université PARIS-SACLAY

C/K interactomics in oil palm metabolism and allocation related to yield

Thèse de doctorat de l'Université Paris-Saclay

École doctorale n° 567, Science du végétal : du gène à l'écosystème (SdV)

Spécialité de doctorat : Sciences agronomiques

Unité de recherche : Université Paris-Saclay, CNRS, AgroParisTech, Ecologie Systématique et Evolution, 91405, Orsay, France

Référent : Faculté des sciences d'Orsay

Thèse présentée et soutenue à Montpellier, le 7 Février 2020, par

Cathleen MIRANDE-NEY

Composition du jury :

Eric Gomès Professeur, UMR 1287 EGFV, Université de Bordeaux	Président
Estelle Jaligot Chercheure EPIC (HDR), CIRAD, Montpellier, France	Rapportrice & examinatrice
Benoit Lacombe Directeur de Recherche, CNRS, Montpellier, France	Rapporteur & examinateur
Nathalie Nesi Directrice de Recherche INRAE, UMR 1349 IGEPP	Examinatrice
Paul Leadley Professeur ESE, Dép. Ecophysiologie Végétale, Orsay, France	Examinateur
Jaleh Ghashghaie Professeure, ESE, Dép. Ecophysiologie Végétale, Orsay, France	Directrice
Guillaume Tcherkez Professeur, Australian National University (ANU), Canberra, Australie	Invité
Emmanuelle Lamade Chercheure, Système de pérennes, CIRAD, France	Invitée

Thèse de doctorat

NNT: 2020UPASS035

Résumé

Le palmier à huile (*Elaeis guineensis* Jacq.) est l'un des oléagineux les plus productifs au monde, avec des rendements d'environ 4 t huile ha^{-1}. Le potassium (K) a une importance considérable pour la production. En effet, l'apport en K est crucial pour le développement des fruits, augmentant non seulement le nombre mais aussi le poids des régimes. Malheureusement, les effets bénéfiques de K sont peu prédictibles car on ignore encore les mécanismes métaboliques sous-jacents. De fait, comprendre ces derniers permettrait aux agronomes de mieux anticiper les effets potassiques sur la production photosynthétique des sucres, les pertes respiratoires et la biosynthèse des lipides.

L'objectif de cette thèse était précisément de regarder les effets de la disponibilité en K sur les voies métaboliques et de voir s'il pouvait y avoir une relation entre les modifications métaboliques et la production d'huile. Pour cela, nous avons réalisé une étude sur le terrain à Sumatra (Indonésie) en utilisant des niveaux de K réalistes évitant l'excès ou la déficience, sur deux croisements largement utilisées commercialement (*Deli x La Mé, Deli x Yangambi*). Nous avons combiné une étude des traits fonctionnels (biomasse, phénologie, analyse des régimes, échanges gazeux), des teneurs élémentaires, et de génomique fonctionnelle (protéomique et métabolomique) dans les folioles et les fruits en cours de maturation. De plus, pour mieux comprendre les effets de K sur l'allocation des photosynthats des feuilles sources aux organes puits et juger si un marquage isotopique sur le terrain est possible, nous avons fait des manipulations préliminaires de marquages avec du $^{13}CO_2$.

Outre les effets attendus sur des traits végétatifs ou les régimes (nombre et/ou poids), nos résultats montrent que l'apport en K impacte le métabolisme primaire du carbone et de l'azote aussi bien dans les folioles que dans les fruits. Dans les feuilles, à K élevé, il y a une capacité photosynthétique accrue que reflètent des teneurs en enzymes-clef (ex. sucrose phosphatase) ou en sucres (disaccharides notamment), et ce de façon croisement-dépendante. De plus, le K élevé reprogramme le catabolisme, avec une augmentation de la respiration, et de la teneur en enzymes du cycle de Krebs et de protéines de la chaîne de transport d'électrons mitochondriale. Dans les fruits, à K élevé, il y a une accélération de la cinétique de dépôt des lipides (synthèse et élongation des acides gras) et des voies associées, comme la synthèse transitoire des sucres et de l'amidon, la remobilisation des acides aminés ou l'activité du cycle des pentoses phosphate. Pourtant, la composition finale des lipides du mésocarpe reste inchangée.

Cette thèse présente ainsi, pour la première fois, une étude détaillée du métabolisme du palmier à huile au champ, et montre que certains traits métaboliques (métabolites ou enzymes) sont liés à la disponibilité en K, mettant en abyme une potentielle utilisation de biomarqueurs foliaires pour piloter la nutrition minérale du palmier.

Abstract

Oil palm (*Elaeis guineensis* Jacq.) is one of the most productive oil crop in the world, with yield values of about 4 t oil ha^{-1}. Potassium (K) is of considerable importance for oil palm production. In fact, K availability is crucial for fruit development by increasing bunch weight and number. Unfortunately, such positive effects of K fertilization remain rather difficult to predict because of the lack of knowledge of underlying metabolic mechanisms. In effect, understanding these mechanisms would allow agronomists to better anticipate oil palm responses in terms of photosynthetic sugar production, respiratory loss, or lipid biosynthesis.

The objective of this thesis was precisely to assess the effect of K availability on oil palm metabolic pathways and determine if metabolic changes could be related to oil production. To do so, we conducted our research work in situ, that is, in plantations in Sumatra (Indonesia), using realistic K levels far from excess or deficiency, with two contrasted oil palm crosses (*Deli x La Mé* and *Deli x Yangambi*) that are widely used in commercial planting. We combined analysis of functional traits (vegetative biomass, phenology, production and fruit analysis, gas exchanges), elemental analyses, functional genomics (proteomics and metabolomics) in leaflets and fruits during maturation. Furthermore, in order to gain knowledge on the effect of K on the redistribution of photosynthetic products from source to sink organs and show the feasibility of isotopic tracing in the field, a preliminary $^{13}CO_2$ labelling experiment was carried out.

In addition to expected effects of potassium on vegetative traits and bunches (number of fruits and/or total fruit biomass), our results show that K availability affected carbon and nitrogen primary metabolism in both leaflets and developing fruits. In leaves, high K conditions led to an increased photosynthetic capacity reflected by higher content in several enzymes (e.g. sucrose phosphatase) and sugar content (in particular disaccharides), in a cross-dependent manner. In addition, high K reconfigured catabolism, with an increase in respiration, Krebs cycle enzyme content and proteins of the mitochondrial electron transfer chain. In fruits, high K accelerated the kinetics of lipid production (fatty acid synthesis and elongation) and associated pathways, including transitory sugar and transitory starch storage and utilization, amino acid remobilization or activity of the oxidative pentose phosphate cycle. However, final mesocarp lipid composition at maturity appeared to be unchanged by K availability.

This thesis presents, for the first time, a detailed metabolic exploration of oil palm in the field and shows that some metabolic traits (metabolites or enzymes) are linked to K availability, thereby opening avenues for the use of leaf biochemical markers to monitor oil palm mineral nutrition.

Acknowledgments

I would like to warmly thank all the people who contributed in many different ways to this Ph.D. work, and more particularly my supervisors: Emmanuelle Lamade, Guillaume Tcherkez and Jaleh Ghashghaie. They contributed widely to the elaboration, the comprehension and the writing of this Ph.D. thesis. I just want to say thank you for your time, your patience and for sharing your knowledge and your skills with me during this 3 years.

I also thank all the Ph.D. board members for their patience during the steering committee meetings and their numerous comments and advice: Jean Ollivier, Edward Gerardeaux and Arthur Gessler.

I thank all colleagues of my research teams UPR34 - Système de pérennes, who welcomed me at CIRAD in Montpellier, and I thank also the team Ecophysiologie Végétal, who welcomed me at Ecology Systematic and Evolution (ESE), and also the doctoral school Science du végétale.

I also thank all members of research teams who welcomed me as a visitor, for trainings or field work:

- *the team of PSBB, Socfindo in Indonesia, including Indra, Dadang, Deni, Chandra, the field workers and the students, who widely helped me on the field,*
- *the team of the platform PAPPSO, INRA, Le Moulon, with Dr. Michel Zivy and Mr. Thierry Balliau,*
- *the team of the platform Metabolism - Metabolome at IPS2, with Dr. Françoise Gilard, Mme. Florence Guérard and Pr. Bertrand Gakière,*
- *the team of the Research School of Biology at Australian National University, including Jing and Illa,*
- *and the team SMS in INRA at Angers with Pr. Anis Limami and Jean-Baptiste.*

I would like to thank Chantal Fresneau from ESE for helping me in the lab with starch extractions and Clément Piel from the ecotron, CNRS at Montpellier, who had the kindness to lend me all the materials necessary for my labelling experiment.

I thank also the greenhouse workers Mr. Christian Chaine and Mr. Semi Melliti at CIRAD in Montpellier who helped me built and organize my pre-labelling experiment in the greenhouse.

I also would like to thank all the members of the oral defence jury, the co-authors of our research articles, and anonymous reviewers, for their time and the thorough comments which really helped me to integrate new skills in research and scientific writing.

To my mother, my sisters Priscilia and Oleecya, my brothers Ruddy and Yannick, my uncle Patrick, my cousin Tracy, Maeva and my grand-mother who believed in me, support me and without them, any of this work would not be possible.

Finally, I warmly thank all my family and friends for their support throughout this Ph.D.: my niece Morgane, nephews, Lynda, uncles, aunts, cousins, and friends; Selima, Tatiana, Mélissa, Suvethighaa, Myriam, Morgan and Yang.

Table of contents

List of figures

List of tables

Context of the study

Oil palm is one of the most productive vegetable oil crop in the world with an oil yield of about 4 t ha^{-1}. Palm oil is the leading vegetable oil in terms of production, volume and consumption (Statista, 2019). Oil palm represents only 5.5% of agricultural land surface area planted with oil crops, but accounts for 35% of global consumption in oils and fats, a number larger than of any other crops (Statista, 2019). In 2017 and 2018, worldwide palm oil production represented roughly 70.5 million metric tons.

Oil palm grows in Asia, Africa and Latin America. Indonesia and Malaysia are the main palm oil producers, followed by Thailand, Colombia, and Nigeria (**FIG. 1**). According to FAOSTAT, Asia accounts for around 89% of global production of palm oil in 2013. Palm oil production is also of importance in India (province of Goa) and Brazil (province of Para) (Sparks, 2012). The global demand in palm oil is expected to rise in the coming years, primarily for food consumption, due to population growth and rising living standards. As such, by 2027, an increase of about 25 million tons of palm oil per year is anticipated (www.oilworld.biz, 2019).

Oil palm is cultivated mainly on tropical soils (and humid tropical climate) with low-to-average level of fertility (i.e., with limited cation exchange capacity) like ultisols (red clay soil) and oxisols (e.g. ferralitic soils) (**FIG. 2**) and therefore requires fertilization, in particular with potassium. In fact, higher potassium application rates are found in Asia on ultisol soils and in Latin America on oxisol and ultisol soils (**FIG. 3**).That is, the particularly high potassium requirement in oil palm comes not only from the dependency of bunch production on nutrient availability, loss via leaching and cultural practices (potassium removal from bunches harvesting and leaf pruning) but also from nutrient scarcity in oil palm cultivation areas (Omoti *et al.*, 1983; Foong, 1991; Chang *et al.*, 1995). Potassium is known to sustain both vegetative growth and fruit production. As a result, there is an increase in potassium consumption in oil palm cultivating countries (Ollivier *et al.*, 2017). It represents up to 114 kg of potash per hectare and thus an annual cost of about US$ 1b at the global scale.

Figure 1. Palm oil production by country in 1000 MT in 2019 – Source: United States Department of Agriculture, www.indexmundi.com

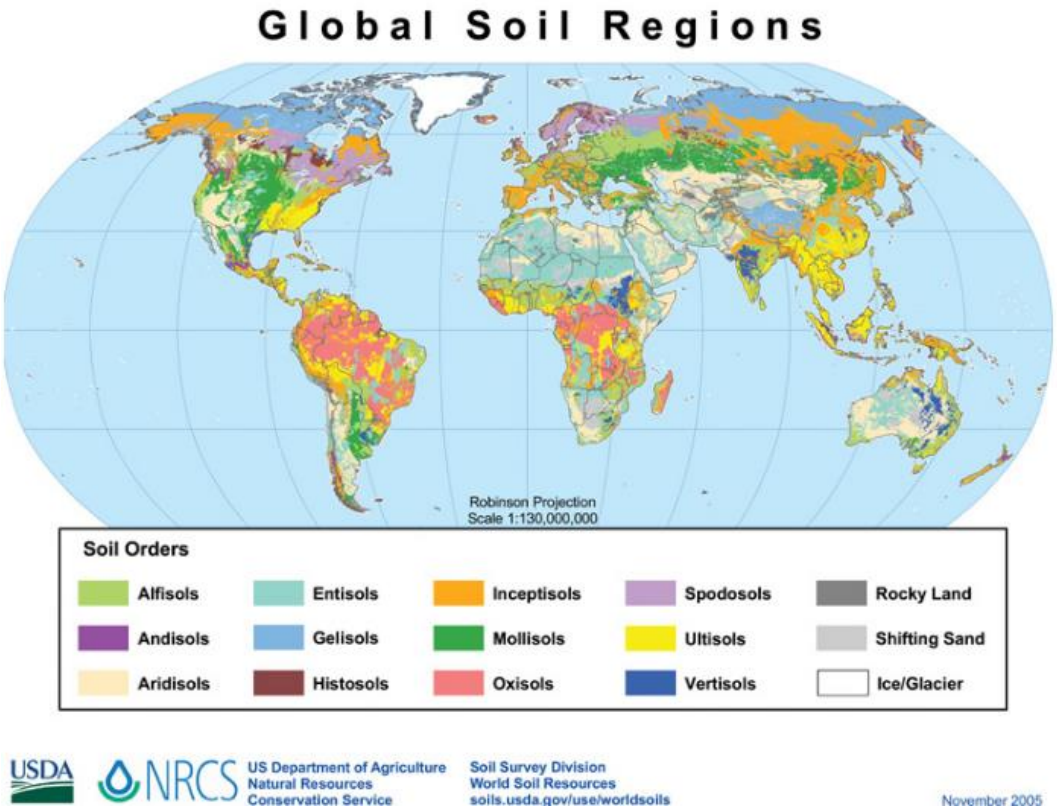

Figure 2. Global soil regions types. Source: www.nrcs.usda.gov, November 2005.

Fertilization management thus represents a crucial aspect of oil palm agriculture and economy. Considerable advances have been made in understanding nutrient requirements in oil palm over the past few decades (Woittiez *et al.*, 2017). However, because of the complexity of oil palm agrosystems (considering soil properties, climatic conditions, nutrient sources and oil palm varieties), fertilization management is still an intense field of research and unsurprisingly therefore, a better understanding of physiological aspects of potassium fertilization related to yield is needed.

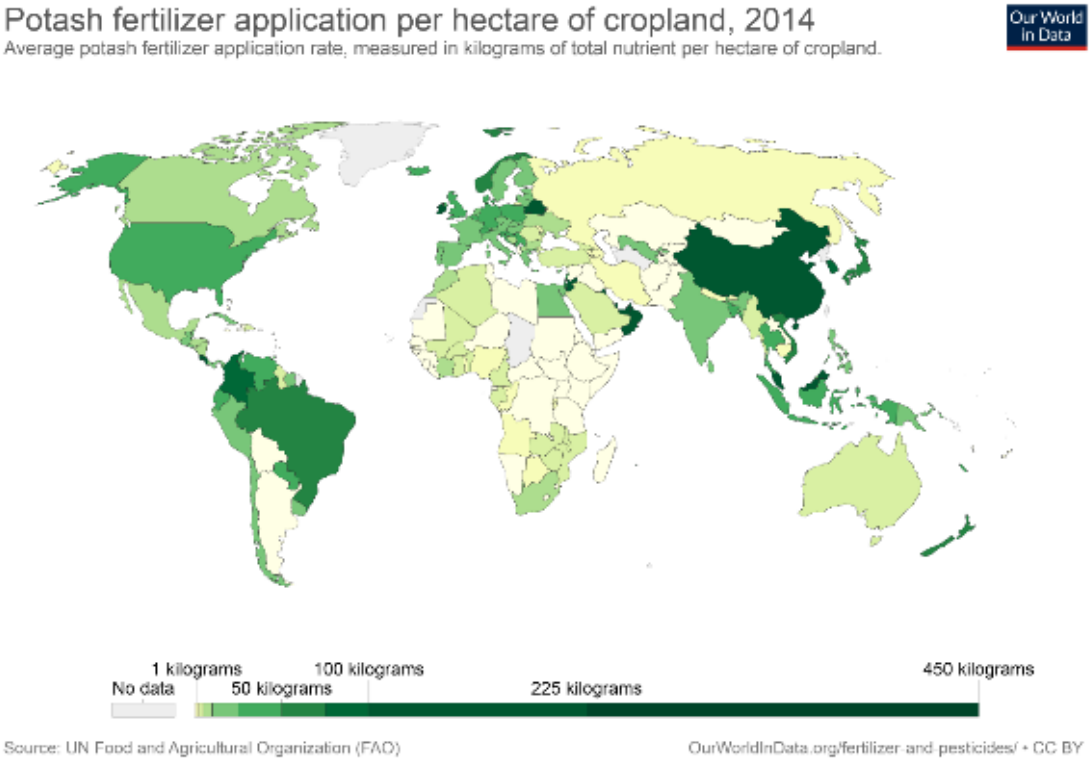

Figure 3. Potassium application rate (in kilograms of total nutrient per hectare of cropland) by region in 2014. Source FAO, from www.ourworldindata.org

Chapter I. General introduction

A. The oil palm tree

1. Overview

Oil palm *Elaeis guineensis* Jacq. was named by Jacquin in 1763 using specimens collected in Martinique, and originates from the tropical rain forest of West Africa (Henson, 2012). Along with coconuts, oil palm is a perennial C_3 monocotyledonous plant of the *Arecaceae* family. Characterized as a ripicole (riparian) species, oil palm grows naturally in forest fringes, river banks, and swampy areas at low altitudes forming natural palm grove galleries (Zeven, 1967).

Within *E. guineensis*, several genetically distinct forms are recognized based on the structure and coloration of fruits. The major structural character is the thickness of the shell or endocarp that surrounds the seed or kernel. Three main forms are referred to as *dura*, *tenera*, and *pisifera*, (more details in paragraph II.A.3). The most producing oil palm trees (*tenera* type) derives from *dura x pisifera* crosses and *dura* × *tenera* crosses (illustrated below in **FIG. I.1**) (Billotte *et al.*, 2005; Cochard *et al.*, 2009). Amongst *tenera* forms, the crosses *Deli x La Mé* and *Deli x Yangambi* are the most widely commercialized families. They have been obtained by crossing the Asian *dura* line *Deli* with the *tenera* African lines *La Mé* (Ivory Coast) or *Yangamb*i (Democratic Republic of Congo). In general, these crosses show differences in morphology, yield and oil composition. Usually, *Deli* lines have a small number of large bunches and *La Mé* and *Yangambi* have a large number of smaller bunches (Meunier & Gascon, 1972). ‰

Oil palm is cultivated mainly as a source of oil but there are side utilizations such as production of palm wine. Two types of oil can be extracted: (1) crude palm oil extracted from the mesocarp of the fruit, and (2) the palmist oil extracted from the kernel. Palm oil is a multipurpose oil since it has several useful properties. It can be used as cooking oil, to manufacture margarine, bakery and confectionery fats (substitute for cocoa butter), or to produce oleochemicals for cosmetics, domestic and industrial products or biofuels.

While oil palm was widely present in West Africa, Central America and Asia, the use of palm oil in the international market expanded significantly as a result of the British Industrial Revolution and the expansion of overseas trade. Major importers of palm oil worldwide in 2018

were India (import of USD 6916.13 million), followed by Pakistan, Netherlands and USA (FIG. 4) (Statista 2019). Import volume of palm oil has increased worldwide over the past few years. According to the World Bank, in 2017, the average price for palm oil was about 649 nominal U.S. dollars per metric ton. It is expected to rise to about 744 nominal U.S. dollars per metric ton by 2025.

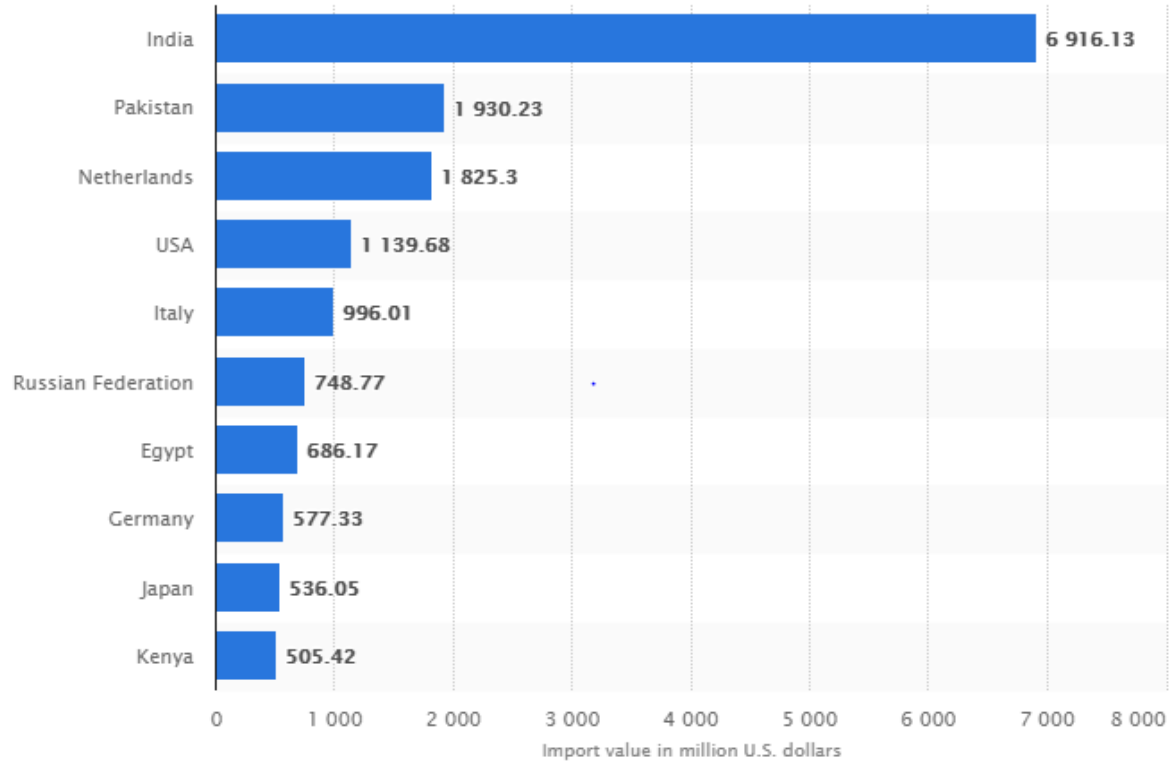

Figure I.1. Leading importers of palm oil worldwide in 2018 (in million U.S. dollars).

While there is an obvious increase in global palm oil need, oil palm production has to face strong criticism in recent years, mostly due to the negative impact of oil palm cultivation on environment. In particular, the development of oil palm plantations at the expense of tropical forest in Indonesia (also in Papua) is believed to cause biodiversity loss, with near-extinction of emblematic species like the orangutan, pygmy elephant and the Sumatran rhino. As a result, public and private efforts led by both consumer and producer countries have been devoted to improve standards of palm oil production. This process is at the origin of the Roundtable of Sustainable Palm Oil (RSPO). RSPO is a non-profit organization that unites stakeholders from several sectors of the palm oil industry in order to develop and implement global standards and produce Certified Sustainable Palm Oil (CSPO) (www. rspo.org).

2. Oil palm ecophysiology

Oil palm is characterized by a simple architecture and indefinite growth which produces successive leaves ("palms") on an unique cylindrical trunk (Jacquemard, 2012; Corley & Tinker, 2016). At adult stage, the palm tree has a crown of 30 to 45 leaves (5 to 9 m long). In the first year after planting, the number of new leaves produced each year increases progressively, reaches 40 leaves yr^{-1} 2 years after planting and then declines with age (Jacquemard, 1979; Gerritsma & Soebagyo, 1999). After 8-12 years, leaf emission is thus about 20-24 leaves yr^{-1} while leaf area and dry weight increase steadily with palm age. Leaf area reaches a plateau at 8-10 years after planting, but petiole cross section and presumably leaf dry weight continue to increase slowly (Corley & Tinker, 2016). At the adult stage, a new leaf is therefore emitted approximatively every two weeks (17 days in fact) with a divergence (phyllotaxic) angle of about 137.5°. The crown is organized in eight spirals where leaves are numbered (as ranks) following emergence sequence, from the youngest (rank 1) to the oldest (for example, rank 42). That is, leaf no. 1 is the starting point of the spiral "one". By convention, leaf rank no. 1 is the youngest leaf presenting 75% of leaflets opened and is considered to be the first functional (i.e. autotrophic) leaf by planters (**FIG. I.2**). At adult stage, the leaf emission rate also depends considerably on water availability (a dry period causes an accumulation of spear leaves), temperature (low temperature decreases growth rate) and also probably on carbon reserves of the tree. By contrast, leaf area and specific leaf weight are not very sensitive to external factors but may show significant responses to fertilizers (Corley & Tinker, 2016).

Oil palm trees can reach 20-25 m height at adult stage, with a trunk diameter varying between 60 and 90 cm, depending on varieties and carbon reserve accumulation. The growth of trunk diameter is limited and usually stops when the tree reaches 4 years. Annual height increment varies from 0.3 to 0.6 m yr^{-1}. It depends on environment and crosses but also on leaf production rate and the internode length (Hartley, 1988a; Corley & Tinker, 2016).

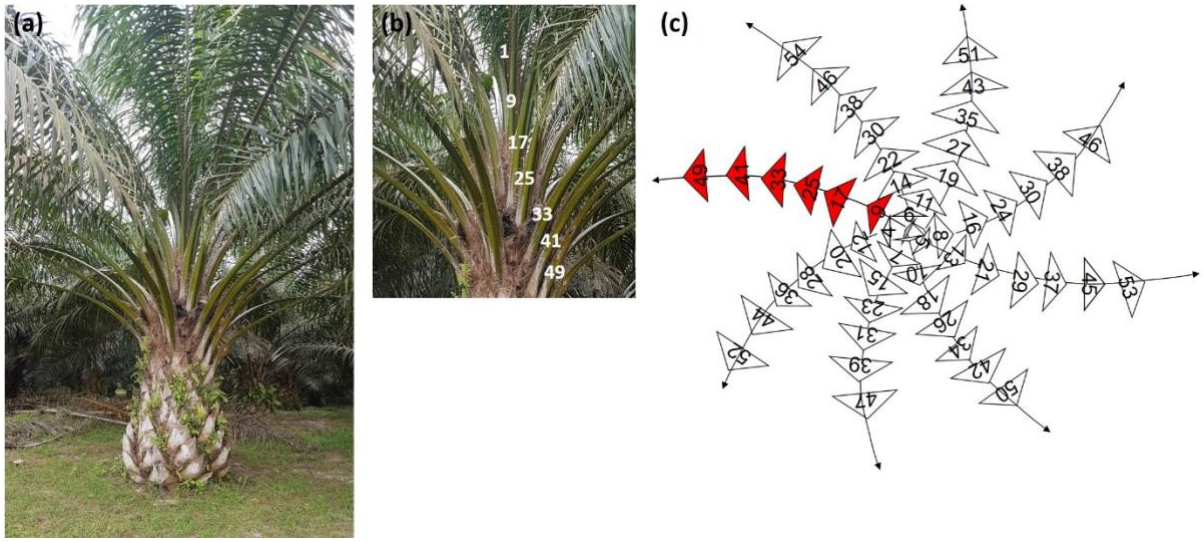

Figure I.2. Oil palm leaf organization. (a) Photography of an oil palm tree. (b) Photography of an oil palm tree crown with associated leaf rank number on spiral one (c) Diagram of an oil palm crown with leaf rank number as a function of their chronological emergence, spiral one in red (Lamade *et al.*, 2009).

The roots system originates from the trunk base and form a fasciculate rootstock, which spreads around the tree, reaching neighbor trees with a potential length at soil surface larger than 9 m. Furthermore, roots can grow up to 6 m depth when grown on sandy soil. The root system is made of four-fold branched roots (the primary roots (I): responsible for sap circulation and anchorage; the secondary roots (II): which are devoted to resources prospections; the tertiary and quaternary roots (III+IV): which form the absorption system) (Jourdan & Rey, 1997a).

Oil palm is a C_3 plant with a high leaf surface area (from 6 to 12 m^2 $leaf^{-1}$, depending on crosses), and a large carbon storage mostly in the form of starch and glucose located in the trunk (Legros *et al.*, 2006; Legros *et al.*, 2009c). Oil palm leaves have high photosynthesis rates, with a maximum for leaves at rank 8 to 10 (from 23 up to 30 µmol m^{-2} s^{-1}) (Dufrene & Saugier, 1993; Lamade & Setiyo, 1996) even in trees that are 4-5 years old only. Concerning photosynthesis activity, a mid-day depression is generally observed due to stomatal closure when the VPD (Vapor Pressure Deficit) reaches 1.7 kPa. In young palms, the rate of photosynthesis goes up with developmental stage but also appears to be controlled by the presence of developing bunches, acting as sinks for assimilates (Gerritsma, 1988). This feedback control is believed to be mediated by carbohydrate accumulation in leaflets during the day (Dufrene, 1989). In fact, Henson (1990) found higher leaf non-structural carbohydrate

levels in non-fruiting than fruiting palms. However, on mature oil palm under drought condition, no negative feedback has been observed with strong sink limitation on light-saturated leaf CO_2 assimilation rate (A_{max}) (Legros *et al.*, 2009b). In such conditions, strong sink limitation, has led to non-soluble carbohydrates (NSC) accumulation in the trunk (mainly as starch), reaching up to 50% (dw:dw) in trunk top. Leaf physiological parameters also vary with leaf ageing. The study of Suresh and Nagamani (2006) has shown that in leaf number 9, net photosynthesis, transpiration, and stomatal conductance, for an adult palm tree, are higher than in younger or older leaves, meaning that leaf gas exchange progressively declines with leaf age (TABLE I.1). In addition, photosynthetic rate has been found to be positively correlated to stomatal conductance and negatively correlated to leaf mass per area (Lamade & Setiyo, 1996). Dark respiration rates are also lower in older and shaded leaves compared to young and unshaded leaves (Henson, 1991). In oil palm leaflets, the dark respiration rate is about 1.5-2.5 µmol m^{-2} s^{-1} (Lamade & Setiyo, 1996; Lamade *et al.*, 2009). At the whole oil palm tree level, about 60 to 80 % of gross assimilation is thought to be respired not only by leaf respiration but also by other organs (Dufrene, 1989; Lamade *et al.*, 2016).

Table I.1. Physiological parameters variations with leaf age. Variation in net photosynthetic rate (P_N in µmol m^{-2} s^{-1}), stomatal conductance for CO_2 (g_s in mol m^{-2} s^{-1}), transpiration rate (E in mmol m^{-2} s^{-1}), leaf area (LA in m^2), leaf dry mass (LDM in kg) and and leaf mass per area (LMA kg m^{-2}). Values with the same letters do not differ significantly from each other. Adapted from Corley et *al*. 2016.

Leaf n°	P_N	g_s	E	LA	LDM	LMA
1	2.94 e	0.01 a	0.72 c	2.15 b	1.80 c	0.85 ab
9	9.18 a	0.03 a	2.26 a	3.38 a	2.61 b	0.78 ab
17	6.16 b	0.03 a	1.58 b	3.28 a	3.08 a	0.94 a
25	5.23 c	0.02 a	1.32 b	3.26 a	2.59 b	0.81 ab
33	4.38 d	0.02 a	1.27 b	2.96 a	2.37 b	0.75 b
LSD (p=0.05)	0.64	0.05	0.36	0.43	0.46	0.19

Assimilates produced during photosynthesis are redistributed to developing leaves, inflorescences (and bunches), trunk and roots, depending on sink strength. Assimilate partitioning among growing organs is generally a function of active sinks (and organ growth rates) in plants (Marcelis, 1996; Heuvelink, 1997). Dufrene (1989) and Dufrene and Saugier

(1993) have estimated that oil palm photosynthates are used in priority for vegetative growth and maintenance. Also, Henson (Henson, 2006; Henson, 2007) reported that vegetative growth and development does not vary much and has priority for photosynthate allocation perhaps due to the low architectural plasticity, whereas fruit production and thus fruit sink strength can adjust to available resources (**FIG. I.3**). In fact, severe leaf pruning reduces vegetative dry matter (VDM) production by 4% only and reduces fruit yield by 65%; conversely, removing bunches increases VDM with an increase in leaf production, leaf dry weight, trunk height and diameter, as well as leaf area (Corley & Breure, 1992). Therefore, fruit development seems to occur only when fixed carbon (gross production) is larger than the demand of vegetative development, and thus is very sensitive to photosynthetic conditions. In fact, it has been shown that intercepted radiation per tree and photosynthesis were linearly related to bunch yield (Squire, 1986; Squire & Corley, 1987) suggesting that bunch yield is source limited, that is, limited by the supply of carbohydrates from photosynthesis. Moreover, in the fruit, the kernels had a higher priority for carbohydrate supply for their development than the mesocarp or shell (Harun & Noor, 2002). It is worth noting that according to Corley and Tinker (2016), roots may have, like leaves, priority over bunches for photosynthates utilization. The physiology of roots is far less documented than leaves and thus this suggestion awaits further evidence. Still, root biomass certainly differs with oil palm age, between crosses, soils and environments and this add to the complexity of physiological determinants of fruit production. Root turnover represents about 9-11.5t ha^{-1} $year^{-1}$, made of 15% primary roots, 31% secondary and 57% fine roots (Dufrene, 1989; Lamade *et al.*, 1996; Jourdan & Rey, 1997a; Jourdan & Rey, 1997b).

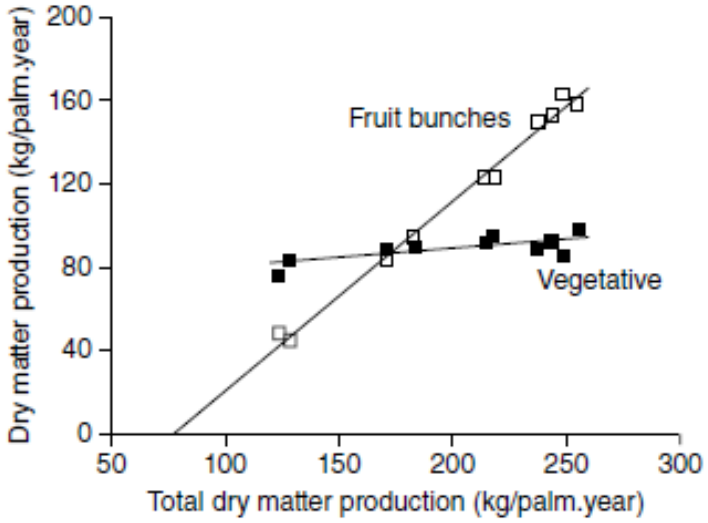

Figure I.3. Dry matter partitioning between vegetative tissues and fruit bunches. Dry matter (DM) per palm incorporated into vegetative tissues and bunches, compared with total dry matter production. The lines are fitted regressions (both with slopes significantly different from zero) and indicate that 91% of all additional dry matter, above a threshold of 77 kg palm^{-1} year^{-1}, goes into bunches. Bunch dry matter is adjusted for the energy content of the oil. Data are from Corley (1973) for 6–7 year-old palms in a density trial, plotted as in Squire (1990).

To our knowledge, the precise photosynthate allocation pattern in oil palm has never been examined with isotopic tracers (^{13}C or ^{14}C labelling), likely due to the scale of experiments required (tree-scale) and thus the induced cost. Nevertheless, a recent study (Lamade *et al.*, 2016) used ^{13}C at natural abundance ($\delta^{13}C$ values) to compute the most probable allocation pattern (**FIG. I.4**). It suggests that fruits and roots represent the largest carbon sinks (20-30% each) while heterotrophic leaves represent about 11-15% (Lamade *et al.*, 2016). Ecophysiological modelling and biomass measurements have suggested that in mature trees, fruit bunches and roots are responsible for a respiratory loss of 18 and 14% of gross primary production, respectively and that carbon partitioning to fruits and roots stands for 30 and 10% of gross carbon fixation, respectively (Dufrene, 1989; Lamade & Setiyo, 1996). However, $\delta^{13}C$ values suggest that fruit development represents by far the largest respiratory loss (40% of tree respiratory loss) while leaves and roots represent only 12 and 5-10% of respiratory loss (Lamade *et al.* 2016). Although more data are certainly needed to provide a more precise picture of allocation and respiratory losses in oil palm, a high respiratory loss in fruits would be consistent with the low metabolic carbon use efficiency of oil (fatty acid) production.

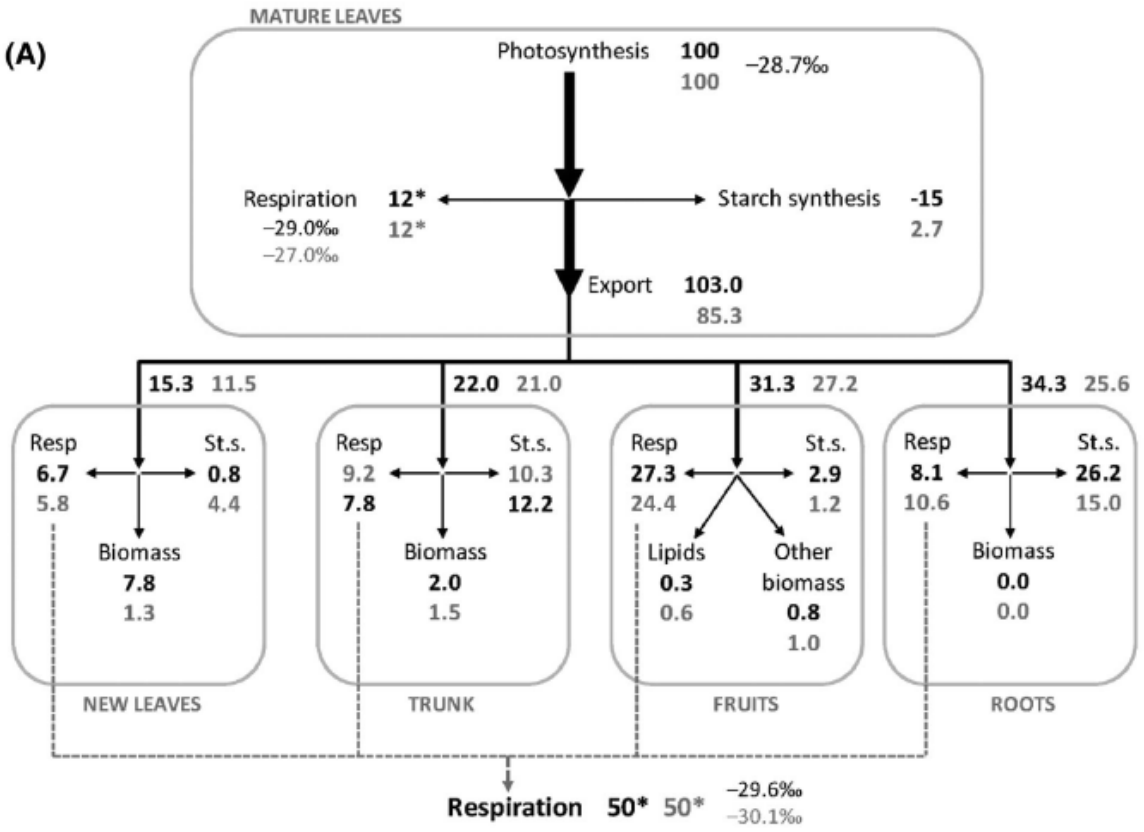

Figure I.4. Allocation pattern in oil palm computed from $\delta_{13}C$ values, using a model based on sucrose redistribution directly from leaves. Numbers are in percent that is, expressed relative to photosynthetic C fixation fixed at 100. Values in black and grey were obtained at stages 0 and 6 of fruit maturation, respectively. $\delta_{13}C$ values shown for respired CO_2 were obtained by mass balance with e=+1‰ (dark) or -1‰ (grey), where e is the isotope fractionation associated with respiratory CO_2 evolution in the light, with respect to net fixed CO_2. Asterisks indicate that the values were fixed as a model constraint: leaf respiration (12% of fixed CO_2), total respiration (fixed CUE of 0.38) and trunk growth [in (B)]. Resp, respiration; St.s., starch synthesis. (See (Lamade *et al.*, 2016) for further details).

In adult oil palm trees under favorable conditions, non-structural carbohydrates (NSC) represents about 20% of vegetative plant dry matter (DM) including roots, with 65% located in the trunk (Legros *et al.*, 2006). In general, it is believed that perennials plants accumulate NSC during periods of excess production of photoassimilates and use them when the demand exceeds production (Kozlowski, 1992). In oil palm, reserves are predominantly located in the trunk, however, other organs like petioles or leaves may also play a role of a transitory storage. Zahari *et al.* (2012) observed also substantial carbon reserves in the form of glucose in petioles. The chemical nature of NSC reserves varies among perennial species (Kozlowski, 1992) but in adult oil palm, glucose is an important reserve sugar (50% of NSC), followed by starch and sucrose

(20% each) and a small amount of fructose (Legros *et al.*, 2006). In other words, oil palm is one of the rare species using glucose as a transitory reserve sugar. However, starch is the main metabolic "buffer" compensating for source and sink variations, whereas glucose dynamics remain poorly explained (Legros *et al.*, 2009d). The same authors suggested that the glucose content might be directly driven by environmental variables. Still, sucrose is by far the major carbon transport form in the tree from source leaves to sinks (fruits) (Houngbossa & Bonnemain, 1985; Obahiagbon *et al.*, 2012). In fact, sucrose is the prevalent sugar in oil palm phloem sap extracted from leaves, and furthermore, it is the major ^{14}C-compound in sap upon ^{14}C-labelling (Houngbossa & Bonnemain, 1985; Obahiagbon *et al.*, 2012). Thus presumably, sucrose is the carbon source for lipid and starch biosynthesis in fruits (starch being then used as a carbon source for lipid synthesis) (Dussert *et al.*, 2013). In fact, genomics analyses have suggested that fruit development is primarily sustained by sucrose, since fruit tissues have a high expression level of sucrose synthase (Susy; which catalyzes sucrose cleavage) during maturation (Wong *et al.*, 2017).

3. Oil production and composition in fruits

Oil palm is a monoecious species, with successive male and female inflorescences that develop separately on the same plant. Pollination, which must be crossed between two individual palm trees at least, is usually anemophilous but can done either by insects such as *Elaeidobius kamerunicus* (Coleoptera Curculionidae), or manually. After pollination, fruits start maturation, which takes 5 to 6 months until ripe. Generally, bunches are harvested from the third to fourth year after planting. Fresh fruit bunch yield increases for 10 years, then reaches a maximum and declines progressively (Corley & Gray, 1976) or stay stable (see https://www.palmelit.com, Catalogue-PalmElit-Oil-Palm-Seeds.pdf)

The oil palm fruit is a sessile drupe composed of five different parts: (1) the exocarp (outer skin); (2) mesocarp (oily fibrous layer containing palm oil): (3) the endocarp (kernel shell); and (4) the kernel containing palmist oil (Teh *et al.*, 2013b). As already mentioned page 10, there are three forms of oil palm fruit: a thick-shelled form (2-8 mm) with a thin mesocarp (35-65 % mesocarp/fruit) called *dura*, a shell-less form, usually female sterile called *pisifera* and a thin shelled form (0.5-4 mm) with a high mesocarp content (55-96 %) called *tenera* (**FIG. I.5**). The *pisifera* is not well spread as a commercial planting material as it is mostly infertile.

Oil represents up to 90% of mesocarp dry weight, and this is the highest lipid content in oil-producing crops. The bunch has a main stalk, spikelet stalks, spines (transformed bracts), fruits and parthenocarpic (seedless) fruits, which are developed in case of poor pollination conditions. The parthenocarpic fruits in the inner bunch increased with fruit set and contain very little oil due to decreased mean fruit size (Harun & Noor, 2002).

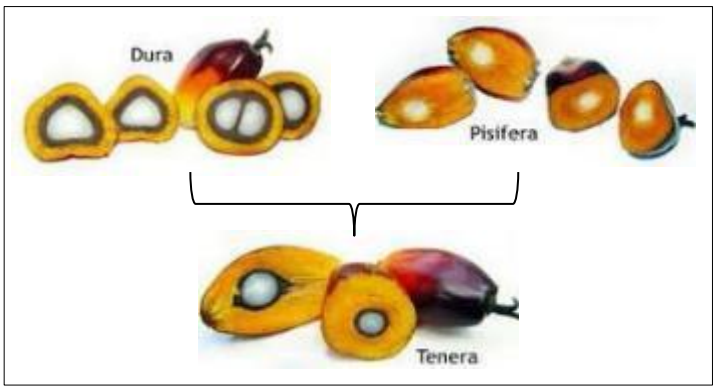

Figure I.5. Oil palm fruits forms of *dura, pisifera* and *tenera*. *Tenera* forms are the products of *dura x pisifera* crosses or *dura x tenera* crosses (or *tenera x tenera*).

Oil palm fruit development and oil deposition has been well-described by Thomas *et al.* (1971) and Hartley (1988a). After anthesis, the mesocarp is visible and composed of 92% of water. At this stage, the kernel is still liquid and the endocarp is thin. Twenty days after anthesis, the endocarp becomes thicker and the kernel hardens. By 11 weeks after anthesis (WAA), depending on varieties, the kernel completely fills the seed cavity and the endocarp starts dehydration while sclerifying to isolate and protect the kernel (Hermine Bille *et al.*, 2013). By 15 WAA, the mesocarp begins a continuous dehydration by transpiration which is associated with active lipid biosynthesis through fatty acids (FA) synthesis until maturation (around 20-21 WAA) (Jeje *et al.*, 1978; Teh *et al.*, 2013a). Reciprocally, fruit sugar content tends to decrease to very low level by 18 WAA (Neoh *et al.*, 2013; Teh *et al.*, 2013a).

Fatty acids (FA) are mostly produced in plastids, and are then assembled into triglycerides and other lipids in the cytoplasm (oil bodies). In fact, Bourgis *et al.* (2011) has established a precise oil biosynthesis pathway for oil palm. Briefly, imported sucrose is cleaved

to hexoses, and intermediates are transported to the plastids, where glycolysis and FA synthesis are massively up-regulated. The large flux of de novo FA synthesis is then channeled to the endoplasmic reticulum, where "housekeeping" levels of enzymes of the Kennedy pathway (**FIG. I.6**) and associated enzymes are sufficient to assemble triacylglycerols (TAG), which simply accumulate as oil droplets in the cytoplasm (**FIG. I.7**). Also, Bourgis *et al.* (2011) found that (i) plastid glycolysis is up-regulated in oil palm temporally during ripening, and (ii) glucose-6-phosphate transporter (GPT2) and phospho*enol*pyruvate (PEP) transporter (PPT) provide glycolytic substrates (hexose P) and intermediates (triose phosphate, PEP) to the plastid by transport from the cytosol, a trend that is accentuated during ripening. This implies a strong funneling of carbon towards pyruvate in the plastids of oil palm. Thus, increased fatty acid synthesis, together with plastid carbon supply, is crucial for the accumulation of oil in the mesocarp.

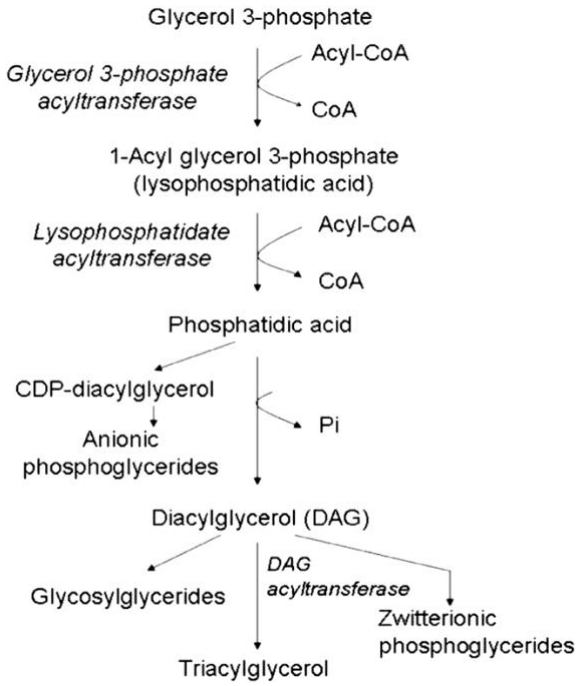

Figure I.6. The basic Kennedy pathway for glycerolipid biosynthesis. From (Guschina *et al.*, 2014)

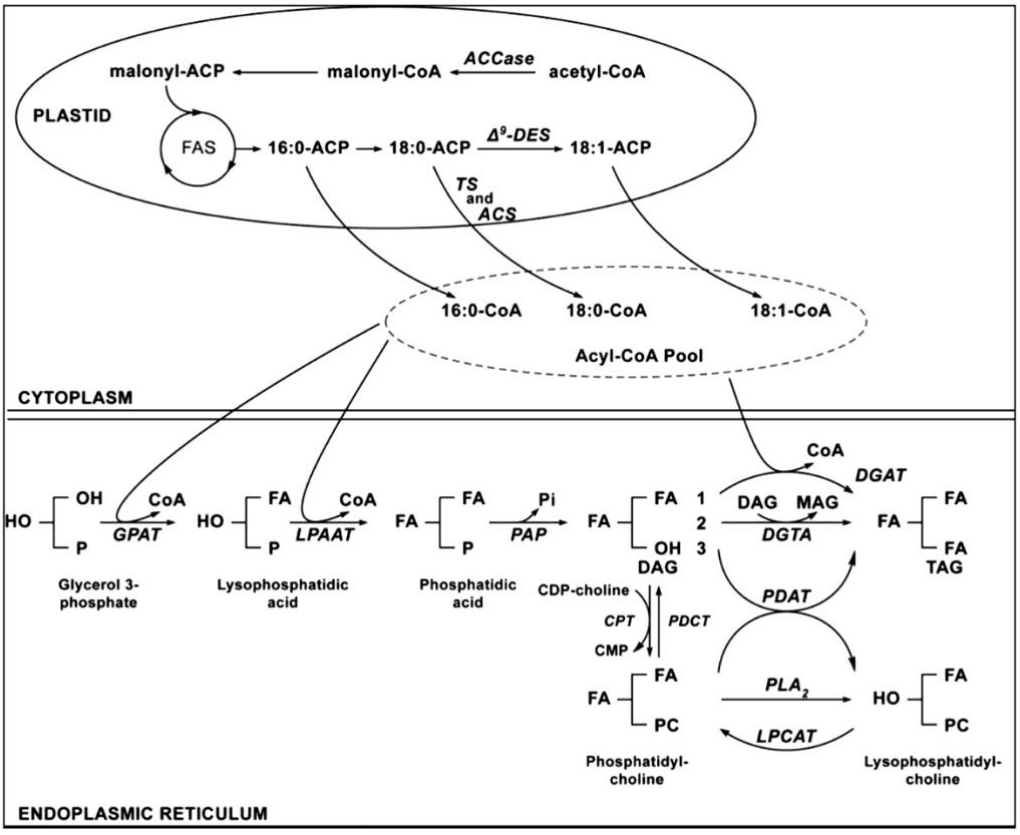

Figure I.7. Simplified scheme of TAG biosynthesis in plants. ACCase, acetyl-CoA carboxylase; ACP, acyl carrier protein; ACS, acyl-CoA synthase; CPT, CDP-choline:1,2-diacylglycerol cholinephosphotransferase; Δ9-DES, Δ9-desaturase; DGAT, DAG acyltransferase; DGTA, diacylglycerol transacylase; FAS, fatty acid synthase; GPAT, glycerol 3-phosphate acyltransferase; LPAAT, lysophosphatidate acyltransferase; LPCAT, lysophosphatidylcholine acyltransferase; PAP, phosphatidate phosphohydrolase; PDAT, phospholipid:diacylglycerol acyltransferase; PDCT, phosphatidylcholine:diacylglycerol cholinephosphotransferase; PLA2, phospholipase A2; TS, acyl-ACP thioesterase. From (Guschina *et al.*, 2014).

Changes in lipid class and fatty acid composition during development of the oil palm mesocarp are well reviewed in Sambanthamurthi *et al.* (2000). Before oil deposition, phospholipids are the major lipid class, accounting for about 60% of the total lipids at 8–12 WAA (with 51% of phosphatidylcholine (PC), followed by phosphatidylinositol (PI) and lysophosphatidyl-choline (LPC)). At maturity, however, glycolipids form the major component of the polar lipids (Bafor & Osagie, 1986). Triacylglycerols (TAG) increase rapidly from 16 WAA and reaches a maximum at 20 WAA (Sambanthamurthi *et al.*, 2000). Palmitoleic and linolenic acids are present in significant amounts in the early stages of lipid synthesis. These fatty acids (FA) are typical constituent of chloroplast and membrane, suggesting a high ratio of

chloroplast and cellular synthesis to storage lipid synthesis at this stage. These fatty acids, however, are undetectable after 16 WAA, probably because of a dilution effect by the accumulation of storage lipids (Sambanthamurthi *et al.*, 2000). In addition, immature mesocarp contains large amounts of chlorophyll, which decline by about 17 WAA, accompanied by a massive accumulation of carotenes as the fruit ripens (Ikemefuna & Adamson, 1984). Also immature mesocarp tissue is characterized by high amounts of sterols. As the fruit matures, sterols decrease as a consequence of dilution by the huge amount of TAG synthesized (Ikemefuna & Adamson, 1984).

When ripe, fruits (including kernels) not only contain lipids but also structural constituents (lignin, hemicellulose, cellulose and pectic substances) at 18-20%, soluble proteins and sugars accounting for 2-3% of mesocarp weight. On average, crude palm oil contains 44% palmitic acid (C16:0), 5% stearic acid (C18:0) and traces of myristic acid (C14:0), which together constitute half of fatty acids found in triacylglycerols (TAG) in fruit mesocarp (Sambanthamurthi *et al.*, 2000). TAG with unsaturated fatty acids are represented by 40% oleic acid (C18:1), 10% linoleic acid (C18:2) and traces of linolenic acid (C18:3) (Barcelos *et al.*, 2015). This right balance between saturated and unsaturated fatty acids makes palm oil suitable for a number of food applications.

In oil palm agronomy, the term “production” refers to fresh fruit bunch (FFB), completed by bunch number, bunch weight and oil-to-bunch ratio. The number of bunches results from leaf emission rate, sex ratio, early and late abortion rate. The weight of a mature bunch depends on the number of spikelets, the number of flowers per spikelet, the fruit set (percentage of flowers that develop into fruit or pollination efficiency), the mean weight per fruit and the weight of the stalk (Corley & Tinker, 2016). The oil-to-bunch ratio is defined as the amount of oil recovered in a bunch (i.e. the oil extraction rate) (Rahim *et al.*, 2003). The oil extraction rate (OER) is calculated as:

$$\mathrm{OER} = \frac{\mathrm{F/B} \times \mathrm{M/F} \times \mathrm{OFM}}{10,000} \times 0.855$$

where F/B, M/F and OFM stand for the percentage of fruits biomass in bunch total biomass, the percentage of mesocarp biomass in total fruit biomass, and the percentage of oil in mesocarp biomass, respectively. The correction factor of 0.855 is used to account for losses in factory oil extraction. Of course, the OER is influenced by oil palm crosses, environmental conditions or

the addition of fertilizers (Menon, 2000). At maturity, bunch weight is in average 23-27 kg and OER is about 23% of fresh weight (**TABLE I.2).**

Table I.2. Oil palm fruit bunch composition under ideal climatic conditions and good management. Data are given in kilograms and percentage of fresh weight. Source: www.fao.org.

Bunch component	Standard range
Bunch weight	23-27 kg
Fruit/bunch	60-65 %
Oil/bunch	21-23 %
Kernel/bunch	5-7 %
Mesocarp/bunch	44-46 %
Mesocarp/fruit	71-76 %
Kernel/fruit	21-22 %
Shell/fruit	10-11 %

B. Potassium nutrition in plants: overview

Potassium (K) is one of the most important macronutrients, along with nitrogen (N) and phosphorous (P), required for plant growth and development. It is also the most abundant (in terms of elemental composition) macronutrient in many species (Leigh & Wyn Jones, 1984), such as oil palm. Potassium plays a significant role in several plant physiological processes related to cation-anion balance, osmoregulation, water movement, phloem transport and energy transfer, and takes part in protein synthesis, carbohydrate metabolism, enzyme activation and stress resistance.

1. Potassium sources and fertilization

Potassium geological reserves are generally large and represent about 2.1 to 2.3 % of Earth's crust (Schroeder, 1978). However, potassium is not readily accessible in soils since its availability for plants depends on exchange capacity and most of soil potassium is fixed in minerals or non-exchangeable and embedded in silicates. In addition, due to intensive agricultural production systems leading to coarse-textured or organic soils, and specific soil composition (sandy, waterlogged, saline, or acidic), K can be limiting for plant growth

(Goulding & Loveland, 1986). This is the case in the tropical region where oil palm is cultivated, where strong weathering leads to clay-rich or ferralitic soils with limited cation exchange capacity and low K bioavailability. Many sources of K are used as fertilizers, including potassium chloride (KCl, the most used by far), potassium nitrate (KNO_3), potassium sulfate (K_2SO_4), potassium carbonate (K_2CO_3) and potassium-malate ($C_4H_4O_5K_2$). Of course, the efficiency of K^+ fertilization depends on soil texture, propensity for leaching, soil moisture content, pH, etc.

In some cases such as sandy soil or waterlogged conditions, K is applied as a foliar spray. In fact, Ashraf *et al.* (2011) reported that foliar spray application of potassium alleviated the adverse effects of waterlogging on cotton plants. In olive tree, potassium nitrate (KNO_3) or mono potassium phosphate (MPK) enhanced leaf mineral status, yield and fruit quality in a sandy soil (Sarrwy *et al.*, 2010). However, while K^+ is highly soluble in water and diffuses relatively easily through the cuticle and the free space of the cell wall, K foliar spray application can only partially compensate for insufficient uptake by roots (Mengel, 2002).

2. Potassium absorption

Plants uptake of K as a cation (K^+) occurs via root hairs and then cortical roots cells and once in the stele, K^+ is transported to the shoot and distributed to the leaves and others organs via the xylem. K^+ can be stored in the vacuole, from which it can be remobilized to keep cytoplasmic K^+ concentration constant. In fact, the concentration of K^+ in the cytoplasm is kept relatively constant at about 50–150 mM, while the concentration in the vacuole varies substantially depending on supply status. In the soil, potassium concentration is between 0.1 and 1 mM (Britto & Kronzucker, 2008; White & Karley, 2010). Therefore, K^+ enters root cells against the concentration gradient but follows the transmembrane potential, which favors the entry of cations. The cornerstone of cation and charge distribution across the plasma membrane is the activity of H^+-ATPases that pumps H^+ out of the cell by consuming ATP.

Potassium uptake is facilitated by different transporters or channels allowing transport of K^+ between the outer environment and the cytoplasm or between different cellular compartments. Two transport systems are involved in K^+ uptake based on their affinity. The high-affinity system operates at low external concentrations. Electrophysiological evidence

indicates that this pathway involves a H^+:K^+ symporter coupled to the activity of the plasma membrane H^+-ATPase (Maathuis & Sanders, 1994). The low affinity pathway, which operates at higher concentrations, usually more than 0.3 mM external K^+, has the characteristics of a channel-mediated transport. Channels of the Shaker family have been implicated in K^+ permeation through the plasma membrane. Other channels have been also identified in plants (**FIG. I.8**). In *Arabidopsis thaliana*, the voltage-gated K^+-selective channel protein K^+ Transporter 1 (AKT1) has been shown to be essential for K^+ uptake by roots (Spalding *et al.*, 1999; Xu *et al.*, 2006). In *Elaeis guineensis*, the transporter EgKUP8 has been shown to be transcriptionally activated in roots under K^+-deficiency, indicating its importance for high affinity K^+ uptake in K^+-limited environment (Husri & Ong-Abdullah, 2018). Stelar K^+ Outward Rectifier (SKOR) is structurally similar to AKT1 but mediates K^+ efflux in root stellar cells to facilitate K^+ loading into the xylem (Gaymard *et al.*, 1998). In *Arabidopsis* guard cells, where K^+ fluxes mediate stomatal movements, stomatal opening driven by K^+ entry occurs mainly through K^+ channel in *Arabidopsis thaliana* 1 (KAT1) and KAT2, whereas stomatal closing is caused by K^+ efflux through Gated Outwardly Rectifying K^+, a channel activated by membrane depolarization (Ache *et al.*, 2000; Hosy *et al.*, 2003; Lebaudy *et al.*, 2010).

Potassium distribution in the plant has been reviewed recently (Ahmad & Maathuis, 2014; Wigoda *et al.*, 2014). K is allocated to growing and metabolically active tissues, often at the cost of older and less crucial cell types. Sensing of and response to K^+ appears to be mediated by several cellular events. These include cell membrane potential (depolarization), reactive oxygen species (ROS), Ca^{2+}, hormones such as ethylene, jasmonic acid or cytokinins and direct sensing of the environmental K^+ concentrations by K^+ channels.

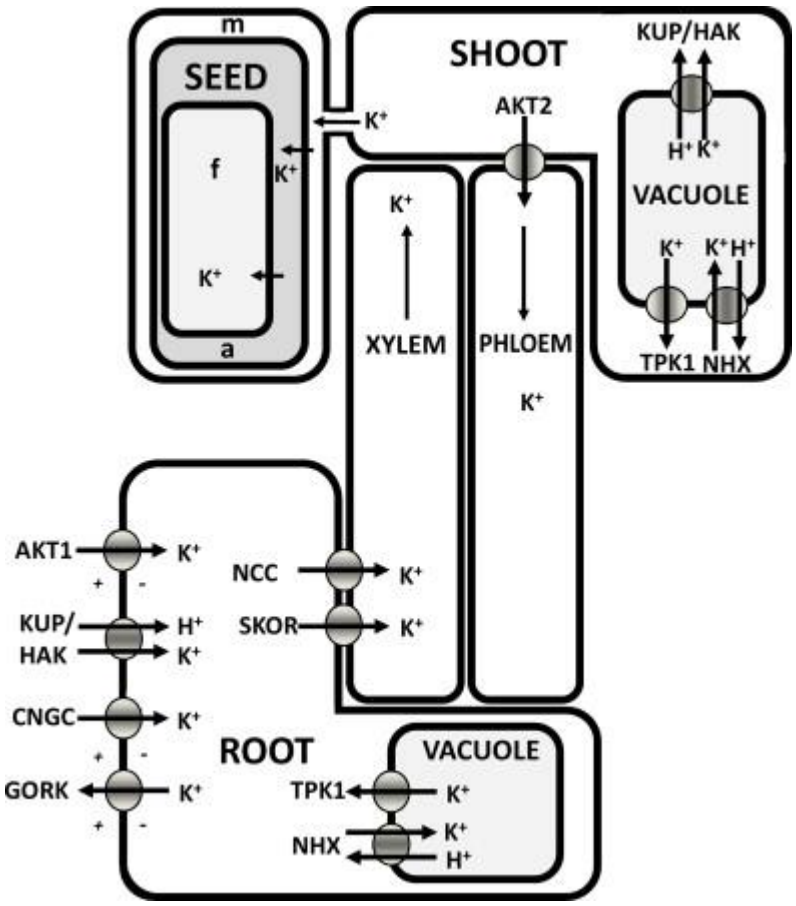

Figure I.8. Overview of transport processes and proteins that are involved in K^+ uptake, efflux and distribution. At the external soil:root interface transport functions are shown for passive [AKT1 and CNGC (cyclic nucleotide gated channel)] and energized (KUP/HAK) K^+ uptake and channel mediated K^+ release (guard cell outward rectifying K^+ channel; GORK); Xylem loading mainly happens through K^+ selective (SKOR) and non-selective (NCC) cation channels though energized systems may also play a role; Phloem loading of K^+ for recycling and/or sucrose loading may involve the AKT2 channel; K^+ flux to the seed is phloem mediated but K^+ is unloaded into the seed apoplast (a) at the junction between maternal (m) and filial (f) tissues; vacuolar K^+ accumulation is primarily driven by H^+-coupled antiporters such as NHX while vacuolar K^+ release is either passive through TPK1 type channels or, in K^+ starvation conditions, active through H^+-coupled KUP/HAK transporters. From Ahmad and Maathuis (2014).

3. Physiological roles of potassium

a) Cells turgor and guard cells

As stated above, plant cells contain two major pools of K^+, one in the vacuole and one in the cytosol (while mitochondria represent a smaller pool but of physiologic ,al importance). K^+ plays the role of an osmoticum in the vacuole and as such, is involved in turgor and cell

enlargement. Similarly, K^+ plays a role in the opening and closing of stomata, which regulate leaf conductance for water vapor and CO_2. Thus K nutrition has been suggested to be essential for water use efficiency (Mengel & Forster, 1973). In general, K-deficient plants have a low stomatal conductance, and a low water use efficiency because of the concurrent decrease in the synthesis of the photosynthetic machinery component (for a recent example in oil palm, see Cui *et al.* (2019b)).

Stomatal opening starts with membrane hyper- or re-polarization caused by H^+-ATPases, leading to K^+ uptake through inward-rectifier K^+ channels (Ache *et al.*, 2000). The influx of K^+, Cl^-, and NO_3^- and the synthesis of malate (accumulated in the vacuole) increases the concentration in osmoticum and thus a water influx thereby ensuring turgor of the guard cells and stomatal opening. The rapid loss of K^+ from guard cells during stomatal closure stems from anion efflux, which causes plasma membrane depolarization and the opening of outward K^+ channels that leads to K^+ efflux from the vacuole and across the plasma membrane. Among ions released from guard cells, it is believed that >90% originate from vacuoles.

b) Cation-anion balance

Potassium has also a function in the transport of water and nutrients throughout the plant in the xylem and participate therefore to the cation-anion balance. Although, evidence has been provided that when K availability is low, translocation of nitrates, phosphates, calcium (Ca), magnesium (Mg), and amino acids is depressed (Schwartzkopf, 1972), increasing amount of potassium in all plant tissues and decreasing amounts of sodium, calcium, magnesium, iron and copper in certain tissues were found in potassium fertilization conditions (from complete deficiency to luxury consumption levels) (Ward, 1959; Cui *et al.*, 2019a). In fact, there is a well-known antagonistic effect between potassium and calcium and between potassium and magnesium in the leaf and stem (Ward, 1959).

Previous research has indicated a close relationship between K^+ and NO_3^- uptake by roots (Marschner & Rengel, 2012), while evidence has been provided that the nitrate reduction rate does not decrease in the short and mid-term with low K (Agüera *et al.*, 1990). That is, K^+ represents the major counter cation for nitrate and thus is transported together with NO_3^- in the xylem (Wang *et al.*, 2013; Coskun *et al.*, 2017).

In addition, NH_4^+ has also a marked inhibitory effect on the high-affinity K^+ uptake system (Coskun *et al.*, 2010; Coskun *et al.*, 2013). This inhibition appears to be reciprocal, resulting in an 'antagonism' between the two ions, with both competitive and non-competitive components.

4. Potassium and metabolism

Although K^+ itself is not metabolized by plants, it plays a vital role in many aspects of plant metabolism. Potassium is involved in the activity of some 46 enzymes (Leigh & Wyn Jones, 1984; Britto & Kronzucker, 2008; Armengaud *et al.*, 2009), it acts as a cofactor of pyruvate kinase (PK), starch synthase, Rubisco or nitrate reductase (NR) amongst other enzymes (Sorger *et al.*, 1965; Evans & Sorger, 1966; Nitsos & Evans, 1966; Beevers & Hageman, 1969; Peoples & Koch, 1979)

a) Carbohydrate metabolism

- *Photosynthesis and sugar synthesis*

As mentioned above, potassium is essential for stomatal movement and therefore photosynthetic gas exchange. The effect of K on photosynthesis has been investigated in a wide range of plants including: maize (Du *et al.*, 2019), bean (O'Toole *et al.*, 1980), cotton (Zhao *et al.*, 2001), eucalyptus (Battie-Laclau *et al.*, 2014), sugar beet (Terry & Ulrich, 1973) and *Brassica napus* L. (Lu *et al.*, 2016b). In all cases, K deficiency significantly decreased the rate of photosynthesis. The role of K on photosynthesis has been associated to stomatal and chloroplast functions but also to non-stomatic pathway.

Since leaf chlorosis appeared on K deficient plant, a direct effect of K on chlorophyll content has been suggested (Bolle-Jones & Notton, 1953). In fact, in potatoes, high potash evidently suppressed chloroplast pigment formation (Schertz, 1929). Moreover, evidences showed in maize at seedling stage that Chlorophyll a, b and (a + b) were significantly decreased under different K deficiency treatments (Zhao *et al.*, 2016). However, such effect has not been observed in rice (Watanabe & Yoshida, 1970) and maize (Baszynski *et al.*, 1972).

Several studies have showed that insufficient leaf K^+ content generally leads to decreased stomatal conductance (g_s), decreased mesophyll conductance (g_m) and a decreased content in ribulose-1,5-bisphosphate carboxylase/oxygenase (RuBisCO), thereby inhibiting photosynthesis per unit leaf area (Zhao *et al.*, 2001; Pettigrew, 2008). However, results from Jin *et al.* (2011) in hickory seedlings indicate that the photosynthetic rate is primarily limited by the biochemical processes of photosynthesis such as the maximum carboxylation rate of Rubisco ($V_{c,max}$) and the maximum rate of electron transport (J_{max}), rather than by g_m and g_s in K-deficient plants. The mesophyll conductance limitation contributed to more than one-half of photosynthesis decline (Lu *et al.*, 2016b). Additionally, g_m was closely correlated with g_s and the leaf dry mass per unit area (SLW) in hickory seedlings, which indicates that decreased g_m and g_s may be a consequence of leaf anatomical adaptation.

In fact, potassium level affects photosynthesis through changes in leaf morphology and anatomy, as the SLW as well as the leaf thickness and density, stomatal size and intercellular air spaces in bean (O'Toole *et al.*, 1980) and cotton (Zhao *et al.*, 2001). In fact, under long term K deficiency, the total stomatal pore area decreases, resulting in lower stomatal conductance in eucalyptus (Battie-Laclau *et al.*, 2014), and in higher mesophyll resistance to CO_2 in sugar beet (Terry & Ulrich, 1973). At the opposite, sufficient K availability increases the volume fraction of intercellular air space and gas-phase internal conductance in eucalyptus (Battie-Laclau *et al.*, 2014), enhances the chloroplast surface area exposed to intercellular air space per leaf area and reduces the gas-phase resistance of CO_2 in the cytoplasm in *Brassica napus* L. (Lu *et al.*, 2016b). Therefore, total CO_2 conductance from the sub-stomatal cavity to the site of carboxylation in the chloroplast is enhanced at high K, which also stimulates total Rubisco enzyme activity (Galmés *et al.*, 2011), although, previous studies have showed that K excess does not stimulate CO_2 transport ability (O'Toole *et al.*, 1980; Jin *et al.*, 2011; Lu *et al.*, 2016a) and Rubisco activity (Weng *et al.*, 2007).

Potassium can also modulate photosynthesis by non-stomatic pathways. K plays a role in the conversion of light energy into chemical energy by pumping proton out of the stroma into the cytosol and maintains therefore the balance of electric charges in chloroplasts. In fact, the two-pore potassium (K^+) channel TPK3, a component of the thylakoid membrane, modulates the size and the composition of the light-induced proton motive force (pmf) across the thylakoid membrane of chloroplasts through ion counterbalancing. A study of (Carraretto

et al., 2013), in *Arabidopsis*, has showed that silencing *TPK3* led to reduced growth and altered thylakoid membrane organization, resulting in reduced CO_2 assimilation and deficient non-photochemical dissipation of excess absorbed light. Hence, K improves the transfer of radiation energy into primary chemical energy in the form of ATP (photophosphorylation) (Pfluger & Mengel, 1972; Tester & Blatt, 1989) and NADPH (Wallingford, 1980) which are produced both in photosynthesis and transpiration processes.

Through its action on photosynthesis, K affects sugar synthesis. The most consistent observation is an accumulation of soluble sugars in K-deficient plants both in leaves ((Cakmak *et al.*, 1994) (bean), (Pettigrew, 1999) (cotton), (Ward, 1959) (potato)) and in roots ((Volenec, 1999) (alfalfa), (Farley & Draycott, 1975) (sugar beet)). Nevertheless, in another study opposite effect of K on sugar contents was found in cabbage (Freeman & Mossadeghi, 1970). The observed accumulation of soluble sugars in K-deficient plants can be explained with K-dependence of both starch synthase and pyruvate kinase as they determine the rate of incorporation of C into starch or organic/amino acids respectively (Amtmann *et al.*, 2008). In fact, evidence has been provided that the activity of starch synthase, which is involved in starch synthesis in the chloroplast, depends on K concentration (Läuchli & Pflüger, 1978). Thus, with insufficient K supply, the level of starch declines in general. In potato leaves, Ward (1959) has showed that the amount of starch was a direct function of the amount of potassium applied. However, Pettigrew (1999) has revealed that in cotton, only glucose content was consistently altered by the K deficiency in leaflet while K deficiency increased root tissue concentrations of starch, glucose and fructose. K is also necessary for ribulose bisphosphate carboxylase activity in alfalfa plants (Peoples & Koch, 1979) and sucrose synthesis (SuSy) is highly sensitive to K deficiency in cotton (Hu *et al.*, 2018).

- *Sugar transport*

As the major cation in phloem sap, K^+ availability has dramatic effect on phloem functions such as sugar transport. Sugar produced during photosynthesis are transported through the phloem to others organs to insure their growth or storage. The energy necessary for the transport of sugars is provided by an H^+/pumping ATPase which establishes a proton gradient and a trans-membrane potential regulated by potassium channels of the AKT2/3 type (Lemoine *et al.*, 2013). Evidences showed that loss of the AKT2/3 potassium channel affects sugar loading into the phloem of Arabidopsis (Deeken *et al.*, 2002). As mentioned above, K deficiency in plant

leads therefore to accumulation of sugars in leaves (sucrose as in cotton see (Gerardeaux *et al.*, 2009)). However, according to (Huber, 1984) decreased rates of assimilate export are associated with decreased activities of sucrose phosphate synthase, a key enzyme involved in sucrose formation, and accumulation of hexose sugars may occur because of increased hydrolysis of sucrose in K-deficient leaves.

- *Respiration*

Respiration is also affected by K availability in plants. Low K progressively decreased the photorespiratory evolution of CO_2 into CO_2-free air, but steadily increased the rate of CO_2 flux in darkness (Terry & Ulrich, 1973). Okamoto (1969) suggested that at low K, respiratory CO_2 production may be uncoupled from oxidative phosphorylation in leaves. High respiration rates under K deficiency are believed to be due, in part, to increased activity of the tricarboxylic acid cycle (Okamoto, 1969). Recently, (Cui *et al.*, 2019a) observed that leaf respiration rate correlated to putrescine and citramalate, two metabolites also associated with low K, and anti-correlated to succinate, malate, and fumarate. Potassium is required for maximal activity (in the forward direction) of succinate thiokinase (Bush, 1969; Besford & Maw, 1976), which catalyzes the reversible reaction of succinyl-CoA conversion to succinate (Yamashita & Fujiwara, 1966), but also of pyruvate kinase. In fact, low K^+ impedes pyruvate formation from phospho*enol*pyruvate (Evans, 1963; Nowak & Mildvan, 1972; Besford & Maw, 1976). Therefore, K shortage must in principle lead to a drastic change in mitochondrial metabolism.

b) Nitrogen assimilation and protein synthesis

Potassium is involved directly and indirectly in plant protein metabolism not only for its role in enzyme activation but also for ribosome synthesis and mRNA turnover (Evans & Wildes, 1971; Blevins, 1985; Pettigrew, 2008) and K dependency of nitrate and amino acid transport (Amtmann & Rubio, 2001). Generally, K supply promotes the incorporation of N into proteins leading to higher levels of proteins and lower concentrations of amino acids in K-sufficient plants (in cotton (Hu *et al.*, 2016b), in tobacco (Koch & Mengel, 1974), in rice (Mengel *et al.*, 1976) and in barley (Helal & Mengel, 1979)). However, an increase of both protein and amino acid levels with increased K supply was found for tea leaves (Ruan *et al.*, 1998) and cucumber (Ruiz & Romero, 2002), while in several other studies, no effect of K on protein and/or amino

acid levels was detected (Amtmann & Rubio, 2001). Moreover, K deficiency increases the content in several free amino acids in oil palm (Ollagnier & Ochs, 1973) as well as *Arabidopsis* (Armengaud *et al.*, 2009).

In fact, potassium is further involved in the partitioning of NR activity between the root and the shoot (Blevins *et al.*, 1978b; Armengaud *et al.*, 2009), which also depends on plant species, external nitrate supply, temperature and light intensity (Pate, 1973; Smirnoff & Stewart, 1985; Andrews, 1986). As mentioned earlier, K promotes long-distance transport of NO_3^- from roots to the leaves and thus improves NO_3^- contents and nitrate reductase activity in leaves, facilitating N use efficiency and metabolism in tobacco (Zioni *et al.*, 1971), barley (Blevins *et al.*, 1978b) and soybean (Touraine *et al.*, 1988), while less N assimilation occurs in barley (Blevins *et al.*, 1978b) or corn (Rufty *et al.*, 1981) roots. At the opposite, K deficiency leads to lower translocation of NO_3^- and then a higher N assimilation in corn roots (Rufty *et al.*, 1981). Moreover, K was found to be involved in ammonium assimilation by up-regulating glutamine synthetase (GS), ferredoxin-glutamine-2-oxoglutarate aminotransferase (Fd-GOGAT) and glutamate dehydrogenase (GDH) (Armengaud *et al.*, 2009; Hu *et al.*, 2016b), suggesting a K effect as a compensatory response to maintain C flux through the TCA cycle and into amino acids and proteins. It is also important to note that individual amino acids show different responses to K. For example, in rice seedlings, K deficiency causes an increase in glutamine but a decrease in glutamate and aspartate (Yamashita & Fujiwara, 1967).

c) C/N metabolism

According to Yamada *et al.* (2002), K deficiency decreased carbon flux into the TCA cycle and amino acids and restricted the distribution of carbon from serine into other amino acids in sunflower, while rice and soybean were less affected. In fact, metabolite analysis in *Arabidopsis* roots revealed a decrease in nitrate, glycolytic intermediates (pyruvate), organic acids (malate, 2-oxoglutarate (2-OG), isocitrate), and negatively charged amino acids (glutamate, aspartate) and an increase in the levels of soluble carbohydrates (sucrose, glucose, fructose) and many amino acids, notably those with high N-carbon (C) ratio and/or a positive charge (glutamine, glycine, arginine) in K-deficient plants (Armengaud *et al.*, 2009). **FIGURE I.9** exemplifies the type of information that was obtained in this study by mapping the changes of transcript levels, enzyme activities and metabolites into a given branch of the metabolic network. In this study,

most metabolite changes were at least partially reversed within 24 hours of K re-supply, a notable exception being sucrose, glucose and fructose in the shoots. In roots, pyruvate levels were replenished within minutes, whereas malate and 2-oxoglutarate levels recovered more slowly (Armengaud *et al.*, 2009). According to Amtmann and Rubio (2001), the reversible change in the metabolite profile was accompanied by a reversible change in the activity of enzymes, including those involved in sugar metabolism, glycolysis, TCA cycle and nitrogen assimilation. Amtmann and Rubio (2001) suggested that regulation of the enzymes is post-translational rather than transcriptional and that the changes in enzyme activities were the result of negative feedback control through the reaction products. Moreover, Amtmann and Rubio (2001) suggested that pyruvate kinase can be viewed as a central integrator of C and N metabolism since it is the primary enzymatic target of K deficiency. The genome microarray study by (Armengaud *et al.*, 2004) showed that several enzymes in glycolysis and anaplerosis are regulated during K stress; in particular, the upregulation of two genes for malic enzyme, which catalyses an alternative pathway for pyruvate synthesis, was observed (Armengaud *et al.*, 2009).

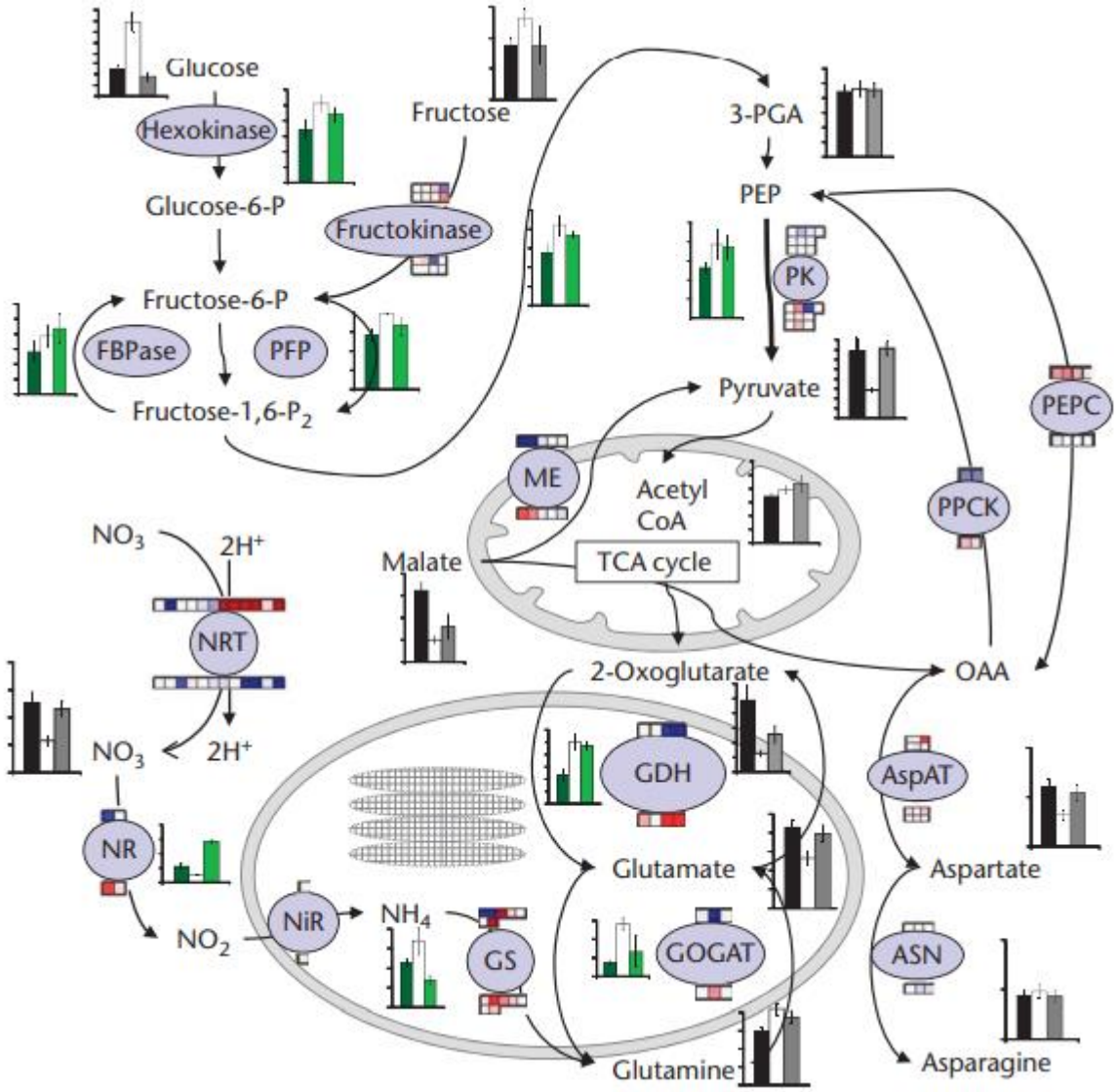

Figure I.9. Example of data obtained in multi-level analysis of the effect of K deficiency and K re-supply on plant primary metabolism. A subset of reactions occurring in root cell cytoplasm, mitochondria and plastids of A. thaliana plants were quantified with respect to changes in metabolite concentrations (grey-scaled bar graphs), transcript levels (blue for increase, red for decrease) and enzyme activities (green bar graphs) of important enzymes (purple). Bar graphs show data for plants grown in control conditions (left), K-deficiency for 14 days (centre) and K re-supply for 24 h (right). Transcript changes in response to K-deficiency and re-supply are shown above and below the enzymes respectively. Individual boxes represent individual genes encoding different enzyme isoforms. For details see (Armengaud *et al.*, 2009). From (Amtmann & Rubio, 2001).

d) K role in plant growth, morphology and yield

Considering the multiple roles of potassium in physiology, it is unsurprising that potassium fertilization has a positive effect on plant growth and increases plant biomass (Ebelhar *et al.*,

1987; Mullins *et al.*, 1994; Pettigrew & Meredith Jr, 1997). In the case of potassium deficiency, plant biomass is reduced and accompanied also by a reduction in leaf area mainly because of a slower rate of leaf appearance and a reduced final size of individual leaves (Kimbrough *et al.*, 1971; Pettigrew & Meredith Jr, 1997; Jordan-Meille & Pellerin, 2004). In fact, for *eucalyptus*, the leaf area reduction can come from a reduction in the number of leaves produced, a reduction in the size of individual leaves or both (Laclau *et al.*, 2009).

Taken as a whole, potassium plays also a crucial role in crop yield (Pettigrew, 2008). In soybean plants, K affects positively the yield by increasing yield component such as the number of pods per plant (Nelson *et al.*, 1946; Jones *et al.*, 1977; Bharati *et al.*, 1986) and the weight of individual seeds (Bharati *et al.*, 1986) or the number of seed per pods (Coale & Grove, 1990). In wheat, K increases yield by increasing in the number of heads per unit area and the number of kernels per head (Haeder & Beringer, 1981), but in other study, this trend was not observed (Sweeney *et al.*, 2000).

Fruit crop quality is also enhanced by K through its influence on size, appearance, color, soluble solids, acidity, vitamin contents, disease resistance, and shelf-life of fruits. K improves quality of the fruits in several species by maintaining desirable sugar-to-acid ratio, ripening of fruit and many other processes (Kumar *et al.*, 2006). In oil crop, effect of potassium on oil composition is still unclear. In some studies, K was found to increase seed linoleic acid content and decrease oleic acid content (Gaydou & Arrivets, 1983), while other studies did not find consistent results from K^+ fertilization on seed oil and protein content (Haq & Mallarino, 2005; Seguin & Zheng, 2006). Similarly, effect of K on isoflavones soybean seeds is controversial (Yin & Vyn, 2004; Seguin & Zheng, 2006).

C. Oil palm mineral nutrition

1. K needs in oil palm

a) Fertilization recommendation

Oil palm is amongst C_3 crops that has a very high fruit production rate. However, as mentioned above, oil palm growth requires high fertilization rates since physiological requirements (to get optimal yield) are high in this species, and furthermore, soils on which oil palm is grown is

generally K-poor. Potassium chloride (KCl) is the most widely used fertilizer in oil palm plantations and also the most expensive. As mentioned above, other forms of potassium fertilizers are also used, such as potash sulphate (K_2SO_4), (potassium and magnesium sulfate, $K_2Mg_2(SO_4)_3$), compound fertilizers (mix of two or three nutrients of N, P, K) or palm leaf and trunk residues.

According to Corley and Tinker (2016), the total K demand is assumed to have two components: “growth” demand and “deficiency” demand. The “growth” demand is determined by the balance between initial content of mineral nutrient, enlargement of plant organs and production of parts that are removed such as leaves, bunches and inflorescences. The growth demand can therefore be calculated as the K demand for the increasing dimensions of the palm trunk, the production of new organs as bunches (or inflorescences) and leaves, less any return of K nutrient. Conversely, when the oil palm is not in a satisfactory nutrient balance, a deficiency situation can take place. In case of K deficiency, a supply is therefore necessary in order to replenish oil palm K mineralomass but also potassium soil content. The “deficiency” demand is thus defined as the amount of K required to fulfill optimum yield and growth.

In mature oil palm, K elemental content differs greatly between organs. Most of the K applied can be stored in the trunk and represents a useful reserve (Goh & Po, 2005). Teoh and Chew (1988a) estimated that trunk reserve can be sufficient to support growth and yield for 2 to 6 years. Under standard cultivation conditions in Sumatra, K content is between 0.6 and 1.2 % of dry matter in leaflet and 1.3-1.5% in rachis. In fruit bunches, potassium is by far the most abundant macroelement. The highest K content can be found in stalks (5-8% of dry matter), which account for up to 26% of total bunch K content. Due to its high biomass, the trunk alone represents 34 to 50% of the total palm K (Teoh & Chew, 1988b; Teoh & Chew, 1988a). According to Goh and Po (2005), most of the increase in K in the plant is accounted for in vegetative parts. The partitioning of absorbed K by the oil palm to its vegetative parts seemed to be related to its nutritional status and K requirement. It is worth noting that within a crown, leaflet K content varies with palm age (Tinker & Smilde, 1963) and leaf rank. Samples taken from leaf 9, 17, 25, and 33 show decreasing in K content in leaflet with increasing palm age (Fairhurst, 1996).

Ng et al. (1999) have proposed that on tropical soils of poor fertility, the total demand in potassium of a mature plantation producing 20 tons fresh fruit bunches (FFB) per year is

about 205 kg K ha^{-1}. The annual nutrient demand of oil palm, depending on tree age, has been characterized further in several studies (TABLE I.3). Table I.3 summarizes data from several sources on the annual nutrient demand of oil palm of various ages based on the need of different plant parts.

Table I.3. Annual K demand of oil palm of various ages (kg ha^{-1}). (Adapted from Tiemann *et al.* (2018)).

Palm age	Plant part	K	Reference
0–3	Whole palm excluding roots	55	Tan (1977) citing Tan (1976)
3–9	Palm including prune fronds and male inflorescences	387	Tan (1977)
3–9	Palm excluding prune fronds & male inflorescences	287	Tan (1977)
9–12	Trunk + root + FFB	167	Tarmizi and Mohd Tayeb (2006)
15–19	FFB + Trunk only	199	Prabowo et al. (2006)
15–19	FFB + Trunk + Frond + male inflorescences	368	Prabowo et al. (2006)

In practice, K is usually applied once to twice a year. Increasing the frequency of fertilizer application up to 6 times a year does not improve the yield but rather the risk of loss by leaching.

b) K nutrition monitoring

In oil palm plantations, potassium deficiency is mainly due to removing bunches (up to 248 kg K ha^{-1} y^{-1} is abstracted from oil palm agrosystems during bunch harvesting (Heffer, 2009)) and losses by leaching (up to 30% of potassium applied (Omoti *et al.*, 1983; Foong, 1991; Chang *et al.*, 1995)). K deficiency is also common on peat soils, sandy soils with low pH derived from sandstone and granite and acid soils with low cation exchange capacity. To characterize or predict the deficiency demand, and to monitor oil palm K requirements, there are different agronomical tools such as fertilization trials, leaf diagnosis, observation of leaf symptoms and soil analysis.

• Fertilization trials are used to determine the response curve of yield with respect to K input, and therefore to provide recommendations for fertilization to achieve optimum production. This will be illustrated further below in Section 2.

• According to Goh and Po (2005), K deficiency symptoms are rare in established plantations. Leaf diagnosis (LD) is therefore widely used to detect sub-optimal nutrition as leaf nutrient status is directly correlated with FFB yield (See Chapter I.2), and nutrient imbalance. Leaf diagnosis is based on the potential relationship between the nutrient content in leaflet tissue and in other organs. Usually, palm rank 17 is used as the standard sample for analysis. Main mineral contents are measured and compared to known critical values. Potassium deficiency may happen when leaflet K elemental content is lower than 0.7% in mature oil palm (Jacquemard, 2012). However, leaf nutrient concentration is also influenced by different factors such as leaf age, leaflet rank, leaf number, tree age, sampling time along the fruiting cycle, planting material (cross), palm density, fertilizer treatment, rainfall and soil properties (Fairhurst, 1996), but also ratio to other nutrient concentrations (See Chapter I.3). Therefore, all these parameters have to be taken into account for potassium fertilization. But quite often, it is assumed that leaflet K content reflects the K status of the tree (Chapman & Gray, 1949). However, in general, leaf K content does not directly reflect K availability depending on soil properties or oil palm varieties (Ollivier *et al.*, 2017; Dubos *et al.*, 2018; Dubos *et al.*, 2019). In fact, on soils of volcanic origin, rachis potassium concentration has been found to be better correlated to soil potassium than was leaf potassium content but not to the yield (Ollivier *et al.*, 2017) and then rachis cannot be used as a better proxy than leaflet for K as recommended by Foster (2002).

• Observation of leaf symptoms are also used to detect deficiency. In case of potassium deficiency, pale green spot becoming gradually colored with yellow or orange appear on leaflets. Symptoms expand across and between veins, until necrotic spots appear, with possible fungus invasion giving thus a ‘bronzed’ appearance to the palm. However, leaf symptoms as an indicator of potassium deficiency are not very reliable, since sometimes potassium deficiency is not accompanied by visible leaf symptoms. In general, symptoms appear on older leaves as K is translocated to young fronds, thereby exaggerating K deficiency in old leaves (Rankine & Fairhurst, 1999).

• In oil palm, soil analysis is used either as a diagnostic tool to group the soil types and to approximate the soil nutrient supply to oil palm, or as a prognostic tool to predict the yield response curve of oil palm to fertilizer rates (Foster, 1985; Foster *et al.*, 1985). Both methods are briefly reviewed in Goh and Po (2005). In both cases, the soil physical, chemical and mineralogical properties are determined. The diagnostic tool is based on a general classification table for soil nutrients. For example, potassium deficiency may occur when the concentration in exchangeable K in soil is less than 0.2 cmol kg^{-1}. Also, soil exchangeable Mg/K has to be above two to avoid magnesium deficiency on acid soils in West Africa (Goh & Po, 2005). In addition, a soil-based system to predict the optimum N and K rates for oil palm in West Malaysia has been described in (Fairhurst & Härdter, 2003). This system was developed by Foster and his associates, using around 50 factorial fertilizer experiments in West Malaysia. The system, which was statistical in nature, attempted to reconstruct the yield response curve to N and K fertilizer inputs based on site characteristics. The system essentially had three steps (Foster, 1985; Foster *et al.*, 1985): (1) predict yield without N and/or K (starting point of the system) (2) predict yield response to N at non-limiting K and vice-versa and (3) predict yield at any combination of N and K fertilizers. However, this system depended on statistical relations, and not on a basic understanding of the underlying mechanisms for plant nutrient uptake, growth and yield (Goh & Po, 2005). In fact, soil fertility is affected not only by soil nutrient content but also texture, structure, consistency, terrain, moisture status and mineralogy. Moreover, soil nutrient variation is extremely high between soil types and within the palm area, and error in sampling a fertilized field is too large, making interpretation difficult and probably unreliable.

• Metabolic signature : as suggested by (Corley *et al.*, 1976), some metabolites could be affected by K content and thus their analysis could be helpful to monitor oil palm K status. For example, putrescine accumulates in several species under potassium deficiency, more or less specifically (Hoffman & Samish, 1970; Cui *et al.*, 2019b). However, this point has never been used in practice in the field so far.

2. Oil palm growth and yield responses to K availability

In oil palm, the positive effects of K fertilization on growth and yield are well-established (Ochs, 1965; Hartley, 1988a; Corley & Tinker, 2016). In immature oil palm (aged 1 to 3 years),

potassium fertilization affects significantly plant morphology, and increases plant height, trunk diameter, leaf number, leaf length, and leaf area of the reference palm rank no. 17 (Purwanto *et al.*, 2018). An increase in leaf area has also been found in mature oil palm under potassium fertilization, partly due to an increase in petiole cross section (Ruer & Varéchon, 1964; Corley, R & Mok, CK, 1972).

The beneficial effects of potassium fertilization on oil palm growth probably come from an increased carbon metabolism. Evidences showed that potassium application significantly increases carbon assimilation via higher chlorophyll and Rubisco contents, and stomatal density and conductance in plant (Pettigrew, 2008; Battie-Laclau *et al.*, 2014). Reciprocally, in oil palm saplings cultivated in the greenhouse, K deficiency leads to a considerable increase in respiratory CO_2 production and a decline in the biosynthesis of proteins involved in photosynthetic machinery (Cui *et al.*, 2019b). In addition, high K availability stimulates nitrogen metabolism while K deficiency (or K excess) leads to oxidative stress (Cui *et al.*, 2019b). However, higher K availability seems to decrease specific leaf weight (g DW m^{-2}), perhaps because it changes non-structural carbohydrate metabolism and thus leaf starch and glucose contents. For example, potassium is essential for phloem sugar movement (Deeken *et al.*, 2002), and thus the remobilization of soluble sugars from vegetative parts like trunk base and leaves (incl. petioles) to sustain fruit development (Lamade *et al.*, 2014). Therefore, high K availability tends to accelerate sugar movement and decrease sugar content in leaflets. However, excess of K may lead to an inhibition of the transport of assimilates from source leaves to sink organs and consequently to an inhibition of the photosynthesis (Senbayram *et al.*, 2016).

The response curve of fresh fruit bunch production to K fertilization is well known (Foster, 2002; Corley & Tinker, 2016). **FIG. I.9** shows the relationship between leaflet potassium content and yield. Fresh fruit bunch production increases with K fertilization level up to an optimum at 2.0 kg K $tree^{-1}$ yr^{-1} (**TABLE I.4**) simultaneously with K leaflets and rachis contents. Above this amount of K, there is no significant increase in fresh fruit bunch production (**TABLE I.4**) (Imogie *et al.*, 2012). Increasing yield using K fertilization involves a change in bunch components. Bunch number, bunch weight and fresh fruit bunch production are indeed significantly higher with increasing K fertilization (Ochs & Ollagnier, 1977; Breure, 1982; Ollagnier & Olivin, 1984a; Ollagnier & Olivin, 1984b). However, in some studies, potassium has been shown to decrease the oil-to-bunch ratio significantly on inland soils while this ratio

increased on coastal soils, but in both cases potassium fertilization led to a significant increase in oil yield (Ochs & Ollagnier, 1977).

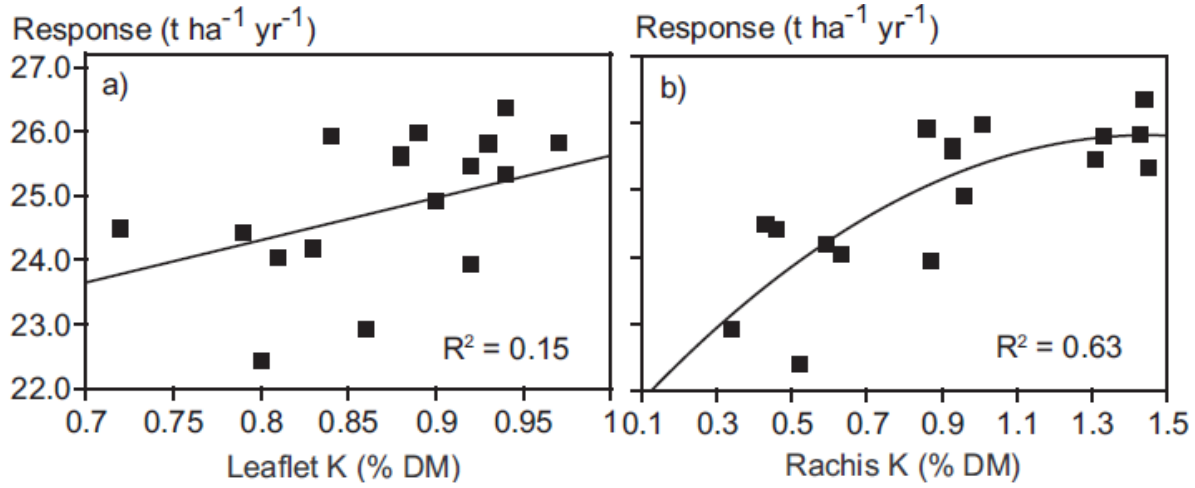

Figure I.9. Comparison of the relationship between oil palm yield and K concentration in leaflets (a) and rachis (b) tissue in a fertilizer experiment on volcanic soil in North Sumatra (Foster & Prabowo, 1996). From Foster (2002).

Table I.4. Effect of K application rate on Fresh Fruit Bunch (FFB) production at Okomu Oil Palm plc, from 1999 to 2008. Oil palm plantation was established in 1993 with NIFOR EWS Seedlings G99 at Okomu. The trial commenced in 1998 when the palms were about 5 years old. K was applied as muriate of potash in addition to 0.5 kg urea, 0.5 kg single super phosphate (SSP) and 0.5 kg dolomite / palm tree yr-1. Means with the same alphabet in the same column are not significantly different from each other at 5% level of probability by the New Duncan's Multiple Range Test (DMRT). Adapted from Imogie *et al.* (2012).

Rate of K application	**Mean bunch Number / palm / year**									
kg/palm/year	**1999**	**2000**	**2001**	**2002**	**2003**	**2004**	**2005**	**2006**	**2007**	**2008**
0.0	8.9c	7.5b	8.01c	9.2c	10.5c	11.0c	11.3d	8.7d	9.5	10.5d
1.0	10.4a	11.9a	12.0b	13.0b	12.0b	14.0b	14.0c	10.5c	12.0	12.5c
1.5	9.5b	11.7a	13.0a	13.5b	13.1a	15.5a	15.0b	12.3b	14.5	15.0b
2.0	11.6a	12.0a	14.0a	15.0a	13.6a	16.5a	17.5a	14.5a	16.0	17.5a
2.5	10.5a	11.7a	13.5a	14.0a	13.4a	16.1a	16.5a	13.1b	15.6	17.0a

While the effect of K on bunch number is well -established, its effect on lipid accumulation in mesocarp (oleosynthesis) is unclear. There are specific dynamics of K content

in fruits that suggest a role in fruit metabolism. In fact, in fruit mesocarp, the K content has been shown to increase progressively for 15 weeks after anthesis (WAA) and then decreases during last developmental stages where lipid biosynthesis occurs (Desassis, 1962). Several studies have shown that higher K availability tends to increase average mesocarp oil content (as well as the proportion of oleate in oil fatty acid composition) (Ochs & Ollagnier, 1977; Ollagnier & Olivin, 1984b) while others found a negative effect (Ochs & Ollagnier, 1977). It has been suggested that this occasional negative effect may come from an increased tissue chloride (Cl^-) concentration (which inevitably comes along with KCl-based fertilization), resulting in lower mesocarp-to-kernel biomass ratio in fruits (Breure, 1982; Ollagnier & Olivin, 1984a; Ollagnier & Olivin, 1984b). *Deli x Yangambi* trees subjected to different forms of chloride fertilization (either as NaCl or KCl) have been shown to form heavier bunches with more and bigger fruits, and higher proportion of kernel biomass, with no change in OER (Ollagnier & Olivin, 1984a), and this effect might also be related to Cl^-. The positive effect of potassium fertilization on lipid synthesis seems to partially come from its effect on moisture content. In other words, if increasing potassium is associated to a lower fruit water content, higher lipid accumulation is observed by mass-balance. Interestingly, fruit transpiration rate (water loss) has been found to be positively related to lipid biosynthesis (Jeje *et al.*, 1978; Teh *et al.*, 2013a).

3. Interaction of K and others nutrients

In oil palm, optimum leaf nutrient ranges varied from 2.24 to 2.97 %, 0.08 to 0.14 % and 0.78 to 0.91 % for N, P and K, respectively, from 0.74 to 1.53 %, 0.25 to 0.98 % and 0.72 to 1.09 % for Ca, Mg and sulfur (S), respectively, and from 5.71 to 31.0 mg kg^{-1}, 7.42 to 12.9 mg kg^{-1}, 33.6 to 58.6 mg kg^{-1}, 82.5 to 681 mg kg^{-1} and 82.8 to 936 mg kg^{-1} for boron (B), copper (Cu), zinc (Zn), manganese (Mn) and iron (Fe), respectively (Behera *et al.*, 2015). As expected, there is an interaction between K fertilization and others nutrients, with an antagonistic response that has been documented recently in oil palm saplings, between K, Na, Ca and Mg (Cui *et al.*, 2019b). The antagonism simply comes from (i) competition for exchange sites in soil and (ii) competition for transporters in roots. In some cases, tissues K concentration may be low due to uptake competition such as between K and Mg, while soil K is sufficient (Pushparajah, 1994). This antagonistic effect is particularly visible for K and Mg fertilization so that an excess of one may interfere with the availability of the other (Senbayram *et al.*, 2016). Studies have shown that optimum K in leaflet depends strongly on soil Mg content (Ochs, 1965; Corley &

Tinker, 2016). Particularly, in sandy soils, application of high rates of K fertilizer often enhances the risk of Mg deficiency, however, at a higher Mg concentration in the soil solution, generally K uptake is not disturbed (Senbayram *et al.*, 2016). This is due to the fact that in the root, the specific K transporters cannot be blocked by others nutrients, whereas Mg transporters are non-specific and can be used by other cations such as K. Therefore, when K concentration in the soil–root interface is high, plant ability to take up sufficient Mg is limited. It is therefore useful to consider (Ca, Na, Mg)/K ratio under K deficiency for a better K fertilization (Fallavier *et al.*, 1989; Corley & Tinker, 2016). However, as mentioned above, in the oil palm such correlations may disappear when the sum K + Ca + Mg is lower than 2.0% (Fairhurst & Härdter, 2003).

At the opposite, there is a synergy between K and N nutrition. For example, leaf analysis may indicate both N and K deficiencies, but a parallel soil analysis may reveal that soil K is adequate and only N needs to be added, allowing significant cost savings (Pushparajah, 1994). According to Teoh and Chew (1985), in mature oil palm, N and K fertilizers are usually applied once or twice a year on coastal marine, nutrient-rich clay soils, and at least twice per year on alluvial, nutrient-poor inland soils. Both nutrients are normally applied together to avoid imbalances and allow optimum yield. In fact, N increased yield by 49% in the presence of high K level rate and there was a 25% positive yield response to K when high N rate was applied (Harun & Noor, 2002). By contrast, in the absence of N, increasing K application rates depressed yield but had no effect on growth (Foster & Mohammed, 1988). Positive effects on oil-to-bunch ratio have been observed too (Foster & Mohammed, 1988).

Moreover, as N has a linear relationship with phosphorus (P) content in leaflet (Tampubolon *et al.*, 1990; Foster, 2002), potassium interacts indirectly with P. In particular, K has an effect on rachis P content and modifies therefore P allocation at the plant level. Also, because of the synergism between N and P uptake, leaf P concentration must be assessed in relation to leaf N concentration during field monitoring (Ollagnier & Ochs, 1981). This is due to the constant N/P ratio in protein compounds found in plant tissue (Fairhurst & Härdter, 2003).

D. Specific objectives of the thesis

The positive effect of K fertilization in oil palm yield has been well known for several decades. However, it is still poorly predictable, mainly because of a lack of understanding of underlying physiological mechanisms. Recent studies taking advantage of mineral nutrition trials in Indonesia, have shown the co-occurrence of K^+ and hexoses (glucose) in heterotrophic tissues (trunk, rachis, rachis bunch (Lamade *et al.*, 2014)). While this suggests that K^+ availability has repercussions on the translocation and the metabolism of sugars, underlying mechanisms are not known, and furthermore, other metabolic pathways could be affected. In addition, recently, a first metabolic model based on photosynthesis and respiration related to sugar allocations (starch and sucrose) in vegetative and reproductive parts, has been elaborated for oil palm (Lamade *et al.*, 2016) on standard conditions of fertilization. It has pointed out the huge cost of fruit filling due to respiration loss. The next step, which is important to consider in oil palm agrosystem husbandry practices, is the investigation of the impact of K on this metabolic aspect.

Then the following research questions are central to the present thesis; they all relate to defining the effect of K availability on metabolic pathways and metabolic changes related to yield:

(A) What is the impact of K fertilization on proteomic and metabolomic responses of leaflets on two genetically contrasted material, presenting different leaflet K mineral signature?

(B) What is the impact of K fertilization on omics responses of the oil palm fruit mesocarp during maturation, on two genetically contrasted material?

(C) Can a $^{13}CO_2$ labelling help identifying sugars produced and C allocation and is all this can be affected by K availability?

In this PhD thesis, we used realistic K conditions in the field in Sumatra, K0 to K3 (that is, no KCl applied for 3 yr before and also during the experiment (K0), 1.5 kg KCl tree^{-1} yr^{-1} (K1), 3 kg KCl tree^{-1} yr^{-1} (K2), and 4.5 kg KCl tree^{-1} yr^{-1} (K3)), far from excess or deficient potassium conditions, with two contrasted oil palm crosses (*Deli x La Mé* and *Deli x Yangambi*).

We took advantage of several methods, combining functional traits (production and fruit analysis), elemental analyses, functional genomics (proteomics and metabolomics) in *(i)* leaflets and *(ii)* fruits during maturation. In addition, a preliminary $^{13}CO_2$ labelling experiment

has been carried out on a palm as a perspective to study carbon flux from source to sink organs and to appreciate the feasibility of isotopic tracing in oil palm in the field.

A mid-term objective of this overall study “K/omics” for oil palm is to identify molecular biomarkers susceptible to precise the K nutritional status of trees studied and then allow the monitoring of K fertilization with higher accuracy than with LD which takes into account only elemental analyses.

In order to answer our first question, which is “What is the impact of K fertilization on proteomic and metabolomic responses of leaflets on two genetically contrasted material, presenting different leaflet K mineral signature?”, the following chapter explores key leaf metabolic pathways under K fertilization treatments, linked to functional traits and yield. This chapter is in the form of a research article that has been submitted to *Environmental and Experimental Botany*.

Chapter II. Metabolic leaf responses to potassium availability in oil palm (Elaeis guineensis Jacq.) trees grown in the field

Cathleen Mirande-Ney[1,5*], Guillaume Tcherkez[2], Thierry Balliau[3], Michel Zivy[3], Françoise Gilard[4], Jing Cui[2], Jaleh Ghashghaie[5], Emmanuelle Lamade[1]

[1]Unité PERSYST, UPR34, Système de pérennes, Centre de Coopération Internationale en Recherche Agronomique pour le Développement, F-34398 Montpellier, France.

[2]Research School of Biology, Australian National University, Canberra 2601, ACT, Australia.

[3] PAPPSO, GQE – Le Moulon, INRA, Univ. Paris-Sud, CNRS, AgroParisTech, Université Paris-Saclay, 91190, Gif-sur-Yvette, France

[4] Plateforme Métabolisme-Métabolome, Institute of Plant Sciences Paris-Saclay, CNRS, INRA, Université Paris-Sud, Université d'Evry, Université Paris-Diderot, Sorbonne Paris-Cité, Université Paris Saclay, Orsay, France

[5]Ecologie Systématique Evolution, Université Paris-Sud, CNRS, AgroParisTech, Université Paris-Saclay, 91400, Orsay, France.

*Contact author to whom correspondence must be addressed: cathleen.mirandeney@gmail.com

Submitted to *Environmental and Experimental Botany*

Abstract

Oil palm growth and production is highly dependent on potassium (K) fertilization. Presently, monitoring K fertilization is difficult since it depends on soil properties, crosses and other nutrients. To adjust K fertilization precisely during cultivation, leaf biomarkers that can indicate changes in tree K status before the appearance of symptoms on fruit production and yield, are required. However, the metabolic response of oil palm leaves to K availability is poorly documented. Here, we investigated the response of oil palm leaf metabolome and proteome to K availability in two crosses (Deli x La Mé, and Deli x Yangambi) grown in the field. Our result show that one to two years only after the onset of K fertilization treatments, there were changes in N metabolism, photosynthesis and mitochondrial metabolism, with a differential effect in the two crosses. In particular, there were changes in sugars, amino and organic acids pointing to modifications in photosynthetic and catabolic (Krebs cycle) capacity and this agreed with the effect seen on enzyme content. Therefore, K availability led to rapid changes in leaf primary metabolism, opening avenues for the utilization of leaf metabolic signature as a marker of K nutrition in oil palm.

Keywords: oil palm, potassium, metabolomics, proteomic, leaflet

A. Introduction

Oil palm (*Elaeis guineensis* Jacq., Arecaceae) is the most widely cultivated oil crop in the world. Because of both its economic efficiency as a high-yielding source of edible and technical oils, the global demand in palm oil for food industry, already very high, will probably increase in the next decade. Presently, palm oil represents the largest oil production globally (about 75 Mt y^{-1}, FAOSTAT). Oil palm plantations are widespread in tropical countries such as Indonesia and Malaysia. In the past decades, intense efforts have been devoted to improve oil palm yield, and this includes not only the generation of better cultivars (crosses) but also the identification of optimal mineral nutrition. Nitrogen (N), phosphorus (P) or potassium (K) fertilization are used, sometimes intensively, to increase fruit development and thus palm oil production. Typical K fertilization consists, on average, of 180 kg K ha^{-1} y^{-1} (≈1.5 kg K $tree^{-1}$ y^{-1}) (Heffer, 2009), which represents an annual cost of about US$ 1b at the global scale.

In fact, potassium supply (generally in the form of potassium chloride, KCl) is by far the most important input in oil palm agrosystems. In general, oil palm biomass contains more K than N, and K elemental content can reach very high values, up to 8% in rachis bunch (about 1% in leaf organic matter) (Lamade *et al.*, 2014; Corley & Tinker, 2016). In addition, fruit bunch harvesting removes substantial amounts of K and this has to be compensated for by K fertilization (Heffer, 2009). The positive effects of K fertilization on tree development are now well established: K fertilization increases total leaf biomass by increasing total leaf area (by increasing rachis length), and depending on the cross, increases bunch weight and/or bunch number (Ochs, 1965; Hartley, 1988a; Corley & Tinker, 2016; Mirande-Ney *et al.*, 2019). However, potassium requirements in oil palm depend on soil quality (such as the Ca or Mg content), other nutrients (N and P fertilization) as well as other environmental conditions (such as water availability) (Corley & Tinker, 2016). Therefore, K fertilization as KCl commonly carried out in the field can be inadequate. This may have side effects, such as Cl^- excess in tissues (causing a decline in fruit quality) (Breure, 1982; Ollagnier & Olivin, 1984a; Ollagnier & Olivin, 1984b), oxidative stress, or potassium and chloride losses by leaching (Omoti *et al.*, 1983; Foong, 1991; Chang *et al.*, 1995).

It is only recently that physiological mechanisms of the response to K availability have been examined in oil palm. In oil palm trees cultivated in North Sumatra (Indonesia) in an agronomic trial with contrasted K fertilization levels, it has been shown that elemental K

content and glucose concentration generally correlate positively, with substantial differences in K content between organs (Lamade *et al.*, 2014). Since fruits are fed with sugars (glucose, sucrose) from other organs to sustain oleosynthesis (Dussert *et al.*, 2013; Lamade *et al.*, 2014; Wong *et al.*, 2017), this correlation may explain why K availability is related to yield. In oil palm saplings cultivated in the greenhouse, leaf metabolism and proteins have been found to respond strongly to K availability, with a considerable increase in respiratory CO_2 and a decline in the biosynthesis of photosynthetic machinery under K deficiency; in addition, changes in K availability were associated with modifications in metabolism, such as polyamine synthesis under K deficiency and oxidative stress under both K deficiency and K excess (Armengaud *et al.*, 2009; Hussain *et al.*, 2011; Ahmad & Maathuis, 2014; Cui *et al.*, 2019b). In species other than oil palm, K availability is well known to play an important role in several biochemical processes such as protein synthesis (translation), carbohydrate metabolism, phloem transport, and enzyme activation (Corley, RHV & Mok, CK, 1972; Mengel, 1980; Marschner, 2002; Pettigrew, 2008; Zörb *et al.*, 2014; Hu *et al.*, 2015; Hu *et al.*, 2016a; Hu *et al.*, 2016b; Zahoor *et al.*, 2017). In particular, K deficiency leads to a strong decrease in key enzymatic activities such as pyruvate kinase, thereby impeding glycolysis (Cui *et al.*, 2019b). Other enzymes are also K-dependent (such as starch synthase, succinate thiokinase, etc.) and this biochemical effect probably contributes to changes in metabolite contents (Cui *et al.*, 2019b). Also, many studies have shown that K deficiency affects nitrogen metabolism, with lower nitrate assimilation, higher putrescine biosynthesis from glutamate, and changes in some amino acids due to the restriction of protein synthesis and pyruvate synthesis (Mengel, 1980; Blevins, 1985; Hu *et al.*, 2016b). At the leaf level, K deficiency lowers stomatal conductance, and thus causes a decline in the photosynthesis rate (Pettigrew, 2008; Favreau *et al.*, 2019). Conversely, K fertilization leads to an increase in stomatal and mesophyll conductances and in the biosynthesis of ribulose 1,5-bisphosphate carboxylase/oxygenase (Rubisco) leading thus to a larger photosynthesis rate (Hu *et al.*, 2015; Hu *et al.*, 2016a). Taken as a whole, K availability may have primarily an impact on oil palm tree photosynthesis (via total leaf surface area, photosynthate export or synthesis of photosynthetic machinery) and leaf primary C and N metabolism and thus on the efficiency of leaves to sustain fruit development.

However, this question has never been examined precisely, in particular in oil palm grown in the field. This lack of knowledge is problematic not only because K availability is an important determinant of palm oil production (see above) but also because most studies looking at the effect of K availability on metabolism take advantage of extreme situations (deficiency,

or excess) that are unlikely to reflect realistic field conditions. In other words, the actual physiological effect of changes in K availability is poorly known, in particular before symptoms become visible. In the case of oil palm, a tree crop, the question as to whether changes in tree K provision (fertilization) might have rapid effects on leaf metabolism is of particular significance since in principle, low K availability could be compensated for by K remobilization from other K-rich organs (such as the trunk) to sustain leaf photosynthesis and fruit development instead of a lower yield or a deficiency. A better knowledge of leaf metabolism under varying K availability would also be of interest to monitor K requirements and thus adjust K fertilization before consequences on fruit production and yield. Presently, K fertilization decisions are based on leaflet K content (about 10 mg g^{-1} dry weight (DW) under K-sufficient conditions) using the so-called LD (leaf diagnosis) method (Chapman & Gray, 1949), but in some agronomic trials, LD has been found not to reflect perfectly K requirements (Foster, 2002).

As an aid in clarifying physiological mechanisms involved in early leaf response to K availability, we conducted here an analysis of leaf metabolism (proteome and metabolome) coupled to tree phenology and elemental analyses, using oil palm trees of two crosses, *Deli x La Mé* (referred to as DL) and *Deli x Yangambi* (referred to as DY), grown in the field in North Sumatra (Indonesia). Here, the objective of the study was not to describe the agronomical effects of K availability but rather, to elucidate biochemical ("omics") leaf responses to K availability in the field and thus compare with greenhouse conditions that have been documented previously (Cui et al., 2019b). We used different K fertilization regimes maintained for two years, with conditions far from deficiency and excess, such that final leaf K varied within a rather narrow range (18-38 mmol m^{-2}), similar to what is usually observed in the field. Our results show that K availability altered N metabolism, photosynthesis and reorchestrated mitochondrial metabolism in leaves, with changes not only in respiratory efflux, but also in mitochondrial metabolites and proteins involved in catabolism.

B. Material and methods

1. Field location, fertilization and leaf traits

The field was located at the SOCFINDO station (North Sumatra, Indonesia; 3°18'19.60"N, 99°3'24.33"E) and sampling was carried out in July 2017 and November 2018. Overall, 40 oil

palm trees were planted in Aug 2013 and organized inside a K factorial agronomic trial. They belonged to two crosses: *Deli x La Mé* (DL) and *Deli x Yangambi* (DY). DL and DY have been chosen here since they are two very common crosses used in oil palm agroforestry. The agronomic trial comprised four levels of potassium fertilization with KCl applied proportionally with growth until 2015 (TABLE II.1). At the beginning of the production stage (starting in 2016) fertilization levels were: no KCl added (K0), 1.5 kg KCl tree^{-1} y^{-1} (K1), 3 kg KCl tree^{-1} y^{-1} (K2), and 4.5 kg KCl tree^{-1} y^{-1} (K3). Therefore, at the first sampling date, in 2017, trees had just experienced 1 year of K treatment plus 3 years of preconditioning, and in 2018, 2+3 years (TABLE II.1).

	Date	Urea (g/tree)	KCl (g/tree)			
		N1	K0	K1	K2	K3
Pre-conditioning	**2013,** *October*	**450**	**25**	**50**	**75**	**100**
	2014, *February*		**300**	**600**	**900**	**1 200**
	2015					
	1st application: April	**750**	**1 000**	**1 000**	**1 000**	**1 000**
	2nd application: September	**1 000**	**1 000**	**1 000**	**1 000**	**1 000**
K treatment	**2016**					
	1st application: May	**1 000**	**0**	**750**	**1 500**	**2 000**
	2nd application: September	**1 000**	**0**	**750**	**1 500**	**2 000**
	2017					
	1st application: March	**1 000**	**0**	**750**	**1 500**	**2 250**
	2nd application: September	**1 000**	**0**	**750**	**1 500**	**2 250**
	2018					
	1st application: April	**1 000**	**0**	**750**	**1 500**	**2 250**
	2nd application: September	**1 000**	**0**	**750**	**1 500**	**2 250**

Table II.1. Fertilization design. Trees were planted in August 2013. From 2013 to 2015, trees were "pre-conditioned", that is, received urea and KCl in accordance with growth demand from 2013 to 2015. Then in 2015, the same amount of fertilizers was applied to all trees (1.75 kg of urea and 2 kg of KCl per tree) so as to sustain growth and avoid extreme differences between K0 and K3 treatments that would not be close enough to realistic field conditions. K fertilization treatments began in May 2016 with 2 kg of urea tree^{-1} and 0, 1.5, 3 or 4.5 kg of KCl tree^{-1} y^{-1}.

Trees were fertilized with nitrogen using 2 kg urea tree^{-1} y^{-1}. There was no K deficiency under K0 conditions, since natural K in the soil under K0 treatment represents about 0.2 meq

exchangeable K per 100 g soil, and some K remained from previous agronomic trials conducted before ours on the same location (information from soil analysis). As such, oil palm tree tissues were not under very low or very high K conditions and K content was always in the 18-38 mmol m^{-2} range (see **FIG. II.1**).

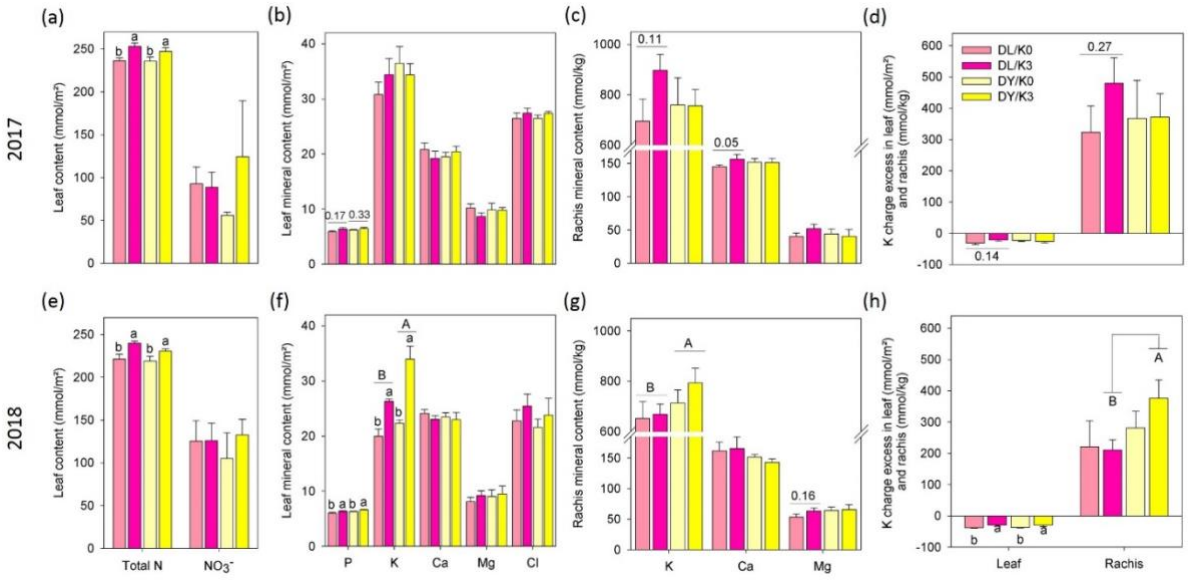

Figure II.1. Leaflet and rachis mineral composition: (a,e) Leaf total nitrogen (N) and nitrate (NO_3-) content, (b, f) leaf phosphorus (P), potassium (K), calcium (Ca), magnesium (Mg) and chlorine (Cl) content, (c, g) rachis K, Ca and Mg content and (d, h) potassium charge excess in 2017 (top) and 2018 (bottom) without (K0, light shade) or with (K3, dark shade) potassium treatments in *Deli x La Mé* (DL, pink) and *Deli x Yangambi* (DY, yellow) crosses. Potassium charge excess corresponds to the charge difference between K and Ca + Mg, i.e. K-2(Ca+Mg). Elemental data are given in millimoles per surface area in leaf and millimoles per kilogram in rachis. Mean ± SE (n = 5). Letters stand for statistical classes (two-way ANOVA, P<0.05).

The number of leaves and bunches (males and females) present on trees at the time of sampling was determined by visual inspection of trees. Specific leaf weight (SLW) was measured in 2017, as dry weight per leaf surface area (g DW m^{-2}) by weighing precisely 30 leaflet samples of 10 cm^2 on a representative palm of the crown. Leaf area was determined in 2017 on the leaf rank number 17 following the method of Tailliez and Ballo, 1992 (Tailliez & Ballo, 1992). Overall foliar emission rate was calculated as the number of leaves present on the tree plus petiolar bases (corresponding to cut leaves) divided by tree age. Leaflets and rachises used for analyses were sampled on leaves number 8 and 9, at leaf B point (**FIG. II.2D**). Leaflet samples

were taken on the blade at a distance of two third of total leaflet length from the base (attachment zone region to the rachis), using leaflets on both sides of the leaf. For memory, the palm crown is composed of 8 spirals which grow indefinitely, with leaves emerging from the apical meristem with a specific phyllotaxic angle (**FIG. II.2C**). Leaves were numbered following tree age, leaf #1 being the youngest (**FIG. II.2B**).

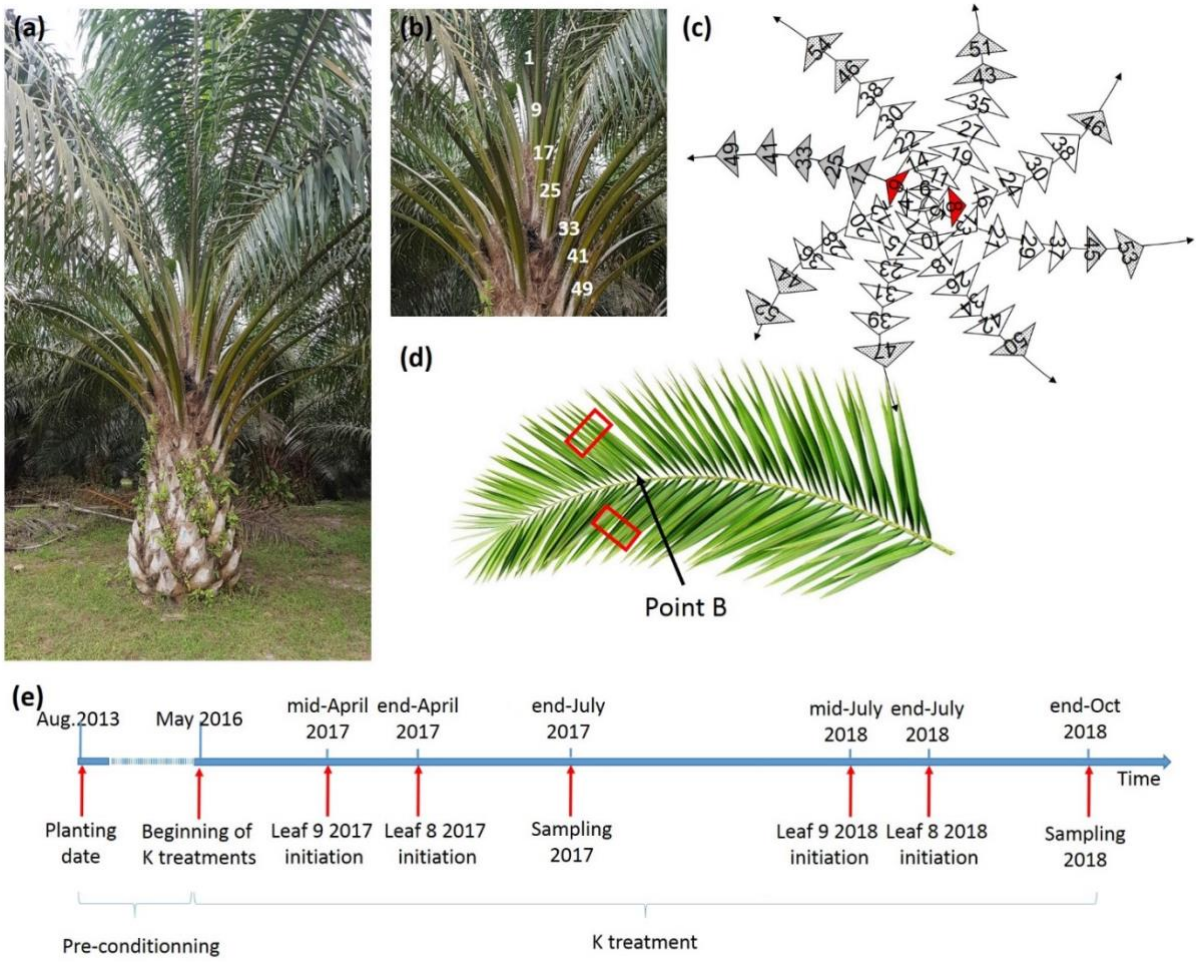

Figure II.2. Leaf sampling design. (a) Photograph of an oil palm tree. (b) Photograph of an oil palm tree crown to show leaf rank number. (c) Diagram of an oil palm crown with leaf rank number as a function of chronological emergence, after Lamade *et al.* (2009). (d) Picture of an oil palm leaf showing the sampling location (red rectangles) at point B of the leaf. (e) Timeline showing the life cycle of leaves sampled in our study (July 2017 and October 2018).

2. Climatic conditions

Climatic conditions (solar radiation, rainfall, temperature and relative humidity) were recorded near the fertilizer trial at Bangun Bandar (Nord Sumatra, Indonesia) using a mini-meteorological station (Watchdog, Spectrum, France). The local weather was characterized by a rainy season in September-December for both years with low solar radiation and temperature and high relative humidity (**FIG. II.3**). Solar radiation varied between 428 MJ/m² and 603 MJ/m², with a maximum in June 2017 and a minimum in December 2017. Temperature varied from 21.6 to 35.6 °C. Rainfall peaked at 682 mm in October 2018.

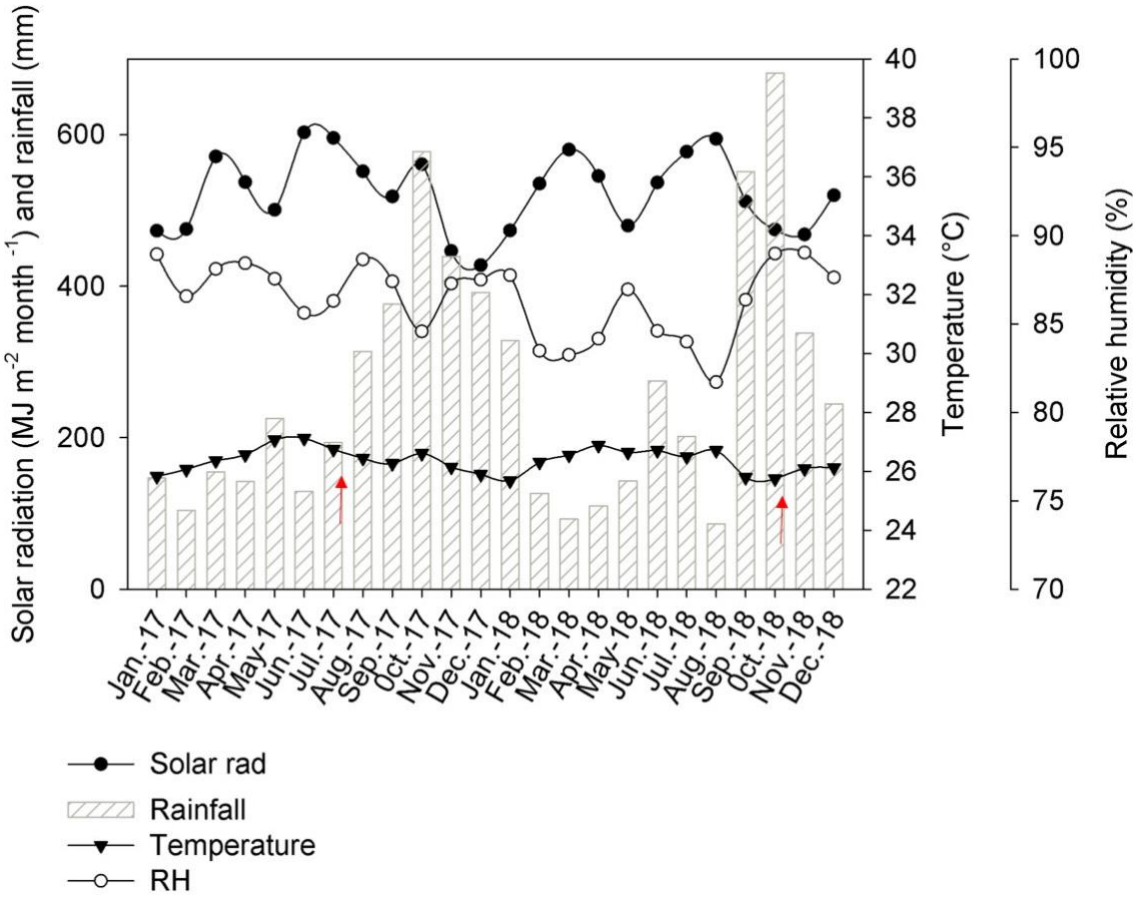

Figure II.3. Climatic conditions in the field. Monthly solar radiation and rainfall precipitation, monthly average temperature and relative humidity in 2017 and 2018 during the agronomical trial BBCP07 at Bangun Bandar (North Sumatra, Indonesia). Red narrow indicates sampling dates.

The two sampling dates (**FIG. II.3**, red arrows) were associated with rather different conditions, since the first sampling in July 2017 was done just after a relatively dry period, while the second sampling in October 2018 was done in the middle of a rainy period. Nevertheless, such differences had no substantial impact on the water status of leaves, due to the very high relative humidity and no sign of water stress was detected in the field in July 2017. Leaf sampling design is shown in **FIG. II.2E**.

3. Elemental analysis

Mineral content analysis was done on leaf and rachis by PSBB (Pusat Seleksi Bangun Bandar) at the SOCFINDO laboratory (Bangun Bandar, Indonesia). Leaflet samples were first cleaned with deionized water, then oven-dried and ground into fine powder. Analyses (N, P, K, Ca, Mg and Cl elemental contents) were carried out either by titration (N), spectrophotometry (P and Mg) or by flame photometry (K, Ca, Cl) following methods from Van Ranst *et al.* (1999). Leaflet nitrate was analyzed using the LAQUA Twin Nitrate Tester® (Spectrum Technologies) using 3-fold diluted leaf extracts (3 mg leaf powder extracted with 4 mL deionized water).

4. Sampling for omics

For proteomics and metabolomics, leaflets were sampled between 8 and 10 am. Samples were rapidly cleaned with deionized water, frozen in liquid nitrogen then freeze dried (lyophilized) for metabolomics, and kept frozen prior to total protein extraction (for proteomics). Proteomics and metabolomics analyses were performed on leaflets only.

5. Metabolomics analysis

After lyophilization, leaflets were ground into fine powder and 10 mg of powder of each sample was extracted with 1 mL cold (–20°C) water-acetonitrile-isopropanol mixture (2:3:3, v:v:v) containing 4 pg mL^{-1} ribitol as an internal standard. Samples were placed for 10 min at 4°C and 1,400 rpm shaking in a thermomixer (Eppendorf). After centrifugation (10 min, 4°C, 13,500 rpm), 10 µL d_{27}-myristic acid (30 pg mL^{-1}; internal standard for retention time calculation) was added to 75 µL of supernatant. The solution was spin-dried under vacuum for 4 h and stored at

−80°C until further analysis. Extracts were derivatized with methoxylamine and N-methyl-N-(trimethylsilyl) trifluoroacetamide (MSTFA) in pyridine and metabolomics analyses were carried out by gas chromatography coupled to mass spectrometry (GC-MS) as in Mirande-Ney *et al.* (2019). Peak integration and identification was done using Metabolome Express as in Cui *et al.* (2019b) and a verification was manually done for each peak using NIST database. Peak areas were normalized to ribitol (internal standard) and sample dry weight, and the sum of metabolites by sample. Similar results were found with both normalization methods. Here we choose to show results normalized with the sum.

6. Proteomics analysis

Proteomic analysis was performed using a method adapted from Cui *et al.* (2019b). Proteins were extracted using TCA-acetone, digested and after desalting on solid phase extraction, peptides were purified using the column Pipette Tip ZipTipSCX according to the protocol of the supplier (Millipore). (http://www.merckmillipore.com, document no. 201306-4805). Column Pipette Tips ZipTipSCX were first equilibrated with 3×10µL washing solution (0.1% TFA, 30% methanol in MilliQ water), then the sample was loaded, washed with 5×10 µL washing solution and eluted with 10 µL 5% ammonium hydroxide, 30% methanol in MilliQ water. Eluted peptides were speed-vac dried and re-suspended in a solution containing 2% acetonitrile, 0.05% TFA and 0.05 % formic acid. Samples were then analyzed by LC-MS/MS (nano-HPLC coupled to mass spectrometry via a nano-electrospray interface). Except for the separation parts of the chromatographic run that is achieved in 110 min against 75 min, acquisition parameters are the same as in Cui *et al.* (2019b). Protein identification, filtering and grouping were carried out using the X!Tandem pipeline, after Langella *et al.* (2017) by querying the MS/MS data against the *Elaeis guineensis* sequenced genome (GCF_000442705.1_EG5, 41887 entries from https://bigd.big.ac.cn/ (Singh *et al.*, 2013)) together with a custom contaminant database (trypsin, keratins, 58 entries). The false discovery rates (FDRs) at the peptide and protein levels were 0.02% and 0.15%, respectively. Relative peptide quantification by peak-area integration on eXtracted ion chromatogram (XICs) was performed using the MassChroQ software (version 2.2.16; pappso.inra.fr/bioinfo/masschroq/) (Valot *et al.*, 2011). Relative protein abundance was calculated and defined as the sum of peptide intensities considering only (1) reproducible peptides, (2) unique peptides, and (3) correlated peptides

belonging to the same protein, which correspond to peptides-mz whose intensity profile do not deviates from the average profile of the peptides-mz from the same protein.

7. Statistical and hierarchical clustering analysis

For all analyses, 3 to 5 replicates were taken for all conditions each year. Univariate and multivariate analyses of omics data were conducted using an ANOVA (MeV version 4.9) and orthogonal projection on latent structures (OPLS, SIMCA version 14.0, Umetrics), respectively. Phenological data and elemental content were analyzed separately in each sampling year using a 2-way ANOVA (with a threshold *P*-value of 0.05) with crosses and K as factors, followed by a post-hoc Tukey test. For each sampling year, we used also a 2-way ANOVA with a threshold *P*-value of 0.05 (metabolomics) or Benjamini-Hochberg-adjusted *P*-value to keep a false discovery rate < 0.05 (proteomics), with cross and K as factors. Omics results were analyzed using a heatmap associated with a hierarchical clustering analysis (Pearson correlation) for significant metabolites. The OPLS analysis used the K level (quantitative) and cross (qualitative) as predicted Y variables and metabolites or proteins as predicting X variables. The goodness of the OPLS model was assessed using the determination coefficient R_2 and the predictive power was quantified by the cross-validated determination coefficient, Q_2. Best discriminating metabolites were identified using volcano plots whereby the logarithm of the *P*-value obtained in univariate analysis (ANOVA) was plotted against the rescaled loading (p_{corr}) obtained in the OPLS. In such a representation, best discriminating metabolites have both maximal –log(*P*) and p_{corr} values. Also, to investigate correlations between leaf proteome and metabolome, a multivariate analysis was performed with proteomics data as X variables and metabolomics data as Y variables (presented in Supplementary Material).

C. Results

1. Functional traits

Elemental contents (nitrogen (N), phosphorus (P), potassium (K), calcium (Ca), magnesium (Mg) and chlorine (Cl)) in leaflet and rachis were analyzed in two different conditions of K availability (K0, K3) and two crosses (DL, DY) for both sampling years (2017, 2018). Using a two-way ANOVA, only the nitrogen content in leaflet was found to be significant for the K

effect (P<0.05) in 2017, with no significant effect of the cross nor the interaction cross × K, regardless of the element. In 2018, N and P contents in leaflet and K content in rachis were significantly different between the two crosses, while leaflet N P, K contents were significant for the K effect (P<0.05) with no significant effect of the interaction. In other words, in 2017, despite the significant effect of K fertilization treatments on total leaflet N, there was no significant effect on leaflet K content while K fertilization had a significant effect in rachis K in DL only (**FIG. II.1**). By contrast, in 2018, there was a significant effect on both leaflet K and N (but no significant effect on leaflet nitrate content), and leaflet K content was higher in DY comparing to DL (**FIG. II.3E-F**). As expected, the increase in leaflet K under K3 conditions was associated with a concurrent increase in average Cl content, but this appeared to be insignificant. It is worth noting that K availability did not affect significantly the Ca or Mg content in leaflets and caused an increase in Ca in rachis in 2017 (**FIG. II.3C**). The balance between cations was examined here by calculating the "potassium charge excess" (PCE), which is the difference between K and the double of Ca + Mg. Interestingly, there was a significant effect of K availability on leaflet PCE in 2018 in both crosses, showing that the increase in K^+ was accompanied by a relative decline in divalent cations (**FIG. II.3D,H**). This was probably compensated for by an increase in Na^+ (not analyzed here). In rachis, as opposed to leaflets, PCE was positive due to the very large K content (about 800 mmol kg^{-1} DW, i.e. 3.2%). Leaflet P content also increased very slightly but significantly with K availability (**FIG. II.3B,F**).

In terms of phenology, there was a strong effect of the cross on female and male inflorescences in 2018 and on leaf area in 2017 (P<0.05). As expected, there was a change in total leaf number between the two years (with more leaves in 2018), and a slight change in the male/female bunch number ratio (**FIG. II.4A**). There were significant differences between crosses, with DY having more apparent leaves with lower leaf surface and less apparent female bunches, reflecting the higher production in DL comparing to DY (about 2 leaves are cut by bunch harvested). K availability did not change significantly the apparent leaf number, bunch number, leaf area nor foliar emission rate (**FIG. II.4**). By contrast, an increase in specific leaf weight was observed in both K2 and K3 conditions, in both crosses (**FIG. II.4C**), consistent with higher N content at higher K availability (**FIG. II.1**).

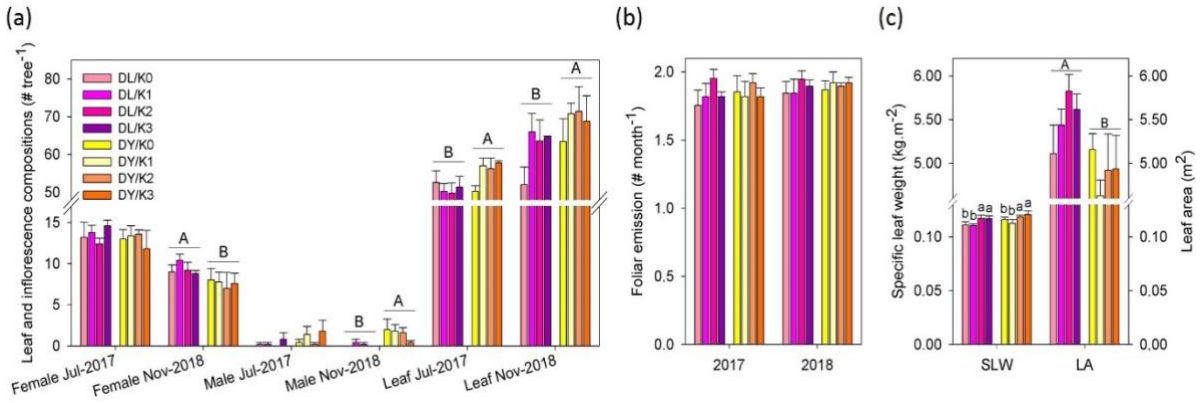

Figure II.4. Oil palm phenology. (a) Total leaf and inflorescence composition of oil palm crown, (b) foliar emission rate, and (c) specific leaf weight and total leaf area of oil palm trees in 2017, under different potassium treatments (K0, K1, K2 and K3) in *Deli x La Mé* (DL) and *Deli x Yangambi* (DY) crosses. Total leaf area was determined on leaf no. 17. Mean ± SE (n = 5). Letters stand for statistical classes (two-way ANOVA, P<0.05).

2. Leaf proteome

Total leaf protein content was quantified prior to proteomics analyses and found to increase with K availability in DL (**FIG. II.5**).

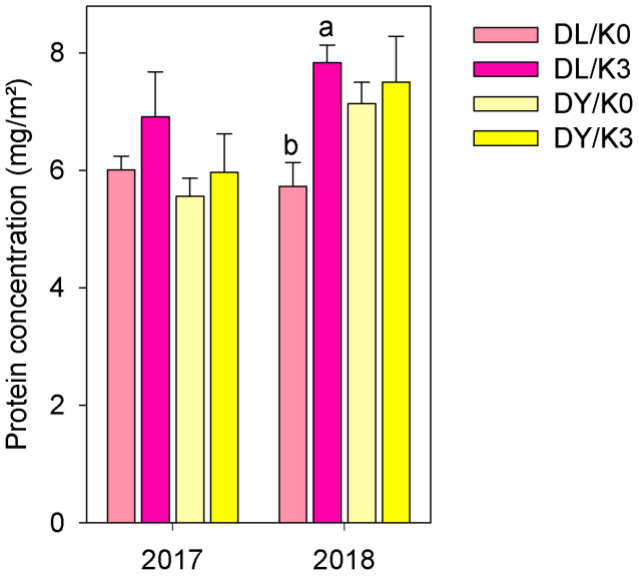

Figure II.5. Differential effect of potassium nutrition on total leaf protein content in *Deli x La Mé* (pink) and *Deli x Yangambi* (yellow) crosses sampled in 2017 (left) and 2018 (right). Protein concentration is given in milligrams per surface area. Mean ± SE (n = 5). Letters stand for statistical classes (two-way ANOVA, P<0.05).

The proteomics analysis allowed us to identify and quantify 1,125 and 1,636 unique proteins in 2017 and 2018, respectively. There was a very clear difference in protein composition between

K conditions and crosses, with an easy discrimination between sample groups in the multivariate analysis (O2PLS) (**FIG. II.6**).

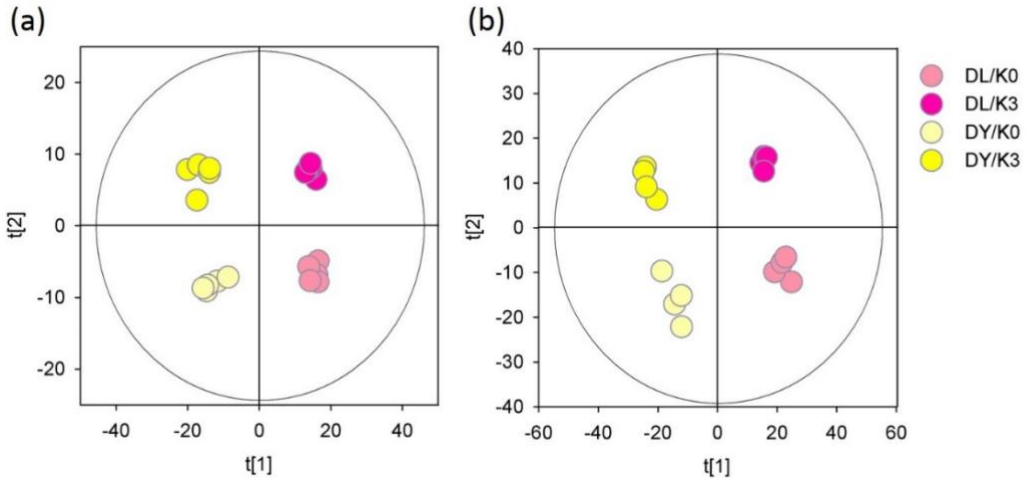

Figure II.6. Output of the multivariate analysis of proteome: score plots of the O2PLS analyses using K and cross as predicted Y variables in 2017 (a) and 2018 (b) analysis. Samples are well-discriminated along the *y* axis (K) and *x* axis (cross).

When tested via a χ^2 test against a random model (average±random error), the OPLS model was insignificant for the K effect and highly significant for the cross effect ($P_{CV\text{-}ANOVA}$ = 0.14 [K effect] and 0.0008 [cross effect]) in 2018. However, it explained most of total variance (R^2 = 0.977) and was very predictive (Q^2 = 0.833). Similarly, the OPLS model was insignificant for the K effect and highly significant for the cross effect ($P_{CV\text{-}ANOVA}$ = 0.99 [K effect] and $2.81 \cdot 10^{-5}$ [cross effect]) in 2017. It explained most of total variance (R^2 = 0.98) and was predictive (Q^2 = 0.591). Using the Benjamini-Hochberg correction in univariate analysis to identify significant proteins, 51 proteins appeared to be significantly affected by K availability, 477 by the cross and 20 by the interaction K × cross in 2018 (**FIG. II.7A-C**; the full list of proteins significant for the cross effect is given in **TABLE S1**). In 2017, no protein was significantly affected neither by K availability nor the interaction K × cross, and 301 were significant for the cross effect (full list given in **TABLE S2**). The 51 proteins that were significant for the K effect in 2018 could be gathered in 4 groups using hierarchical clustering. The two first groups comprised proteins that decreased with K availability, in a slightly more pronounced manner in DL (group 1) or DY (group 2). Group 3 and 4 comprised proteins that

increased with K availability and such a decrease was slightly more pronounced in DL (group 3) or DY (group 4) **FIG. II.7A**). Also, proteins significant for the interaction effect increased with K availability only in DL (group 3) or DY (group 2), while others decreased with K availability in DL only (group 1) (**FIG. II.7C**).

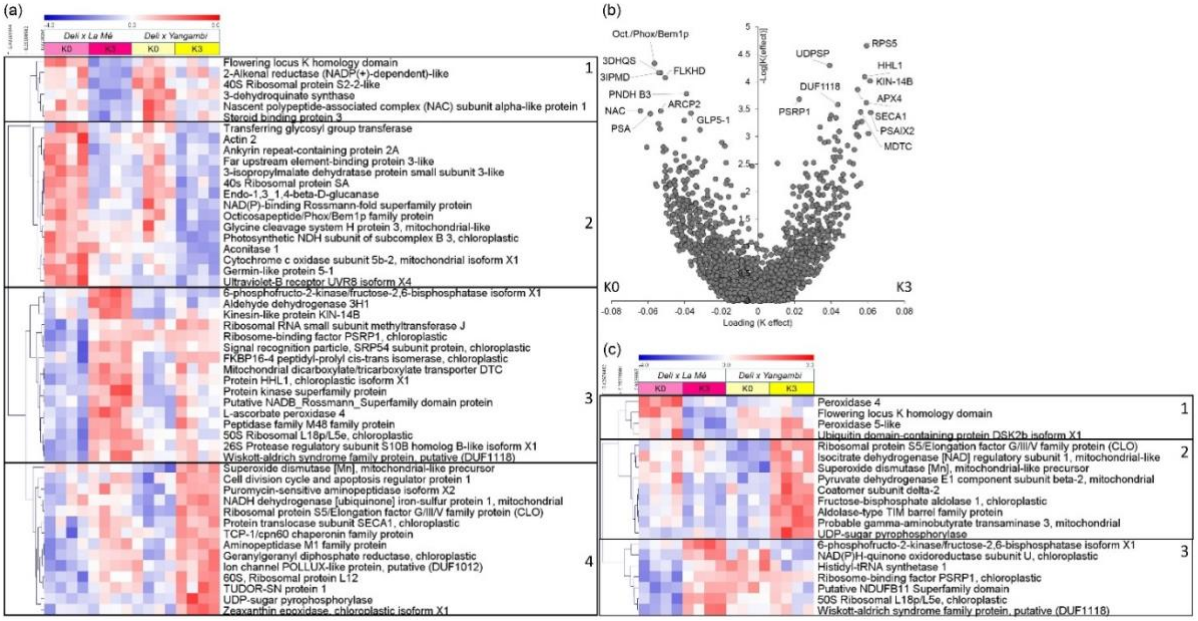

Figure II.7. Proteomics pattern of oil palm leaves under two K fertilization treatments, for *Deli x La Mé* (pink) and *Deli x Yangambi* (yellow), in 2018. (a,c) Heatmaps of proteins that were significant for the K effect (a) and the interaction effect K × cross (c). Scale from blue (lowest) to red (highest) to show the relative content (mean-centered). (b) Volcano plots (−log(*P*) from two-way ANOVA versus O2PLS loading, p_{corr}) associated with the effect of K availability. *Abbreviations*: RPS5, Ribosomal protein S5/Elongation factor G/III/V family protein (CLO); Oct./Phox/Bem1p, Octicosapeptide/Phox/Bem1p family protein; UDPSP, UDP-sugar pyrophosphorylase; 3IPMD, 3-isopropylmalate dehydratase protein ; 3DHQS, 3-dehydroquinate synthase ; HHL1, Protein HHL1, chloroplastic isoform X1; FLKHD, Flowering locus K homology domain; KIN-14B, kinesin-like protein KIN-14B; APX4, Probable L-ascorbate peroxidase 4; PNDH B3, Photosynthetic NDH subunit of subcomplex B 3, chloroplastic; PSRP1, Ribosome-binding factor PSRP1, chloroplastic; SECA1, Protein translocase subunit SECA1, chloroplastic; DUF1118, Wiskott-aldrich syndrome family protein, putative (DUF1118); NAC, Nascent polypeptide-associated complex (NAC) subunit alpha-like protein 1; ARCP2, Ankyrin repeat-containing protein 2; MDTC, Mitochondrial dicarboxylate/tricarboxylate transporter DTC; PSAIX2, Puromycin-sensitive aminopeptidase isoform X2; GLP5-1, Germin-like protein 5-1; PSA, 40s ribosomal protein SA.

Amongst proteins that increased with K availability (in one cross only or both crosses) were proteins related to (**FIG. II.7A-B**): photosynthesis and sucrose synthesis (UDP-sugar

pyrophosphorylase, phosphofructokinase/fructose-2,6-bisphosphatase, HHL1 protein, zeaxanthin epoxidase, NADPH-quinone oxidoreductase, chloroplastic aldolase), mitochondrial metabolism (ubiquinone-NADH dehydrogenase, mitochondrial dicarboxylate/tricarboxylate transporter, γ-aminobutyrate transaminase), redox homeostasis (superoxide dismutase, ascorbate peroxidase), protein turn-over (ribosomal proteins, peptidases, signal recognition particle protein and chloroplastic translocase, chloroplastic ribosome binding factor, histidinyl-tRNA synthetase) as well as other proteins involved in secondary metabolism and housekeeping functions. Interestingly, a K^+ channel of the nuclear envelope was also found to increase with K availability (DUF 1012 domain-containing ion channel POLLUX). Quite similarly, proteins decreasing with K availability were associated with photosynthesis and photorespiration (NDH subunit, protein H of the glycine decarboxylase complex), mitochondrial metabolism (aconitase, cytochrome c oxidase, 3-isopropylmalate dehydratase), redox homeostasis (peroxidase), protein turn-over (ribosomal proteins, nascent polypeptide associated complex subunit, ubiquitin-domain containing protein), and well as other proteins involved in secondary metabolism (e.g., alkenal reductase) and housekeeping functions (e.g. actin). Taken as a whole, rather than a general protein increase or decrease, changes in K availability led to a reconfiguration of photosynthetic, mitochondrial or protein synthesis machinery.

3. Leaf metabolome

Overall, 208 and 181 analytes were quantified and identified in 2017 and 2018, respectively. Multivariate analysis conducted separately on the two sampling years showed that the cross and K availability could well be discriminated along axis 1 and 2 of the OPLS score plot, respectively (**FIG. II.8A-B**).

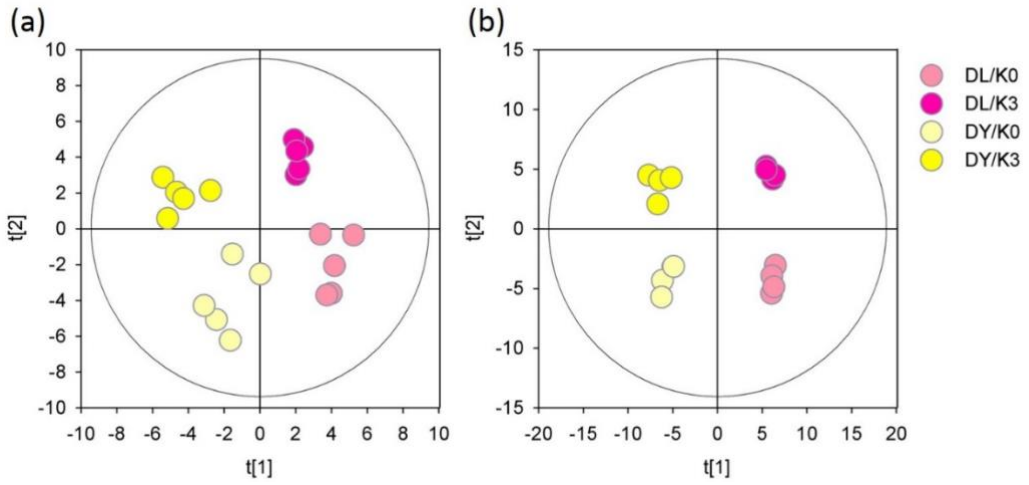

Figure II.8. Output of the multivariate analysis of metabolome: score plots of the O2PLS analyses using K and cross as predicted Y variables in 2017 (a) and 2018 (b) analysis. Samples are discriminated along the *y* axis (K) and *x* axis (cross).

However, the OPLS model was not significant in 2017 ($P_{CV\text{-}ANOVA}$ = 1 [K effect] and 0.96 [cross effect]), and was significant for the cross effect in 2018 ($P_{CV\text{-}ANOVA}$ = 0.67 [K effect] and 0.036 [cross effect]). It explained most of total variance (R_2 = 0.908 and 0.899) and was predictive in 2018 but not in 2017 (Q_2 = 0.583 and < 0, respectively). Unsurprisingly, the two crosses exhibited significant differences in many metabolites (**FIG. S1**). DY had more hexoses (glucose, fructose), Krebs cycle intermediates (citrate, fumarate, isocitrate), amino acids (glycine, isoleucine, serine, threonine) than DL. Conversely, DL had more lipids (such as stearate, digalactosylglycerol, arachidate). Also, crosses differed in their secondary metabolite composition such as phenylpropanoids (blue rectangle, **FIG. S1**): DY had more cis-caffeate, ferulate and vanillin, while DL had more trans-caffeate, catechin and sinapate. In univariate analysis, 12 analytes were significant for the K effect and 10 for the interaction K × cross in 2017 (**FIG. II.9B-C**), and 21 were significant for the K effect and 23 for the interaction K × cross in 2018 (**FIG. II.9E-F**). The importance of metabolites in sample discrimination associated with K availability was easily visible in the volcano plot which combined univariate and multivariate analyses (−log(*P*) obtained in the two-way ANOVA was plotted against the loading (p_{corr}) along axis, Fig. 5a-b). In both sampling years, higher K availability led to an increase in amino acids (methionine, glutamate, serine, aspartate and methyl-aspartate), sugars and their derivatives (sucrose, gluconate, and a disaccharide), polyamines (spermidine and

cadaverine), organic acids (3-methylglutarate, dehydroascorbate, succinate, and citrate), a polyol (galactitol) and an alkaloid (dopamine).

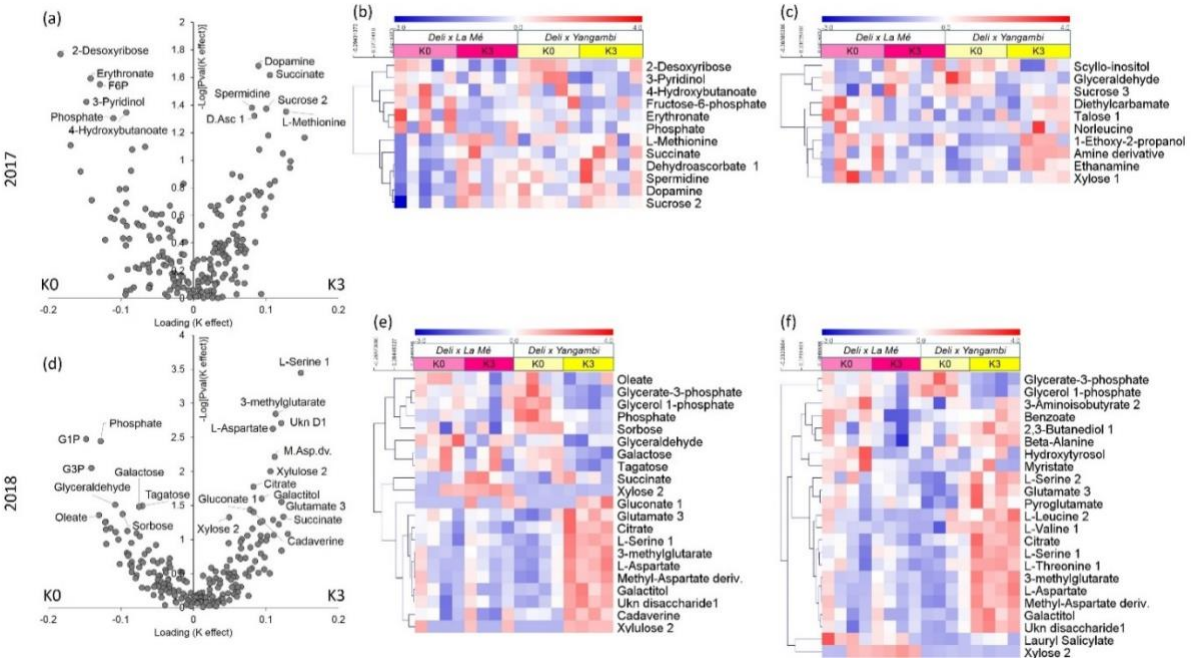

Figure II.9. Metabolomics pattern of oil palm leaves under two K fertilization treatments, in *Deli x La Mé* (pink) and *Deli x Yangambi* (yellow) crosses, in 2017 (top) and 2018 (bottom). (a,d) Volcano plots (−log(*P*) from two-way ANOVA versus O2PLS loading, p_{corr}) associated with the effect of K availability, in 2017 (a) and 2018 (d). Heatmaps of metabolites significant for the K effect ($P<0.05$) (b,e) and the interaction effect K × cross ($P<0.05$) (c,f). Scale from blue (lowest) to red (highest) to show the relative content (mean-centered). Hierarchical clustering (Pearson correlation) is shown on left. Abbreviation 1, 2 or 3 indicate different isomers of the same compound. *Abbreviations*: F6P, fructose-6-phosphate; D.Asc 1, dehydroascorbate 1; Ukn D1, unknown disaccharide from the family of turanose; G1P, glycerol-1-phosphate; G3P, glycerate-3-phosphate; M.Asp.dv., methyl aspartate derivative.

Lower K availability was associated with an increase in some sugars and their derivatives (fructose 6-phosphate, galactose, glyceraldehyde, glycerate 3-phosphate, 2-desoxyribose, tagatose, sorbose), organic acids (erythronate, 4-hydroxybutanoate), lipids (oleate, glycerol-1-phosphate) and phosphate. Higher K availability led to cross-specific changes, here an increase in amino acids (norleucine, leucine, valine, β-alanine, threonine) in DY (**FIG. II.9F**). Taken as a whole, K availability decreased the content in phosphorylated metabolites, reconfigured sugar metabolism and increased the content in nitrogenous metabolites (amino acids and polyamines). It is worth noting that metabolomics indicate that K

fertilization increased the content in some disaccharides such as sucrose (**FIG. II.9**). This tendency was further confirmed using absolute quantitation by ^{1}H-NMR, which also suggested an effect of K on sucrose (**FIG. II.10**).

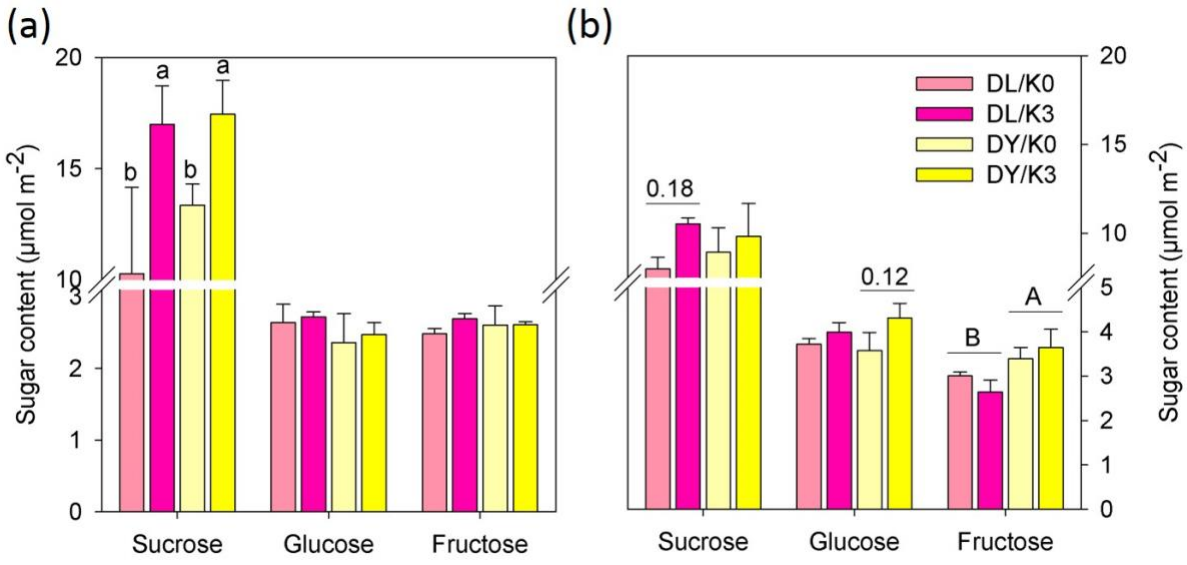

Figure II.10. Differential effect of potassium nutrition on leaf sugar content in *Deli x La Mé* (pink) and *Deli x Yangambi* (yellow) crosses sampled in 2017 (a) and 2018 (b). Sucrose, glucose and fructose leaf content were determined by ^{1}H-NMR and are given in micromoles per square meter of leaf. Mean ± SE (n = 5). Letters stand for statistical classes (two-way ANOVA, P<0.05).

4. Correlation between proteome and metabolome

A bidimensional statistical multivariate analysis (O2PLS) was conducted to investigate the potential linkage between proteome and metabolome. In such an analysis, it is not necessary to give classes (K0/K3, DY/DL) as an input to discriminate samples, since samples should be discriminated from their metabolomics pattern (Y variable). Interestingly, samples appeared to be naturally discriminated following crosses (axis 1) and K availability (axis 2), demonstrating that the proteome-metabolome association was K- and cross-specific (**FIG. II.11A**). However, the O2PLS model was not significant, the minimal individual $P_{CV\text{-}ANOVA}$ value being obtained for caffeate (P = 0.102). Caffeate correlated to various proteins involved in metabolism (adenosine kinase, cinnamoyl CoA reductase, cytosolic phosphoglycerate kinase, phosphopyruvate hydratase, linoleate lipoxygenase, tryptophan synthase, V type proton

ATPase) and anti-correlated to some proteins involved in photorespiration and photosynthesis (glutamate glyoxylate aminotransferase, rubisco activase, sucrose phosphatase) (*P*-value of correlations < 0.01). The loading bi-plot of the O2PLS analysis further showed that metabolite and protein families were not randomly distributed (**FIG. II.11B**).

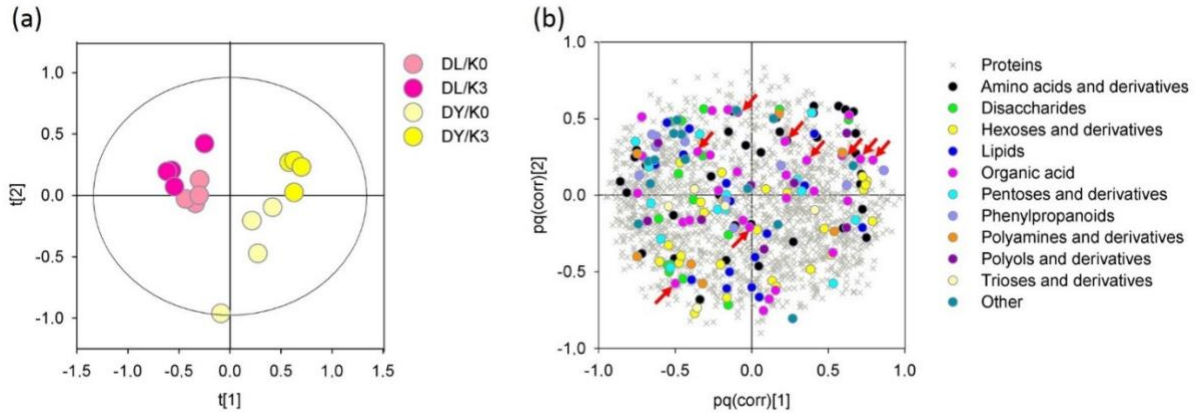

Figure II.11. Bidimensional multivariate analysis of metabolome and proteome: (a) Score plots of the O2PLS analysis using proteomic and metabolomic data as predicting (X) and predicted (Y) variables, respectively. Samples are mostly discriminated along the *y* axis (K) and *x* axis (cross). (b) Loading plot showing the first two components (loading pq(corr)[1] plotted against pq(corr)[2]). Metabolistes are colored by classes to facilitate reading and red arrows indicate metabolites from the tricarboxylic acid cycle pathway (Krebs cycle).

In fact, disaccharides (green dots) and some proteins of photosynthesis (sucrose-phosphatase, glycerate dehydrogenase, carbohydrate kinase domain-containing protein, Rubisco activase, transketolase) co-localized (i.e. correlated) on the DL side (left). Moreover, most intermediates of the Krebs cycle (red arrows) co-localized with proteins involved in catabolism (phospho*enol*pyruvate carboxylase, phosphopyruvate hydratase, etc.) on the DY side (right), and appeared to be anti-correlated to mitochondrial malate dehydrogenase (Table S4). Most hexoses and their derivatives (yellow dots) appeared to correlate with several chloroplastic proteins involved in photosynthesis (NADH dehydrogenase subunit, PSII subunit PsbP, PSI chlorophyll a/b-binding protein) in the lower part of the plot, i.e., under low K availability. Taken as a whole, the O2PLS analysis suggests that there were differences in both photosynthetic capacity and mitochondrial metabolism between crosses. In particular, it suggests that the abundance of organic acids of the Krebs cycle was dictated by the balance

between phospho*enol*pyruvate carboxylase and malate dehydrogenase. Also, K availability impacted on photosynthesis, with changes in both the protein composition of the photosynthetic machinery and an increase in free hexoses.

D. Discussion

1. Time lag between K treatment and visible effects

The present study shows that unsurprisingly, the effect of K fertilization on leaf K content (and proteome) was minimal after one year (in 2017) plus three years preconditioning (**FIGS. III.1 AND III.9**). That is, it took two years to see a significant effect of K fertilization on leaf K content (**FIG. II.1F**). This is consistent with past agronomic trials that show potassium fertilization affects leaf K pools about four years after the treatment onset (Corley *et al.*, 1976). Also, it is worth noting that in 2017, based on the weighted tree-average elemental K content (1.1%), considering that tree total standing biomass is about 295 kg DW, tree K mineralomass was about 2.6 kg K tree^{-1}. Since, on average, 1.8 leaves (**FIG. II.4**) are produced each month and 23 bunches each year (Mirande-Ney *et al.*, 2019), this represents about 107 kg y^{-1} DW produced, and a K demand of about 1.1 kg K tree^{-1} y^{-1}. If we also account for K represented by leaves cut when bunches are harvested, the overall K requirement was about 43% of total K mineralomass of trees (note this value is slightly underestimated due to the K demand by trunk growth). Without any supply of potassium (no fertilization), standing K mineralomass may be sufficient to feed growth explaining the lack of effects in 2017. In addition, during preconditioning, all trees received 2 kg KCl tree^{-1}, which compensate for the K0 treatment in 2016 onwards. The lack of significant effect of K fertilization on leaf K content in 2017 could have also come from changes in allocation, with more inflorescences and less leaves compared to 2018 (**FIGS. III.1 AND III.4**). That is, some K could have been remobilized from leaves or trunk to fruits to cover the K demand of bunch maturation, thereby dampening changes in leaf K despite the K fertilization treatment. Parenthetically, with 4.5 kg KCl tree^{-1} y^{-1} (i.e. 2.3 kg K tree^{-1} y^{-1}), fertilization in the K3 conditions represented therefore an excess, i.e. twice as much the K demand.

However, despite the lack of effect of fertilization on leaf K content and proteome in 2017, several metabolites appeared to be significant (**FIG. II.9**), suggesting that there were

some changes in, e.g., K^+ distribution amongst leaf tissues or cellular compartments. In fact, we found that there was more succinate, spermidine and methionine at high K (K3 conditions), suggesting a higher activity associated with two well-known K^+-dependent enzymes, succinyl-CoA thiokinase (Krebs cycle enzyme which forms succinate) and S-adenosylmethionine synthase (required for spermidine synthesis and the methionine salvage pathway). That is, it is probable that even in 2017, K0/K3 conditions were associated with subtle changes in cytosolic and mitochondrial K^+ concentration.

2. K availability interacts with N and P

Both elemental and omics analyses suggested that K availability impacted on nitrogen metabolism. Our results show that potassium fertilization increased N content in leaflets of both crosses (**FIG. II.1**). This agrees with previous agronomical observations that increasing K stimulates N use efficiency and eventually, increases %N in leaflets (Ollagnier & Ochs, 1973). However, despite a tendency to increase leaf nitrate (NO_3^-) in DY (**FIG. II.1A,E**), no significant effect of K was found on nitrate overall, in contrast to what has been observed elsewhere in other species (Blevins, 1985; Hu *et al.*, 2016b). In fact, it is believed that K plays a key role in nitrate absorption and circulation, as a counter-cation (Blevins *et al.*, 1978a; Hu *et al.*, 2016b; Coskun *et al.*, 2017; Wang & Wu, 2017). An effect of K availability on both leaf nitrate content and natural ^{15}N abundance ($\delta^{15}N$) has also been found in sunflower, showing a change in nitrate influx-to-reduction ratio in leaves (Cui *et al.*, 2019a). Nitrate reductase isoforms were not detected in our proteomics analyses. However, leaf glutamate synthase (Fd-GOGAT) content increased with K availability (P=0.008) (not shown) and we also found an increase in glutamate (**FIG. II.9**), suggesting a stimulation of N assimilation by K availability (**FIG. II.12**). That said, it is worth noting that, in accordance with usual agronomical practices, N fertilization was here done with urea, using 1 kg $tree^{-1}$ y^{-1}. The mineralization rate in tropical soils like those found in oil palm fields in Indonesia is in principle sufficient to mineralize such an amount of urea to nitrate within 1 year (Allen *et al.*, 2015) but it is likely that at least for a brief period after urea fertilization, available soil nitrogen was made of a mixture of urea and nitrate. It has been found in maize that while urea can be assimilated directly via urease, urea potentializes N assimilation, in particular the expression of genes encoding GOGAT and glutamine synthetase (Zanin *et al.*, 2015). This effect probably explains why the effect of K on leaf nitrogen was more pronounced on glutamate metabolism (and thus on many amino acid contents) than on nitrate content.

Several amino acids increased with K availability, such as methionine, serine, leucine or valine as a likely consequence of both augmented synthesis and proteolysis (protein-turn-over). In fact, amongst significant proteins were isopropyl malate dehydratase (involved in leucine biosynthesis), and peptidases (**FIGS. III.7, III.9 AND III.12**). However, the effect of K availability appeared to depend on the cross. DY was generally enriched in amino acids compared to DL (**FIG. S1**). K availability had also an effect on protein synthesis machinery, in particular ribosomal proteins (**FIG. II.7**). K^+ is also required for translational activity (Blevins, 1985) and it is thus likely that protein synthesis was higher at high K availability. In fact, total leaf protein content was larger under K3 conditions (**FIG. II.5**). Previous study showed that in cotton, tea and oil palm, K fertilization improved leaf protein content and changed free amino acids concentration, depending on the species and variety (Ollagnier & Ochs, 1973; Ruan *et al.*, 1998; Hu *et al.*, 2016b)

In addition to its effect on nitrogen, K fertilization impacted on phosphorus content and metabolism (**FIGS. II.1 AND II.9**). This may have in turn had an effect on protein synthesis and leaf N content (Marschner, 2002). The concurrent effect of K on N and P metabolism comes as no surprise since in oil palm, P and N contents have been found to be linearly correlated in leaflets (Tampubolon *et al.*, 1990). Transcriptomics analysis of *Eucalyptus* leaves have shown that K supply influenced the expression of genes involved in phosphate homeostasis and the response to phosphate starvation (Favreau *et al.*, 2019). Here, we show that leaf free phosphate (Pi), fructose 6-phosphate, glycerol 1-phosphate and 3-phosphoglycerate decreased at high K (**FIG. II.9)**, in contrast to elemental P content, which was found to increase slightly in leaflets (**FIG. II.1**) and in rachis elsewhere (Cui *et al.*, 2019b). The decrease in Pi was further confirmed by ^{31}P-NMR (data not shown). Therefore, it is likely that higher K availability was associated with an increase in P-containing compounds that could not be analysed here, such as phospholipids, nucleotides or non-soluble phosphates (such Ca/Mg phytate and phosphate). More generally, K fertilization affected the cation balance, with, in 2017, a lower content in Ca and Mg in leaflets (but higher content in rachis). We also found an increase in the content of the ion channel POLLUX, which is a Ca-gated, potassium channel of the nuclear envelope. Evidence has been provided that POLLUX modulates nuclear envelope membrane potential and therefore opening of nuclear calcium channels or conversely, and compensate for calcium efflux by playing a role of a nuclear K^+ inward rectifier (Charpentier *et al.*, 2008; Chen *et al.*, 2009; Checchetto *et al.*, 2016). Thus, our data suggests that K availability directly impacted

cellular K^+ and Ca^{2+} pools. Of course, our present analysis does not cover all aspects related to channels since the protocol used for protein extraction was generic. A targeted analysis on membrane-associated proteins would provide more insight on cellular ion balance.

3. Potassium modulates photosynthesis and respiration and perhaps carbon use efficiency

It is well-known that potassium has beneficial effects on photosynthesis via stomatal regulation, photosynthetic capacity and photosynthate export (see *Introduction*). Here, we found that K availability had a significant effect on several proteins involved in photosynthesis and photorespiration, including sucrose metabolism (UDP-sugar pyrophosphorylase) (**FIG. II.7**). At the transcript level, it has also been shown in *Eucalyptus* that K availability impacted on the expression of genes involved in photosynthesis (Favreau *et al.*, 2019). The net effect of such changes is likely to be an increase in photosynthetic CO_2 assimilation rate, as shown in oil palm saplings grown under different K conditions (Cui *et al.*, 2019b) and here, using gas exchange in a separate agronomic trial (**FIG. II.13**). This effect is also associated with a higher content in sugars, here disaccharides such as sucrose (**FIGS. II.9 AND II.10**). It is interesting to note that leaf sucrose accumulation can also been found in K deficient plants not due to an increase in photosynthetic rate but rather, because of inhibited phloem loading (Cakmak *et al.*, 1994; Zhao *et al.*, 2001; Gerardeaux *et al.*, 2010).

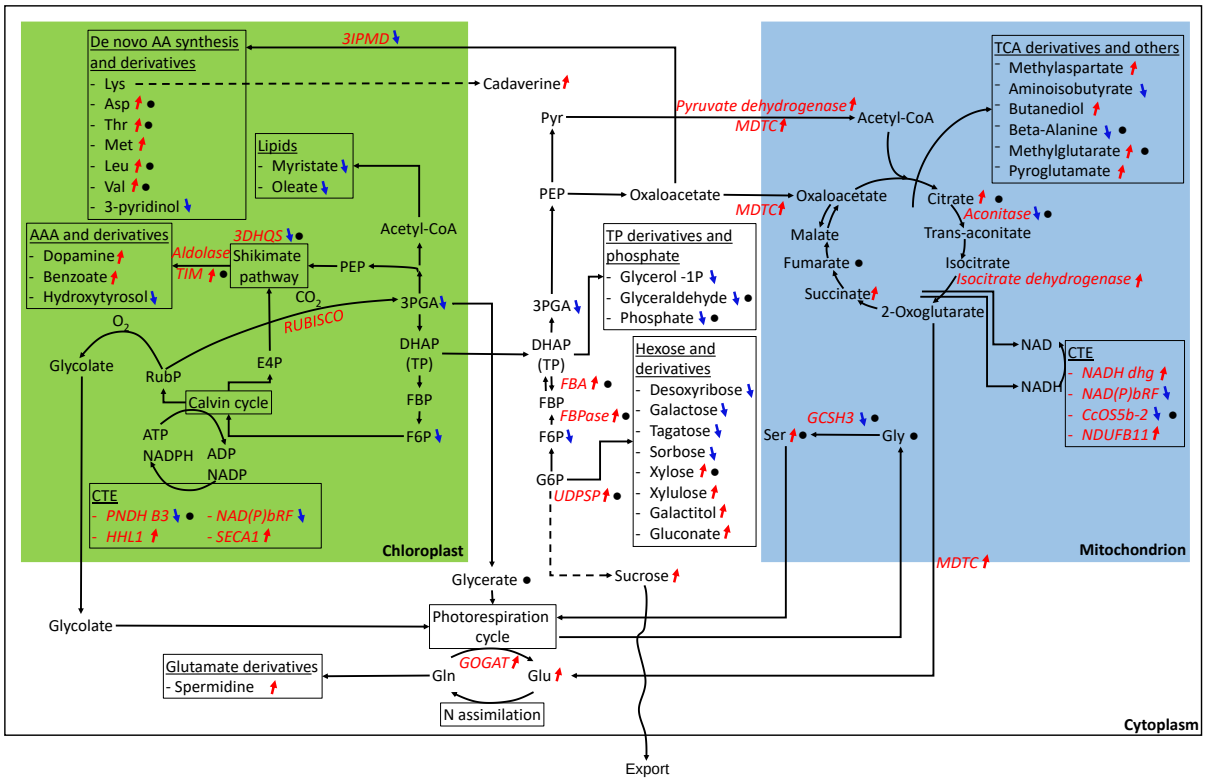

Figure II.12. Tentative summary of the effect of K on leaf metabolism. Blue arrows (↘) indicate metabolites/enzymes that decrease with K fertilization while red arrows (↗) indicate an increase. Black dots (●) indicates metabolites/enzymes that differ significantly between crosses. Enzymes are written in red italics. Abbreviation: 3DHQS, 3-dehydroquinate synthase; 3IPMD, 3-isopropylmalate dehydratase protein; 3PGA, 3-phosphoglycerate; AA, amino acid; AAA, aromatic amino acid; ADP, adenosine diphosphate; Asp, aspartate; ATP, adenosine triphosphate; Aldolase TIM, aldolase-type tim barrel family protein; CcOS5b-2, cytochrome c oxidase subunit 5b-2; CoA, coenzyme A; CTE, chain transport electron; DHAP, dihydroxyacetone phosphate; E4P, erythrose-4-phosphate; F6P, fructose-6-phosphate; FBA, fructose-bisphosphate aldolase 1; FBP, fructose biphosphate; G6P, glucose-6-phosphate; GCSH3, glycine cleavage system H protein 3; Gln, glutamine; Glu, glutamate; glycerol-1P, glycerol-1-phosphate; Gly, glycine; GOGAT, ferredoxin-dependent glutamate synthase; HHL1, Protein HHL1, chloroplastic isoform X1; MDTC, mitochondrial dicarboxylate/tricarboxylate transporter DTC; Met, methionine; N, nitrogen; NADH dhg, NADH dehydrogenase; NADH/NAD, nicotinamide adenine dinucleotide; NADPH/NADP, nicotinamide adenine dinucleotide phosphate; NAD(P)bRF, NAD(P)-binding Rossmann-fold superfamily protein; NDUFB11; Putative NDUFB11 Superfamily domain; Leu, leucine; Lys, lysine; PEP, phospho*enol*pyruvate; PNDH B3, Photosynthetic NDH subunit of subcomplex B 3; Pyr, pyruvate; RubP, ribulose 1,5-bisphosphate; SECA1, Protein translocase subunit SECA1; Ser, serine; TCA; tricarboxylic acid cyle; TP, triose-phosphate; Thr, threonine; UDPSP, UDP-sugar pyrophosphorylase; Val, valine.

In effect, bi-dimensional multivariate analysis (O2PLS) of leaf proteome and metabolome suggested that here, disaccharides correlated to proteins involved in photosynthesis such as sucrose phosphatase or Rubisco activase (**FIG. II.11 AND TABLE S3**), suggesting that sugar

concentration reflected photosynthetic activity. However, the effect on photosynthesis and sugar concentration appeared to be cross-dependent, with a differential effect on 3-phosphoglycerate, disaccharides, photorespiratory intermediate (serine) and stomatal conductance (**FIGS. II.9F AND II.13**). That is, the increase in photosynthetic capacity under K3 conditions was not accompanied by an increase in stomatal conductance and thus led to a decline in the intercellular-to-atmospheric CO_2 mole fraction ratio (c_i/c_a) and more photorespiration in DL. By contrast, stomatal conductance increased in DY, leading to a small increase in c_i/c_a. Such an effect on conductance was probably caused by a lower leaf K content in DL than in DY (**FIG. II.1**).

Potassium fertilization had an effect on mitochondrial metabolism, with changes in Krebs cycle enzyme contents (decrease in aconitase, increase in NAD-dependent isocitrate dehydrogenase, IDH) and associated changes in Krebs cycle intermediates: an increase in citrate (due to lower aconitase activity) and succinate (due to both larger IDH and succinate thiokinase activity). We nevertheless recognize that the increase in succinate content could have also been due to the increase in γ-aminobutyrate (GABA) transaminase, which can generate succinate semialdehyde in the GABA shunt. There was also an increase in other mitochondrial proteins (cytochrome c oxidase subunit 5b-2, NADH dehydrogenase, di/tricarboxylate transporter, etc.). Altogether, these changes point to an increase flux in organic acid metabolism and thus an increase in respiratory activity. In fact, we found nearly a 2-fold increase in dark respiration (CO_2 evolution) using gas-exchange measurements (**FIG. II.13**). The rationale of such an important stimulation of mitochondrial metabolism at higher K availability is presently unclear. In fact, it might have been driven by ion balance (generation of organic acids carrying a negative charge to compensate for changes in relative K^+ excess, Fig. 1), the demand in carbon skeletons for nitrogen assimilation (discussed above), or the increase in growth rate and sucrose export. In that regard, it is very different from the stimulation of respiration observed under K deficiency, which is linked to a loss in ATP generation efficiency and the onset of CO_2-producing alternative pathways (Cui *et al.*, 2019b).

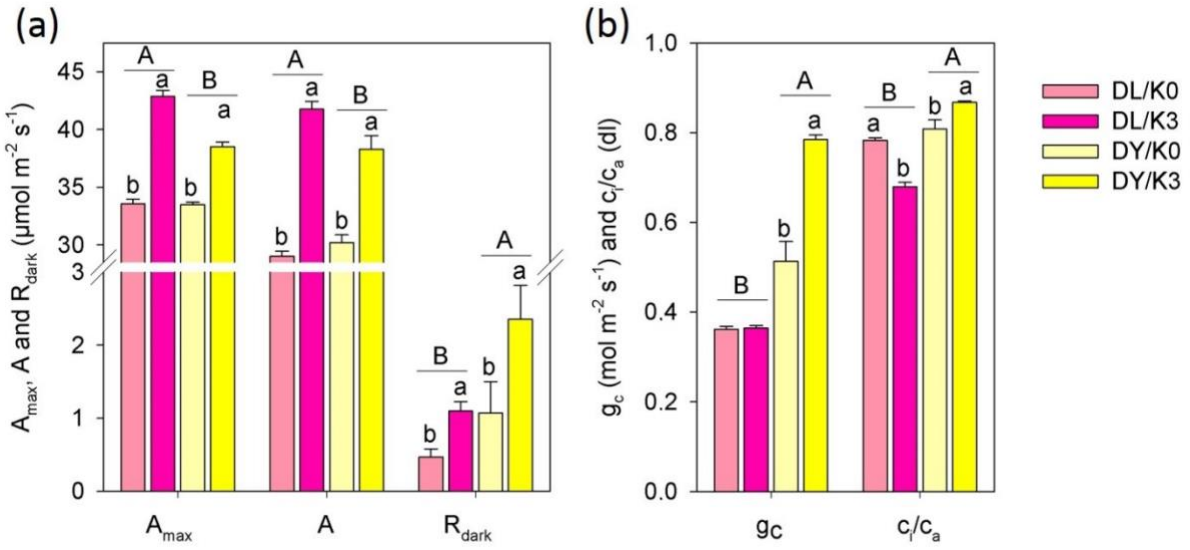

Figure II.13. Differential effect of K fertilization on leaf gas-exchange parameters for *Deli x Lamé* (pink) and *Deli x Yangambi* (yellow) under K0 and K3 treatments from a similar fertilization trial in a SOCFINDO plantation at Aek Loba, North Sumatra (Indonesia). (a) Carbon assimilation under saturated light (A_{max}), carbon assimilation at standard light (A) and dark respiration (R_{dark}), measured with the WALZ GFS 3000 (Germany), in µmol CO_2 per square meter per second. (b) Stomatal conductance and intercellular-to-external CO_2 mole fraction ratio (c_i/c_a). Mean ± SE (n = 5). Letters stand for statistical classes (two-way ANOVA, P<0.05).

E. Conclusions and perspectives

Taken as a whole, K availability had important effects on several metabolic pathways in leaflets of oil palm trees grown in the field (summarized in **FIG. II.12**). These effects were visible one to two years only after the onset of K fertilization regime, that is, before significant changes could be found on bunch number (**FIG. II.4**) and fresh fruit bunches weight (Mirande-Ney *et al.*, 2019). As such, our results obtained at the leaf scale suggest that it could be of interest to conduct experiments at the plantation scale (agronomical trials) to assess the potential of the metabolic signature of leaflets as a technique for K fertilization monitoring. In addition, the simultaneous effect of K availability on photosynthesis and respiration suggests that the carbon use efficiency could have also been impacted. Recent studies have shown that in oil palm saplings, K deficiency leads to ≈10% loss in carbon use efficiency only (Cui et al., 2019b) and under field conditions similar to ours, the effect of K availability on total fruit and oil production was rather small (Hartley, 1988). That is, despite significant changes in photosynthetic capacity and respiratory efflux, K availability has, perhaps, a limited effect on tree-scale carbon use

efficiency. Of course, measuring the overall effect of K availability on tree carbon balance would require further work, e.g. to monitor biomass and respiration of all organs and estimate total tree photosynthesis. This will be addressed in a future study.

F. Acknowledgements

C. Mirande-Ney is grateful to CIRAD for the PhD fellowship funding and for financial support of the experiments and divers analyses, and also to IDEEV for financial support. The authors would like to thank the company SOCFINDO for their material and technical support during field experiment, as well as Bertrand Gakiere from the facility Metabolism-Metabolome (IPS2). We also thank Jean Ollivier for providing agronomical data.

Proteomics analyses were performed on the PAPPSO platform (http://pappso.inra.fr) which is supported by INRA (http://www.inra.fr), the Ile-de-France regional council (https://www.iledefrance.fr/education-recherche), IBiSA (https://www.ibisa.net), CNRS (http://www.cnrs.fr) and SPS (https://www6.inra.fr/saclay-plant-sciences).

In Chapter III, fruit mesocarp metabolome was explored during five steps of maturation from pollination to harvesting, and the quality and quantity of mesocarp oil was assessed. This Chapter is now published as a research article in *Journal of Agricultural and Food Chemistry*.

Chapter III. Effects of potassium fertilization on oil palm fruit metabolism and mesocarp lipid accumulation

Cathleen Mirande-Ney[1,4*], Guillaume Tcherkez[2], Françoise Gilard[3], Jaleh Ghashghaie[4], Emmanuelle Lamade[1]

[1]Unité PERSYST, UPR34, Système de pérennes, Centre de Coopération Internationale en Recherche Agronomique pour le Développement, F-34398 Montpellier, France.
[2]Research School of Biology, Australian National University, Canberra 2601, ACT, Australia.
[3] Plateforme Métabolisme-Métabolome, Institute of Plant Science Paris-Saclay, University of Paris-Sud, 91405 Orsay cedex, France.
[4]Ecologie Systématique Evolution, Université Paris-Sud, CNRS, AgroParisTech, Université Paris-Saclay, 91400, Orsay, France.
*Contact author to whom correspondence must be addressed: cathleen.mirande-ney@cirad.fr

Published in *Journal of Agriculture and Food Chemistry*
J. Agric. Food Chem.201967339432-9440
Publication Date: August 1, 2019
https://doi.org/10.1021/acs.jafc.9b04336
The Supporting Information is available free of charge on the ACS Publications website at DOI: 10.1021/acs.jafc.9b04336.

Abstract

Potassium fertilization is common practice in oil palm (*E. guineensis*) plantation to increase yield. However, its effect on fruit oil content and composition are not well documented. Here, we conducted bunch, metabolomics and oil composition analyses in two contrasting crosses (*Deli x La Mé* and *Deli x Yangambi*) grown under different K fertilization conditions. K availability impacted on bunch oil content, due to lower water content and higher oil proportion in fruit mesocarp in *Deli x La Mé* only, showing differential responses of crosses to K. Oil composition at maturity did not significantly change under low K conditions despite clear alterations in fruit metabolism associated with lipid production during maturation, demonstrating the resilience of oil biosynthetic metabolism. However, the analysis of variance in oil content (across K treatments and crosses) demonstrates that sugar availability, lipid synthesis rate and metabolic recycling are all important in determining the oil content.

Keywords: oil palm, potassium, metabolomics, oil, fruit, mesocarp

A. Introduction

Oil palm (*Elaeis guineensis* Jacq.) is a major oil crop with a global production of about 77 Mt y^{-1} in 2018. Oil palm is also the world highest yielding oil crop species, with a productivity (production per hectare) up to 10 times larger than other leading vegetable oil crops like canola. Due to its unique chemical composition (relatively rich in saturated fatty acids), palm oil has a long shelf-life. In addition, it offers a number of nutritional benefits since it is cholesterol-free and rich in carotenoids, representing a natural source of vitamin A.

Oil palm growth is highly dependent on potassium (K) provision, and the elemental K content in total oil palm tissues is often larger than that of nitrogen. As such, K fertilization is common practice in the field, with potassium chloride (KCl) or potassium sulphate (K_2SO_4), representing an annual cost of about US$ 1b at the global scale. Typical oil palm K fertilization consists, on average, of 180 kg K ha^{-1} y^{-1} (≈2.5 kg KCl $tree^{-1}$ y^{-1}), while N and P represent about 95 and 11 kg ha^{-1} y^{-1}, respectively (Heffer, 2009). The particularly high K requirement in oil palm comes not only from the dependency of bunch production to K availability, but also from K scarcity in soils of oil palm cultivation areas, and the considerable loss of K applied, via leaching (up to 30% (Omoti *et al.*, 1983; Foong, 1991; Chang *et al.*, 1995)). Elemental bunch analyses have shown that K is by far the most abundant macroelement in fruit bunches. The highest K content can be found in stalks (5-8% of dry matter), which account for up to 26% of total bunch K content (Teoh & Chew, 1988b; Teoh & Chew, 1988a). Also, it has been estimated that up to 248 kg K ha^{-1} y^{-1} is abstracted from oil palm agrosystems during bunch harvesting (Heffer, 2009), and therefore K efflux (harvesting) can exceed K influx (fertilization). K fertilization is thus crucial to allow proper development and avoid progressive K depletion in soils and trees.

Furthermore, high K availability is beneficial to fruit development, bunch biomass and bunch number and thus increases yield (Hartley, 1988b; Corley & Tinker, 2016). In fruit mesocarp, the K content has been shown to increase progressively for 15 weeks after anthesis (WAA) and then decreases during last developmental stages where lipid biosynthesis occurs (Desassis, 1962). K^+ has also been suggested to drive phloem sugar movement, in particular for the remobilization of soluble sugars from the trunk base (and petioles) to sustain fruit development (Lamade *et al.*, 2014). However, to our knowledge, there is considerable uncertainty as to whether K fertilization affects mesocarp oil content and composition. Some

studies have shown that on average, higher K availability tends to increase mesocarp oil content (as well as the proportion of oleate in oil fatty acid composition) (Ochs & Ollagnier, 1977; Ollagnier & Olivin, 1984b) but a negative effect of K on oil content has been found elsewhere (Ochs & Ollagnier, 1977). It has been suggested that this negative effect may stem from an increased tissue chloride (Cl^-) concentration (which inevitably comes along with KCl-based fertilization), resulting in lower mesocarp-to-kernel biomass ratio in fruits (Breure, 1982; Ollagnier & Olivin, 1984a; Ollagnier & Olivin, 1984b). On average, crude palm oil triacylglycerols (TAG) contain unsaturated and saturated fatty acid chains in near-equal proportions, which makes palm oil suitable for a number of food, medicinal or biofuel applications. Saturated fatty acid chains are formed by 44% palmitic acid (C16:0), 5% stearic acid (C18:0) and traces of myristic acid (C14:0) (Sambanthamurthi *et al.*, 2000). Unsaturated fatty acid chains are formed by 40% oleic acid (C18:1), 10% linoleic acid (C18:2) and traces of linolenic acid (C18:3) (Barcelos *et al.*, 2015). In other species such as olive tree, it has been shown that K affects oil composition by increasing the proportion of mono-unsaturated (C20:1) and long saturated (C22:0) fatty acids (Dag *et al.*, 2009). Similarly, high K availability leads to increased fatty acid unsaturation in linseed, sunflower and sesame oil (Seo *et al.*, 1986; Salama, 1987; Froment *et al.*, 2000). K availability has a well-known effect on metabolism, via its action on several enzymatic activities such as pyruvate kinase, the last step of glycolysis that generates pyruvate from phospho*enol*pyruvate. In oil palm cultivated under low K conditions in the greenhouse, a general reorchestration of carbon primary metabolism has been shown in leaves, with drastic changes in organic acid content and the involvement of an alternative pathway (parapyruvate aldolase) to synthesize pyruvate (Cui *et al.*, 2019b). Since pyruvate is the key metabolite that links glycolysis to fatty acid synthesis (via acetyl-CoA production), an impact of K availability on oil production and composition can be anticipated. However, amongst metabolomics analyses conducted in oil palm fruits (Neoh *et al.*, 2013; Teh *et al.*, 2013a), none has looked at the effect of K availability on fruit development and oil biosynthesis.

This lack of knowledge impedes our current understanding of how K availability regulates lipid biosynthesis and thus oil palm productivity. In particular, since the impact of K fertilization on oil composition and final oil content in mature fruits has never been assessed precisely, K fertilization strategies that are best adapted to fruit metabolic efficiency are unknown. To address this issue, we examined fruit metabolism during maturation, using oil palm cultivated in the field under different K availability conditions. Bunch analysis, mesocarp metabolomics and ^{1}H-NMR oil analysis were carried out using two oil palm crosses (*Deli x*

La Mé (DL) and *Deli x Yangambi* (DY)) grown under different K fertilization treatments (from 0 to 4.5 kg KCl tree^{-1} y^{-1}) in a plantation located in North Sumatra (Indonesia). Fruit metabolism and bunch analysis were monitored at five developmental maturation stages (depicted in Fig. S1 and explained in Supplemental Text S1), and metabolomics and lipid analyses were carried out.

B. Material and Methods

1. Field location, fertilization and sampling

The experimental field was located at SOCFINDO plantation (Bangun Bandar Estate, North Sumatra, Indonesia; 3°18'19.60"N, 99°3'24.33"E) and sampling was carried out in Oct-Nov 2018. Average monthly temperature was 26°C, ranging from 18 to 42°C. In this geographical region, there is a soft rainy season from Sept to Dec, and a precipitation peak (460 mm) has been observed in Dec 2017. Total annual precipitation is about 2,500 mm. Overall, 40 oil palm trees planted in Aug 2013 were organized in a K-factorial agronomic trial. They belonged to two crosses: *Deli x La Mé* (DL) and *Deli x Yangambi* (DY). DL and DY have been chosen here since they are two very common crosses used in oil palm agroforestry. The agronomic trial comprised four levels of potassium fertilization with KCl: no KCl applied for 3 y before and also during the experiment (K0), 1.5 kg KCl tree^{-1} y^{-1} (K1), 3 kg KCl tree^{-1} y^{-1} (K2), and 4.5 kg KCl tree^{-1} y^{-1} (K3). In an effort to examine the influence of K under realistic conditions, we used K availability levels that are far from extreme situations (i.e., K deficiency or K excess). In fact, residual K in soil under the K0 treatment represents about 0.2 meq exchangeable K per 100 g soil, showing that there was no K deficiency during the experiment. Trees were also fertilized with nitrogen using 2 kg urea tree^{-1} y^{-1}. Leaflets used for mineral analysis were sampled on trees fertilized under treatments K0, K2 and K3 on leaf rank number 9, at point B and a distance of two third of the leaflet length from the rachis, using leaflets on both sides of the leaf (Lamade *et al.*, 2009). Leaf samples were cleaned with deionized water, frozen in liquid nitrogen and then oven-dried prior to analysis. Fruit sampling for metabolomics analysis was performed with treatments K0 and K3 at five different developmental maturation stages (30 d between them) numbered from 1 (1 month after anthesis) to 5 (at ripening) so as to follow fruit formation and maturation described by (Thomas *et al.*, 1971) (stages are further described in **FIG. III.1** and **SUPPLEMENTAL TEXT S1**). Five fruits (per stage) were randomly collected on

each respective bunch the same day for all maturation stages and all trees studied. Sampled fruits were rapidly cleaned with deionized water, cut in small pieces, frozen in liquid nitrogen then frozen-dried (lyophilized). Once dried, fruit mesocarp was ground and stored at –20°C. Leaf samples were ground in a fine powder and mineral analyses (N and K elemental content) were carried out by ICP-OES by SOCFINDO.

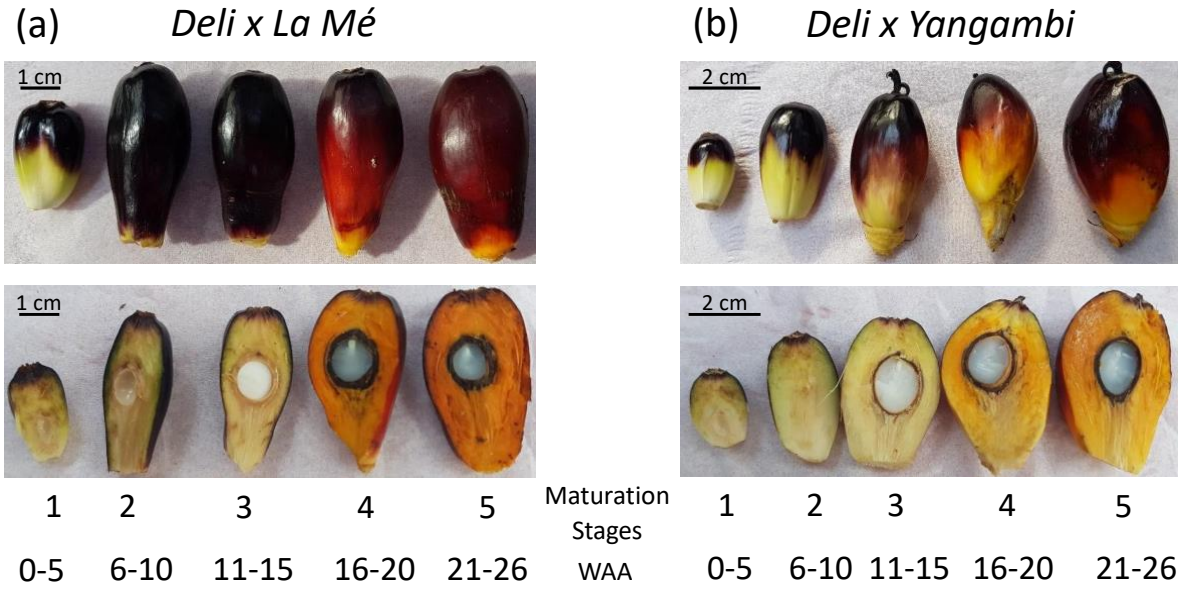

Figure III.1. Fruit developmental maturation stages. Fruit morphology (top) and longitudinal sections (bottom) of (a) *Deli x La Mé* (DL) and (b) *Deli x Yangambi* (DY) oil palm trees at 5 different developmental maturation stages, along with associated time-windows (in week after anthesis, WAA). These time-windows are averages and depend on crosses (maturation takes about 5.8 months in DL and 5.5 months in DY).

2. Starch and metabolites extraction

Starch was extracted following the procedure described in Duranceau *et al.* (1999). Briefly, 50 mg of ground mesocarp was extracted with 1 mL MilliQ water, centrifuged and the supernatant was discarded. The pellet was rinsed with absolute ethanol and starch was extracted using solubilization with 6 M HCl and subsequent flocculation in methanol at 5°C. For metabolomics, 10 mg of ground dried mesocarp was extracted with 1 mL cold (–20°C) water-acetonitrile-isopropanol mixture (2:3:3, v:v:v) containing 4 pg mL^{-1} ribitol as an internal standard, using 2 stainless steel 3-mm balls for tissue lysing (1.5 min, 30 Hz). Samples were placed for 10 min

at 4°C and 1,400 rpm shaking in a thermomixer (Eppendorf). After centrifugation (10 min, 4°C, 13,500 rpm), 10 µL d_{27}-myristic acid (30 pg mL^{-1}; internal standard for retention time locking (RTL) using the Agilent software (Tavares *et al.*, 2018; Fu *et al.*, 2019)) was added to 50 µL of supernatant. The solution was spin-dried under vacuum for 4 h and stored at −80°C until further analysis.

3. Metabolomics by gas chromatography-mass spectrometry (GC-MS)

GC-MS analyses were carried out as in Fiehn (2006); Fiehn *et al.* (2008). Frozen samples were warmed up for 15 min and vacuum-dried for 1.5 h at 35°C. Extracts were derivatized with 10 µL methoxyamine in pyridine (20 mg mL^{-1}) for 90 min at 30°C with continuous shaking then 90 µL of N-methyl-N-trimethylsilyl-trifluoroacetamide (Regis Technologies) was added and the reaction ran for 30 min at 37°C. After cooling to ambient temperature, 100 µL was transferred to a glass vial. Four hours after derivatization, 1 µL was injected in split-less mode into the GC-MS (GC Agilent 7890B coupled to MS Agilent 5977A). The GC column contained a standard low-polarity phase with 1,4-bis(dimethylsiloxy)phenylene dimethyl polysiloxane (RXI-5SIL MS, 30 m with 10 m integra-guard column, Restek). Injection in split mode (ratio 1:30) was also done for saturating (highly concentrated) compounds quantification. Oven temperature was 60°C for 1 min then ramped at 10°C min^{-1} up to 325°C for 10 min. Helium was used as vector gas under a constant flow at 1.1 mL min^{-1}. Other temperature values were as follows: injector 250°C, transfer line 290°C, source 230°C, and quadrupole 150°C. The solvent delay was 5.9 min, and the scan window during acquisition was 50-600 amu. Retention indexes were calculated against the internal standard (d_{27}-myristic acid) using the RTL system provided in Masshunter® (Agilent) in order to reduce run-to-run variations. In addition, a fatty acid methyl ester mix (from C_8 to C_{30}) was injected each 8 samples for external retention index calibration. Samples were randomized amongst treatments and crosses to avoid statistical bias. Raw data files were analyzed with AMDIS (http://chemdata.nist.gov/mass- spc/amdis), and the Fiehn GC-MS Metabolomics RTL Library (version June 2008) was employed for metabolite identification, which was also checked using the NIST library and authentic standards injected separately. Peak areas were determined with Masshunter® (quantitative analysis version, Agilent). Because automated peak integration was occasionally erroneous, integration was verified manually for each compound in all analyses. Resulting areas were compiled in one single Excel file for comparison. Peak areas were normalized to ribitol (internal standard) and

dry weight. In addition to GC-MS metabolomics, we also conducted the analysis of total lipids by NMR in order to measure saturated and unsaturated fatty acid contents and the iodine index (**SUPPLEMENTAL TEXT S2**).

4. Bunch analysis

Components of oil extraction rate were determined by SOCFINDO using standard procedures adapted from Blaak *et al.* (1963). Bunch recording was performed from the onset of the productive period of the trial. One mature bunch (5 to 6 months after pollination) per tree was sampled for analysis: bunch, stalk and spikelet fresh biomass was measured and fruit biomass, mesocarp-to-fruit (M/F), oil-to-mesocarp (OFM) and kernel-to-fruit (K/F) ratios (expressed in %) were computed using a set of 30 fruits. Mesocarp relative water content (in %) was calculated as the difference between fresh and dry mesocarp biomass divided by fresh mesocarp biomass. The oil extraction rate (OER) was calculated as:

$$\mathrm{OER} = \frac{\mathrm{F/B} \times \mathrm{M/F} \times \mathrm{OFM}}{10,000} \times 0.855$$

where F/B, M/F and OFM stand for the percentage of fruit biomass in bunch total biomass, the percentage of mesocarp biomass in total fruit biomass, and the percentage of oil in mesocarp biomass, respectively. The correction factor of 0.855 is used to account for losses in factory oil extraction. The proportion of kernels in bunch biomass was computed as:

$$p_{\mathrm{kernel}} = \frac{\mathrm{F}}{\mathrm{B}} \times \frac{\mathrm{K}}{\mathrm{F}} \times \frac{0.91}{100}$$

where, K/F stands for the percentage of kernel biomass in fruit biomass and 0.91 represent the fraction of non-parthenocarpic fruits.

5. Statistical and hierarchical clustering analysis

For OER components, elemental content and metabolomics, 4 to 5 replicates were taken for all conditions. Univariate and multivariate analyses of metabolomics data were conducted using an ANOVA (MeV version 4.9) and orthogonal projection on latent structures (OPLS, SIMCA version 14.0, Umetrics), respectively. For each cross, we used a 2-way ANOVA (threshold *P*-value for significance 0.01) with developmental stage and K as factors and results are presented as a heatmap associated with a hierarchical clustering analysis (Pearson correlation) for

significant metabolites. The OPLS analysis used the K level (qualitative) and maturation stage (quantitative) as predicted Y variables and metabolites as predicting X variables. The goodness of the OPLS model was assessed using the determination coefficient R^2 and the predictive power was quantified by the cross-validated determination coefficient, Q^2. Best discriminating metabolites were identified using volcano plots whereby the logarithm of the *P*-value obtained in univariate analysis (ANOVA) was plotted against the rescaled loading (p_{corr}) obtained in the OPLS. In such a representation, best discriminating metabolites have both maximal –log(*P*) and p_{corr} values. Metabolic pathway enrichment was analyzed with the tool MetaboAnalyst(Xia & Wishart, 2016) using as input metabolites significant for the K effect (*P*<0.01) for DL and DY mixed and the plant metabolite database (*Arabidopsis thaliana*; the database for oil palm is not currently available). A Pearson correlation analysis was also performed on metabolomics data with R (version 3.6.0, R Development Core Team 2005) in order to identify correlations between metabolites and agronomical parameters such as OER and OFM. OER components, elemental content and lipid content (^{1}H-NMR) were analyzed separately using a 2-way ANOVA (with a threshold *P*-value of 0.05) with developmental stage and K as factors, followed by a post-hoc Tukey test.

C. Results and discussion

1. Differential effect of K on bunch composition

As expected, K fertilization conditions were reflected in leaf K elemental content while N content remained constant. In fact, there was about 0.75% K under K0 conditions and significantly more (up to 1.15%) at K2 and/or K3 (**FIG. III.2**).

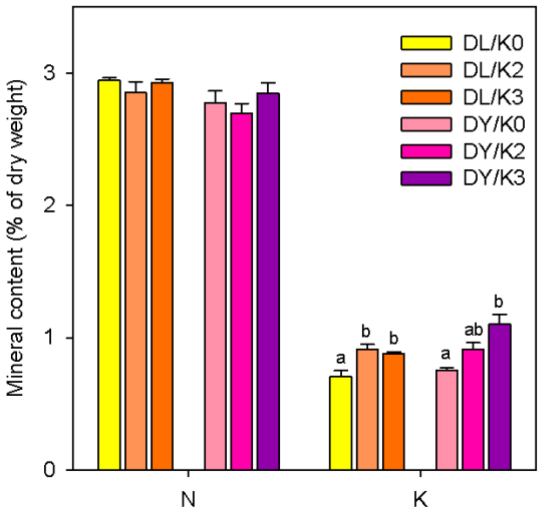

Figure III.2. Leaf nitrogen and potassium elemental contents in the two crosses *Deli x La Mé* (DL) and *Deli x Yangambi* (DY) under three K treatments (K0, K2 and K3). The elemental content is given in percentage of dry weight. Mean ± SE (n = 4). Letters stand for statistical classes (P<0.05) using a Tukey test

K availability had a differential effect on bunch parameters depending on the cross (**FIG. III.3**). DY trees produced less bunches (**FIG. III.3A**) with less fruits and more stalk and spikelet biomass (**FIG. III.3B**) but formed bigger fruits (**FIG. III.3D**) with higher mesocarp water content (MWC, **FIG. III.3F**), as compared to DL. As a result, there was a higher oil content in fruit mesocarp (OFM) and larger oil extraction rate (OER) in DL (**FIG. III.3G**). High K availability tended to decrease the number of bunches per tree (**FIG. III.3A**) but increased significantly the number of fruits (**FIG. III.3B**) as well as mesocarp and kernel biomass proportion in bunches (**FIG. III.3C**). Interestingly, while previous studies have shown that K availability ameliorates yield by increasing bunch biomass and number (Corley & Mok, 2008), we find here that the increase in bunch number is visible only under K2 conditions, with even a slight decrease at high K (K3) in DY (**FIG. III.3A**). In DL, MWC clearly decreased with K availability (**FIG. III.3F**) and accordingly, there was an increase in OFM and OER (**FIG. III.3G**). In contrast, higher K availability caused an increase in kernel biomass proportion in bunches and MWC in DY, thus leading to lower OFM. Our results are in agreement with previous studies that showed a correlation between fruit transpiration (water loss) and lipid biosynthesis (Jeje *et al.*, 1978; Teh *et al.*, 2013a). The negative effect of high K (K3 conditions)

on oil content (OFM) in DY fruits could have come from excess chloride in tissues, which is also known to increase the kernel-to-mesocarp ratio, as observed here (Breure, 1982).

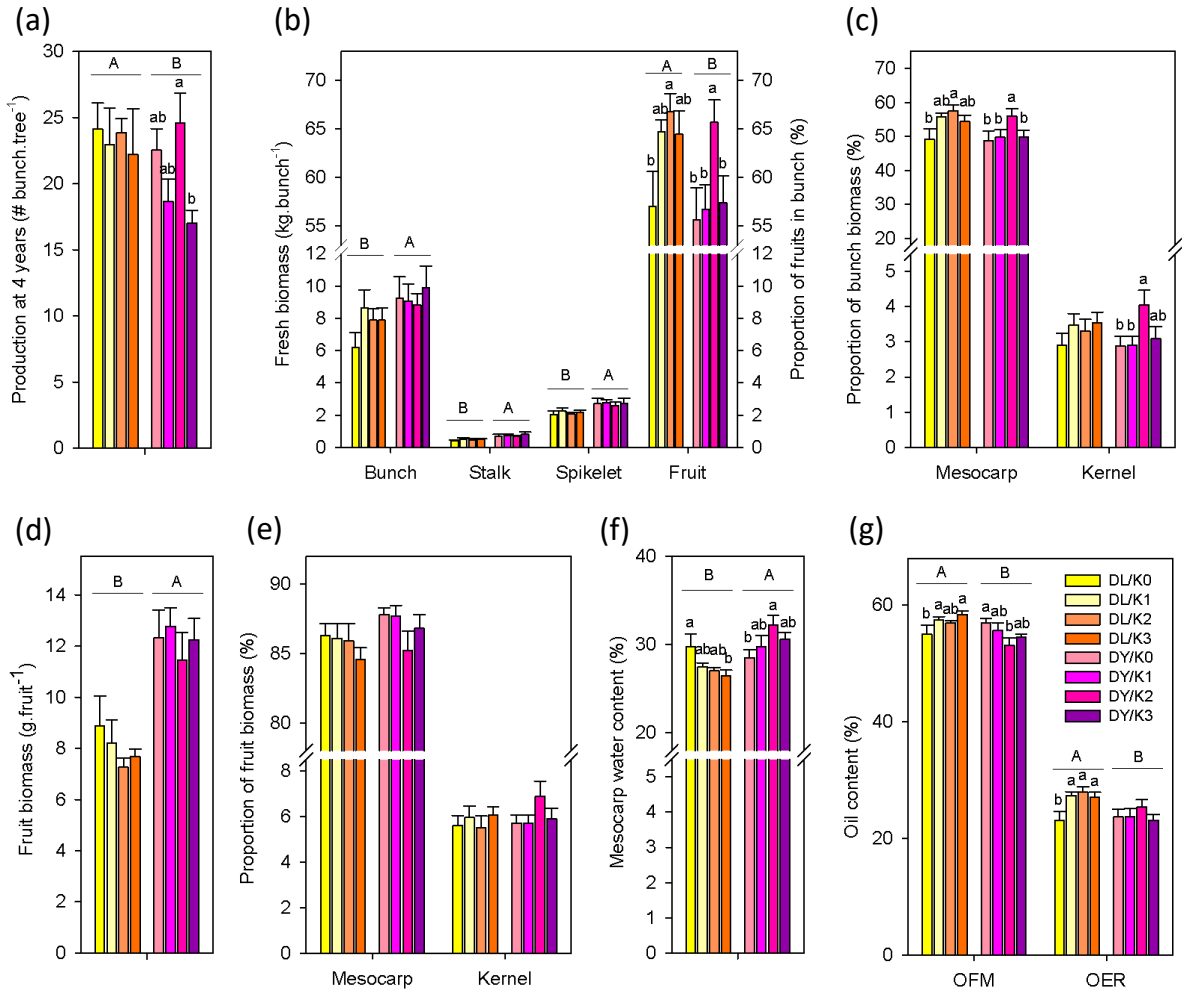

Figure III.3. Effect of potassium availability on bunch production: (a) Production at 4 years, (b) Bunch, stalk and spikelet fresh biomass and proportion of fruits in bunch, (c) Proportion of mesocarp and kernel in bunch biomass, (d) Fruit biomass, (e) Proportion of mesocarp and kernel in fruit biomass, (f) Mesocarp water content and (g) Oil content in mesocarp (OFM) or in bunch (OER), under different K fertilization treatments (K0 to K3) and two contrasting oil palm crosses *Deli x La Mé* (DL) and *Deli x Yangambi* (DY). Production at 4 years corresponds to the number of bunches harvested along the 4th year. Fresh biomass is given in kilograms (b) or grams (d). Proportions are given in percentage and were defined as the ratio of fruits, mesocarp or kernel biomass to that of the bunch or fruit. Abbreviations: OFM, oil content in fresh mesocarp; OER, oil extraction rate (proportion of oil in mesocarp). Mean ± SE (n = 5). Letters stand for statistical classes (Tukey test, P<0.05).

In fact, DY trees subjected to different forms of chloride fertilization (either as NaCl or KCl) have been shown to form heavier bunches with more and bigger fruits, and higher proportion

of kernel biomass, with no change in OER (Ollagnier & Olivin, 1984a). We also note that leaf K elemental content was more impacted by fertilization in DY than in DL (**FIG. III.2**), suggesting that KCl absorption was more efficient in DY trees. In other oil-producing species such as castor bean, higher K availability is accompanied by lower Na^+ and/or Ca^{2+} and less chloride in phloem sap and tissues, suggesting that electroneutrality at high K requires less (not more) anions, and is achieved with anion species other than chloride (Peuke *et al.*, 2002). That is, ion balance leads to an antagonistic relationship between K and Cl and therefore explains the effect (or the lack thereof) of high KCl fertilization in which Cl^- inevitably comes along with K^+.

2. Metabolic profiling during fruit development

The metabolome of fruit mesocarp was analysed at five different developmental stages, across two K conditions (K0, K3) and two crosses (DL, DY). Overall, 131 analytes were quantified and identified and amongst them, about 100 (103 in DL, 97 in DY) were found to be significant for the developmental stage effect ($P<0.01$, **FIG. S2**). As expected, carbohydrates, organic acids and amino acids decreased between stage 2 and 3 and conversely, there was a clear increase from stage 3 to 5 not only in free fatty acids (FAs) but also in glycerol, glycerol 1-phosphate, monostearin, and oleoylglycerol, reflecting increased triglycerides synthesis. At maturity, mesocarp metabolome distribution was made of 72% FAs, 27% carbohydrates and less than 1% other metabolites across all conditions (as estimated from GC-MS signals; **FIG. III.4A**). Thus, fruit development was associated with a general change in tissue composition and metabolic content, along with a typical accumulation of lipids (**FIGS. III.4A AND S2**) as described elsewhere (Hartley, 1967; Thomas *et al.*, 1971; Neoh *et al.*, 2013; Teh *et al.*, 2013a).

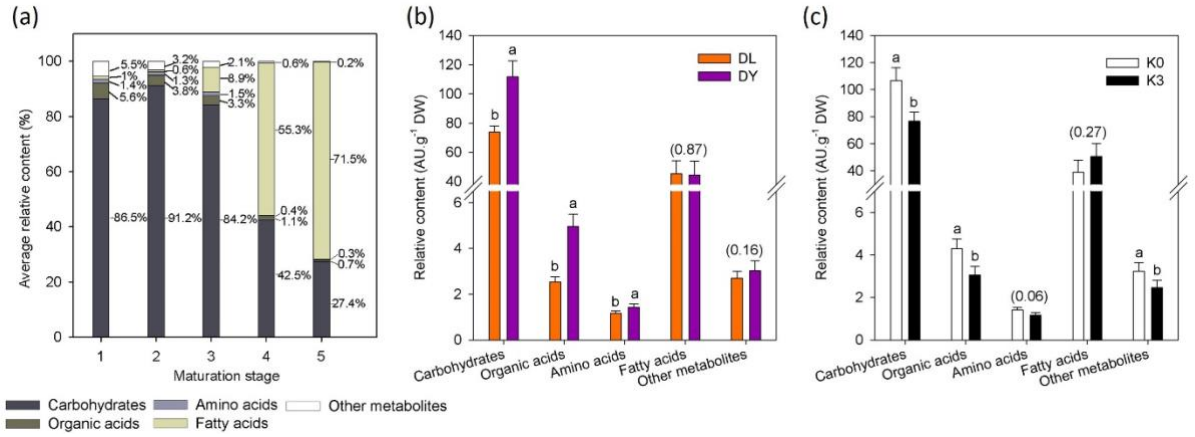

Figure III.4. Overview of mesocarp metabolism: (a) Average mesocarp composition (across K conditions and crosses) during fruit development (relative content in % of total GC-MS signal). (b) Average content (in arbitrary unit (AU) relative to internal standard, normalized to dry weight (DW)) in carbohydrates, organic acids, amino acids, fatty acids and others metabolites across developmental stages in *Deli x La Mé* (DL) and *Deli x Yangambi* (DY). (c) Average K effect (K0 vs. K3) on metabolite classes across developmental stages and crosses. Mean ± SE (n = 10). Letters stand for statistical classes (Tukey test, P<0.05). When non-significant, the P-value is written between parentheses.

Interestingly, sucrose decreased from stage 1, glucose and fructose increased until stage 2 and then decreased, while starch peaked at stage 3 and reached a minimal level at stage 5 (**FIGS. S2, III.5 AND III.6**). It strongly suggests that sucrose was used first as the carbon source for lipid and starch biosynthesis, and then starch was used as a carbon source for lipid synthesis (Dussert *et al.*, 2013). Accordingly, sucrose is the prevalent sugar in oil palm phloem sap (Houngbossa & Bonnemain, 1985; Obahiagbon *et al.*, 2012). Also, genomics analyses have suggested that fruit development is primarily sustained by sucrose, which is hydrolysed by sucrose synthase (Susy) in the mesocarp (Wong *et al.*, 2017). The involvement of starch metabolism is also demonstrated here by the occurrence of maltose (non-phosphorolytic starch degradation product), which increased in both crosses during stages 4 and 5 (**FIG. III.4**).

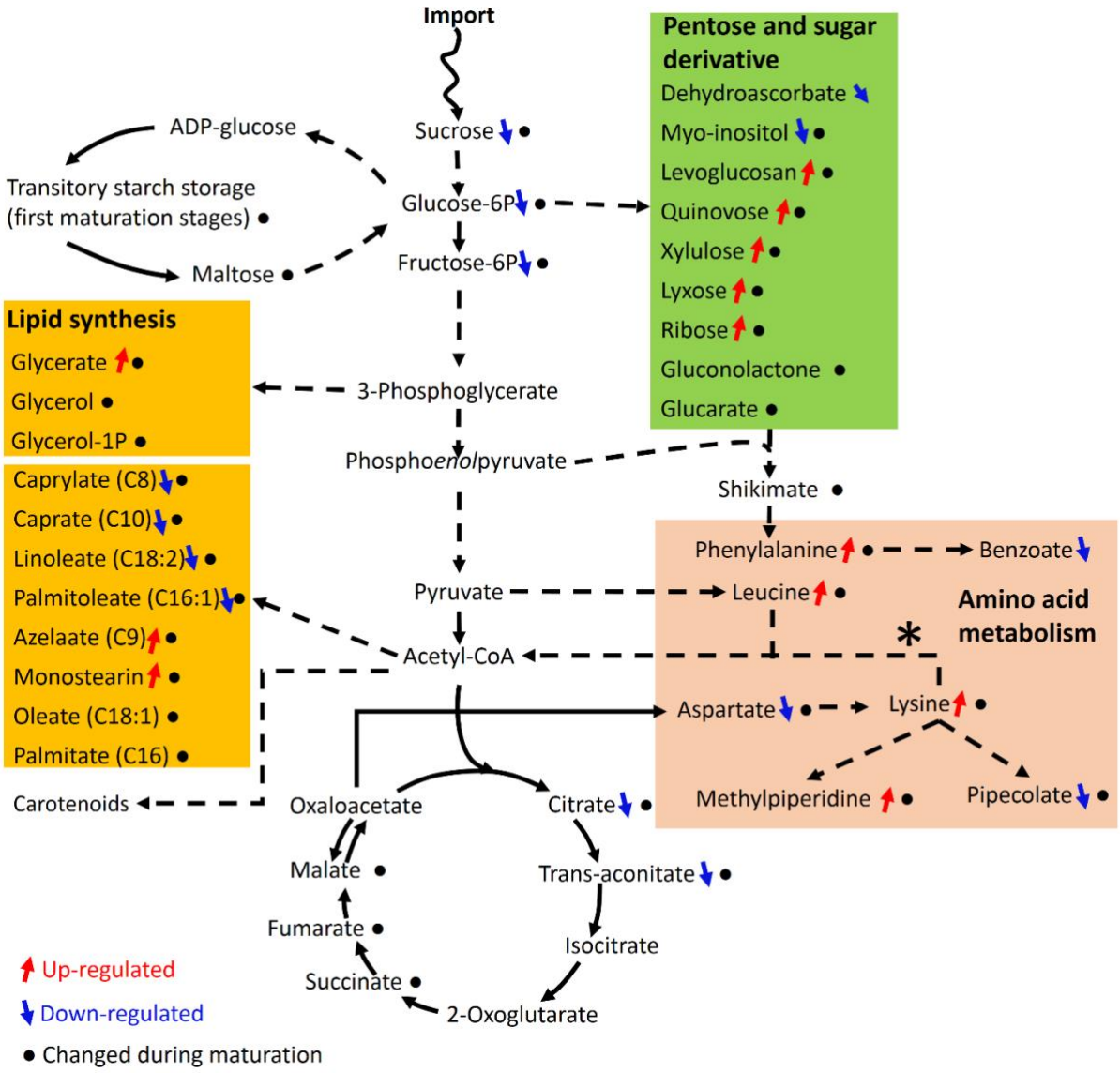

Figure III.5. Effect of K availability on oil palm mesocarp lipid biosynthesis. Blue arrow indicates metabolites which decrease with K fertilization and red arrow indicates those which increase. Abbreviation: ADP-glucose: adenosine diphosphate glucose, Susy: Sucrose synthase

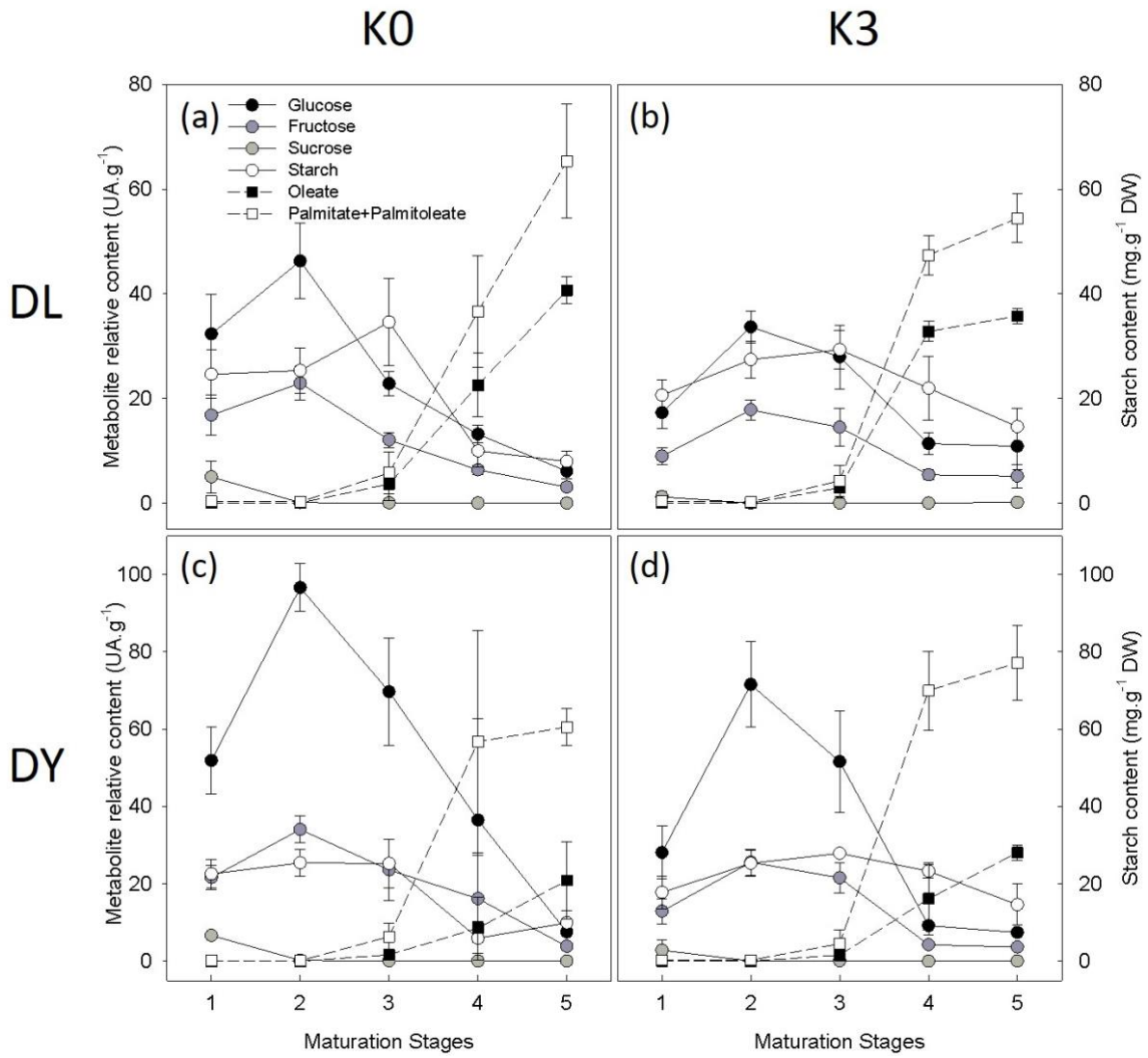

Figure III.6. Effect of K availability on FAs synthesis. Sugars (glucose, fructose, sucrose and starch) and FAs (oleate and palmitate + palmitoleate) variations during mesocarp maturation under different K fertilization treatments (K0 and K3) in two contrasting oil palm crosses (a-b) *Deli x La Mé* (DL) and (c-d) *Deli x Yangambi* (DY). Metabolites are given in UA g^{-1} (from GC-MS profiling) and starch is given in mg g^{-1} DW. Mean ± SE (n = 4).

Lipid accumulation was also accompanied by an increase in glucarate and gluconolactone, which are both associated with the oxidative pentose phosphate pathway. Maturation was associated with a general depletion in fumarate, citrate or succinate, probably reflecting the progressive increase in energy generation and thus the consumption of Krebs cycle intermediates. The importance of respiration and oxidative phosphorylation in oil palm fruit development has also been demonstrated by protein content analysis (Loei *et al.*, 2013). It is worth noting that other compounds were found to accumulate during fruit maturation, such

as caffeate, suggesting changes in secondary metabolism as fruits mature. In addition to changes during developmental stage, our results also show some differences between crosses. In fact, there were more carbohydrates, amino acids and organic acids in DY compared with DL (**FIG. III.4**). Furthermore, we found an increase in putrescine in DL fruits during maturation, as found elsewhere (Teh *et al.*, 2014). Polyamines such as putrescine have been shown to be involved as signaling metabolites in fruit enlargement, maturation, and ripening (Serrano *et al.*, 2016; Guo *et al.*, 2018). Sugars have a signaling role in lipid synthesis. In particular, hexokinase acts as a glucose sensor and generates glucose 6-phosphate (which will then be used by the oxidative pentose phosphate pathway) and is essential for fatty acid synthesis (Aguilera-Alvarado & Sánchez-Nieto, 2017; Zhai *et al.*, 2017). Overall, the kinetics of lipid biosynthesis and sugar remobilization seem to be faster in DL, maybe linked to higher catabolism, or differences in metabolic signaling.

3. Potassium availability impacts on kinetics of lipid synthesis

K availability had an effect on fruit metabolism during maturation, with lower carbohydrate and organic acid content at high K (**FIG. III.4C**, pathways summarized in **FIG. III.5**). At high K, glucose, fructose and sucrose were lower (by 40-70%) compared with K0 in particular at stage 1 (**FIG. III.6**). Multivariate analysis conducted separately on the two crosses showed that both the developmental stage and K availability could be well discriminated along axis 1 and 2, respectively (**FIG. III.7A-B**). The OPLS model was significant in both DL ($P_{CV\text{-}ANOVA} = 3 \cdot 10^{-4}$ [K effect] and $7 \cdot 10^{-11}$ [stage]) and DY ($P_{CV\text{-}ANOVA} = 4.9 \cdot 10^{-2}$ [K effect] and $6 \cdot 10^{-13}$ [stage]), explained most of total variance ($R^2 = 0.892$ and 0.739, respectively) and was predictive ($Q^2 = 0.69$ and 0.54, respectively). The importance of metabolites in sample discrimination associated with K0 and K3 conditions was assessed using the combination of univariate and multivariate analysis whereby $-\log(P)$ obtained in the two-way ANOVA (univariate) was plotted against the loading value (p_{corr}) along axis 2 (volcano plot; **FIG. III.7C-D**). In DL, high K availability led to an increase in methylpiperidine and glucose derivatives 1,6-anhydroglucose (levoglucosan) and 6-deoxyglucose (quinovose) and in DY, there was an increase in amino acids (leucine, phenylalanine, lysine) as well as glucose derivatives (xylulose, lyxose, ribose).

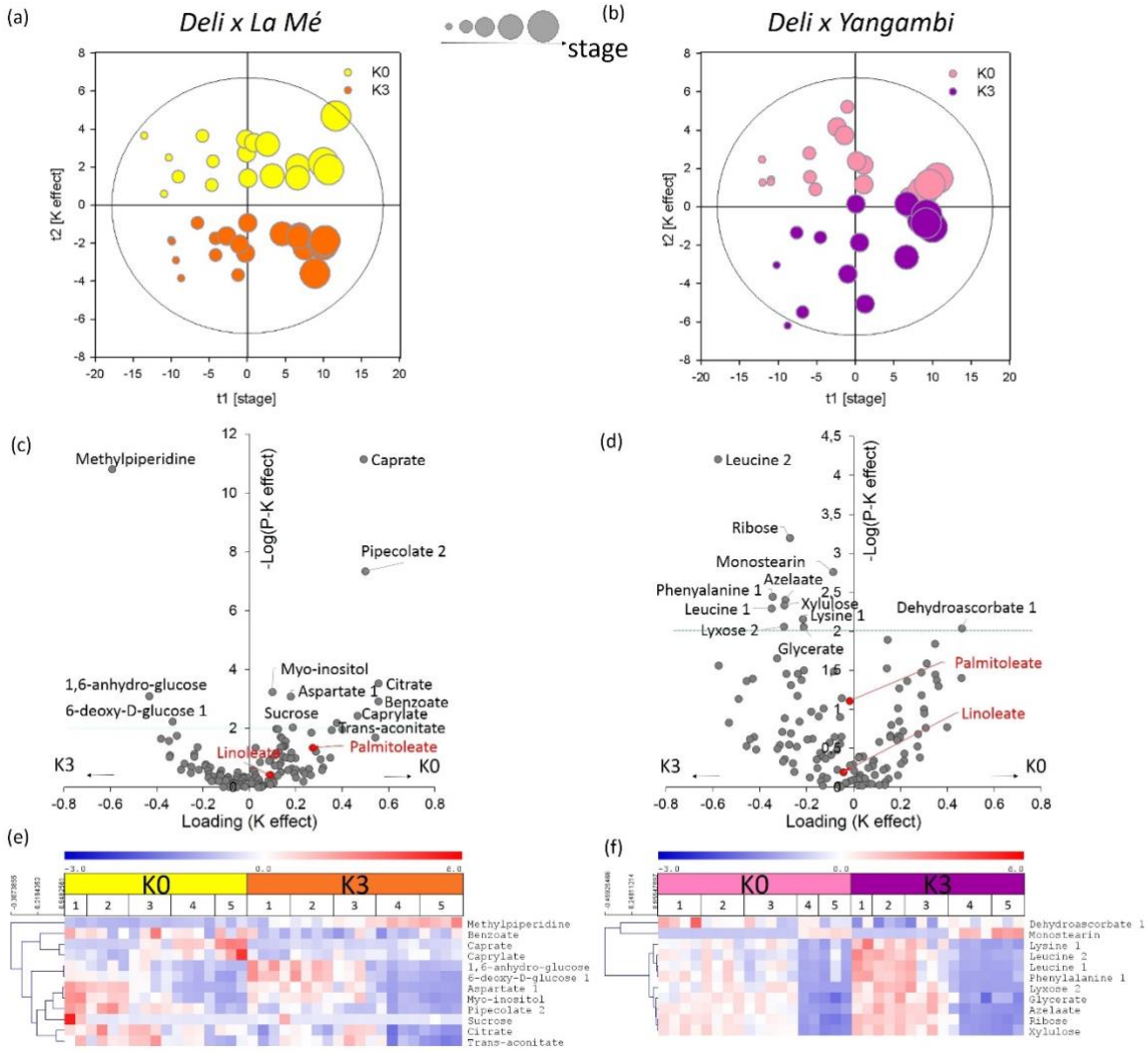

Figure III.7. Metabolomics response of mesocarp to K fertilization during fruit maturation in *Deli x La Mé* and *Deli x Yangambi* crosses. (a-b) Score plots of the O2PLS analysis using K and developmental stage as predicted Y variables in DL (a) and DY (b). Samples are discriminated along the *y* axis (K) and *x* axis (stage). (c-d) Volcano plots (−log(*P*) from two-way ANOVA versus O2PLS loading p_{corr}) showing best discriminating metabolites associated with K availability, in DL (c) and DY (d). (e-f) Heatmap of metabolites significant for the K effect ($P<0.01$; the threshold of 0.01 is shown with the green dotted line) in DL (e) and DY (f). Scale from blue (lowest) to red (highest) to show the relative content (mean-centered). To facilitate reading, a magnified version of this figure is available as Supplementary Figure S3.

This reflected the increase in glucose catabolism via the oxidative pentose phosphate pathway (which generates NADPH for fatty acid synthesis), and the redistribution of nitrogen to specific compounds (methylpiperidine, amino acids). Interestingly, pipecolate (product of lysine catabolism) was found to decrease at high K in DL and lysine found to increase in DY, suggesting that in both crosses, high K availability likely slowed down lysine catabolism.

Similarly, phenylalanine was more abundant in DY at high K and benzoate (product of phenylalanine catabolism) was less abundant in DL, suggesting that phenylalanine catabolism was also slowed down. This K effect on amino acid catabolism was mostly visible at early stages (1-3) of fruit development since lysine and phenylalanine contents were very low at late stages (4-5) (**FIG. III.7E-F**). In DY, high K was associated with more intermediates of lipid synthesis (glycerate, monostearin and azelaate) and in DL, less short-chain fatty acids (caprate, caprylate), showing that K stimulated fatty acid chain elongation and triglyceride synthesis. These suggested changes in metabolic pathways as affected by K availability were further supported by pathway enrichment analysis (**FIG. III.8**).

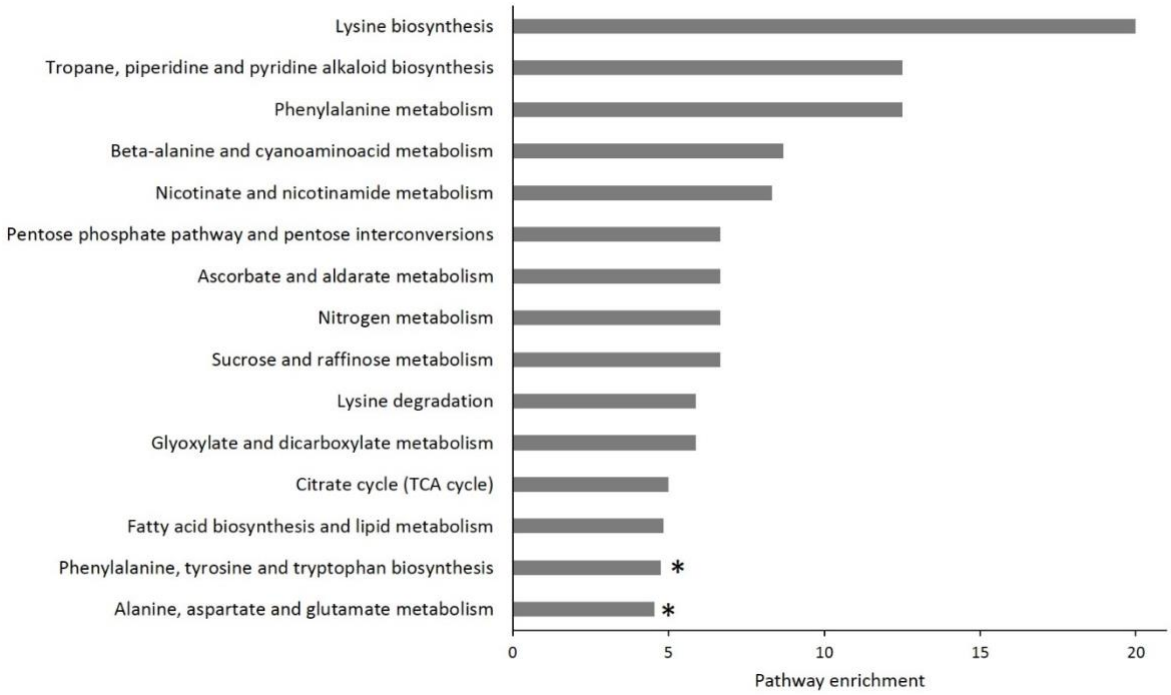

Figure III.8. Pathway enrichment analysis (PEA) associated with the effect of potassium fertilization in both crosses (DL, DY). PEA was performed with MetaboAnalyst and shows metabolic pathways affected by the K treatment in DL and DY (i.e., where at least one metabolite is significantly impacted by K fertilization with $P<0.01$, Fig. 3). The asterisk (*) indicates when pathways are not significantly affected as per PEA analysis ($P>0.05$).

4. Differential effect of potassium on mesocarp lipid composition

Despite metabolic changes during fruit development (see above), the relative quantity in fatty acids in mesocarp and final oil composition at maturity were not significantly modified by K availability (**FIGS. III.4C AND III.9**). Accordingly, oil NMR profiles were extremely similar

(FIG. III.10). However, at high K (K3), GC-MS showed an increase in average oleate and a decrease in linoleate content in both crosses, although it was found to be insignificant in each cross taken separately (FIG. III.9A). Consistently, NMR analyses showed a slight increase in both average mono-unsaturated fatty acids and iodine index in both crosses (FIG. III.9B). A similar effect of K has been suggested previously in oil palm (Ochs & Ollagnier, 1977; Ollagnier & Olivin, 1984a; Ollagnier & Olivin, 1984b) and other species (Seo *et al.*, 1986; Salama, 1987; Froment *et al.*, 2000; Dag *et al.*, 2009). Here, we show that its effect is quantitatively small (≈1-2% change in mono-unsaturated FA content) but found in both crosses even though they had very different lipid compositions (nearly 10% difference in mono-unsaturated FAs, FIG. III.9B). Furthermore, in the present study the difference in leaf tissue K content was modest (0.3-0.7% of dry weight (DW)) suggesting that very large changes in oil composition are to be anticipated under K deficiency or very high K fertilization.

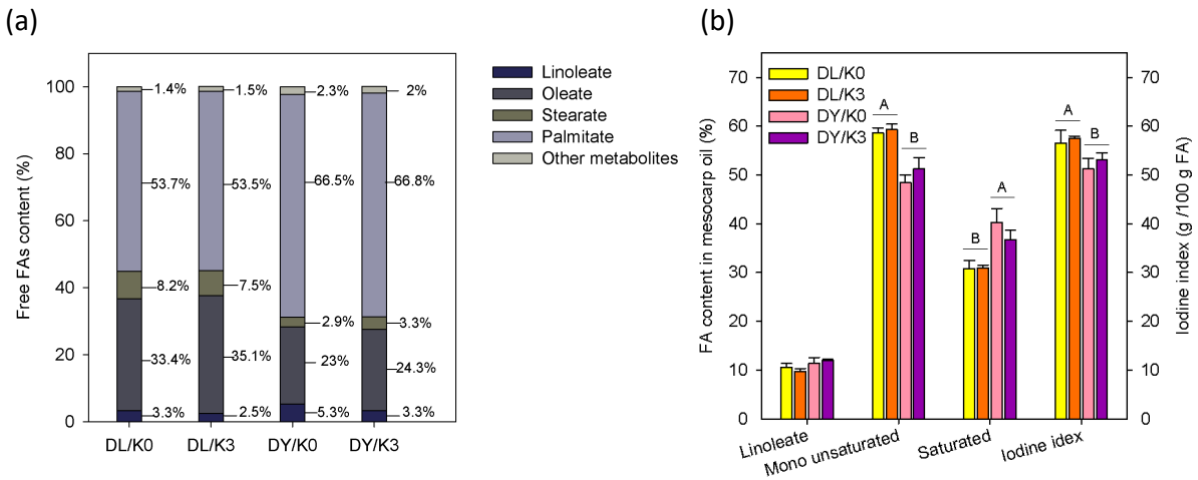

Figure III.9. Differential effect of potassium nutrition on mesocarp oil quality: (a) Average mesocarp free fatty acid (FA) composition of both crosses (*Deli x La Mé*, DL, and *Deli x Yangambi*, DY) under K0 and K3 conditions, with FA contents given in percentage of total FAs as measured by GC-MS. (b) Mesocarp content in linoleate, mono-unsaturated and saturated fatty acids, and iodine index, measured using $_1$H-NMR, in both crosses under K0 and K3 conditions. FA contents are given in percentage of total FAs and iodine index in (g iodine/100 g FA). Mean ± SE (n = 3). Letters stand for statistical classes (Tukey test, P<0.05).

Interestingly, the biochemical response to K availability differed slightly in minor oil components between the two crosses. In fact, linoleate and palmitoleate correlated positively (positive loading value) with K in DY whereas they anti-correlated (negative loading value) with K in DL (FIG. III.7C-D). Accordingly, linoleate decreased significantly at high K at stage 5 and so did palmitoleate in DL (FIGS. S2 AND III.5). Also, in terms of kinetics of lipid production, high K decreased significantly the pool of short-chain fatty acids (caprate,

caprylate), showing the stimulation of fatty acid chain elongation in DL, while both a short-chain fatty acid (azelaate) and esterified stearate (monostearin) increased in DY, suggesting a general increase in lipid synthesis (**FIGS. III.7 AND III.8**). In addition, high K increased the average content in carotenoids in mesocarp oil, and this effect was easily visible from the color of chloroform oil extracts (**FIG. III.11**). Estimating carotenoids quantity with NMR showed an increase of the average content by 25% in DL and almost 100% in DY (**FIG. III.11**) at high K but this was not significant due to substantial variability between individuals. Such a variability was also due to the fact that carotenoids formed small peaks in the NMR spectrum (**FIG. III.10**) and this was detrimental to quantitation precision.

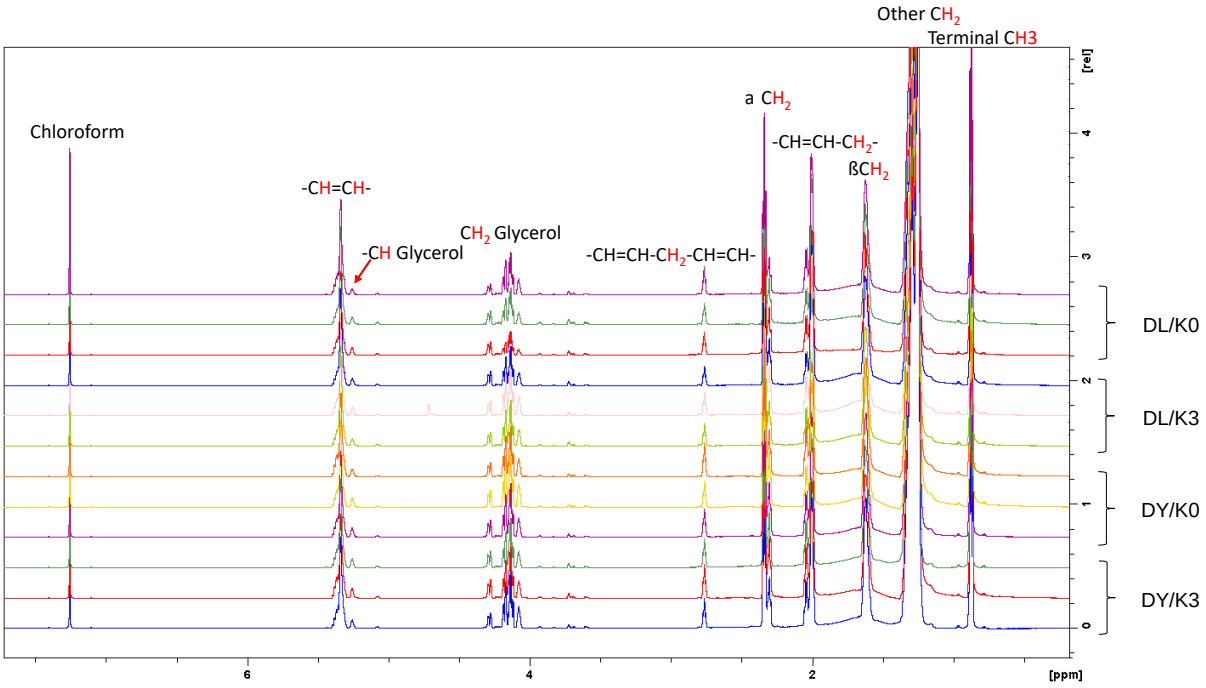

Figure III.10. Overview of NMR spectra in DL and DY chloroform-extracted oil, under different K fertilization treatment (K0 and K3). Spectra were obtained by $_1$H-NMR analysis (see *Materials and Methods*) and are presented as the relative signal at the same scale, with the chemical shift (relative to TMS) on the *x*-axis.

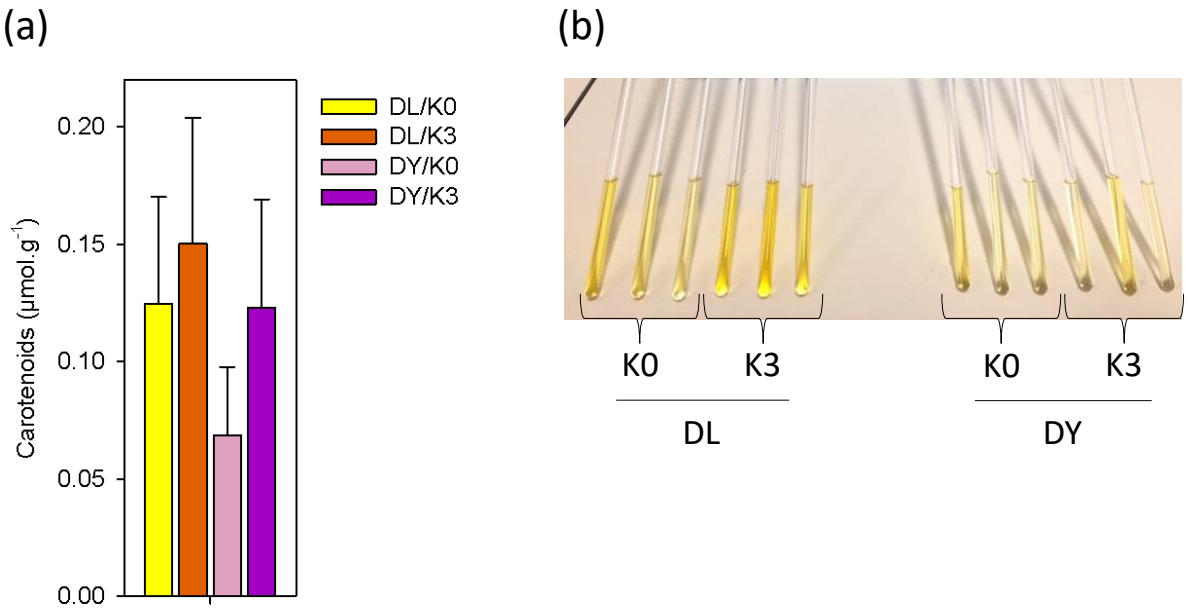

Figure III.11. Effect of potassium availability on mesocarp carotenoids content. (a) Carotenoids content from total chloroform extracted lipids of mesocarp at stage 5 of DL and DY under K0 or K3 conditions. Carotenoids content is given in µmol mL^{-1} as measured by ^{1}H-NMR analysis. Mean ± SE (*n* = 3). (b) Photograph of mesocarp chloroform oil extracts at stage 5, used for ^{1}H-NMR analysis.

5. Key determinants of oil production

Oil palm production not only depends on the number and the biomass of bunches formed by trees each year but also on the amount of oil that can be recovered from bunches. In other words, the oil content in fresh mesocarp (OFM) and oil extraction rate (OER) are two critical parameters to assess lipid synthesis capability of trees. Both OFM and OER depend on K availability and crosses (Menon, 2000) (**FIG. III.3**). Here, we took advantage of the variance in OFM and OER values and statistical methods to find potential biomarkers of oil production rate. Univariate Pearson correlation and OPLS multivariate analysis (where OFM or OER were used as predicted Y variable) were computed. Since our metabolomics analyses showed that kinetics of lipid production may vary, we used relative changes in metabolite content from stage 3 to 5 as predictive X variables rather than metabolite contents at individual maturation stages. OPLS models were insignificant ($P_{CV\text{-}ANOVA}$>0.05) demonstrating that the variance in metabolic composition and oil production was too small to generate a very strong statistical model. This result is unsurprising since the window of OER or OFM values across all conditions was narrow

(a few %, FIG. III.3). However, OPLS models explained nearly all of the variance (R^2=0.999 and 0.922 for OER and OFM, respectively) and were robust for OER (Q^2= 0.511) (FIG. III.12).

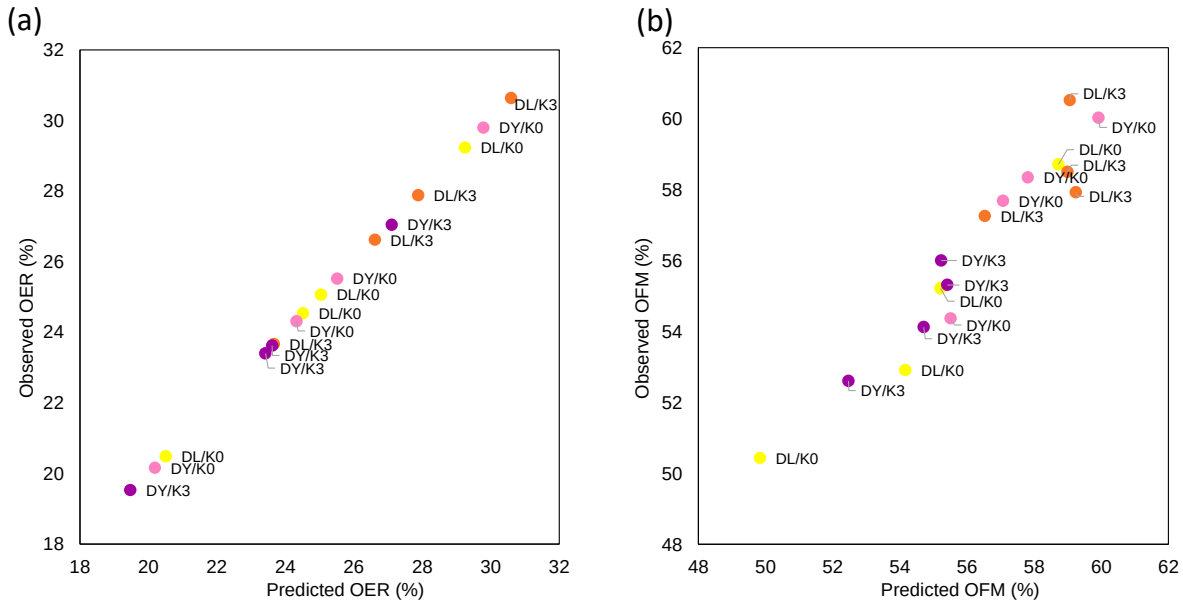

Figure III.12. Robustness of the relationship between oil content and mesocarp metabolome in the OPLS statistical models with OER or OFM as a quantitative predicted Y variable. This figure shows the linear relationship between observed (*y*-axis) and predicted (*x*-axis) values of (a) OER and (b) OFM

Univariate Pearson correlation analysis showed that OER was strongly correlated not only to morphological parameters (fruit-to-bunch ratio and bunch biomass) but also to 2-hydroxypyridine (TABLE III.1). The correlation with morphological parameters comes as no surprise since it reflects the importance of fruit set rather than fruit size per se (FIG. III.3). OFM appeared to be positively correlated to hexoses (fructose, glucose) as well as pipecolate, aminoisobutyrate and dopamine (which are products of lysine, leucine and tyrosine degradation, respectively) and β-alanine and triethanolamine (TABLE III.1). In contrast, OFM was negatively correlated to caprate, glycerol 1-phosphate and a compound possibly identified as lauryl salicylate. This shows that final oil content in mesocarp is related to *(i)* the velocity of lipid production (and thus anticorrelates to pools of intermediates of lipid synthesis), *(ii)* the availability of carbon source (sugars) and *(iii)* the ability to break down amino acids and thus metabolic recycling to other N-containing metabolites (β-alanine, triethanolamine, in addition to putrescine discussed above in DL).

Table III.1. Correlation analysis between oil content and mesocarp metabolome. List of

agronomical factors and metabolites significantly correlated to (a) oil extraction rate (OER) and (b) oil content in fresh mesocarp (OFM). The correlation coefficient (which is equal to p_{corr} in the OPLS analysis) and the *P*-value (significance of the correlation with univariate analysis) are listed for all features with a *P*-value lower than 0.05.

(a)

OER	Pcorr	P-value
Fruit/bunch	0.892	0.0001
Bunch weight	0.578	0.019
2-Hydroxypyridine	0.572	0.021

(b)

OFM	Pcorr	P-value
Triethanolamine	0.608	0.012
Caprylate	-0.578	0.019
Pipecolate	0.575	0.020
3-aminoisobutyrate	0.555	0.026
Glucose 1	0.553	0.026
Beta-alanine	0.549	0.028
Glucose 2	0.543	0.030
Caprate	-0.536	0.033
Ukn	-0.531	0.034
Fructose 2	0.524	0.037
Glycerol 1-phosphate	-0.520	0.039
Dopamine	0.509	0.044
Fructose 1	0.504	0.047

Taken as a whole, our study shows that K availability had a significant effect on mesocarp metabolism but composition of fruit oil at maturity was not significantly affected. This demonstrates that even though K changed metabolic fluxes in lipid synthesis and source sugar utilization and recycling, it had little effect on oil production.

D. Acknowledgements

C. Mirande-Ney is grateful to CIRAD for the PhD fellowship funding and for financial support of the experiments and divers analyses. The authors would like to thank the company SOCFINDO for their material and technical support during field experiment, as well as Bertrand Gakiere from the facility Metabolism-Metabolome (IPS2). We also thank Jean Ollivier for providing agronomical data.

E. Associated content:

Analysis of leaf mineral content and metabolites involved in oil palm mesocarp maturation and oil biosynthesis. This material is available free of charge via the Internet at http://pubs.acs.org.

Preamble

In Chapters II and III of this thesis, we have identified main metabolic pathways impacted by potassium fertilization in leaflets and fruits. In order to better understand metabolic dynamics and the flux of carbon from leaflet assimilation to fruits, further physiological studies are necessary. The idea of this last part is to offer a new perspective for analysing carbon fluxes in adult trees upon different conditions of potassium fertilization using stable isotope of carbon, ^{12}C and ^{13}C. More precisely, our intention was to know how K reshaped sugar production and allocation from source organ (leaflets) to sink organs.

The experiment was performed in 2017, where rather small effects of potassium were found due to previous fertilization and therefore, there was little modification of leaflet metabolism by K treatments (despite significant changes in some metabolites, see Chapter II). Nevertheless, this study represents an innovative work using, for the first time, $^{13}CO_2$ labelling in oil palm in the field. This was a challenging part of the thesis, because of leaf size and field conditions, which both made gas-exchange coupled to ^{13}C tracing rather difficult. In addition, a purpose-built chamber was designed and constructed to enclose leaves for labelling them with $^{13}CO_2$. It should also be noted that this experiment was expensive (typically due to the cost of travel, $^{13}CO_2$ and subsequent isotopic analyses) and could not be repeated in 2018. In what follows, the results are structured using the general form of an article draft that has not been submitted for publication to a journal yet.

Chapter IV. A $^{13}CO_2$ labelling experiment to study carbohydrates production and transport from leaves to sink organs under different potassium conditions in oil palm tree.

Cathleen Mirande-Ney[1,4*], Guillaume Tcherkez[2], Jaleh Ghashghaie[3], Emmanuelle Lamade[1]

[1]Unité PERSYST, UPR34, Système de pérennes, Centre de Coopération Internationale en Recherche Agronomique pour le Développement, F-34398 Montpellier, France.

[2]Research School of Biology, Australian National University, Canberra 2601, ACT, Australia.

[3]Ecologie Systématique Evolution, Université Paris-Sud, CNRS, AgroParisTech, Université Paris-Saclay, 91400, Orsay, France.

Abstract

In this study, we performed for the first time a $^{13}CO_2$ pulse-labelling experiment on oil palm leaves, submitted to two potassium fertilization conditions and two crosses in the field. The goal of this study was a better understanding of metabolic dynamics and the flux of carbon from leaflet assimilation to fruits of oil palm. Preliminary results showed that $^{13}CO_2$ injected into the chamber was effectively fixed into leaflet organic matter (OM), demonstrating that the labelling experiment was successful. However, the efficacy of labelling was much less than expected. For technical reasons, such as high temperature or air relative humidity, less than 27% of $^{13}CO_2$ added to air composition in the chamber was assimilated by leaflets. Also, $\delta^{13}C$ values after labelling were found to be sensitive to climatic variations such as temperature and RH, there was a strong variability between replicate that made difficult the interpretation of the data in terms of effect of K on carbon metabolism in the leaflet. However, we could observe some tendency for K to increase leaflet starch content, and the kinetics of the decline in $\delta^{13}C$ after labelling suggests there were 2 pools of C: a bigger pool representing (or feeding) leaf biomass, and a smaller “labile” (exportable) pool. The labile pool had a mean turn-over time of up to 130 h suggesting that photosynthate export rate is low.

A. Introduction

The oil palm (*Elaeis guineensis* Jacq.) is one of the most productive oil crops, with a potential yield reaching 40 t fresh fruit biomass ha^{-1} yr^{-1} due to its high photosynthetic capacity (from 23 to 30 µmol m^{-2} s^{-1}) for a C_3 plant and an important carbon allocation to fruits (Lamade *et al.*, 2009). Among the ten major oil seeds, oil palm accounted for only 5.5% of agricultural land surface area planted with oil crops, and oil palm represents 35% of global consumption in oils and fats, a number that is larger than for any other crop (Statista, 2019). Moreover, with growing demand for food and decreasingly available arable land, improving yield becomes central in oil palm producer interests. According to FAO (2012), the global demand for palm oil will double by 2020, and triple by 2050. The positive effect of potassium on fresh fruit yield is well known. While oil composition at maturity did not significantly change under low K conditions, we found clear alterations in fruit metabolism associated with lipid production during maturation with K fertilization (Mirande-Ney *et al.*, 2019).

Some (eco)physiological studies allowed to get a better understanding of oil palm physiology, with the ultimate objective to improve fruit bunch production. They concerned (i) distribution of assimilated carbon (Lamade *et al.*, 2016); (ii) reserve carbon pools under source constraints such as pruning (Legros *et al.*, 2009b); (iii) plant response to variable environmental conditions (Legros *et al.*, 2009a); (iv) functional relationship and dependency between autotrophic source organs and heterotrophic sink tissues (Lamade *et al.*, 2009); and (v) the carbon transfer and allocation pathways at the tree scale (Lamade & Setiyo, 1996; Lamade *et al.*, 2009). In particular, in a recent study, Lamade *et al.* (2016) have computed plausible carbon fluxes (allocation patterns) using natural ^{13}C abundance ($\delta^{13}C$ values) and a steady-state model of ^{13}C-distribution. However, the effect of potassium fertilization on oil palm carbon fluxes related to yield has been not investigated yet.

Stable isotopes are sensitive and multipurpose tools to study various climatic and environmental effects on plant physiology since their natural abundance responds to key parameters such as CO_2 mole fraction, humidity, etc. (Saurer *et al.*, 2016). In particular, the ^{13}C natural abundance (isotope composition, $\delta^{13}C$) in plant organic matter gives information on photosynthesis. In fact, photosynthates of C_3 plants are ^{13}C-depleted by about 20‰ compared to atmospheric carbon dioxide because of the isotope discrimination during photosynthesis. Importantly, the $\delta^{13}C$ value of net assimilated carbon (photosynthates) not only depends on the

isotope composition of the inorganic source (atmospheric CO_2) but also on isotope fractionation processes associated with transport, diffusion, phase transition, and enzyme reactions in the plant. Here, the term "fractionation" refers to the change in the $\delta^{13}C$ between substrate and product due to different velocity of isotopic molecules (isotopologues) (i.e., the ratio of rates $^{12}v/^{13}v$ differs from unity). In practice, the $\delta^{13}C$ value of organic plant material can be modelled as (neglecting the denominator, and neglecting internal resistance):

$$\delta^{13}C_{leaf} \approx \delta^{13}C_{atm} - a - (b - a)\cdot c_i/c_a \quad (1)$$

where $\delta^{13}C_{atm}$ is the carbon isotope ratio of atmospheric CO_2 (about –8‰), a is the fractionation caused by diffusion (4.4‰), b is the apparent biochemical fractionation associated with carbon dioxide fixation by primary carboxylating enzymes, mainly Rubisco (here, 27‰), and c_i/c_a is the intercellular-to-ambient ratio of CO_2 mole fraction (Francey & Farquhar, 1982). It is clear in Eq (1) that the $\delta^{13}C$ value of a given plant tissue reflects both the carbon source and fractionations along metabolism, thereby providing physiological information (Offermann *et al.*, 2011). At the whole plant scale, the carbon isotopic signal is primarily determined by photosynthesis, that is, by the $\delta^{13}C$ value of photosynthates. Sugars exported by leaves via the phloem to sink tissues (like fruits) are used to synthesize organic matter and thus sink organs are isotopically close to leaves, but with some further fractionation steps referred to as "post-photosynthetic" fractionation may take place (Gessler *et al.*, 2009). As a result, sink organs are generally ^{13}C-enriched compared to leaves, by a few ‰.

Here we took advantage of ^{13}C labelling and quantified how the isotope composition in leaf matter and respired CO_2 deviated from natural abundance after photosynthesis in a $^{13}CO_2$-containing atmosphere. Labelling of plants with isotopically enriched CO_2 has been used for decades (mostly with ^{14}C up to the 80s) to study the fate of carbon into photosynthetic products in leaves. Pulse-labelling has already been used to examine where photosynthetically fixed carbon is allocated and how fast it is transferred in trees (Epron *et al.*, 2012). In this study, we performed for the first time a $^{13}CO_2$ pulse-labelling experiment on oil palm leaves, submitted to two potassium fertilization conditions: K0 (no KCl applied) and K3 (with 4.5 kg KCl tree^{-1} yr $^{-1}$), and two crosses (*Deli x La Mé* (DL) and *Deli x Yangambi* (DY)), in the field. Our primary objectives were to (i) determine the nature of the prevalent sugar exported by leaves (sucrose or glucose); (ii) follow the export of carbon from leaves to other organs; (iii) understand carbon dynamics in leaves after photosynthesis (in particular, utilization by respiration); and (iv) know

whether all these processes are affected by K availability. Amongst these objectives, mainly (iii) is addressed here. Objective (i) is still in progress (samples collected in this experiment were not of sufficient quality to allow reliable NMR analyses) and will not be reported here. Objective (ii) has been partly addressed and will be discussed at the end. As stated above in the Preamble, objective (iv) is superficially dealt with here and awaits further experiments when the K treatment has more tangible effects on photosynthesis and allocation.

B. Material and methods

1. Field location and fertilization

The field was located at the SOCFINDO station (North Sumatra, Indonesia; 3°18'19.60"N, 99°3'24.33"E). The experiment was carried out in July 2017 on oil palm trees planted in August 2013 and organized inside a K factorial agronomic trial. They belonged to two crosses: *Deli x La Mé* (DL) and *Deli x Yangambi* (DY). DL and DY have been chosen here since they are two very common crosses used in oil palm agroforestry and presented, at nursery stage, contrasting K foliar signature with DL "K--"and DY K++. Two levels of potassium fertilization were studied: (K0), no KCl added and (K3) with 4.5 kg KCl $tree^{-1}$ yr^{-1}.Trees were fertilized with nitrogen using 2 kg urea $tree^{-1}$ yr^{-1}. There was no K deficiency under K0 conditions, since K content in soil under the K0 treatment represents about 0.2 meq exchangeable K per 100 g soil, coming from some K remained from previous agronomic trials conducted before on the same location (information from soil analysis). As such, oil palm tree tissues were not under very low or very high K conditions and K content was always in the 18-38 mmol m^{-2} range.

2. Climatic conditions

Climatic conditions (solar radiation, rainfall, temperature and relative humidity) were recorded near the fertilizer trial at Bangun Bandar (Nord Sumatra, Indonesia) using a mini-meteorological station (Watchdog, Spectrum, France). The local weather was characterized by a rainy season in September-December for both years (2017-2018) with low solar radiation and temperature and high relative humidity. Solar radiation varied between 428 MJ/m^2 and 603 MJ/m^2, with a maximum in June 2017 and a minimum in December 2017. Temperature varied

from 21.6 to 35.6 °C. Rainfall peaked at 460.3 mm in December 2017, with almost no rain between May and July 2017. Nevertheless, no sign of water stress could be detected in the field in July 2017. In fact, each tree studied were watered on the night before the labelling to make sure that stomates were fully opened at the beginning of the experiment in the following morning at 7 am.

3. Functional traits

Specific leaf weight (SLW) was measured, as dry weight per leaf surface area (kg DW m^{-2}) by weighing precisely 30 leaflets samples of 10 cm^2 of each on a representative palm of the crown. Leaf area was determined in 2017 on the leaf rank number 17 following the method of Tailliez and Ballo (1992). Overall foliar emission rate was calculated as the number of leaves present on the tree plus petiolar bases (corresponding to cut leaves) divided by tree age. Trunk heights (from the limit of the trunk basal bud to the petiole insertion of leaf rank number 33) were determined using a meter, and diameters were measured (at 1 m high from trunk base) with a specific caliper, respecting CIRAD standard procedure. Functional traits were determined on 5 replicates per condition for a better representation of the treatment effect.

4. Experimental design and sampling

Overview. The $^{13}CO_2$ pulse-labelling experiment was carried out on 12 oil palm trees (3 replicates per condition) using a closed chamber system where CO_2 is injected to maintain its mole fraction. For this purpose, a palm portion of 1m of rachis length, centered at point B of potential leaf rank number for gas exchanges (usually 10 but mainly varied until 14). In some cases, when palm 10 was absent or in bad shape, other palms (11, 12 or 14) which have approximatively the same age were used instead. See **PICTURES S1-S7** illustrating the whole experiment.

The labelling chamber. For this labelling, we did a purpose-built transparent chamber with a rectangular form and a volume of 0.38 m^3 (1.9 m x 1 m x 0.2 m). It was made of stainless steel half-plates covered with a polypropylene film with rectangular openings to allow the entrance of the rachis (**FIG. IV.1**). Air tightness was obtained with mastic (Terobon RB VII) and

adhesive tape. Six axial fans (12 V) were placed in the labelling chamber to ensure good air mixing and a cold water bath (located outside) was used to help to cool air tube (connected to the pump) for maintaining air temperature inside the labelling chamber. Temperature, humidity and solar radiation were recorded inside the labelling chamber using a small meteorological station. $^{13}CO_2$ circulation was obtained through the chamber and tubing (BEV A LINE IV 3.2 x 6.4 mm, Fischer Scientific, Illkirsh, France) using a pump (IP00-T 230V50HZ N828KNE, KNF, Village-Neuf, France). Silica gel was used to decrease humidity generated by high leaf transpiration rates after the closing of chamber. The labelling chamber is held by a scaffold made of wood. In the field, electricity was provided using a generator. Because the chamber was installed in the canopy, upper leaves were folded away to avoid shading.

The $^{13}CO_2$ - labelling experiment. The central B leaf region (composed of around 20 leaflets) was enclosed with care in the chamber and both entrances were then sealed with mastic (See **FIG. IV.2**). During all this time and after closing the chamber, the CO_2 concentration inside the labelling chamber was continuously monitored with a gas analyzer (WALZ GFS 3000, Germany) that was designed and calibrated for $^{12}CO_2$ and exhibited low sensitivity to $^{13}CO_2$. When the chamber was closed, the CO_2 mole fraction decreased linearly from ambient (≈400 ppm) with an average of 0.37 ppm s^{-1} due to CO_2 uptake by photosynthesis. When the CO_2 mole fraction reached 200 ppm, $^{13}CO_2$ was added to reach again 400 ppm inside the chamber (which equals external conditions). Pure $^{13}CO_2$ (99.3%, Euriso-top, Saint-Aubin, France) was then constantly injected at a flow rate that compensated for photosynthetic consumption, using a mass flow controller (EL-FLOW Prestige, Bronkhorst, Montigny-Les-Cormeilles, France). Because of the low sensitivity of the gas analyzer to $^{13}CO_2$, the slope of the CO_2 decline in the beginning of the experiment was used to calculate net CO_2 uptake and thus adjust immediately the flow rate of the $^{13}CO_2$ injector. The observed flow rate for all trees was 6-10 mL min^{-1}. The labelling was stopped when 1 L of $^{13}CO_2$ had been injected in the chamber. The time required to do so was 2-5 hours, depending on individual CO_2 palm absorption and leaf surface area. At the end, the chamber was rapidly opened and removed and leaflets were sampled. Labelling started at about 8:00 AM local time and ended no later than 3:00 PM.

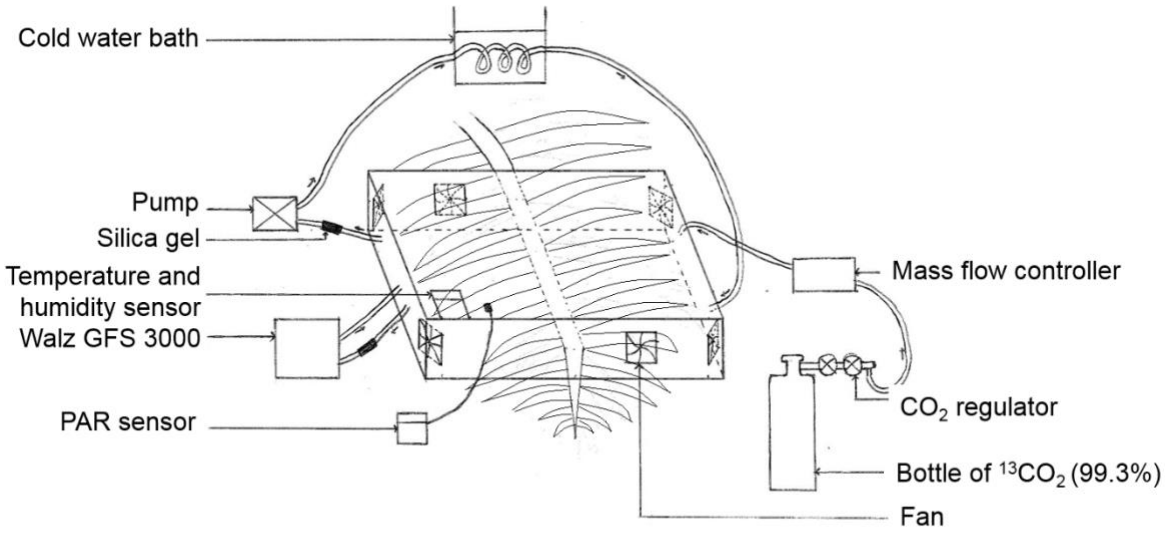

Figure IV.1. Scheme of the 13CO2 labelling. The closed system used is alimented by pure 13CO2 (99.3%) with a CO2 and mass flow regulator allowing a constant flow that compensated for photosynthetic consumption. The flow is also maintained using a pump, silica gel was used to decrease humidity generated by high leaf transpiration rates after the closing of chamber, CO2 level was controlled with a gas analyzer (WALZ GFS 3000, Germany), a cold water bath was used to help to cool air tube, air inside the chamber was homogenized with fans and, temperature, humidity and solar radiation (PAR) were monitored with sensors. Small arrows indicates the sens of the flow.

Figure IV.2. Photographs of (a) the whole $^{13}CO_2$ labeling experiment installation in the field and (b) external view of an oil palm leaf enclosed in the labeling chamber.

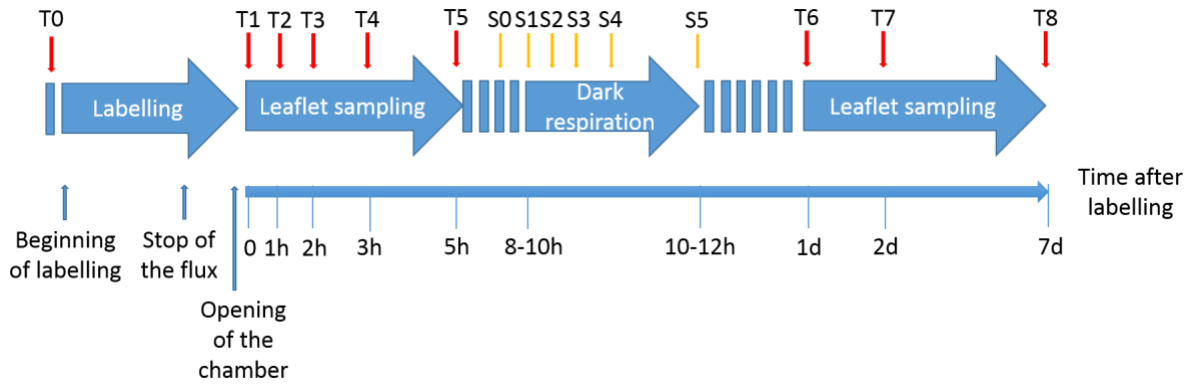

Figure IV.3. Temporal design of the experiment. The labelling duration was about 2-5h depending on the CO_2 consumption of each tree. The chamber was opened 1h after the stop of the flux. Leaflet were sampled at: T0, before the labelling, T1, just after opening after labelling, and then at T2-T8, 1h, 2h, 3h, 5 h and 1, 2 and 7 days later. Dark respiration analysis started 8 to 10h after the labelling depending on the tree and was performed during 2h. CO_2 sampling inside the chamber took place at: S0, before the installation of the chamber (control with no respired CO_2) and S1-S5, 5 min, 10 min, 30 min, 1h and 2h later using a 25 mL syringe.

Samples preparation and isotope analysis. Leaflets were collected just before placing the leaf in the labelling chamber and just after opening after labelling, and then 1h, 2h, 3h, 5h and 1, 2 and 7 days later (**FIG. IV.3**). One leaflet was sampled per time point randomly on both sides of the rachis at the point B of the palm labelled. Seven days after the experiment, leaflets from the palm rank 1, 9, 17, 25, 33, 41 and 49 were also sampled (at point B) from the labelled trees. Leaflet samples were cleaned with deionized water, frozen in liquid nitrogen, stored at −20 °C, and finally oven-dried and ground. Leaflet organic matter (OM) samples were weighed in tin capsules and analyzed for C isotope composition and total C using an elemental analyzer (Carlo-Erba) coupled to an isotope ratio mass spectrometer (Isochrom, Elementar) run in continuous flow at the Isotope Facility of the Australian National University.

Calculations

^{13}C excess. The ^{13}C atom fraction (percentage), denoted as $x(^{13}C)$, was calculated from the isotope composition ($\delta^{13}C$) using the isotope ratio ($R_{V\text{-}PDB}$) of V-PDB (Vienna Pee Dee Belemnite standard, 0.0112372):

$$x(^{13}C) = {}^{13}C/({}^{12}C+{}^{13}C) = (\delta^{13}C+1)\times R_{V\text{-}PDB}/((\delta^{13}C+1)\times R_{V\text{-}PDB} + 1) \quad (2)$$

While the isotope composition ($\delta^{13}C$) at natural abundance levels is often expressed as a ratio relative to V-PDB, the isotope composition of an enriched compartment can be better expressed as percent atom excess because in denominators, the isotope ratio is not negligible compared to unity (Dawson *et al.*, 2002). This value is defined using percentages, as the relative ^{13}C abundance in a labelled sample exceeding the natural isotope abundance in an unlabelled sample. Percent atom excess ^{13}C, denoted as $x_E(^{13}C)$, was calculated therefore after accounting for the background ^{13}C atom fraction measured on the same tree before labelling, $x(^{13}C_{UN})$:

$$x_E(^{13}C) = x(^{13}C) - x(^{13}C_{UN}) \quad (3)$$

$x_E(^{13}C)$ in leaflets was calculated for each tree at each sampling time.

Turnover of assimilated C. In order to assess differences in C turnover, we consider two general pools of C turnover within leaflet as in Epron *et al.* (2012); Subke *et al.* (2012): (1) a labile C pool (photosynthates), and (2) leaf biomass C. All assimilated C initially forms part of the labile, non-structural C pool (Pool 1), which includes all water-soluble forms of carbohydrates (i.e. also sugars stored in cell vacuoles). As this labile pool turns over, a small fraction of it becomes incorporated into leaf biomass (Pool 2), whilst the rest is either exported to other plant parts via the phloem, or respired by the leaf.

In order to calculate the export rate of labile C, we fitted the following exponential decay function in Eq. (4) to the excess ^{13}C and x_E (^{13}C) leaflet:

$$x_E(^{13}C) = C_S + C_L * \exp(-\tau t) \quad (4)$$

where t is the time since pulse-labelling (in hours), and C_S, C_L and τ are fitted parameters. In doing so, we assume that the overall pool sizes do not change over the observation period, i.e. that the reduction in ^{13}C abundance in Pool 1 is caused by respiratory loss, phloem export or incorporation into Pool 2 and not by dilution due to an increase in unlabelled C subsequent to the ^{13}C pulse. We recognize that a double exponential decay would be more appropriate to model ^{13}C dynamics, in particular because it is unlikely that only one labile pool is representative of metabolic partitioning. However, we chose to use a simple exponential decay because it fitted satisfactorily our data and our time resolution would be insufficient to fit a

double exponential function reliably. We estimated the mean residence time (MRT) of labile C with Eq. (5) as the reciprocal of the decay constant (τ):

$$MRT=\tau_{-1} \qquad (5)$$

The asymptote of the exponential decay function (C_S) indicates the amount of labelled C not affected by the exponential decay, i.e. the amount of C that would remain in the leaf once the labile pool of labelled C (C_L) is completely turned over.

Dark respiration. The night following the labelling experiment, dark respiration was quantified by analyzing CO_2 respired by the same palm portion labelled in the morning using the same chamber. Experiment started at about 8:00 PM and lasted for 2h. Immediately after closing the chamber, the CO_2 mole fraction inside the chamber was continuously monitored with the gas analyzer. The CO_2 mole fraction increased linearly after the chamber was closed because of CO_2 release by respiration and the slope was computed. The CO_2 respired was sampled just before the installation of the chamber (control with no respired CO_2) and directly after the closing, 5 min, 10 min, 30 min, 1h and 2h later (**FIG. IV.3**) using a 25 mL syringe, collected inside 5 mL air tight glass vials and sealed with parafilm. Glass vials were kept at -20°C until analysis. The analysis was carried out by the platform GISMO (Bourgogne, France) using a GC-C-IRMS (Gas Chromatography- Combustion- Isotope Ratio Mass Spectrometry). The isotope composition of respired CO_2 was obtained by linear regression using a Keeling plot.

5. Statistical analysis

For all analyses, 3 replicates were taken for all conditions. Univariate analyses were conducted using a two-way ANOVA (SigmaPlot version 11.0) (Fisher test with a threshold P-value of 0.05) with crosses and K as factors, followed by a post-hoc Tukey test. Also, to investigate correlations between leaflet K content or carbon isotopic signature and functional traits, a Pearson correlation was assessed. MRT was determined using a fitted exponential decay model with SigmaPlot.

C. Results and discussion

1. Functional traits and leaflet starch content of oil palms studied

Foliar emission (FE), leaf area (LA), SLW, trunk height and diameter were determined for each K and cross conditions. Fisher tests showed, as expected, that except for trunk diameter significantly affected by both K level (P=0.01) and crosses (P=0.02), potassium and crosses did not affect significantly other traits such as FE, LA, SLW or trunk height (**FIG. IV.4**), as observed elsewhere (Ruer & Varéchon, 1964; Corley, R & Mok, CK, 1972; Purwanto *et al.*, 2018). Trees emitted approximatively two new leaves by month with a leaf area of 5 m² in average with a specific weigh of about 0.102 kg DW m^{-2}. In 2017, trees were 4 - years old, with a trunk height of about 87 cm and a diameter of 76 cm. They produced between 18 and 25 bunches per year (Mirande-Ney *et al.*, 2019). Trunk diameter increased slightly by 5% at high K (K3) and was higher in DL compared to DY. At this stage, K3 had a small positive effect on bunch production in DY only, but not in DL. FFB was higher in DL compared to DY (see Mirande-Ney *et al.* (2019)).

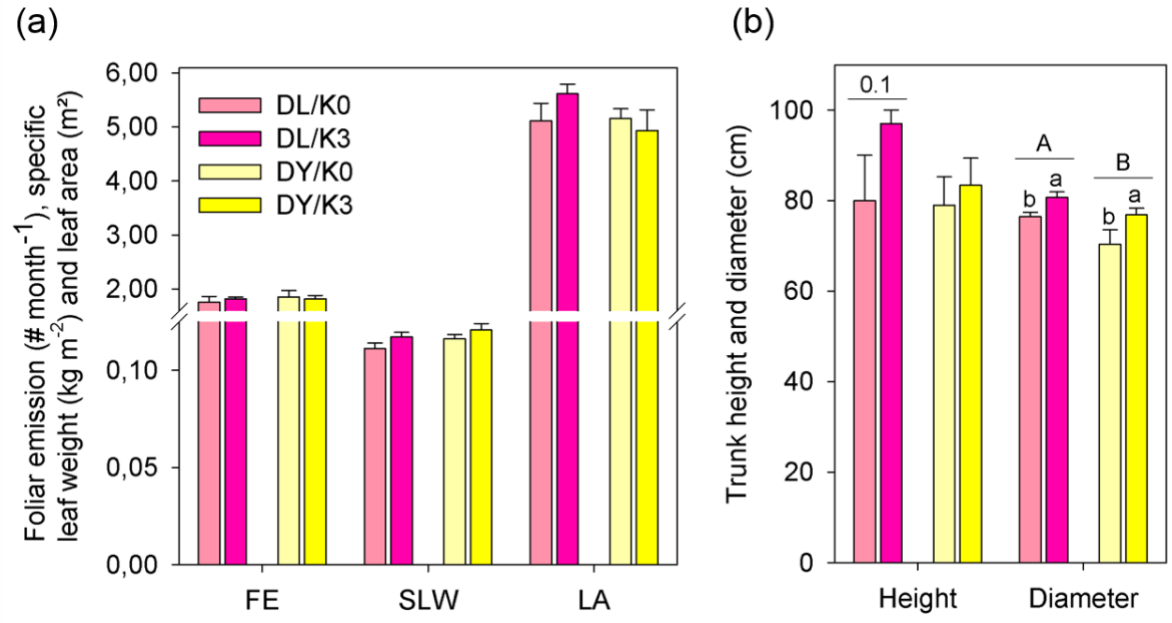

Figure IV.4. Overview of functional traits of oil palm in DL and DY under K0 and K3 treatments. (a) Foliar emission (FE), specific leaf weight (SLW), leaf area (LA), (b) trunk height and trunk diameter variations with K0 and K3 and in DL and DY. FE stands for the number of leaf emitted per month and SLW, LA and trunk height and diameter are given in kg m^{-2}, m^2 and cm. Mean ± SE (n = 5). Letters stand for statistical classes (Tukey test, P<0.05). When non-significant, the P-value is written.

Although K fertilization had small effects on tree morphology and phenology, leaf K content (documented further in Chapter II) was found to be correlated to crosses (R = 0.82, P-value = 0.01), but also (i.e. with positive R) to photosynthesis, leaflet chlorine content and oil-to-bunch ratio, while it appeared to be insignificant (TABLE IV.1). These results are not surprising since K was added as KCl thereby providing chlorine. Also the positive effect of K on photosynthesis is well known (see Introduction of the thesis). However, univariate analysis showed no significant effect of potassium fertilization conditions or cross on photosynthesis (FIG. IV.5). In Chapter II, we have seen effectively that there was no significant effect of potassium fertilization or cross on leaflet K content in 2017. It seems therefore that, although leaflet mineral composition does not reflect yet fertilization condition, oil palm reacts to small variations of leaflet K content to modulate its photosynthesis. Under our labelling conditions, photosynthesis was on average about 6 µmol m^{-2} s^{-1} in DL and 5.3 µmol m^{-2} s^{-1} in DY, far from average usually admitted for oil palm, around 11 µmol m^{-2} s^{-1} (Lamade *et al.*, 2016) for the same ecology and age. This was perhaps due to poor air conditioning of the chamber while under tropical conditions in Sumatra, incident radiation was high, with PAR values about 2000 µmol m^{-2} s^{-1} and high air temperature was also high, above 30 °C.

Table IV.1. Correlation analysis between leaflet K content and oil palm functional traits.

Leaflet K content	R	Pvalue
Palm 17 length	-0.70	0.05
Bunch biomass (kg DW)	-0.68	0.07
Leaflet N content	-0.66	0.08
%C T0	-0.65	0.08
Average diameter	-0.65	0.08
Labelling time	-0.57	0.14
Trunk biomass	-0.54	0.93
Trunk volume	-0.54	0.17
Leaf area	-0.51	0.20
Bunch number (2017)	-0.51	0.20
Photosynthesis	0.52	0.19
Leaflet Cl content	0.54	0.73
Oil-to-mesocarp ratio	0.62	0.10
Cross	0.82	0.01 **

Moreover, when we looked at starch content variations in leaflets under different K fertilization conditions and crosses, no significant effect of K or cross was observed while high K caused a decrease in leaflet starch content in DL and an increase in DY (**FIG. IV.6**). This is surprising considering that via its action on starch synthase, potassium is known to be positively correlated to leaflet starch content (Ward, 1959; Läuchli & Pflüger, 1978). The effect of K on leaflet starch content seemed to be therefore cross-dependent. Starch content varied between 15 and 35 kg g_{-1} DW.

Interestingly, leaflet K content was also anti-correlated to palm length, bunch biomass, leaflet N and C content and average diameter (**TABLE IV.1**), while these parameters are also cross-dependent. It is possible that K has an effect on carbon partitioning but further investigations are required to differentiate the effect of K from that of the cross (genotype) itself. Having said that, an effect of K on carbon partitioning would not be surprising because of its action on sugar synthesis and transport. Lamade *et al.* (2014) have shown in fact a co-occurrence of K_+ and hexoses (glucose) in heterotrophic tissues (trunk, rachis, rachis bunch), suggesting an effect of K on sugar redistribution. While insignificant, it seems also that potassium addition tends to increase dark respiration rate in DY (**FIG. IV.5**).

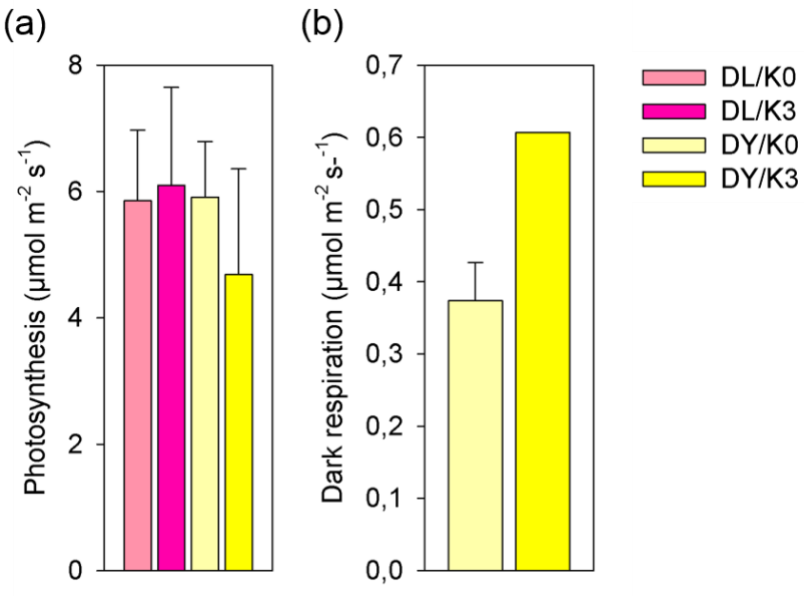

Figure IV.5. Photosynthesis and respiration rate variation upon K fertilization for both crosses DL and DY. Photosynthesis and respiration rate are given in micromoles per square meter per second. Respiration rate was calculated only in DY. Mean ± SE (n = 3).

In another trial with the same conditions (reported in Chapter II), potassium also had a positive

effect on photosynthesis and respiration. Dark respiration was on average 0.47 µmol m^{-2} s^{-1} in DY, similar to the values observed in the other trial.

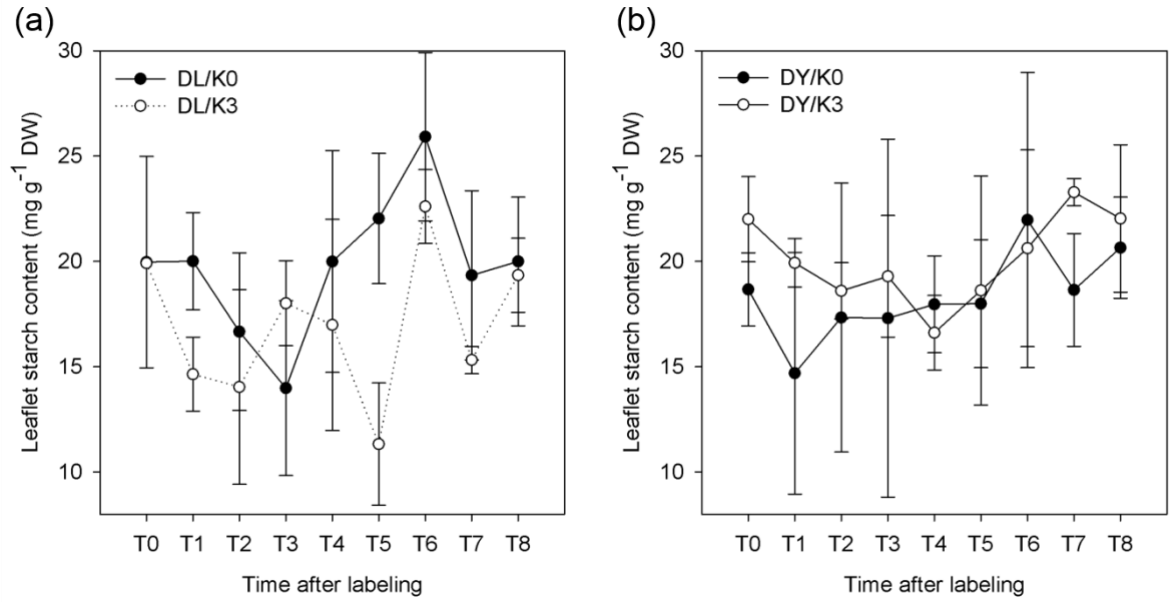

Figure IV.6. Variations of leaflet starch content upon K fertilization in (a) DL and (b) DY over different time periods after the $^{13}CO_2$ labelling. Leaflet starch content are given in milligrams per gram of dry weight. They were measured on labelled leaflet until 7 days after labelling. T0 correspond to the time before the labelling and T1-T8 correspond to 1h, 2h, 3h, 5 h and 1, 2 and 7 days after the labelling. Mean ± SE (n = 3).

2. ^{13}C natural abundance in leaflet total organic matter (OM)

At natural abundance, on average, $\delta^{13}C$ (OM) was about -30.3 ‰ in DL (K0, -30.5 ‰ and K3, -30.67 ‰) and -29.9 ‰ in DY (K0, -30.44 ‰ and K3, -29.41 ‰) close to the $\delta^{13}C$ value observed in leaflet by Lamade *et al.* (2009); Lamade *et al.* (2016); Muhammad *et al.* (2017). Univariate analysis on $\delta^{13}C$ value of OM between conditions showed no significant effect of K or cross. Since K availability is known to affect photosynthesis and carbon allocation in oil palm (Legros *et al.*, 2006), an impact on leaflet $\delta^{13}C$ could have been expected. Here, the effect of K fertilization was too small to affect significantly c_i/c_a and thus the photosynthetic fractionation.

In general, leaf $\delta_{13}C$ values at natural abundance depends on many factors such as climatic conditions but also leaflet functional traits (Saurer *et al.*, 2016). In our study, $\delta_{13}C$ values at T0 (i.e. at natural abundance) were correlated to average air relative humidity in the cultivation field and leaflet starch content determined just after photosynthesis in the chamber, but anti-correlated to average temperature and leaf length (TABLE IV.2). These relationships may indicate a link between the natural abundance and photosynthetic capacity since at high carboxylation velocity for a fixed stomatal conductance, c_i/c_a is low. Although insignificant, leaflet $\delta_{13}C$ was also correlated to fruit starch content at stage 3 as reported in Mirande-Ney *et al.* (2019), crosses, leaflet chlorine (Cl) content and replicates, and anti-correlated to leaf area, bunch biomass, bunch weight and bunch number. This tendency might be driven by K considering its known effects on bunch production, leaf area or carbohydrate metabolism (Legros *et al.*, 2006; Legros *et al.*, 2009b; Battie-Laclau *et al.*, 2014).

Table IV.2. Correlation analysis between leaflet carbon isotopic signatures at natural abundance ($\delta_{13}C$ (T0)) and just after the labelling ($\delta_{13}C$ (T1)), and oil palm functional traits. Significant correlation are written in red.

$\delta^{13}C$(T0)	R	P value
Palm 17 length	-0.71	0.05
Leaf area	-0.67	0.07
Bunch biomass (kg DW)	-0.67	0.07
Bunch weight	-0.64	0.09
Average T(°C)	-0.60	0.04
Bunch number (2017)	-0.56	0.15
Rep	0.54	0.17
Leaflet starch content (T1)	0.60	0.04
RH avg	0.62	0.03
Leaflet Cl content	0.65	0.13
Cross	0.67	0.07
Fruits starch content (Stage 3)	0.69	0.06

$\delta^{13}C$(T1)	R	P value
Labelling time	-0.65	0.02
SLW (g/m²)	-0.60	0.12
Leaflet starch content (day)	-0.55	0.16
%C T0	-0.51	0.20
Leaflet starch content (T1)	0.52	0.08
Fruit-to-bunch ratio	0.53	0.17
RH max	0.55	0.07
Leaflet Cl content	0.58	0.03
Photosynthesis (µmol/m²/s)	0.69	0.01
Leaflet starch content (night)	0.75	0.03

3. Dynamics of ^{13}C in leaflets after labelling

Clearly, $^{13}CO_2$ injected into the chamber was fixed into leaflet organic matter (OM), showing that the labelling experiment was successful. However, when we compared the amount of ^{13}C found in the leaflet just after labelling to the amount of ^{13}C supposedly assimilated during the labelling time based on photosynthesis rate, it represented sometimes less than 10% (**TABLE IV.3**). The maximum of ^{13}C assimilated by leaflet was about 2623 µg ^{13}C/g C, representing only 27% of efficacy. Even though the export of photosynthates can explain a smaller-than-expected ^{13}C content, we expected to find at least 50%, which is in general the carbon partitioning to starch. Therefore, we can suppose that either there was a leak in the chamber leading to a loss of $^{13}CO_2$, or photosynthesis decreased/changed during the experiment maybe due to an insufficient temperature control. There could also be a problem at the end of the labelling when there was no $^{13}CO_2$ left (1 L $^{13}CO_2$ was consumed) but the leaf continued assimilation for some time. In fact, at this stage, leaflet experienced about 1 h without any supply of $^{13}CO_2$, and therefore CO_2 mole fraction should have decreased down to the compensation point.

Table IV.3. Summary of ^{13}C expected and effectively found in leaflet, according to the different conditions of K and crosses.

Cross	K Treatment	Rep	Expected leaflet ^{13}C content assimilated (µg ^{13}C/g C)	Leaflet ^{13}C content assimilated (µg ^{13}C/g C)	Proportion of ^{13}C effectively incorporated
DL	K0	1	9558	1882	19.7%
		2	10813	2584	23.9%
		3	9153	213	2.3%
	K3	1	9096	985	10.8%
		2	10111	1480	14.6%
		3	9722	2623	27.0%
DY	K0	1	9939	1779	17.9%
		2	9294	114	1.2%
		3	9649	310	3.2%
	K3	1	9098	103	1.1%
		2	9639	617	6.4%
		3	9327	2189	23.5%

When we looked at leaflet $\delta_{13}C$ just after labelling (T1), we could observe a strong variability between replicates in the same conditions (**TABLE IV.4**). Although leaflet $\delta_{13}C$ at T1 (denoted as $\delta_{13}C(T1)$) was not significantly affected by K, cross or replicates conditions, pearson correlation analyses revealed that $\delta_{13}C(T1)$ was strongly correlated to photosynthesis, and leaflet starch content during the night. Considering the fact that leaflets were not in optimal conditions of photosynthesis during the labelling due to high temperature and RH, these correlations showed that leaflet $\delta_{13}C$ was in fact very sensitive to photosynthetic processes (Saurer *et al.*, 2016) and may give insight on starch leaflet composition during the night thus carbon remobilization, thus respiration.

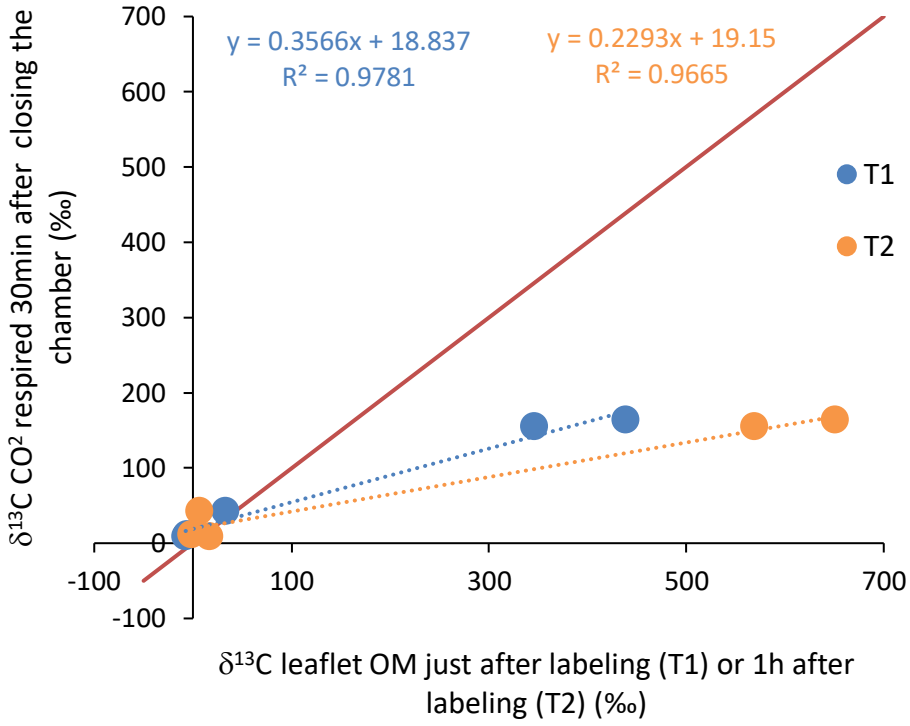

Figure IV.7. Correlation between $\delta_{13}C$ values of respired CO_2 and leaflet organic matter after labelling. Just after (T1) or 1h after (T2) a $^{13}CO_2$ pulse-labelling, leaflets OM of labelled palms were analyzed for C isotope composition using an elemental analyzer coupled to an isotope ratio mass spectrometer. In addition, the night following the labelling experiment CO_2 respired by labelled leaflets were sampled and $\delta_{13}C$ of respired CO_2 was determined for each sample using a GC-C-IRMS at S3, 30 min after closing the chamber. $\delta^{13}C$ values are given in part per million. Each point corresponds to $\delta^{13}C$ values of leaflet OM and CO_2 respired of K0 and K3 from DL trees (n=3). Dotted lines corresponds to linear regressions.

In fact, as shown in **FIG. IV.7**, $\delta_{13}C$ in leaflet OM after labelling was linearly correlated to $\delta_{13}C$ of respired CO_2 (r^2=0.98, *P*=0.001). Respired CO_2 had a $\delta_{13}C$ of about 164 ‰ 30min

after having closed the chamber the night following the labelling experiment. It represents about 0.53 of ^{13}C excess, that is about 64% of the mean of ^{13}C labile pool (C_L) (See **TABLE IV.4)** (maximum values of $\delta^{13}C$ of CO_2 respired were observed 30 min after having closed the chamber).

Unsurprisingly, ^{13}C excess in leaflet total organic matter was maximal just after labelling and decreased thereafter (**FIG. IV.8**). The decrease in leaflet ^{13}C excess with time could be explained by sugar transport to sink organs or losses by dark respiration. As for natural abundance, no significant effect of K or cross was found on excess ^{13}C after labeling. However, in a $^{13}CO_2$ labelling study on Eucalypt trees under K nutrition, (Epron *et al.*, 2016) have shown that K fertilization had a positive effect on crown CO_2 uptake and the amount of ^{13}C in excess recovered in leaves just after labelling. According to (Dannoura *et al.*, 2011), the shape of the curve given by the time course of excess ^{13}C is affected by the duration of the labelling, thus the photosynthesis, but also to seasonal conditions. We found in fact that, $\delta^{13}C(T1)$ was anti-correlated to temperature and leaflet %C.

The time course of excess ^{13}C, $x_E(^{13}C)$ in leaflet of labelled palms (**FIG. IV.8**) was fitted according to Eq. (4). This is based on the assumption there are two pools of ^{13}C in leaflets: representing a "stabilized" (i.e. fixed constant) pool (C_S) and a labile pool (C_L) that is turned-over exponentially (Epron *et al.*, 2012; Subke *et al.*, 2012). C_S accounted for 33% of total ^{13}C (C_S+C_L) in DL (35.5% in K0 and 30.6% in K3) and for 32.5% of total ^{13}C in DY (30.4% in K0 and 33.8% in K3) (**TABLE IV.4**). The ^{13}C pool associated with C_L decreased quite slowly, with a mean residence time ($1/\tau$) ranging from 2h to 130h that was longer in DL than in DY trees (but this difference was insignificant because of large variations within condition) (**TABLE IV.4**).

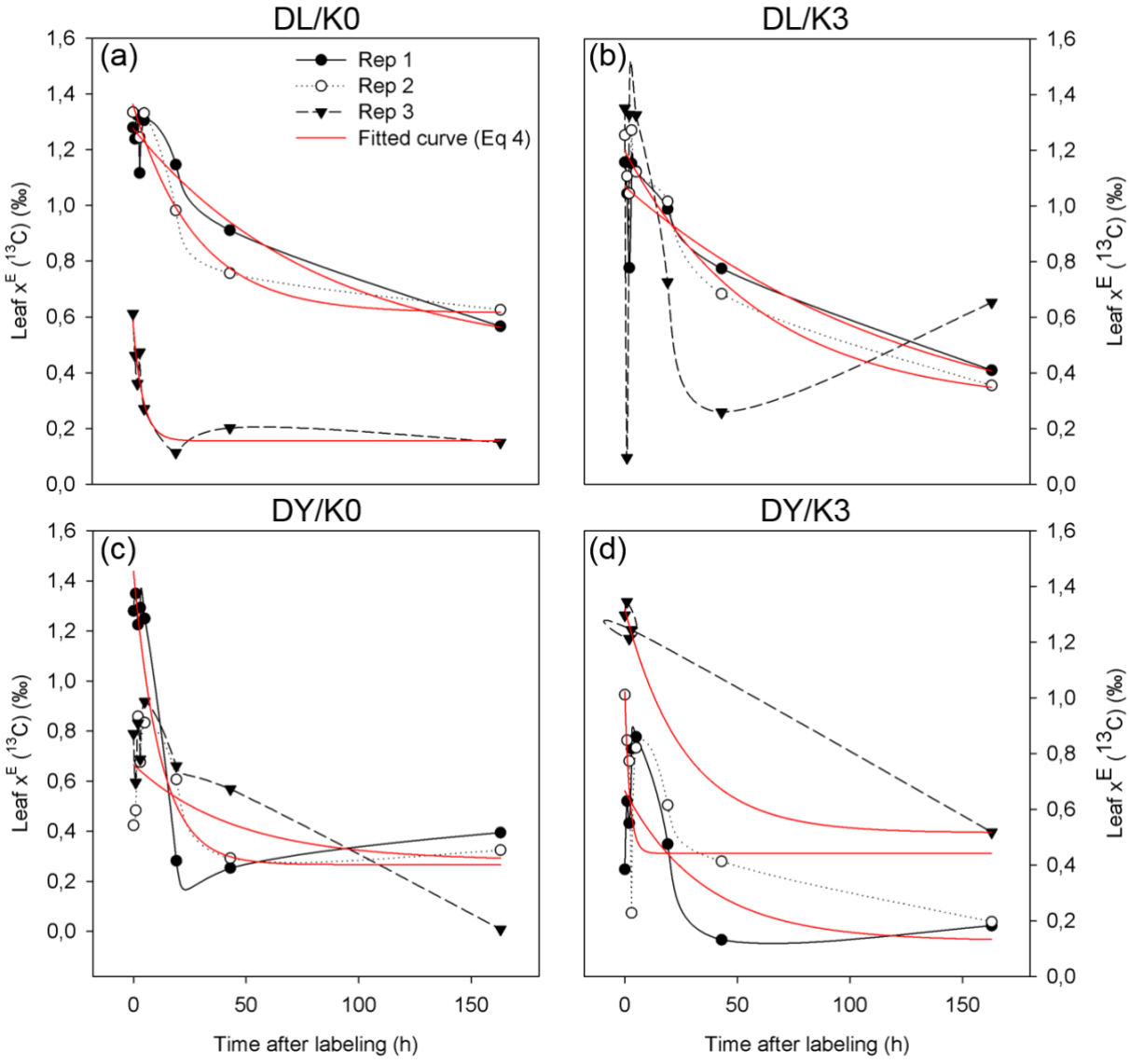

Figure IV.8. Time courses of $x_E(^{13}C)$, the ^{13}C in excess, after pulse labelling in leaflets in DL and DY under K0 and K3 treatments for each replicate. $x_E(^{13}C)$ was calculated according to Eq. (3). Red straight lines represent fitted simple exponential decay (Eq. (4)).

In *Betula nana* (Subke *et al.*, 2012) or eucalypts (Epron *et al.*, 2012), mean residence time of pulse-derived ^{13}C are about 1.1 days or 21-31h respectively. There were also no difference between K conditions (P=0.3). In eucalypts, Epron *et al.* (2012) has observed that $1/\tau$ tended to be shorter in K fertilized trees compared to non-fertilized trees while the difference was found to be insignificant.

Table IV.4. Model parameters describing the decrease in xE(^{13}C), the ^{13}C in excess, with time after labelling in leaflet (Eq. 4). C_L is the labile pool of x_E(^{13}C) at time 0 and C_S is the asymptotic remaining of x_E (^{13}C) in the leaflet. MRT is the mean residence time of labile C in leaflet and as the inverse of the decay constant (τ).

	C_S	C_L	τ	r^2	MRT (h)
DL K0 1	0.45	0.83	0.01	0.93	82.64
DL K0 2	0.61	0.75	0.04	0.98	27.86
DL K0 3	0.16	0.43	0.23	0.90	4.30
DL K3 1	0.14	0.93	0.01	0.77	130.65
DL K3 2	0.29	0.91	0.02	0.93	59.88
DL K3 3	NA	NA	NA	NA	NA
DY K0 1	0.27	1.17	0.08	0.91	11.93
DY K0 2	0.28	0.38	0.02	0.39	45.25
DY K0 3	NA	NA	NA	NA	NA
DY K3 1	0.13	0.54	0.03	0.55	35.21
DY K3 2	0.44	0.58	0.46	0.48	2.16
DY K3 3	0.52	0.80	0.04	0.99	26.18

The presence of the 2 pools was also represented after graphed the probability density of the data according to different conditions (**FIG. IV.9**). We can see in Fig. IV.9 that the data follow a bimodal distribution before and after the labelling, suggesting the occurrence of too carbon pools within a condition. Taken as a whole (**FIG. IV.9 A**), we can see that the first peak representing the biggest pool has a median carbon isotope signature of −30 ‰ which is slightly impacted by ^{13}C labelling (**FIG. IV.9 E**) and the smallest has a median carbon isotope signature of −29.4‰, which is more impacted by ^{13}C labelling (400 ‰ just after labelling). When the probability density of the different conditions taken separately (**FIG. IV.9 H**), we could observe a slight positive shift in the median carbon isotope composition between K0 and K3, suggesting an enrichment of the pool with ^{13}C labelled upon K fertilization, as observed in Epron *et al.* (2016).

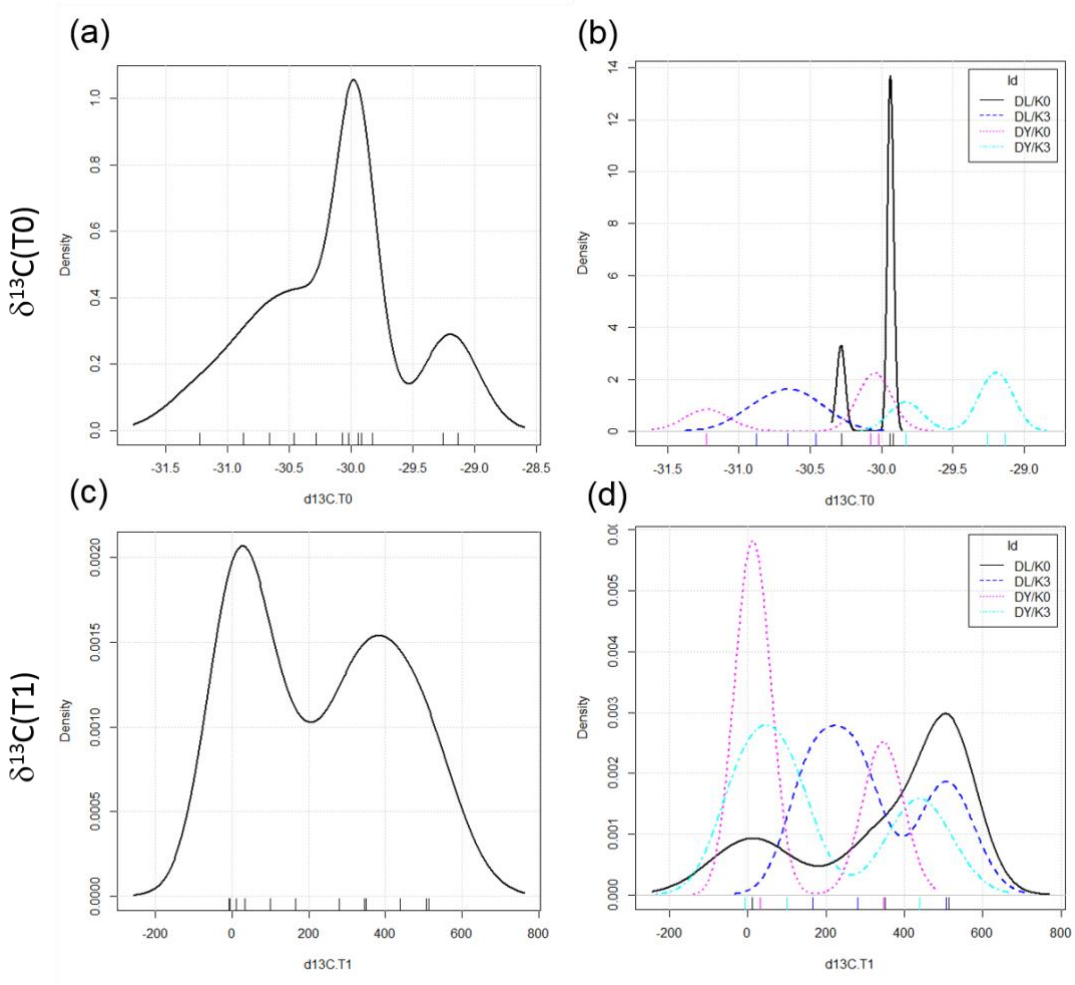

Figure IV.9. Probability density of δ13C values before and after the labelling according to K and cross conditions. (a,c) global probability density with all the data and (b,d) probability density grouped by crosses and treatments.

4. Fate of assimilated 13C in oil palm tree

4.1. Labelling. Analysis of leaflet OM δ13C for different palm ranks 7 days after the labelling experiment revealed that leaflets of leaf ranks number 1, 9, 17, 25, 33, 41 or 49 did not exhibit 13C labelling from leaf number 10 (**FIG. IV.10**). Because past studies have shown that vegetative tissues were priority sinks in carbon partitioning (Henson, 2006; Henson, 2007), we were expecting that some 13C labelling could be found in other leaves and specially young ones like leaf number 1 and 9. However, we are conscious that at this developmental stage, oil palm represents a huge biomass. We estimated that in 2017, trees had a total standing biomass of about 295 kg DW per tree, and 13C effectively assimilated by a tree represented only about 1.2 mg 13C /g C.

4.2. Natural abundance. As observed by Lamade *et al.* (2009), there was a clear difference in $_{13}C$ natural abundance between leaf ranks, suggesting changes in the origin of the carbon source used for leaf growth. In fact, it is found here that $\delta_{13}C$ values decreased with increasing rank number. Thus, leaf number 1 was more enriched than leaf number 49, regardless of the cross or K fertilization, ranging from − 29.5‰ to − 31.5‰ (**FIG. IV.10**). The $\delta_{13}C$ difference between leaf ranks may be due to differences in the ratio of starch/soluble sugars. In young leaves, starch content (which present a less negative $\delta_{13}C$ value, about − 26 ‰) is more important than soluble sugars (which have a more negative $\delta_{13}C$, about − 29 ‰ for glucose and fructose) (Lamade *et al.*, 2016). When the leaf is becoming autotrophic after rank 1, there is a change in the carbon pool participating to leaf biomass elaboration, with a higher proportion of photosynthates that are more negative. In addition, while insignificant, we observed that K tended to increase the $\delta_{13}C$ value in leaflets, regardless of leaf rank (**FIG. IV.10**), suggesting that K either modified leaflet carbohydrate composition with for example an increase in sucrose vs. starch (see Chapter II and **FIG. IV.6**), or was associated with an increase in c_i/c_a.

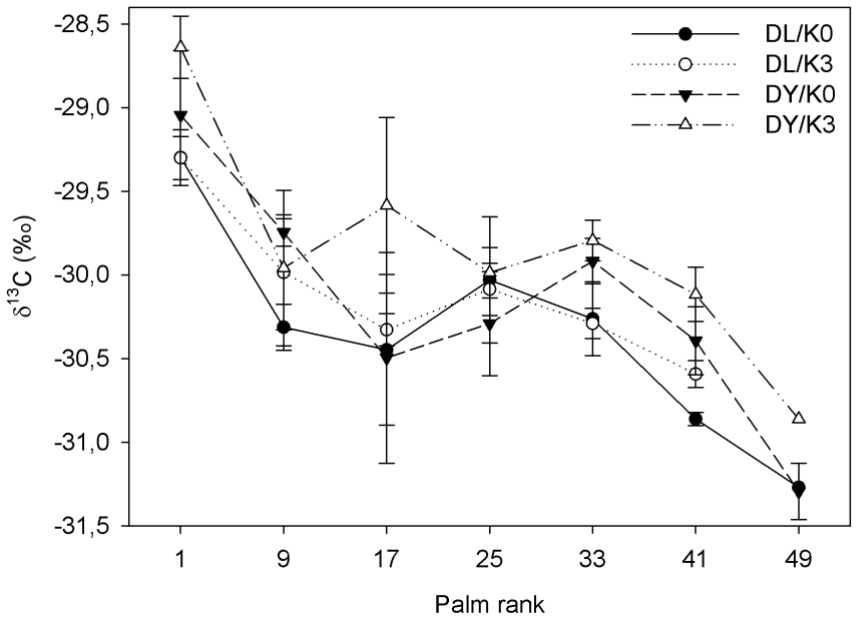

Figure IV.10. Variation of the carbon isotope composition ($\delta_{13}C$) of organic matter (OM) across leaf ranks. Mean ± SE (n = 3).

D. Advantages and disadvantages of the present experiment

In this study, we performed for the first time a $^{13}CO_2$ pulse-labelling experiment on oil palm leaves, submitted to two potassium fertilization conditions and two crosses in the field. Clearly, $^{13}CO_2$ injected into the chamber was fixed into leaflet organic matter (OM), showing that the labelling experiment was successful.

However, the efficacy of the experiment was much less than expected. In reason of uncontrolled conditions in the field, such as high temperature or air relative humidity, leading to water condensation (**PICT. S4**) and the large biomass that a young oil palm tree represents, it was less than 27% of $^{13}CO_2$ added inside the chamber that were assimilated by the leaflets. In fact, according to Dufrene and Saugier (1993) photosynthesis is very low when air temperature is over 36°C. In our experiment, air temperature inside the chamber could reach 49°C. Moreover, because of the high water condensation inside the chamber, we had to add silica gel before the entrance of the analyzer to avoid water entry that could damage the analyzer, which made impossible the measure of water absorbed, transpiration rate and thus the calculation of stomatal conductance and water use efficiency.

Therefore, since $\delta^{13}C$ is very sensitive to climatic variations such as temperature and RH, there was a strong variability between replicate that made impossible the interpretation of the data relative to the effect of K on carbon metabolism in the leaflet. However, we could observe some tendency for K to enrich starch or $\delta^{13}C$ median of the 2 pools. In addition, $\delta^{13}C$ was correlated to leaflet Cl content that could reflect an effect of K on trees experienced more K treatments as K applied as KCl.

Finally, this study sheds light on the basal physiology of the oil palm inside the leaflet that is the existence of 2 pools of C: a bigger pool representing the leaf biomass, and a smaller labile pools. The labile pool had a MRT reaching up to 130 h that is relatively slow comparing to *Betula nana* (Subke *et al.*, 2012) or eucalypts (Epron *et al.*, 2012) trees, suggesting a slow exportation rate of C. It also gave us insight on the proportion of CO_2 lost by respiration, although more $\delta^{13}C$ analysis of leaflets OM during respiration could have informed us on the metabolism of respiration and explained higher mitochondrial activity with K fertilization.

To conclude, this experiment has a strong potential, it can brings insight on the effect of potassium on carbon dynamic and flux related to the yield, which is relatively important for the adjustment of K fertilization in the field. Another experiment of $^{13}CO_2$ labelling is therefore necessary with trees experiencing more K treatments and with controlled climatic conditions to answer the followings objectives: (i) determine the nature of the prevalent sugar exported by leaves (sucrose or glucose); (ii) follow the export of carbon from leaves to other organs; (iii) understand carbon dynamics in leaves after photosynthesis (in particular, utilization by respiration); and (iv) know whether all these processes are affected by K availability. More specifically, compound specific analysis (by LC-c-IRMS or GC-c-IRMS) of labelled leaflets following the labelling are necessary to answer (i). Moreover, as the trees at 4 years old represent a huge amount of carbon biomass, it may be difficult to answer to objective (ii) without performing several analysis for the different organs or labelling during a long time with pure $^{13}CO_2$, which represent both high cost. A solution may be to do a labelling with ^{13}C-depleted CO_2 (i.e., near-natural abundance labelling) during a long period (see (Epron *et al.*, 2012)) or practice a pruning to reduce sink organs before the labelling (see Chapter IA2). In order to answer to objective (iii), analysis of CO_2 respired and compound specific analysis of labelled leaflets during dark respiration should be performed in addition to gas exchange measurements.

Chapter V. General discussion and perspectives

Oil palm is characterized by a simple architecture and indefinite growth which produces successive leaves on an unique cylindrical trunk (Jacquemard, 2012; Corley & Tinker, 2016). It is a C_3 plant with a high leaf surface area and a generally high photosynthesis rate (Legros *et al.*, 2006; Legros *et al.*, 2009c). To sustain growth and get optimal yield, high fertilization is required. Potassium chloride (KCl) is the most widely used fertilizer in oil palm plantations. K has many roles in plant physiology and metabolism related to cation-anion balance, osmoregulation, water movement, phloem transport and energy transfer, and takes part in protein synthesis, carbohydrate metabolism and enzyme activation (see Introduction). However, in oil palm, the effects of K on carbon metabolism related to the yield are not well understood and in some cases, potassium is applied excessively. Nowadays, different agronomical practices and tools are used to monitor K nutrition (fertilization trial, leaf diagnosis, leaf symptoms and soil analysis) for a better prediction and adjustment of K fertilization. However, there is still some possible improvement (and even a slight improvement of a few % in KCl management could save hundreds of k$).

The goal of this study was to assess the effect of K availability on oil palm metabolic pathways and determine if metabolic changes were related to yield. More precisely: (A) What is the impact of K fertilization on proteomic and metabolomic responses of leaflets on two genetically contrasted materials, presenting different leaflet K mineral signature? (B) What is the impact of K fertilization on omics responses of the oil palm fruit mesocarp during maturation, on two genetically contrasted materials? (C) Can a $^{13}CO_2$ labelling help identifying sugars produced and C allocation, with these affected by K availability?

A. Effect of K on oil palm growth and yield

Taken as a whole, we observed that K fertilization, in the first 3-4 years (respecting standard agronomical procedures) had small effects on functional traits. Two years were necessary to see a significant effect of K fertilization on leaf K content. Even so, while potassium fertilization increased N, P and K contents in leaflets of both crosses, no general effect of K was found on

bunch production nor vegetative growth 2 years after the treatment, as observed elsewhere (Ochs, 1965; Hartley, 1988a; Corley & Tinker, 2016). On average, individual bunch production of oil palm studied was up to 25 bunch tree^{-1} yr^{-1} and bunch weight was about 9 kg, with no significant effect of K, which is coherent to the fact that it takes 3 year for a bunch to develop (Corley & Tinker, 2016). However, high K availability increased significantly specific leaf weight, trunk diameter and the number of fruits as well as mesocarp and kernel biomass proportion in bunches, and tended to increase trunk height. This suggests that possible changes in yield and therefore on leaflet and fruit metabolism can be anticipated in the next few years. Moreover, the fact that K increased trunk diameter and tended to increase trunk height without increasing foliar emission rate, may reflect an effect of K on trunk internode length, and therefore on growth rate, carbon transport and storage in the trunk, which would be consistent to literature (Legros *et al.*, 2006; Legros *et al.*, 2009c; Corley & Tinker, 2016).

Our study also shows that while the effect of K fertilization on leaflet K content (and leaflet proteome) was minimal after one year (in 2017) plus three years preconditioning, several metabolites appeared to be significant, suggesting that there were some changes in, e.g., K^+ distribution amongst leaf tissues or cellular compartments. That is, it is probable that even in 2017, K0/K3 conditions were associated with subtle changes in cytosolic and mitochondrial K^+ concentration. In fact, we have observed in Chapter IV that in spite of the absence of significant effect of K fertilization on photosynthesis, leaflet K content was slightly correlated to photosynthesis, while not significant ($R=0.52$, $P=0.19$). It is worth noting that both crosses have contrasted leaflet K content and effect of leaflet K content on photosynthesis may be attributed to the cross effect. In fact, both crosses differed from their metabolism and particularly, the O2PLS analysis from the Chapter II suggests that there were differences in both photosynthetic capacity and mitochondrial metabolism between crosses.

We estimated that the lack of effect of K on vegetative growth and yield in 2017 may be due to K remobilization from leaves or trunk to fruits to cover the K demand of bunch maturation, thereby dampening changes in leaf K despite the K fertilization treatment. Also, in 2017, K3 fertilization (4.5 kg KCl tree^{-1} yr^{-1}) represented twice as much the K demand and may reflect an excess. In a previous study (Imogie *et al.*, 2012), it has been observed that even 1 year after the onset of the K treatment, fresh fruit bunch production increased with K fertilization up to an optimum at 2.0 kg K tree^{-1} yr^{-1} and above this amount of K, there was no significant increase in fresh fruit bunch production (See Chapter I.C.2), reflecting the non-linear

relation between K and bunch production thus oil palm metabolism. Here, we could observe a slight depressive effect of K on bunch production in DY.

We observed that higher K availability caused an increase in kernel biomass proportion in bunches and mesocarp water content (MWC) in DY, thus leading to lower OFM, while in DL, MWC clearly decreased with K availability and accordingly, there was an increase in OFM and OER. Previous studies showed a correlation between fruit transpiration (water loss) and lipid biosynthesis (Jeje *et al.*, 1978; Teh *et al.*, 2013a). It seemed therefore that high K availability had an effect on fruit water loss, and this effect can be positive or negative depending on the cross. Leaflet elemental content analysis showed that DY (supposed to be leaflet K^{++}) was more sensitive to K fertilization than DL (supposed to be leaflet K^{--}) (See Chapter III). In fact, according to Rengel and Damon (2008), genotypic differences in capacity to utilize K have been attributed to (1) differences in partitioning and redistribution of K at cellular and whole plant levels, (2) the substitution of K by other ions e g Na in the vacuole particularly important under salinity, and (3) the partitioning of resources into the economic product. However, the negative effect of high K (K3 conditions) on oil content (OFM) in DY fruits could not be assigned to an excess of K, because the same trend was observed with K1 and K2 in DY (**FIG. III.3**). The change in OFM may have come from excess chloride in tissues, which is also known to increase the kernel-to-mesocarp ratio, as observed in our study (Breure, 1982; Ollagnier & Olivin, 1984a). Moreover, increasing OFM in DL with K without increasing mesocarp proportion in a fruit, suggested therefore that increasing OFM may be associated to increasing lipid accumulation and/or FA synthesis (see Chapter III).

Finally, although no big changes were observed on yield or vegetative growth 2 years after the onset of the treatment, our data indicate that leaflet metabolism is sensitive to small variation of leaflet K content suggesting that possibly, important changes on yield and therefore on leaflet and fruit metabolism will take place in the next few years. It is important to realize that a direct effect of K nutrition on enzyme activity thus on leaflet metabolism requires a considerable change in cytoplasmic K concentration. However, according to Amtmann and Rubio (2001), efficient usage of the vacuole as a reversible K store usually prevents large fluctuations of cytoplasmic K concentration. A considerable increase of cytoplasmic K concentrations would only be expected after prolonged K-supply.

B. Effect of K on leaflet metabolism

In order to understand the possible impact of K fertilization on leaflet metabolism, both proteome and metabolome were analyzed. First, our results showed that higher K availability increased N assimilation. Stimulation of N assimilation encompassed an increase in glutamate metabolism leading to higher amino acid content such as methionine, serine, leucine or valine, due to both augmented synthesis and proteolysis (protein-turn-over). In fact K availability had an effect on protein synthesis machinery, in particular the abundance of ribosomal proteins. This agrees with previous agronomical observations that increasing K stimulates N use efficiency and eventually, increases %N in leaflets (Ollagnier & Ochs, 1973), perhaps through enzyme activation but also ribosome synthesis and mRNA turnover (Evans & Wildes, 1971; Blevins, 1985; Pettigrew, 2008)). K fertilization has been found to be beneficial to ammonium assimilation by up-regulating glutamine synthetase (GS), ferredoxin-glutamine-2-oxoglutarate aminotransferase (Fd-GOGAT) and glutamate dehydrogenase (GDH) in *Arabidopsis* (Armengaud *et al.*, 2009; Hu *et al.*, 2016b). This might imply that K fertilization leads to a high C flux through the TCA cycle so as to sustain amino acids and protein synthesis (Ollagnier & Ochs, 1973; Ruan *et al.*, 1998; Amtmann & Rubio, 2001; Armengaud *et al.*, 2009; Hu *et al.*, 2016b) (See **FIG. IV.1**).

Moreover, higher K availability led to higher proteins contents, which may explain the increase in SLW. We are well aware, that an increase in SLW could have also come from an increase in leaflet structural components (such as lipids, cellulose, lignins, etc.); however, they have not been characterized in this study. Despite a tendency of K to increase leaflet starch content in DL and to decrease it in DY (Chapter IV), high variability between samples did not allow a consistent interpretation of the effect of K on starch content and carbon storage. However, difference in leaflet starch content between both crosses may be consistent with the fact that DY was more sensitive to K fertilization suggesting a higher carbon assimilation and translocation resulting in lower starch content at higher K compared to DL.

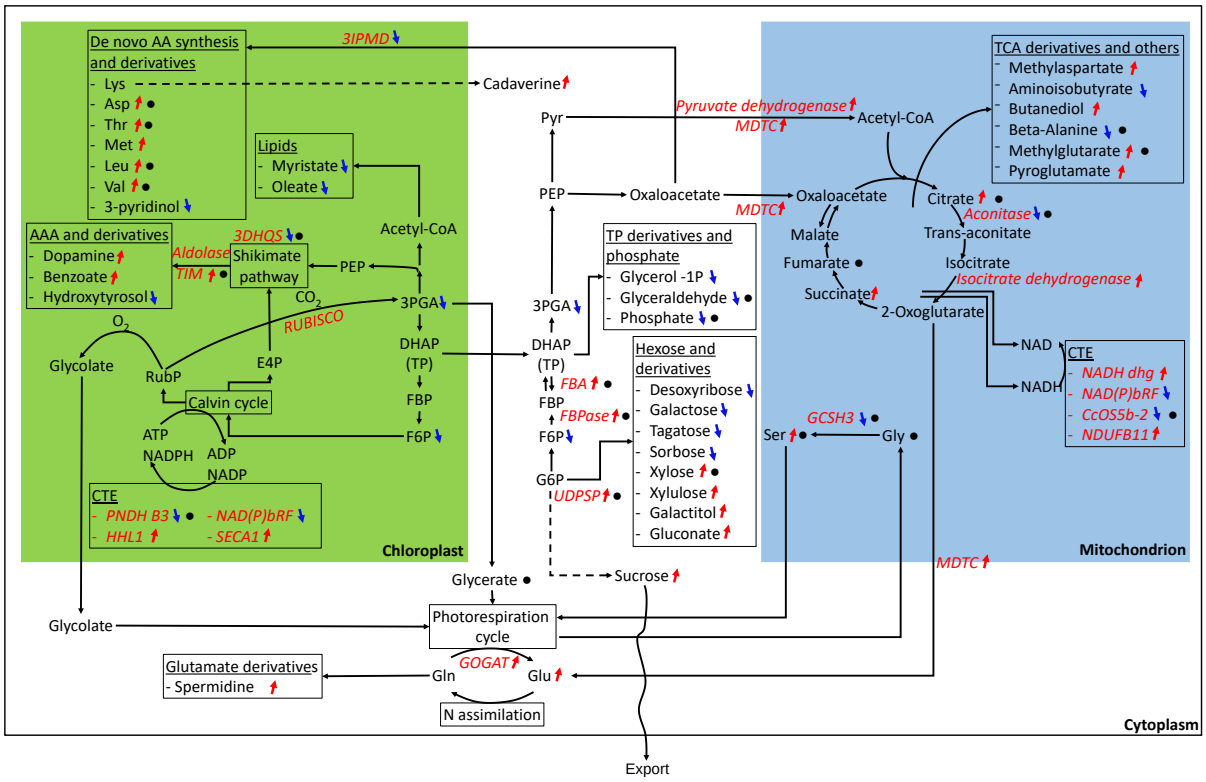

Figure V.1. Tentative summary of the effect of K on leaf metabolism. Blue arrows (↘) indicate metabolites/enzymes that decrease with K fertilization while red arrows (↗) indicate an increase. Black dots (●) indicates metabolites/enzymes that differ significantly between crosses. Enzymes are written in red italics. Abbreviation: 3DHQS, 3-dehydroquinate synthase; 3IPMD, 3-isopropylmalate dehydratase protein; 3PGA, 3-phosphoglycerate; AA, amino acid; AAA, aromatic amino acid; ADP, adenosine diphosphate; Asp, aspartate; ATP, adenosine triphosphate; Aldolase TIM, aldolase-type tim barrel family protein; CcOS5b-2, cytochrome c oxidase subunit 5b-2; CoA, coenzyme A; CTE, chain transport electron; DHAP, dihydroxyacetone phosphate; E4P, erythrose-4-phosphate; F6P, fructose-6-phosphate; FBA, fructose-bisphosphate aldolase 1; FBP, fructose biphosphate; G6P, glucose-6-phosphate; GCSH3, glycine cleavage system H protein 3; Gln, glutamine; Glu, glutamate; glycerol-1P, glycerol-1-phosphate; Gly, glycine; GOGAT, ferredoxin-dependent glutamate synthase; HHL1, Protein HHL1, chloroplastic isoform X1; MDTC, mitochondrial dicarboxylate/tricarboxylate transporter DTC; Met, methionine; N, nitrogen; NADH dhg, NADH dehydrogenase; NADH/NAD, nicotinamide adenine dinucleotide; NADPH/NADP, nicotinamide adenine dinucleotide phosphate; NAD(P)bRF, NAD(P)-binding Rossmann-fold superfamily protein; NDUFB11; Putative NDUFB11 Superfamily domain; Leu, leucine; Lys, lysine; PEP, phospho*enol*pyruvate; PNDH B3, Photosynthetic NDH subunit of subcomplex B 3; Pyr, pyruvate; RubP, ribulose 1,5-bisphosphate; SECA1, Protein translocase subunit SECA1; Ser, serine; TCA; tricarboxylic acid cyle; TP, triose-phosphate; Thr, threonine; UDPSP, UDP-sugar pyrophosphorylase; Val, valine.

In fact, proteins involved in catabolism (phospho*enol*pyruvate carboxylase, phosphopyruvate hydratase, etc.) were up-regulated in DY, whereas disaccharides and some proteins of photosynthesis (sucrose-phosphatase, glycerate dehydrogenase, carbohydrate kinase domain-containing protein, Rubisco activase, transketolase) were up-regulated in DL

(see Chapter II). In fact, according to Yang *et al.* (2004), the higher K concentrations in the rice leaves (especially the lower leaves) of the K-efficient genotypes were associated with higher RuBP carboxylase activities and net photosynthetic rates allowing the leaves to maintain a higher photosynthetic capacity during grain filling. Nevertheless, at high K, the increase in leaflet total phosphorus content concurrent with a decrease in leaflet free phosphate (Pi), fructose 6-phosphate, glycerol 1-phosphate and 3-phosphoglycerate, suggests an increase in P-containing compounds such as phospholipids, which could participate in increasing SLW.

Moreover, we found that K availability had a significant effect on several proteins involved in photosynthesis and photorespiration, including sucrose metabolism (UDP-sugar pyrophosphorylase) that were consistent to the well-known beneficial effects of K on oil palm photosynthesis via stomatal regulation, photosynthetic capacity and photosynthate export (Lamade *et al.*, 2014; Cui *et al.*, 2019b). Nevertheless, in our study, we found that this effect was also associated with a higher content in sugars such as sucrose, which is not in agreement with other findings (Cakmak *et al.*, 1994; Zhao *et al.*, 2001; Gerardeaux *et al.*, 2010) where sugar accumulation was observed at low K because of the inhibition of phloem loading. It is worth noting that in our study case, no K deficiency was observed, explaining therefore why the effect of K on sugar content in our study was different with other findings dealing with K deficiency. Further studies are necessary to evaluate effect of K on sugar transport. Still, in our study, preliminary results of $^{13}CO_2$-labelling experiment (Chapter IV) indicates that leaflet carbon transport rate was relatively slow (high MRT) (Epron *et al.*, 2012; Subke *et al.*, 2012). Dufrene (1989) has effectively demonstrated that carbon assimilation (at saturating light) and SLW in oil palm leaflets are correlated and suggested that assimilate transport is very slow during the day. However, increasing in SLW with photosynthesis may be also due to the fact that up to 20% of carbon are stored as starch (Legros *et al.*, 2006). Also, under our conditions, we observed a link between sugars and photosynthetic capacity. In fact, bi-dimensional multivariate analysis showed that disaccharides did correlate to key proteins involved in photosynthesis such as sucrose phosphatase or Rubisco activase.

In addition, potassium fertilization had an effect on mitochondrial metabolism, with changes in the abundance of some Krebs cycle enzymes and associated changes in Krebs cycle intermediates: an increase in citrate (due to lower aconitase activity) and succinate (due to both larger IDH and succinate thiokinase activity). There was also an increase in other mitochondrial proteins (cytochrome c oxidase subunit 5b-2, NADH dehydrogenase, di/tricarboxylate

transporter, etc.). Altogether, these changes point to an increased flux in organic acid metabolism and thus an increase in respiratory activity. Our results have effectively shown that potassium tended to increase dark respiration rate in DY (Chapters II and IV). However, such an important stimulation of mitochondrial metabolism at higher K availability is slightly surprising. In fact, recent studies have shown that in oil palm saplings, K deficiency rather than high K leads to an increase in respiration rate and ≈10% loss in carbon use efficiency only (Cui *et al.*, 2019b). We have suggested that such increase might have been driven by the demand in carbon skeletons for nitrogen assimilation (discussed above), or the increase in growth rate and sucrose export, or the ion balance (generation of organic acids carrying a negative charge to compensate for changes in the relative K^+ excess). Indeed, we also found an increase in the content of the Ca^{2+}-sensitive ion channel POLLUX suggesting that K availability directly impacted on cellular K^+ and Ca^{2+} pools. Moreover, as shown in (Cui *et al.*, 2019b), effect of K in leaflet metabolism is non-linear, thus explaining similar results observed at K deficiency.

Thus, the simultaneous effect of K availability on photosynthesis and respiration suggests that the carbon use efficiency could have also been impacted. Future measures of biomass, gas exchange and thus carbon use efficiency are necessary to better understand the effect of K on leaflet metabolism.

C. Carbon utilization by fruits

Assimilates produced in the leaflets are redistributed mainly as sucrose to developing leaves, inflorescences (and bunches), trunk and roots, depending on sink strength (Houngbossa & Bonnemain, 1985; Obahiagbon *et al.*, 2012). In fact, in the fruit mesocarp, our data (Mirande-Ney *et al.*, 2019) suggested that sucrose is the carbon source for lipid and starch biosynthesis (starch being stored transiently and then used as a carbon source for lipid synthesis). This is consistent with the findings of Dussert *et al.* (2013). According to Bourgis *et al.* (2011) and Voelker (2011), in the mesocarp, imported sucrose is cleaved into hexoses, and intermediates are transported to the plastids, where glycolysis and FA synthesis occurs. FA are then assembled into triglycerides and other lipids in the cytoplasm. In addition, we found that lipid accumulation was associated with metabolites of the oxidative pentose phosphate pathway (generating NADPH) and a general depletion in fumarate, citrate or succinate, probably

reflecting the progressive increase in energy generation and thus the consumption of Krebs cycle intermediates. In general, we observed that FA biosynthesis was accompanied by a decrease in sugar, amino acids and organic acids to very low levels at maturity (around 20-21 WAA at stage 5) as observed elsewhere (Hartley, 1967; Thomas *et al.*, 1971; Neoh *et al.*, 2013; Teh *et al.*, 2013a). Final oil content in mesocarp was found to be related to *(i)* the velocity of lipid production (and thus anticorrelated to pools of intermediates of lipid synthesis), *(ii)* the availability of carbon source (sugars) and *(iii)* the ability to break down amino acids and thus metabolic recycling to other N-containing metabolites (β-alanine, triethanolamine and putrescine). At maturity, the fruit mesocarp was mostly composed of 71.5% FAs (including palmitate (53-67%), oleate (23-35%), linoleate (2.5-5.3%) and stearate (3-8%)), and 27.4% carbohydrates depending on the cross.

D. Effect of K on fruit mesocarp metabolism during maturation

Despite multiple metabolic changes during fruit development, the relative quantity in fatty acids in mesocarp and final oil composition at maturity were not modified significantly by K availability. However, K availability had an effect on fruit metabolism during maturation, with lower carbohydrate and organic acid content at high K. At high K, glucose, fructose and sucrose were lower (by 40-70%) in particular at stage 1, suggesting therefore (1) that sugar transport to the fruit could be a limiting factor to lipid accumulation as suggested earlier and/or (2) that sugars were rapidly used for FA synthesis under K fertilization.

Our data showed that high K simply led to an increase in glucose catabolism, including via the oxidative pentose phosphate pathway (which generates NADPH for fatty acid synthesis), and in redistribution of carbon skeletons to specific nitrogenous compounds (methylpiperidine, amino acids). More precisely, K slowed down lysine and phenylalanine catabolism during early stages of fruit maturation (stages 1-3). Moreover, in DY, high K was associated with more intermediates of lipid synthesis (glycerate, monostearin and azelaate) and in DL, less short-chain fatty acids (caprate, caprylate), showing that K stimulated fatty acid chain elongation and triglyceride synthesis. (See **FIG. IV.2**), balancing therefore toward the hypothesis (2).

However, it is worth noting that, (1) in young palms, there was a strong competition between vegetative growth and bunch production with a priority for growth and maintenance (Dufrene, 1989; Dufrene & Saugier, 1993) and (2) K increased fruit number and thus sink without increasing leaf area nor foliar emission rate, both leading to a decrease therefore in sugars allowed to the mesocarp for oleosynthesis. In addition, this may be accentuated by the fact that high K increased the leaflet respiration rate, thus the carbon loss. Previous studies have effectively shown that fruit bunches are responsible for a respiratory loss of 18-40% of gross primary production (Dufrene, 1989; Lamade & Setiyo, 1996; Lamade *et al.*, 2016). Although more data are certainly needed to provide a more precise picture of allocation and respiratory losses in oil palm, a high respiratory loss in fruits would be consistent with the low metabolic carbon use efficiency of oil (fatty acid) production.

Moreover, bunch analyses showed that K increased OFM without modifying significantly mesocarp FA content. Therefore, it seems that K slow down sugar transport to the fruit during the day as suggested by Dufrene (1989), but used rapidly the sugar allocated to the fruit for FA elongation. More studies are nevertheless necessary to confirm this hypothesis. Proteomic analysis of oil palm mesocarp at different maturation stages for example could inform us on enzymes activity associated to FA biosynthesis.

Furthermore, although GC-MS showed that there was an increase in average oleate and a decrease in linoleate content in both crosses with K, consistently with NMR analysis and others findings (Ochs & Ollagnier, 1977; Ollagnier & Olivin, 1984a; Ollagnier & Olivin, 1984b; Seo *et al.*, 1986; Salama, 1987; Froment *et al.*, 2000; Dag *et al.*, 2009), it is important to keep in mind that GC-MS is not the best technique to characterize FAs and lipids (a proper lipidomics analysis with LC-MS would be necessary). We choose GC-MS here as the best compromise to study fruit mesocarp metabolism and get broad information on mesocarp metabolome, since it allows the simultaneous identification and quantitation of sugars, amino acids, organic acids, etc.

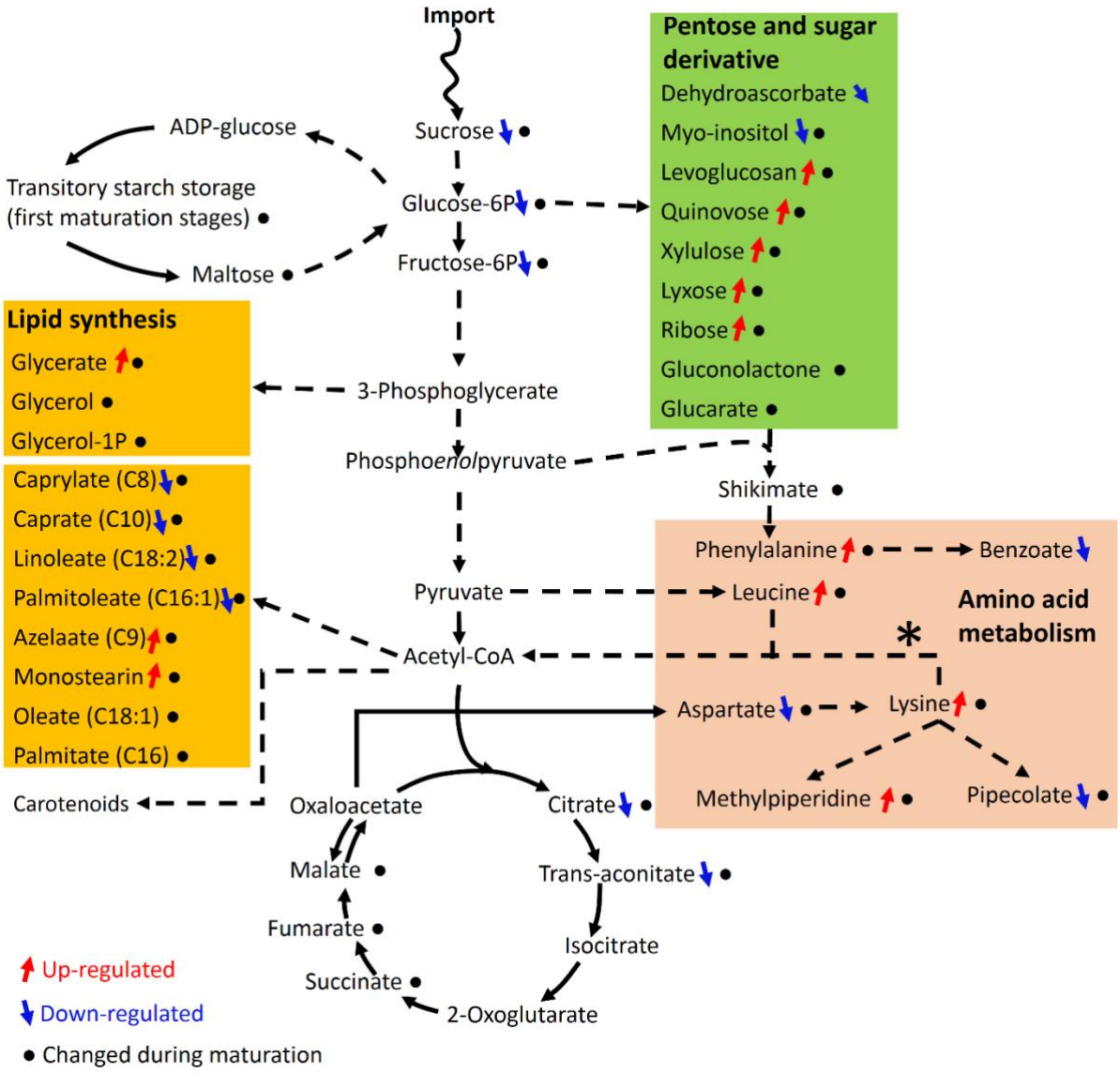

Figure V.2. Effect of K availability on oil palm mesocarp lipid biosynthesis. Blue arrow indicates metabolites which decrease with K fertilization and red arrow indicates those which increase. Abbreviation: ADP-glucose: adenosine diphosphate glucose, Susy: Sucrose synthase

E. Conclusion

Taken as a whole, this study allowed us to assess the effect of K availability on oil palm metabolic pathways. It gives us the opportunity to identify key metabolic pathway impacted by K into leaflet but also in fruit mesocarp. Metabolomics and proteomics analyses gave us insight

on photosynthetic and respiration activity, and metabolomics analyses gave information on mesocarp lipid accumulation. Finally, our results are thus of potential interest to envisage new techniques for K fertilization monitoring using the metabolic signature of leaflets. Further studies with others K fertilization conditions and oil palm tree ages are nevertheless necessary. Also, studies on trunk composition and carbon dynamics in the phloem must be assessed, in particular, analysis of specific sugar in the phloem after a leaf $^{13}CO_2$ labelling could help understanding kinetic of production, utilization and transport of specific sugars related to the yield.

Importantly, our study allowed us to identify metabolic pathways modified in a cross-specific manner and thus key components that are specific to genotypes. As such, this study may be of interest for breeding since it show how integrative analyses (omics) are implementable in oil palm and thus could be used for the selection of genotypes more sensitive (responsive) to K. This perspective would be useful to reduce K fertilization for sustainable agrosystem. More generally, omics-based selection could be interesting for selecting genotypes associated with other traits, such as higher resistance to climatic changes such as increasing air temperature, waterlogging events or decreasing solar radiation induced by fires in oil palm plantations.

References

Ache P, Becker D, Ivashikina N, Dietrich P, Roelfsema MRG, Hedrich R. 2000. GORK, a delayed outward rectifier expressed in guard cells of *Arabidopsis thaliana*, is a K^+-selective, K^+-sensing ion channel. *Febs Letters* **486**(2): 93-98.

Agüera E, De la Haba P, Fontes A, Maldonado J. 1990. Nitrate and nitrite uptake and reduction by intact sunflower plants. *Planta* **182**(1): 149-154.

Aguilera-Alvarado GP, Sánchez-Nieto S. 2017. Plant hexokinases are multifaceted proteins. *Plant and Cell Physiology* **58**(7): 1151-1160.

Ahmad I, Maathuis FJM. 2014. Cellular and tissue distribution of potassium: Physiological relevance, mechanisms and regulation. *Journal of Plant Physiology* **171**(9): 708-714.

Allen K, Corre MD, Tjoa A, Veldkamp E. 2015. Soil nitrogen-cycling responses to conversion of lowland forests to oil palm and rubber plantations in Sumatra, Indonesia. *PLOS ONE* **10**(7): e0133325.

Amtmann A, Rubio F. 2001. Potassium in plants. *e LS*.

Amtmann A, Troufflard S, Armengaud P. 2008. The effect of potassium nutrition on pest and disease resistance in plants. *Physiologia Plantarum* **133**(4): 682-691.

Andrews M. 1986. The partitioning of nitrate assimilation between root and shoot of higher plants. *Plant, Cell & Environment* **9**(7): 511-519.

Armengaud P, Breitling R, Amtmann A. 2004. The potassium-dependent transcriptome of Arabidopsis reveals a prominent role of jasmonic acid in nutrient signaling. *Plant physiology* **136**(1): 2556-2576.

Armengaud P, Sulpice R, Miller AJ, Stitt M, Amtmann A, Gibon Y. 2009. Multilevel analysis of primary metabolism provides new insights into the role of potassium nutrition for glycolysis and nitrogen assimilation in *Arabidopsis* roots. *Plant Physiol* **150**(2): 772-785.

Ashraf MA, Ahmad MSA, Ashraf M, Al-Qurainy F, Ashraf MY. 2011. Alleviation of waterlogging stress in upland cotton (*Gossypium hirsutum* L.) by exogenous application of potassium in soil and as a foliar spray. *Crop and Pasture Science* **62**(1): 25-38.

Bafor ME, Osagie AU. 1986. Changes in lipid class and fatty acid composition during maturation of mesocarp of oil palm (*Elaeis guineensis*) variety dura. *Journal of the Science of Food and Agriculture* **37**(9): 825-832.

Barcelos E, Rios Sde A, Cunha RN, Lopes R, Motoike SY, Babiychuk E, Skirycz A, Kushnir S. 2015. Oil palm natural diversity and the potential for yield improvement. *Front Plant Sci* **6**: 190.

Baszynski T, Brand J, Barr R, Krogmann DW, Crane FL. 1972. Some biochemical characteristics of chloroplasts from mineral-deficient maize. *Plant physiology* **50**(3): 410-411.

Battie-Laclau P, Laclau JP, Beri C, Mietton L, Muniz MR, Arenque BC, M DECP, Jordan-Meille L, Bouillet JP, Nouvellon Y. 2014. Photosynthetic and anatomical responses of *Eucalyptus grandis* leaves to potassium and sodium supply in a field experiment. *Plant Cell Environ* **37**(1): 70-81.

Beevers L, Hageman R. 1969. Nitrate reduction in higher plants. *Annual Review of Plant Physiology* **20**(1): 495-522.

Behera S, Rao B, Suresh K, Manoja K. 2015. Soil nutrient status and leaf nutrient norms in oil palm (*Elaeis guineensis* Jacq.) plantations grown on southern plateau of India. *Proceedings of the National Academy of Sciences, India Section B: Biological Sciences* **86**.

Besford RT, Maw GA. 1976. Effect of potassium nutrition on some enzymes of the tomato plant. *Annals of Botany* **40**(167): 461-471.

Bharati M, Whigham D, Voss R. 1986. Soybean response to tillage and nitrogen, phosphorus, and potassium fertilization. *Agronomy journal* **78**(6): 947-950.

Billotte N, Marseillac N, Risterucci A-M, Adon B, Brottier P, Baurens F-C, Singh R, Herrán A, Asmady H, Billot C, et al. 2005. Microsatellite-based high density linkage map in oil palm (*Elaeis guineensis* Jacq.). *Theoretical and Applied Genetics* **110**(4): 754-765.

Blaak G, Sparnaaij LD, Menendez T. 1963. Breeding and inheritance in the oil palm (*Elaeis guineensis* Jacq.). Part II. Methods of bunch quality analysis. *J. W. Afr. Inst. Oil Palm Res*(4): 146–155.

Blevins DG. 1985. Role of potassium in protein metabolism in plants. *Potassium in agriculture*(potassiuminagri): 413-424.

Blevins DG, Barnett NM, Frost WB. 1978a. Role of potassium and malate in nitrate uptake and translocation by wheat seedlings. *Plant Physiology* **62**(5): 784-788.

Blevins DG, Hiatt A, Lowe R, Leggett J. 1978b. Influence of K on the uptake, translocation, and reduction of nitrate by barley seedlings. *Agronomy Journal* **70**(3): 393-396.

Bolle-Jones EW, Notton BA. 1953. The relative proportions of the chloroplast pigments as influenced by different levels of iron and potassium supply. *Plant and Soil* **5**(1): 87-100.

Bourgis F, Kilaru A, Cao X, Ngando-Ebongue G-F, Drira N, Ohlrogge JB, Arondel V. 2011. Comparative transcriptome and metabolite analysis of oil palm and date palm mesocarp that differ dramatically in carbon partitioning. *Proceedings of the National Academy of Sciences* **108**(30): 12527.

Breure CJ. 1982. Factors affecting yield and growth of oil palm *tenera* in West New Britain. *Oléagineux* **37**(5): 213-227.

Britto DT, Kronzucker HJ. 2008. Cellular mechanisms of potassium transport in plants. *Physiologia Plantarum* **133**(4): 637-650.

Bush LP. 1969. Succinyl CoA synthetase of tobacco. *Physiologia Plantarum* **22**(6): 1097-1104.

Cakmak I, Hengeler C, Marschner H. 1994. Changes in phloem export of sucrose in leaves in response to phosphorus, potassium and magnesium deficiency in bean plants. *Journal of Experimental Botany* **45**(9): 1251-1257.

Carraretto L, Formentin E, Teardo E, Checchetto V, Tomizioli M, Morosinotto T, Giacometti GM, Finazzi G, Szabó I. 2013. A thylakoid-located two-pore K^+ channel controls photosynthetic light utilization in plants. *Science* **342**(6154): 114-118.

Chang KC, Goh KJ, Kee KK, Foong SF, Law KF 1995. Leaching losses of nutrients from a mature oil palm catchment in Malaysia. *International Conference on Soil Resources and Sustainable Agriculture*. Malaysia: Malaysian Society of Soil Science. 33-34.

Chapman GW, Gray HM. 1949. Leaf analysis and the nutrition of the oil palm (*Elaeis guineensis* Jacq.). *Annals of Botany* **13**(52): 415-433.

Charpentier M, Bredemeier R, Wanner G, Takeda N, Schleiff E, Parniske M. 2008. Lotus japonicus CASTOR and POLLUX are ion channels essential for perinuclear calcium spiking in legume root endosymbiosis. *The Plant Cell* **20**(12): 3467-3479.

Checchetto V, Teardo E, Carraretto L, Leanza L, Szabo I. 2016. Physiology of intracellular potassium channels: a unifying role as mediators of counterion fluxes? *Biochimica et Biophysica Acta (BBA) - Bioenergetics* **1857**(8): 1258-1266.

Chen C, Fan C, Gao M, Zhu H. 2009. Antiquity and function of CASTOR and POLLUX, the twin ion channel-encoding genes key to the evolution of root symbioses in plants. *Plant Physiology* **149**(1): 306-317.

Coale F, Grove J. 1990. Root distribution and shoot development in no-till full-season and double-crop soybean. *Agronomy journal* **82**(3): 606-612.

Cochard B, Adon B, Rekima S, Billotte N, de Chenon RD, Koutou A, Nouy B, Omoré A, Purba AR, Glazsmann J-C, et al. 2009. Geographic and genetic structure of African oil palm diversity suggests new approaches to breeding. *Tree Genetics & Genomes* **5**(3): 493-504.

Corley R. 1973. Effects of plant density on growth and yield of oil palm. *Experimental Agriculture* **9**(2): 169-180.

Corley R, Breure CJ. 1992. Fruiting activity, growth and yield of oil palm. I. Effects of fruit removal. *Experimental Agriculture* **28**(1): 99-109.

Corley R, Gray B 1976. Growth and morphology: development in crop science (1), oil palm research: Elsevier Scientific Publishing Company, Amsterdam, Netherlands.

Corley R, Hardon J, Wood B 1976. Oil palm research: Elsevier.

Corley R, Tinker P. 2016. *The oil palm*. Chichester, UK: Wiley Blackwell.

Corley RHV, Mok CK. 1972. Effects of nitrogen, phosphorus, potassium and magnesium on growth of the oil palm. *Experimental Agriculture* **8**(4): 347-353.

Corley RHV, Mok CK. 2008. Effects of nitrogen, phosphorus, potassium and magnesium on growth of the oil palm. *Experimental Agriculture* **8**(04).

Coskun D, Britto DT, Kronzucker HJ. 2010. Regulation and mechanism of potassium release from barley roots: an in planta ^{42}K analysis. *New Phytologist* **188**(4): 1028-1038.

Coskun D, Britto DT, Kronzucker HJ. 2017. The nitrogen–potassium intersection: membranes, metabolism, and mechanism. *Plant, cell & environment* **40**(10): 2029-2041.

Coskun D, Britto DT, Li M, Oh S, Kronzucker HJ. 2013. Capacity and plasticity of potassium channels and high-affinity transporters in roots of barley and *Arabidopsis*. *Plant physiology* **162**(1): 496-511.

Cui J, Abadie C, Carroll A, Lamade E, Tcherkez G. 2019a. Responses to K deficiency and waterlogging interact via respiratory and nitrogen metabolism. *Plant, cell & environment* **42**(2): 647-658.

Cui J, Davanture M, Zivy M, Lamade E, Tcherkez G. 2019b. Metabolic responses to potassium availability and waterlogging reshape respiration and carbon use efficiency in oil palm. *New Phytologist* **223**: 310-322.

Dag A, Ben-David E, Kerem Z, Ben-Gal A, Erel R, Basheer L, Yermiyahu U. 2009. Olive oil composition as a function of nitrogen, phosphorus and potassium plant nutrition. *Journal of the Science of Food and Agriculture* **89**(11): 1871-1878.

Dannoura M, Maillard P, Fresneau C, Plain C, Berveiller D, Gerant D, Chipeaux C, Bosc A, Ngao J, Damesin C, et al. 2011. In situ assessment of the velocity of carbon transfer by tracing ^{13}C in trunk CO_2 efflux after pulse labelling: variations among tree species and seasons. *New Phytologist* **190**(1): 181-192.

Dawson TE, Mambelli S, Plamboeck AH, Templer PH, Tu KP. 2002. Stable isotopes in plant ecology. *Annual review of ecology and systematics* **33**(1): 507-559.

Deeken R, Geiger D, Fromm J, Koroleva O, Ache P, Langenfeld-Heyser R, Sauer N, May ST, Hedrich R. 2002. Loss of the AKT2/3 potassium channel affects sugar loading into the phloem of *Arabidopsis*. *Planta* **216**(2): 334-344.

Desassis A. 1962. *Sur les modalités de formation des matières grasses dans le fruit d'Elaeis guineensis Jacq.* Thèse de doctorat : Sciences naturelles Thèse, Université de Paris Paris, France.

Du Q, Zhao X-h, Xia L, Jiang C-j, Wang X-g, Han Y, Wang J, Yu H-q. 2019. Effects of potassium deficiency on photosynthesis, chloroplast ultrastructure, ROS, and

antioxidant activities in maize (*Zea mays* L.). *Journal of Integrative Agriculture* **18**(2): 395-406.

Dubos B, Baron V, Bonneau X, Dassou O, Flori A, Impens R, Ollivier J, Pardon L. 2019. Precision agriculture in oil palm plantations: diagnostic tools for sustainable N and K nutrient supply.

Dubos B, Baron V, Bonneau X, Flori A, Ollivier J. 2018. High soil calcium saturation limits use of leaf potassium diagnosis when KCl is applied in oil palm plantations. *Experimental Agriculture* **54**(5): 794-804.

Dufrene E. 1989. *Photosynthèse, consommation en eau et modélisation de la production chez le palmier à huile (Elaeis guineensis Jacq.).* Paris 11.

Dufrene E, Saugier B. 1993. Gas exchange of oil palm in relation to light, vapour pressure deficit, temperature and leaf age. *Functional Ecology*: 97-104.

Duranceau M, Ghashghaie J, Badeck F, Deleens E, Cornic G. 1999. $\delta_{13}C$ of CO_2 respired in the dark in relation to $\delta_{13}C$ of leaf carbohydrates in *Phaseolus vulgaris* L. under progressive drought. *Plant, Cell & Environment* **22**(5): 515-523.

Dussert S, Guerin C, Andersson M, Joet T, Tranbarger TJ, Pizot M, Sarah G, Omore A, Durand-Gasselin T, Morcillo F. 2013. Comparative transcriptome analysis of three oil palm fruit and seed tissues that differ in oil content and fatty acid composition. *Plant Physiol* **162**(3): 1337-1358.

Ebelhar S, Kamprath E, Moll R. 1987. Effects of nitrogen and potassium on growth and cation composition of corn genotypes differing in average ear number 1. *Agronomy journal* **79**(5): 875-881.

Epron D, Bahn M, Derrien D, Lattanzi FA, Pumpanen J, Gessler A, Hogberg P, Maillard P, Dannoura M, Gerant D, et al. 2012. Pulse-labelling trees to study carbon allocation dynamics: a review of methods, current knowledge and future prospects. *Tree Physiol* **32**(6): 776-798.

Epron D, Cabral OM, Laclau JP, Dannoura M, Packer AP, Plain C, Battie-Laclau P, Moreira MZ, Trivelin PC, Bouillet JP, et al. 2016. In situ $^{13}CO_2$ pulse labelling of field-grown eucalypt trees revealed the effects of potassium nutrition and throughfall exclusion on phloem transport of photosynthetic carbon. *Tree Physiol* **36**(1): 6-21.

Evans H, Wildes R 1971. Potassium and its role in enzyme activation. *Proc. 8th Colloq. Int. Potash Inst. Bern*. 13-39.

Evans HJ. 1963. Effect of potassium & other univalent cations on activity of pyruvate kinase in *Pisum sativum*. *Plant Physiology* **38**(4): 397.

Evans HJ, Sorger GJ. 1966. Role of mineral elements with emphasis on the univalent cations. *Annual review of plant physiology* **17**(1): 47-76.

Fairhurst T, Härdter R. 2003. Oil palm: management for large and sustainable yields. *Oil palm: management for large and sustainable yields.*

Fairhurst TH. 1996. Management of nutrients for efficient use in small holder oil palm plantations.

Fallavier P, Breysse M, Olivin J. 1989. Etude expérimentale de la dynamique du potassium dans deux sols tropicaux utilisés pour la culture du palmier à huile. *Oléagineux* **44**(5): 197-207.

Farley RF, Draycott AP. 1975. Growth and yield of sugar beet in relation to potassium and sodium supply. *Journal of the Science of Food and Agriculture* **26**(4): 385-392.

Favreau B, Denis M, Ployet R, Mounet F, Peireira da Silva H, Franceschini L, Laclau J-P, Labate C, Carrer H. 2019. Distinct leaf transcriptomic response of water deficient *Eucalyptus grandis* submitted to potassium and sodium fertilization. *PloS one* **14**(6): e0218528-e0218528.

Fiehn O 2006. Metabolite profiling in *Arabidopsis*. In: Salinas J, Sanchez-Serrano JJ eds.

Arabidopsis Protocols. Totowa, NJ: Humana Press, 439-447.

Fiehn O, Wohlgemuth G, Scholz M, Kind T, Lee DY, Lu Y, Moon S, Nikolau B. 2008. Quality control for plant metabolomics: reporting MSI-compliant studies. *The Plant Journal* **53**(4): 691-704.

Foong SF 1991. Potential evapotranspiration, potential yield and leaching losses of oil palm. *PORIM International Palm Oil Conference*. Kuala Lumpur, Malaysia: Palm Oil Research Institute of Malaysia, Ministry of Primary Industries. 105-119.

Foster HL. 1985. *Oil palm yield responses to N and K fertilizers in different environments in peninsular malaysia*: Palm Oil Research Institute of Malaysia, Ministry of Primary Industries, Malaysia.

Foster HL 2002. Assessment of oil palm requirements. In: Fairhurst TH, Härdter R eds. The oil palm, management for large and sustainable yields. . *Potash and Phosphate Institute of Canada (ESEAP)*. Singapore.

Foster HL, Dolmat MTH, Zakaria ZZ. 1985. *Oil palm yields in the absence of N and K fertilizers in different environments in peninsular Malaysia*: Palm Oil Research Institute of Malaysia, Ministry of Primary Industries, Malaysia.

Foster HL, Mohammed AT. 1988. Variation in the fertilizer requirements of oil palm in peninsular Malaysia. I. Within the same soil series. *PORIM Bulletin, Palm Oil Research Institute, Malaysia*(116): 1-9.

Foster HL, Prabowo NE. 1996. *Variation in the potassium fertiliser requirements of oil palm in North Sumatra*: Palm Oil Research Institute of Malaysia.

Francey RJ, Farquhar GD. 1982. An explanation of $^{13}C/^{12}C$ variations in tree rings. *Nature* **297**(5861): 28-31.

Freeman GG, Mossadeghi N. 1970. Studies on potassium nutrition of plants IV.—Effect of potassium nutrition on the composition of leaves of cabbage seedlings (*Brassica oleracea capitata*). *Journal of the Science of Food and Agriculture* **21**(10): 492-495.

Froment M, Turley D, Collings L. 2000. Effect of nutrition on growth and oil quality in linseed. *Tests of Agrochemicals and Cultivars*(21): 29-30.

Fu J, Gong Z, Kelly BC. 2019. Metabolomic profiling of zebrafish (*Danio rerio*) embryos exposed to the antibacterial agent triclosan. *Environmental Toxicology and Chemistry* **38**(1): 240-249.

Galmés J, Ribas-Carbó M, Medrano H, Flexas J. 2011. Rubisco activity in Mediterranean species is regulated by the chloroplastic CO_2 concentration under water stress. *Journal of Experimental Botany* **62**(2): 653-665.

Gaydou EM, Arrivets J. 1983. Effects of phosphorus, potassium, dolomite, and nitrogen fertilization on the quality of soybean. Yields, proteins, and lipids. *Journal of Agricultural and Food Chemistry* **31**(4): 765-769.

Gaymard F, Pilot G, Lacombe B, Bouchez D, Bruneau D, Boucherez J, Michaux-Ferriere N, Thibaud J-B, Sentenac H. 1998. Identification and disruption of a plant shaker-like outward channel involved in K^+ release into the xylem sap. *Cell* **94**(5): 647-655.

Gerardeaux E, Jordan-Meille L, Constantin J, Pellerin S, Dingkuhn M. 2010. Changes in plant morphology and dry matter partitioning caused by potassium deficiency in *Gossypium hirsutum* (L.). *Environmental and Experimental Botany* **67**(3): 451-459.

Gerardeaux E, Saur E, Constantin J, Porté A, Jordan-Meille L. 2009. Effect of carbon assimilation on dry weight production and partitioning during vegetative growth. *Plant and Soil* **324**(1-2): 329-343.

Gerritsma W. 1988. Simulation of oil palm yield. *Wageningen: Dept of Theoretical Production Ecology, Agricultural University Wageningen*.

Gerritsma W, Soebagyo F. 1999. An analysis of the growth of leaf area of oil palms in

Indonesia. *Experimental Agriculture* **35**(3): 293-308.
Gessler A, Brandes E, Buchmann N, Helle G, Rennenberg H, Barnard RL. 2009. Tracing carbon and oxygen isotope signals from newly assimilated sugars in the leaves to the tree-ring archive. *Plant, Cell & Environment* **32**(7): 780-795.
Goh K, Po SB 2005. Fertilizer recommendation systems for oil palm: estimating the fertilizer rates. *Proceedings of MOSTA Best practices workshops-agronomy and crop management. Malaysian Oil Scientists' and Technologists' Association*.
Goulding K, Loveland P. 1986. The classification and mapping of potassium reserves in soils of England and Wales. *Journal of Soil Science* **37**(4): 555-565.
Guo J, Wang S, Yu X, Dong R, Li Y, Mei X, Shen Y. 2018. Polyamines regulate strawberry fruit ripening by abscisic acid, auxin, and ethylene. *Plant Physiology* **177**(1): 339.
Guschina IA, Everard JD, Kinney AJ, Quant PA, Harwood JL. 2014. Studies on the regulation of lipid biosynthesis in plants: application of control analysis to soybean. *Biochimica et Biophysica Acta (BBA) - Biomembranes* **1838**(6): 1488-1500.
Haeder HE, Beringer H. 1981. Influence of potassium nutrition and water stress on the content of abscisic acid in grains and flag leaves of wheat during grain development. *Journal of the Science of Food and Agriculture* **32**(6): 552-556.
Haq MU, Mallarino AP. 2005. Response of soybean grain oil and protein concentrations to foliar and soil fertilization. *Agronomy Journal* **97**(3): 910-918.
Hartley C. 1988a. *The oil palm (Elaeis guineensis Jacq.)*. Harlow, UK: Longman Scientific and Technical.
Hartley C. 1988b. The oil palm (*Elaeis guineensis* Jacq.): Longman group UK Limited.
Hartley CWS. 1967. *The oil palm*. New York: Longman group Limited.
Harun M, Noor M. 2002. Fruit set and oil palm bunch components. *Journal of oil palm research* **14**: 24-33.
Heffer P. 2009. Assessment of fertilizer use by crop at the global level. *International Fertilizer Industry Association*.
Helal H, Mengel K. 1979. Nitrogen metabolism of young barley plants as affected by NaCl-salinity and potassium. *Plant and Soil* **51**(4): 457-462.
Henson I. 1990. Photosynthesis and source-sink relationships in oil palm (*Elaeis guineensis*). *Trans Malay Soc Plant Physiol* **2**(1): 165-171.
Henson I. 1991. Adaptation to light environment by leaves of oil palm (*Elaeis guineensis*). *PORIM Bulletin*(22): 1-8.
Henson IE. 2006. Modelling vegetative dry matter production of oil palm. *Oil Palm Bulletin* **52**: 25.
Henson IE. 2007. Modelling the effects of physiological and morphological characters on oil palm growth and productivity. *Oil Palm Bulletin* **54**: 1.
Henson IE 2012. 1 - A Brief History of the Oil Palm. In: Lai O-M, Tan C-P, Akoh CC eds. *Palm Oil*: AOCS Press, 1-29.
Hermine Bille N, Joseph Martin B, Georges Franck Ngando E, Lambert N, Félix Chancelin N, Godswill Ntsefong N. 2013. Morphogenesis of oil palm fruit (*Elaeis guineensis* Jacq.) in mesocarp and endocarp development. *Journal of Life Sciences* **7**(2).
Heuvelink E. 1997. Effect of fruit load on dry matter partitioning in tomato. *Scientia Horticulturae* **69**(1-2): 51-59.
Hoffman M, Samish RM 1970. Free amine content in fruit tree organs as an indicator of the nutritional status with respect to potassium. *Colloquium on Plant Analysis and Fertilizer Problems, 6th, Tel Aviv*.
Hosy E, Vavasseur A, Mouline K, Dreyer I, Gaymard F, Porée F, Boucherez J, Lebaudy A, Bouchez D, Véry A-A. 2003. The Arabidopsis outward K^+ channel GORK is

involved in regulation of stomatal movements and plant transpiration. *Proceedings of the National Academy of Sciences* **100**(9): 5549-5554.

Houngbossa S, Bonnemain JL. 1985. The nature of organic nutrients exported from the leaf of oil palm (*Elaeis guineensis*): effect of ethylenediaminetetraacetic acid on exudation. *Bulletin de la Societe Botanique de France, Lettres Botaniques* **132**(1): 15-23.

Hu W, Jiang N, Yang J, Meng Y, Wang Y, Chen B, Zhao W, Oosterhuis DM, Zhou Z. 2016a. Potassium (K) supply affects K accumulation and photosynthetic physiology in two cotton (*Gossypium hirsutum* L.) cultivars with different K sensitivities. *Field Crops Research* **196**: 51-63.

Hu W, Yang J, Meng Y, Wang Y, Chen B, Zhao W, Oosterhuis DM, Zhou Z. 2015. Potassium application affects carbohydrate metabolism in the leaf subtending the cotton (*Gossypium hirsutum* L.) boll and its relationship with boll biomass. *Field Crops Research* **179**: 120-131.

Hu W, Yang J, Wang S, Chen B, Zhou Z. 2018. Effects of potassium deficiency on the enzymatic changes in developing cotton fibers. *Acta Physiologiae Plantarum* **40**.

Hu W, Zhao W, Yang J, Oosterhuis DM, Loka DA, Zhou Z. 2016b. Relationship between potassium fertilization and nitrogen metabolism in the leaf subtending the cotton (*Gossypium hirsutum L.*) boll during the boll development stage. *Plant Physiology and Biochemistry* **101**: 113-123.

Huber SC. 1984. Biochemical basis for effects of K-deficiency on assimilate export rate and accumulation of soluble sugars in soybean leaves. *Plant physiology* **76**(2): 424-430.

Husri MN, Ong-Abdullah M. 2018. Importance of KUP8 for K^+ uptake in rooted plantlets of *Elaeis guineensis* under K^+ sufficient conditions. *South African Journal of Botany* **118**: 65-75.

Hussain SS, Ali M, Ahmad M, Siddique KHM. 2011. Polyamines: natural and engineered abiotic and biotic stress tolerance in plants. *Biotechnology Advances* **29**(3): 300-311.

Ikemefuna J, Adamson I. 1984. Chlorophyll and carotenoid changes in ripening palm fruit, *Elaeis guineënsis*. *Phytochemistry* **23**(7): 1413-1415.

Imogie A, Oviasogie P, Ejedegba B, Udosen C. 2012. Effect of potassium (K) source on oil palm yield at Okomu oil palm Plc, Ovia North East LGA of Edo State. *International Journal of Plant Research* **2**(1): 35-38.

Jacquemard J. 1979. Contribution to the study of the height growth of the stems of *Elaeis guineensis* (Jacq.)[oil palm, Ivory Coast]. Study of the L2T x DIOD cross. *Oleagineux*.

Jacquemard JC. 2012. *Le palmier à huile*: Quae.

Jeje AA, Odetola AO, Zimmermann MH. 1978. Transpiration and oil accumulation rates for developing oil palm fruits *Elaeis guineensis* Jacq. R. *Acta Botanica Neerlandica* **27**(3-4): 213-228.

Jin SH, Huang JQ, Li XQ, Zheng BS, Wu JS, Wang ZJ, Liu GH, Chen M. 2011. Effects of potassium supply on limitations of photosynthesis by mesophyll diffusion conductance in *Carya cathayensis*. *Tree physiology* **31**(10): 1142-1151.

Jones G, Lutz J, Smith T. 1977. Effects of phosphorus and potassium on soybean nodules and seed yield 1. *Agronomy Journal* **69**(6): 1003-1006.

Jordan-Meille L, Pellerin S. 2004. Leaf area establishment of a maize (*Zea mays* L.) field crop under potassium deficiency. *Plant and Soil* **265**(1-2): 75-92.

Jourdan C, Rey H. 1997a. Architecture and development of the oil-palm (*Elaeis guineensis* Jacq.) root system. *Plant and Soil* **189**(1): 33-48.

Jourdan C, Rey H. 1997b. Modelling and simulation of the architecture and development of the oil-palm (*Elaeis guineensis* Jacq.) root system. *Plant and soil* **190**(2): 217-233.

Kimbrough E, Blaser R, Wolf D. 1971. Potassium effects on regrowth of alfalfa (*Medicago*

sativa L.). *Agronomy Journal* **63**(6): 836-839.

Koch K, Mengel K. 1974. The influence of the level of potassium supply to young tobacco plants (*Nicotiana tabacum* L.) on short‐term uptake and utilisation of nitrate nitrogen (^{15}N). *Journal of the Science of Food and Agriculture* **25**(5): 465-471.

Kozlowski T. 1992. Carbohydrate sources and sinks in woody plants. *The botanical review* **58**(2): 107-222.

Kumar AR, Kumar N, Kavino M. 2006. Role of potassium in fruit crops-a review. *AGRICULTURAL REVIEWS-AGRICULTURAL RESEARCH COMMUNICATIONS CENTRE INDIA* **27**(4): 284.

Laclau JP, Almeida JC, Goncalves JL, Saint-Andre L, Ventura M, Ranger J, Moreira RM, Nouvellon Y. 2009. Influence of nitrogen and potassium fertilization on leaf lifespan and allocation of above-ground growth in *Eucalyptus* plantations. *Tree Physiol* **29**(1): 111-124.

Lamade E, Djégui N, Leterme P. 1996. Estimation of carbon allocation to the roots from soil respiration measurements of oil palm. *Plant and Soil* **181**(2): 329-339.

Lamade E, Ollivier J, Rozier-Abouab T, Gérardeaux E 2014. Occurrence of potassium location in oil palm tissues with reserve sugars: consequences for oil palm K status determination. *IOPC conference*. Bali: Convention Center.

Lamade E, Setiyo E. 1996. Variation in maximum photosynthesis of oil palm in Indonesia: comparison of three morphologically contrasting clones. *Plantations, recherche, développement* **3**(6): 429-438.

Lamade E, Setiyo IE, Girard S, Ghashghaie J. 2009. Changes in $^{13}C/^{12}C$ of oil palm leaves to understand carbon use during their passage from heterotrophy to autotrophy. *Rapid Commun Mass Spectrom* **23**(16): 2586-2596.

Lamade E, Tcherkez G, Darlan NH, Rodrigues RL, Fresneau C, Mauve C, Lamothe-Sibold M, Sketriené D, Ghashghaie J. 2016. Natural ^{13}C distribution in oil palm (*Elaeis guineensis* Jacq.) and consequences for allocation pattern. *Plant, Cell & Environment* **39**(1): 199-212.

Langella O, Valot B, Balliau T, Blein-Nicolas M, Bonhomme L, Zivy M. 2017. X!TandemPipeline: a tool to manage sequence redundancy for protein inference and phosphosite identification. *Journal of Proteome Research* **16**(2): 494-503.

Läuchli A, Pflüger R. 1978. Potassium transport through plant cell membranes and metabolic role of potassium in plants. 11^{th} congres potash institute, bern.

Lebaudy A, Pascaud F, Véry A-A, Alcon C, Dreyer I, Thibaud J-B, Lacombe B. 2010. Preferential KAT1-KAT2 heteromerization determines inward K^+ current properties in *Arabidopsis* guard cells. *Journal of Biological Chemistry* **285**(9): 6265-6274.

Legros S, Mialet-Serra I, Caliman J-P, Clement-Vidal A, Siregar F, Widiastuti L, Jourdan C, Dingkuhn M. 2006. *Carbohydrates reserves in 9 years old oil palm: nature, distribution and seasonal changes*.

Legros S, Mialet-Serra I, Caliman JP, Siregar FA, Clément-Vidal A, Dingkuhn M. 2009a. Phenology and growth adjustments of oil palm (*Elaeis guineensis*) to photoperiod and climate variability. *Annals of Botany* **104**(6): 1171-1182.

Legros S, Mialet-Serra I, Caliman JP, Siregar FA, Clement-Vidal A, Fabre D, Dingkuhn M. 2009b. Phenology, growth and physiological adjustments of oil palm (*Elaeis guineensis*) to sink limitation induced by fruit pruning. *Annals of botany* **104**(6): 1183-1194.

Legros S, Mialet-Serra I, Clement-Vidal A, Caliman JP, Siregar FA, Fabre D, Dingkuhn M. 2009c. Role of transitory carbon reserves during adjustment to climate variability and source-sink imbalances in oil palm (*Elaeis guineensis*). *Tree Physiol* **29**(10): 1199-1211.

Leigh RA, Wyn Jones R. 1984. A hypothesis relating critical potassium concentrations for growth to the distribution and functions of this ion in the plant cell. *New Phytologist* **97**(1): 1-13.

Lemoine R, La Camera S, Atanassova R, Dédaldéchamp F, Allario T, Pourtau N, Bonnemain J-L, Laloi M, Coutos-Thévenot P, Maurousset L, et al. 2013. Source-to-sink transport of sugar and regulation by environmental factors. *Frontiers in plant science* **4**: 272-272.

Loei H, Lim J, Tan M, Lim TK, Lin QS, Chew FT, Kulaveerasingam H, Chung MC. 2013. Proteomic analysis of the oil palm fruit mesocarp reveals elevated oxidative phosphorylation activity is critical for increased storage oil production. *J Proteome Res* **12**(11): 5096-5109.

Lu Z, Lu J, Pan Y, Li X, Cong R, Ren T. 2016a. Genotypic variation in photosynthetic limitation responses to K deficiency of *Brassica napus* is associated with potassium utilisation efficiency. *Functional plant biology* **43**(9): 880-891.

Lu Z, Lu J, Pan Y, Lu P, Li X, Cong R, Ren T. 2016b. Anatomical variation of mesophyll conductance under potassium deficiency has a vital role in determining leaf photosynthesis. *Plant, cell & environment* **39**(11): 2428-2439.

Maathuis F, Sanders D. 1994. Mechanism of high-affinity potassium uptake in roots of *Arabidopsis thaliana*. *Proceedings of the National Academy of Sciences* **91**(20): 9272-9276.

Marcelis L. 1996. Sink strength as a determinant of dry matter partitioning in the whole plant. *Journal of Experimental Botany*: 1281-1291.

Marschner H 2002. 8 - Functions of mineral nutrients: macronutrients. In: Marschner H ed. *Marschner's mineral nutrition of higher plants (second edition)*. San Diego: Academic Press, 229-312.

Marschner P, Rengel Z 2012. Nutrient availability in soils. *Marschner's mineral nutrition of higher plants*: Elsevier, 315-330.

Mengel K. 1980. Effect of potassium on the assimilate conduction to storage tissue. *Berichte der Deutschen Botanischen Gesellschaft* **93**(1): 353-362.

Mengel K 2002. Alternative or complementary role of foliar supply in mineral nutrition International Society for Horticultural Science (ISHS), Leuven, Belgium. 33-47.

Mengel K, Forster H. 1973. Der Einfluß der Kaliumkonzentration der ‘Bodenlösung’ auf den Ertrag, den Wasserverbrauch und die K‐Aufnahmearten von Zuckerrüben (*Beta vulgaris* ssp. esculenta var. altissima). *Zeitschrift für Pflanzenernährung und Bodenkunde* **134**(2): 148-156.

Mengel K, Viro M, Hehl G. 1976. Effect of potassium on uptake and incorporation of ammonium-nitrogen of rice plants. *Plant and Soil* **44**(3): 547-558.

Menon NR 2000. Factors affecting oil and kernel extraction rates. In: Yusof B, Jalani BS, Chan KW eds. *Advances in oil palm research*. Kajang, Malaysia: Malaysian Palm Oil Board, 697-743.

Meunier J, Gascon JP. 1972. Le schéma général d'amélioration du palmier à huile à l'IRHO. *Oléagineux* **27**(1): 1-12, 11 micro-fiche numéro CP_HO720002.

Mirande-Ney C, Tcherkez G, Gilard F, Ghashghaie J, Lamade E. 2019. Effects of potassium fertilization on oil palm fruit metabolism and mesocarp lipid accumulation. *Journal of Agricultural and Food Chemistry* **67**(33): 9432-9440.

Muhammad SA, AB KADIR MO, RODHI AM, HASSAN‡ HM. 2017. Variations of $\delta_{13}C$ and $\delta_{15}N$ in oil palm tree organs: an insight into C and N distribution. *Journal of Oil Palm Research* **29**(2): 242-250.

Mullins GL, Reeves DW, Burmester CH, Bryant HH. 1994. In-row subsoiling and potassium placement effects on root growth and potassium content of cotton.

Agronomy Journal **86**(1): 136-139.

Nelson W, Burkhart L, Colwell W. 1946. Fruit development, seed quality, chemical composition, and yield of soybeans as affected by potassium and magnesium 1. *Soil Science Society of America Journal* **10**(C): 224-229.

Neoh BK, Teh HF, Ng TL, Tiong SH, Thang YM, Ersad MA, Mohamed M, Chew FT, Kulaveerasingam H, Appleton DR. 2013. Profiling of metabolites in oil palm mesocarp at different stages of oil biosynthesis. *J Agric Food Chem* **61**(8): 1920-1927.

Nitsos RE, Evans HJ. 1966. Effects of univalent cations on the inductive formation of nitrate reductase. *Plant physiology* **41**(9): 1499-1504.

Nowak T, Mildvan AS. 1972. Nuclear magnetic resonance studies of the function of potassium in the mechanism of pyruvate kinase. *Biochemistry* **11**(15): 2819-2828.

O'Toole J, Treharne K, Turnipseed M, Crookston K, Ozbun J. 1980. Effect of potassium nutrition on leaf anatomy and net photosynthesis of *Phaseolvs vulgaris* L. *New Phytologist* **84**(4): 623-630.

Obahiagbon F, Ilori GE, Erhabor J. 2012. Assessment of the nutritional constituents of *Elaeis guineensis* Jacq. exudates from different states of Nigeria. *J. Appl. Sci. Environ. Manage*.

Ochs R. 1965. Contribution à l'étude de la fumure potassique du palmier à huile. *Oléagineux* **N°8-9**(20ème année): 497-501.

Ochs R, Ollagnier M. 1977. Effect of fertilizers on composition of lipids produced by perennial tropical oil plants and on their yield. *Oléagineux* **32**(10): 409-426.

Offermann C, Ferrio JP, Holst J, Grote R, Siegwolf R, Kayler Z, Gessler A. 2011. The long way down—are carbon and oxygen isotope signals in the tree ring uncoupled from canopy physiological processes? *Tree Physiology* **31**(10): 1088-1102.

Okamoto S. 1969. The respiration in leaf disks from younger taro plants under a moderate potassium deficiency. *Soil Science and Plant Nutrition* **15**(6): 274-279.

Ollagnier M, Ochs R. 1973. Interaction entre l'azote et le potassium dans la nutrition des oléagineux tropicaux. *Oléagineux* **28**(11): 493-507, 491 micro-fiche numéro CP_HO730062.

Ollagnier M, Ochs R. 1981. Management of mineral nutrition in industrial oil palm plantations. Fertilizer savings. *Oléagineux* **36**(8/9): 409-421.

Ollagnier M, Olivin J. 1984a. Effets de la nutrition sur la production. Progrès génétiques et effets de la nutrition sur la qualité de l'huile de palme. 1ere partie. *Oléagineux* **39**(7): 349-368.

Ollagnier M, Olivin J. 1984b. Effets de la nutrition sur la production. Progrès génétiques et effets de la nutrition sur la qualité de l'huile de palme. 2e partie. *Oléagineux* **39**(8-9): 401-407.

Ollivier J, Flori A, Cochard B, Amblard P, Turnbull N, Syahputra I, Suryana E, Lubis Z, Surya E, Sihombing E. 2017. Genetic variation in nutrient uptake and nutrient use efficiency of oil palm. *Journal of Plant Nutrition* **40**(4): 558-573.

Omoti U, Ataga D, Isenmila A. 1983. Leaching losses of nutrients in oil palm plantations determined by tension lysimeters. *Plant and Soil* **73**(3): 365-376.

Pate J. 1973. Uptake, assimilation and transport of nitrogen compounds by plants. *Soil Biology and Biochemistry* **5**(1): 109-119.

Peoples TR, Koch DW. 1979. Role of potassium in carbon dioxide assimilation in Medicago sativa L. *Plant physiology* **63**(5): 878-881.

Pettigrew W, Meredith Jr W. 1997. Dry matter production, nutrient uptake, and growth of cotton as affected by potassium fertilization. *Journal of Plant Nutrition* **20**(4-5): 531-548.

Pettigrew WT. 1999. Potassium deficiency increases specific leaf weights and leaf glucose

levels in field-grown cotton. *Agronomy Journal* **91**(6): 962-968.
Pettigrew WT. 2008. Potassium influences on yield and quality production for maize, wheat, soybean and cotton. *Physiologia Plantarum* **133**(4): 670-681.
Peuke AD, Jeschke WD, Hartung W. 2002. Flows of elements, ions and abscisic acid in *Ricinus communis* and site of nitrate reduction under potassium limitation. *Journal of Experimental Botany* **53**(367): 241-250.
Pfluger R, Mengel K. 1972. The photochemical activity of chloroplasts from various plants with different potassium nutrition. *Plant and Soil* **36**: 417-425.
Purwanto OD, Faustina E, Shintarika F. 2018. Roles and optimisation rate of potassium fertiliser for immature oil palm (*Elaeis guineensis* Jacq.) on an Ultisol soil in Indonesia. *Journal of Agriculture and Rural Development in the Tropics and Subtropics (JARTS)* **119**(1): 13-22.
Pushparajah E. 1994. *Leaf analysis and soil testing for plantation tree crops*: ASPAC & FFTC.
Rahim A, Abdullah S, Basran Z. 2003. An economic perspective of oil extraction rate in the oil palm industry of Malaysia. *Oil Palm Industry Economic Journal* **3**.
Rankine I, Fairhurst T. 1999. Management of phosphorus, potassium and magnesium in mature oil palm. *Better Crops International* **13**(1): 11.
Rengel Z, Damon PM. 2008. Crops and genotypes differ in efficiency of potassium uptake and use. *Physiologia Plantarum* **133**(4): 624-636.
Ruan J, Wu X, Ye Y, Härdter R. 1998. Effect of potassium, magnesium and sulphur applied in different forms of fertilisers on free amino acid content in leaves of tea (*Camellia sinensis*L). *Journal of the Science of Food and Agriculture* **76**(3): 389-396.
Ruer P, Varéchon C. 1964. Premières observations sur les caractéristiques du pétiole de la feuille de palmier à huile. *Oléagineux* **19**(8-9): 539-542.
Rufty TW, Jackson WA, Raper CD. 1981. Nitrate reduction in roots as affected by the presence of potassium and by flux of nitrate through the roots. *Plant Physiology* **68**(3): 605-609.
Ruiz JM, Romero L. 2002. Relationship between potassium fertilisation and nitrate assimilation in leaves and fruits of cucumber (*Cucumis sativus*) plants. *Annals of Applied Biology* **140**(3): 241-245.
Salama A. 1987. Yield and oil quality of sunflower as affected by fertilization and growth-regulating hormones. *Novenytermeles* **36**(3): 191-202.
Sambanthamurthi R, Sundram K, Tan Y-A. 2000. Chemistry and biochemistry of palm oil. *Progress in Lipid Research* **39**(6): 507-558.
Sarrwy S, Mohamed EA, Hassan H. 2010. Effect of foliar sprays with potassium nitrate and mono-potassium phosphate on leaf mineral contents, fruit set, yield and fruit quality of picual olive trees grown under sandy soil conditions. *American-Eurasian Journal of Agricultural and Environmental Science* **8**(4): 420-430.
Saurer M, Kirdyanov AV, Prokushkin AS, Rinne KT, Siegwolf RTW. 2016. The impact of an inverse climate–isotope relationship in soil water on the oxygen-isotope composition of *Larix gmelinii* in Siberia. *New Phytologist* **209**(3): 955-964.
Schertz F. 1929. The effect of potassium, nitrogen and phosphorus fertilizing upon the chloroplast pigments, upon the mineral content of the leaves, and upon production in crop plants. *Plant physiology* **4**(2): 269.
Schroeder D. 1978. Structure and weathering of potassium containing minerals. *IPI Research Topics*: 5-25.
Schwartzkopf C. 1972. Potassium, calcium, magnesium—How they relate to plant growth. *USGA Green Section Record*: 1-2.
Seguin P, Zheng W. 2006. Potassium, phosphorus, sulfur, and boron fertilization effects on

soybean isoflavone content and other seed characteristics. *Journal of Plant Nutrition* **29**(4): 681-698.

Senbayram M, Gransee A, Wahle V, Thiel H. 2016. Role of magnesium fertilisers in agriculture: plant–soil continuum. *Crop and Pasture Science* **66**(12): 1219-1229.

Seo G, Jo J, Choi C. 1986. The effects of fertilization level on the growth and oil quality in sesame (*Sesamum indicum* L.). *Korean Journal of Crop Science (Korea R.)*.

Serrano M, Zapata PJ, Martínez-Romero D, Díaz-Mula HM, Valero D 2016. 7 - Polyamines as an ecofriendly postharvest tool to maintain fruit quality. In: Siddiqui MW ed. *Eco-Friendly Technology for Postharvest Produce Quality*: Academic Press, 219-242.

Singh R, Ong-Abdullah M, Low E-TL, Manaf MAA, Rosli R, Nookiah R, Ooi LC-L, Ooi S-E, Chan K-L, Halim MA, et al. 2013. Oil palm genome sequence reveals divergence of interfertile species in Old and New worlds. *Nature* **500**(7462): 335-339.

Smirnoff N, Stewart G. 1985. Nitrate assimilation and translocation by higher plants: comparative physiology and ecological consequences. *Physiologia Plantarum* **64**(2): 133-140.

Sorger GJ, Ford RE, Evans HJ. 1965. Effects of univalent cations on the immunoelectrophoretic behavior of pyruvic kinase. *Proceedings of the National Academy of Sciences of the United States of America* **54**(6): 1614.

Spalding EP, Hirsch RE, Lewis DR, Qi Z, Sussman MR, Lewis BD. 1999. Potassium uptake supporting plant growth in the absence of AKT1 channel activity: inhibition by ammonium and stimulation by sodium. *The Journal of general physiology* **113**(6): 909-918.

Sparks DL. 2012. *Advances in agronomy*: Academic Press.

Squire G. 1986. A physiological analysis for oil palm trials. *Porim Bulletin*(12): 12-31.

Squire G, Corley R. 1987. Oil palm. *Tree crop physiology*: 141-167.

Squire GR. 1990. *The physiology of tropical crop production*: CAB International.

Subke J-A, Heinemeyer A, Vallack HW, Leronni V, Baxter R, Ineson P. 2012. Fast assimilate turnover revealed by in situ $^{13}CO_2$ pulse-labelling in Subarctic tundra. *Polar Biology* **35**(8): 1209-1219.

Suresh K, Nagamani C. 2006. Variations in photosynthetic rate and associated parameters with age of oil palm leaves under irrigation. *Photosynthetica* **44**: 309-311.

Sweeney DW, Granade GV, Eversmeyer MG, Whitney DA. 2000. Phosphorus, potassium, chloride, and fungicide effects on wheat yield and leaf rust severity. *Journal of Plant Nutrition* **23**(9): 1267-1281.

Tailliez B, Ballo K. 1992. A method for measuring oil palm leaf area. *Oléagineux (Paris)* **47**(8-9): 537-545.

Tampubolon FH, Daniel C, Ochs R. 1990. Réponses du palmier à huile aux fumures azotée et phosphorée à Sumatra. *Oléagineux* **45**(11): 475-486.

Tavares G, Venturini G, Padilha K, Zatz R, Pereira AC, Thadhani RI, Rhee EP, Titan SMO. 2018. 1,5-Anhydroglucitol predicts CKD progression in macroalbuminuric diabetic kidney disease: results from non-targeted metabolomics. *Metabolomics* **14**(4): 39.

Teh HF, Neoh BK, Hong MP, Low JY, Ng TL, Ithnin N, Thang YM, Mohamed M, Chew FT, Yusof HM, et al. 2013a. Differential metabolite profiles during fruit development in high-yielding oil palm mesocarp. *PLoS One* **8**(4): 61344.

Teh HF, Neoh BK, Hong MPL, Low JYS, Ng TLM, Ithnin N, Thang YM, Mohamed M, Chew FT, Yusof HM, et al. 2013b. Differential Metabolite Profiles during Fruit Development in High-Yielding Oil Palm Mesocarp. *PLOS ONE* **8**(4): e61344.

Teh HF, Neoh BK, Wong YC, Kwong QB, Ooi TE, Ng TL, Tiong SH, Low JY, Danial

AD, Ersad MA, et al. 2014. Hormones, polyamines, and cell wall metabolism during oil palm fruit mesocarp development and ripening. *J Agric Food Chem* **62**(32): 8143-8152.

Teoh K, Chew P 1985. Investigations on areas and frequencies of fertiliser application in mature oil palms. *International Conference on Soils and Nutrition of Perennial Crops:(icosanp): proceedings, Kuala Lumpur, 13-15 Aug 1984. Organised by Malaysian Society of Soil Science/edited by AT Bachik and E. Pushparajah*: Kuala Lumpur, Malaysia: Malaysian Society of Soil Science, 1985.

Teoh KC, Chew PS 1988a. Potassium in the oil palm ecosystem and some implications to manuring practice.In Halim Hassan ea. *International Palm Oil Conference: Progress and prospects*. Kuala Lumpur, Malaysia: Palm Oil Research Institute of Malaysia. 277-286.

Teoh KC, Chew PS 1988b. Use of rachis analysis as an indicator of K nutrient status in oil palm.In Halim Hassan ea. *International Palm Oil Conference: Progress and prospects*. Kuala Lumpur, Malaysia: Palm Oil Research Institute of Malaysia. 262-271.

Terry N, Ulrich A. 1973. Effects of potassium deficiency on the photosynthesis and respiration of leaves of sugar beet. *Plant Physiology* **51**(4): 783-786.

Tester M, Blatt MR. 1989. Direct measurement of K channels in thylakoid membranes by incorporation of vesicles into planar lipid bilayers. *Plant physiology* **91**(1): 249-252.

Thomas RL, Sew PH, Mok CK, Chan KW, Easau PT, Ng SC. 1971. Fruit ripening in the oil-palm *Elaeis guineensis*. *Annals of Botany* **35**(143): 1219-1225.

Tiemann TT, Donough CR, Lim YL, Härdter R, Norton R, Tao HH, Jaramillo R, Satyanarayana T, Zingore S, Oberthür T 2018. Feeding the palm. 149-243.

Tinker P, Smilde K. 1963. Cation relationships and magnesium deficiency in the oil palm. *JW Afr. Inst. Oil Palm Res* **4**: 82-100.

Touraine B, Grignon N, Grignon C. 1988. Charge balance in NO_3^--fed soybean: estimation of K^+ and carboxylate recirculation. *Plant Physiology* **88**(3): 605-612.

Valot B, Langella O, Nano E, Zivy M. 2011. MassChroQ: a versatile tool for mass spectrometry quantification. *PROTEOMICS* **11**(17): 3572-3577.

Van Ranst E, Verloo M, Demeyer A, Pauwels J. 1999. *Manual for the soil chemistry and fertility laboratory: analytical methods for soils and plants equipment, and management of consumables*.

Voelker T. 2011. Secrets of palm oil biosynthesis revealed. *Proc Natl Acad Sci U S A* **108**(30): 12193-12194.

Volenec J 1999. Physiological control of alfalfa growth and yield. *Crop Yield*: Springer, 425-442.

Wallingford W. 1980. Function of potassium in plants. *Potassium for Agriculture. Potash and Phosphate Inst., Atlanta, Georgia*: 10-27.

Wang M, Zheng Q, Shen Q, Guo S. 2013. The critical role of potassium in plant stress response. *Int J Mol Sci* **14**(4): 7370-7390.

Wang Y, Wu W-H. 2017. Regulation of potassium transport and signaling in plants. *Current opinion in plant biology* **39**: 123-128.

Ward GM. 1959. Potassium in plant metabolism: II. Effect of potassium upon the carbohydrate and mineral composition of potato plants. *Canadian Journal of Plant Science* **39**(2): 246-252.

Watanabe H, Yoshida S. 1970. Effects of nitrogen, phosphorus, and potassium on photophosphorylation in rice in relation to the photosynthetic rate of single leaves. *Soil Science and Plant Nutrition* **16**(4): 163-166.

Weng XY, Zheng CJ, Xu HX, Sun JY. 2007. Characteristics of photosynthesis and

functions of the water–water cycle in rice (*Oryza sativa*) leaves in response to potassium deficiency. *Physiologia Plantarum* **131**(4): 614-621.

White PJ, Karley AJ 2010. Potassium. *Cell biology of metals and nutrients*: Springer, 199-224.

Wigoda N, Moshelion M, Moran N. 2014. Is the leaf bundle sheath a "smart flux valve" for K^+ nutrition? *Journal of Plant Physiology* **171**(9): 715-722.

Woittiez LS, van Wijk MT, Slingerland M, van Noordwijk M, Giller KE. 2017. Yield gaps in oil palm: a quantitative review of contributing factors. *European Journal of Agronomy* **83**: 57-77.

Wong YC, Teh HF, Mebus K, Ooi TEK, Kwong QB, Koo KL, Ong CK, Mayes S, Chew FT, Appleton DR, et al. 2017. Differential gene expression at different stages of mesocarp development in high- and low-yielding oil palm. *BMC Genomics* **18**(1): 470.

Xia J, Wishart DS. 2016. Using MetaboAnalyst 3.0 for comprehensive metabolomics data analysis. *Current Protocols in Bioinformatics* **55**(1): 14.10.11-14.10.91.

Xu J, Li H-D, Chen L-Q, Wang Y, Liu L-L, He L, Wu W-H. 2006. A protein kinase, interacting with two calcineurin B-like proteins, regulates K^+ transporter AKT1 in *Arabidopsis*. *Cell* **125**(7): 1347-1360.

Yamada S, Osaki M, Shinano T, Yamada M, Ito M, Permana AT. 2002. Effect of potassium nutrition on current photosynthesized carbon distribution to carbon and nitrogen compounds among rice, soybean, and sunflower. *Journal of Plant Nutrition* **25**(9): 1957-1973.

Yamashita T, Fujiwara A. 1966. Respiration and organis acid metabolism in potassium deficient rice plant. *Plant and Cell Physiology* **7**(4): 527-532.

Yamashita T, Fujiwara A. 1967. Metabolism of acetate-1-^{14}C in excised leaves from potassium deficient rice seedlings. *Plant and Cell Physiology* **8**(4): 557-565.

Yang X, Liu J, Wang W, Ye Z, Luo A. 2004. Potassium internal use efficiency relative to growth vigor, potassium distribution, and carbohydrate allocation in rice genotypes. *Journal of Plant Nutrition* **27**(5): 837-852.

Yin X, Vyn TJ. 2004. Critical leaf potassium concentrations for yield and seed quality of conservation-till soybean. *Soil Science Society of America Journal* **68**(5): 1626-1634.

Zahari MAKM, Zakaria MR, Ariffin H, Mokhtar MN, Salihon J, Shirai Y, Hassan MA. 2012. Renewable sugars from oil palm frond juice as an alternative novel fermentation feedstock for value-added products. *Bioresource technology* **110**: 566-571.

Zahoor R, Dong H, Abid M, Zhao W, Wang Y, Zhou Z. 2017. Potassium fertilizer improves drought stress alleviation potential in cotton by enhancing photosynthesis and carbohydrate metabolism. *Environmental and Experimental Botany* **137**: 73-83.

Zanin L, Tomasi N, Pinton R. 2015. Measurement of net high-affinity urea uptake in maize plants. *Bio Protoc* **5**: e1490.

Zeven AC. 1967. *The semi-wild oil palm and its industry in Africa*: Pudoc.

Zhai Z, Liu H, Xu C, Shanklin J. 2017. Sugar potentiation of fatty acid and triacylglycerol accumulation. *Plant Physiology* **175**(2): 696-707.

Zhao D, Oosterhuis D, Bednarz C. 2001. Influence of potassium deficiency on photosynthesis, chlorophyll content, and chloroplast ultrastructure of cotton plants. *Photosynthetica* **39**(1): 103-109.

Zhao X, Du Q, Zhao Y, Wang H, Li Y, Wang X, Yu H. 2016. Effects of different potassium stress on leaf photosynthesis and chlorophyll fluorescence in maize (*Zea Mays* L.) at seedling stage. *Agricultural Sciences* **Vol.07No.01**: 10.

Zioni AB, Vaadia Y, Lips SH. 1971. Nitrate uptake by roots as regulated by nitrate reduction products of the shoot. *Physiologia Plantarum* **24**(2): 288-290.

Zörb C, Senbayram M, Peiter E. 2014. Potassium in agriculture – status and perspectives.

Journal of Plant Physiology **171**(9): 656-669.

Appendix

A. Supplementary texts

Supplemental text S1: Oil palm fruit developmental stages and oil deposition kinetics

Here, we use oil palm fruit development and oil deposition kinetics that are well described by previous studies (Hartley, 1967; Thomas *et al.*, 1971):

- Stage 1 | 0-5 weeks after anthesis (WAA): the mesocarp is visible and composed of up to 92% of water. At this stage, the kernel is still liquid and the endocarp is rather thin.
- Stage 2 | 6-10 WAA: the endocarp becomes thicker and the kernel hardens.
- Stage 3 | 11-15 WAA: the kernel completely fills the seed cavity and the endocarp starts dehydrating while sclerification starts to isolate and protect the kernel.
- Stage 4 | 16-20 WAA: the mesocarp starts dehydrating by transpiration and there is active lipid biosynthesis. Sugars decrease.
- Stage 5 | 21-26 WAA: fruit reaches maturation. Structural constituents (lignin, hemicellulose, cellulose and pectins) represent 18-20%, and soluble protein and sugars account for 2-3% of mesocarp biomass.

Supplemental text S2: Total lipids analysis with 1H-NMR analyses

15 mg of ground mesocarp samples (fruits at maturity) were extracted with 500 µL KCl (0.88 %, w:w), 1 mL *d*-chloroform (Sigma-Aldrich), and 20 µL tetramethylsilane (TMS, 0.03% in *d*-chloroform) in 4-mL glass vials (Supelco). Samples were vortexed, kept on ice for 10 min and then re-vortexed. After centrifugation (3 min, 2,500 rpm, 16°C), 600 µL of the organic phase was collected and transferred to 5-mm NMR tubes (Z107373, Bruker). NMR analyses were performed on a 700 MHz Advance spectrometer (Bruker) at 25°C with a standard pulse program (zg30) over 244 scans. Chemical shifts were referenced against TMS.

B. Supplementary figures

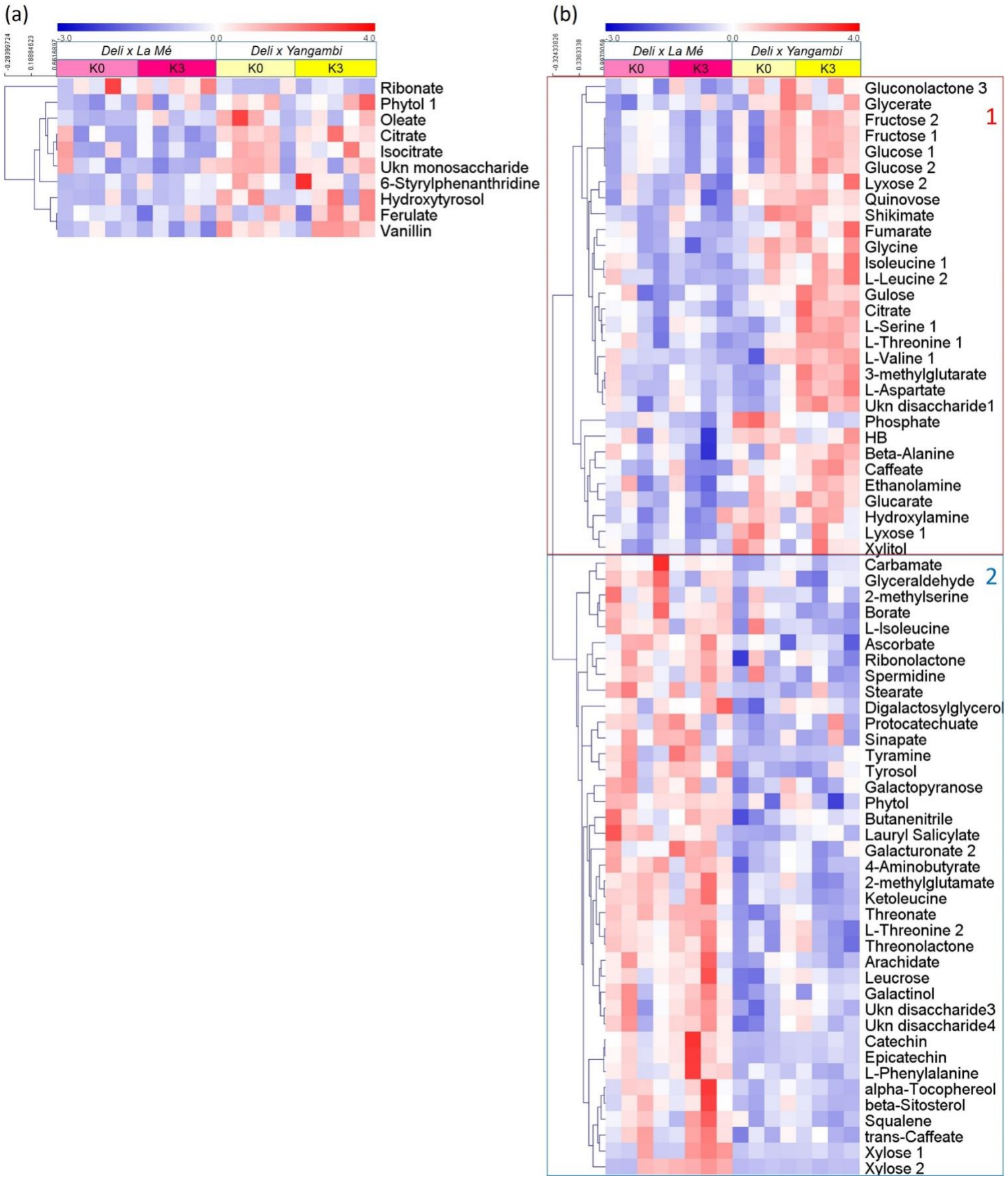

Figure S1. Metabolites significantly different (P<0.05) between crosses in metabolomics pattern, in *Deli x La Mé* (pink) and *Deli x Yangambi* (yellow) crosses sampled in 2017 (a) and 2018 (b). Scale from blue (lowest) to red (highest) to show the relative content (mean-centered). Hierarchical clustering (Pearson correlation) shown on left. Red (2) and blue (1) frames show metabolites that are more or less abundant in *Deli x La Mé* (compared to *Deli x Yangambi*), respectively. Numbers 1, 2 or 3 after metabolite names indicate different isomers obtained after derivation of a same compound. Ukn disaccharide 1-4 correspond to disaccharides (maltose or sucrose family) that could not be identified precisely. HB, hydroxybenzoate

Figure S2. Metabolomics response of mesocarp during fruit maturation in *Deli x La Mé* and *Deli x Yangambi* crosses. (a-b) Heatmap of metabolites significant for the maturation stage (P<0.01) in DL (a) and DY (b). Scale from blue (lowest) to red (highest) to show the relative content (mean-centered). Red frames (labelled A) show metabolites that increased during maturation and blue frames (labelled B) show metabolites that decreased with maturation. Abbreviations: DHB, 3,4-dihydroxybenzoate; HB, 4-hydroxybenzoate; DHS, 3-dehydroshikimate; HC, 4-hydroxycinnamate; GABA, γ-aminobutyrate; HMB, 4-hydroxy-3-methoxybenzoate (vanillate); NADM, N-acetyl-D-mannosamine. On bottom right, two metabolites (caprylate, putrescine) that are did not vary significantly during maturation in DY but did vary significantly in DL are shown to facilitate comparison.

C. Supplementary tables

Table S1. List of proteins significant for the cross effect in 2018 (Benjamini-Hochberg correction).

Accession number	Description	Pvalue (Cross effect)	Loading (Cross effect)
XP_010921685.1	Adenine nucleotide alpha hydrolases-like superfamily protein	2.42E-07	-0.0473331
XP_010926052.1	NAD(P)-binding Rossmann-fold superfamily protein (Cinnamoyl-CoA reductase)	8.27E-08	-0.0461637
XP_010907411.1	Methionine aminopeptidase 2B	2.99E-06	-0.0460055
XP_010941660.1	Phosphoglycerate kinase 3, cytosolic isoform X1	3.83E-06	-0.0454463
XP_010934326.1	Adenosine kinase 2-like	3.09E-07	-0.0448761
XP_010921546.1	Mannosyl-glycoprotein endo-beta-N-acetylglucosaminidase	8.84E-07	-0.0448145
XP_010940458.1	Aldolase superfamily protein	1.80E-05	-0.044642
XP_010930561.1	Glycinamide ribonucleotide (GAR) synthetase	7.36E-07	-0.0444355
XP_010922792.1	V-type proton ATPase subunit E	3.52E-05	-0.0444183
XP_010938781.1	amidase 1	8.68E-06	-0.0434407
XP_010924612.2	Phosphoenolpyruvate carboxylase 2	4.30E-05	-0.0434006
XP_010927580.1	Fructose-bisphosphate aldolase 1, cytoplasmic	6.03E-06	-0.0432054
XP_010914509.1	Pathogenesis-related protein 1-like	7.98E-05	-0.0431729
XP_010923803.1	glutathione S-transferase TAU 19	2.60E-05	-0.0431369
XP_010933076.1	Phosphopyruvate hydratase	3.44E-06	-0.0428156
XP_010915364.1	NADP-malic enzyme 3	4.80E-05	-0.0427539
XP_010941296.1	Chaperone protein htpG family protein	1.58E-04	-0.042726
XP_010931681.1	Fumarylacetoacetate (FAA) hydrolase family	1.44E-04	-0.0424722
XP_010933708.1	nitrilase-like protein 1	1.50E-05	-0.0421827
XP_010928833.1	PLAT/LH2 domain-containing lipoxygenase family protein	2.89E-04	-0.041927
XP_010929587.1	uncharacterized protein LOC105051024	1.11E-04	-0.0418438
XP_010942803.1	phosphoglucose isomerase 1	5.84E-05	-0.0418074
XP_010938666.1	S-formylglutathione hydrolase	3.57E-05	-0.0417312

XP_010941718.1	Inositol monophosphatase family protein	1.12E-06	-0.0417023
XP_010907928.1	enolase 1	2.13E-04	-0.0416507
XP_010908558.2	S-adenosyl-L-homocysteine hydrolase	9.57E-05	-0.0414787
XP_010931551.1	4-(cytidine 5'-phospho)-2-C-methyl-D-erithritol kinase	2.58E-05	-0.0412066
XP_019709780.1	Probable linoleate 9S-lipoxygenase 5	2.58E-05	-0.0410603
XP_010911890.1	aspartate aminotransferase	1.59E-04	-0.0410244
XP_010941303.1	Methenyltetrahydrofolate cyclohydrolase; Methylenetetrahydrofolate dehydrogenase (NADP(+))	6.11E-04	-0.0407506
XP_010914094.1	RNA-binding (RRM/RBD/RNP motifs) family protein	5.80E-04	-0.0406333
XP_010925637.2	SCAR family protein	9.35E-04	-0.0405515
XP_010908643.1	rhodanese-like domain-containing protein / PPIC-type PPIASE domain-containing protein	1.21E-04	-0.0405112
XP_010935251.1	AMP-dependent synthetase and ligase family protein	3.95E-04	-0.0405099
XP_010925701.1	ketol-acid reductoisomerase	6.72E-05	-0.0403843
XP_010908745.1	U2 small nuclear ribonucleoprotein A	1.31E-04	-0.0402851
XP_010915515.1	phosphoenolpyruvate carboxylase 1	7.30E-04	-0.0402352
XP_010930274.1	cysteine synthase D2	4.76E-06	-0.0400136
XP_010907558.1	haloacid dehalogenase-like hydrolase family protein	1.44E-05	-0.0398957
XP_010939360.1	Thioredoxin superfamily protein	6.00E-04	-0.0398849
XP_010930319.1	Aldolase superfamily protein	0.00110523	-0.0398462
XP_010931230.2	NAD(P)-binding Rossmann-fold superfamily protein	6.58E-05	-0.0398273
XP_010918502.1	Heat shock protein 70 (Hsp 70) family protein	2.08E-04	-0.0397847
XP_010943467.1	aconitase 1	3.51E-04	-0.039784
XP_010922296.1	NAD(P)-binding Rossmann-fold superfamily protein	4.43E-05	-0.0396309
XP_010920467.1	pfkB-like carbohydrate kinase family protein	3.29E-04	-0.0394274
XP_010910405.1	glyceraldehyde 3-phosphate dehydrogenase A subunit 2	0.00161413	-0.0393916
XP_010926761.1	pfkB-like carbohydrate kinase family protein	8.25E-04	-0.0392998
XP_010905780.1	TCP-1/cpn60 chaperonin family protein	2.69E-04	-0.0392272
XP_010931117.1	Glycosyl hydrolases family 32 protein	2.21E-04	-0.0391175
XP_010920552.1	NAD(P)-binding Rossmann-fold superfamily protein	2.18E-05	-0.039101
XP_010927782.1	Tyrosyl-tRNA synthetase, class Ib, bacterial/mitochondrial	3.34E-04	-0.0390599
XP_010926050.1	aluminum induced protein with YGL and LRDR motifs	0.00104735	-0.0389989
XP_010907964.1	Immunoglobulin E-set superfamily protein	1.84E-04	-0.0389678
XP_010916885.1	UDP-Glycosyltransferase superfamily protein	3.86E-04	-0.0387989

XP_010909225.1	methionine synthase 2	1.49E-04	-0.0387499
XP_010917850.1	methionine synthase 2	0.00204259	-0.0386529
XP_010926875.1	copper ion binding protein	6.96E-06	-0.0386446
XP_010930636.1	thylakoid lumenal protein (Mog1/PsbP/DUF1795-like photosystem II reaction center PsbP family protein)	2.21E-04	-0.0384408
XP_010943210.1	cinnamyl alcohol dehydrogenase 5	4.35E-04	-0.0384016
XP_010941286.1	Cyclophilin-like peptidyl-prolyl cis-trans isomerase family protein	4.73E-05	-0.038396
XP_010930359.1	GDSL-like Lipase/Acylhydrolase superfamily protein	7.91E-04	-0.0383056
XP_010943064.1	nitrite reductase 1	3.93E-04	-0.0382939
XP_010906459.1	cysteine synthase D2	1.92E-04	-0.0382726
XP_010935079.1	Chaperone protein htpG family protein	0.00317751	-0.038216
XP_010943015.1	alpha/beta-Hydrolases superfamily protein	5.63E-05	-0.0381524
XP_010905354.1	anthranilate synthase 2	3.65E-04	-0.0381055
XP_010941086.1	Cytochrome P450 superfamily protein	0.00118534	-0.038086
XP_010926163.1	aldehyde dehydrogenase 6B2	9.71E-04	-0.037962
XP_010943282.1	xylulose kinase-2	0.00252647	-0.0377297
XP_010938161.1	glutathione S-transferase TAU 8	0.00366096	-0.037691
XP_010928857.1	Translation elongation factor EF1B, gamma chain	0.00107656	-0.0375946
XP_010931733.1	thioredoxin family protein	0.00191442	-0.0374778
XP_010938585.1	annexin 3	0.00323309	-0.0374553
XP_010937618.1	triosephosphate isomerase	2.59E-04	-0.0370001
XP_010921787.1	acetone-cyanohydrin lyase	3.14E-04	-0.0368616
XP_019704990.1	UDP-Glycosyltransferase superfamily protein	8.72E-04	-0.0368176
XP_010916976.1	Oxidoreductase family protein	0.00390832	-0.036815
XP_010905138.1	Selenium-binding protein 1 isoform X2	5.73E-04	-0.0367675
XP_010906556.1	RNA-binding (RRM/RBD/RNP motifs) family protein	0.00699588	-0.0366709
XP_010913586.1	calcium sensing receptor	0.0014242	-0.0365995
XP_010940068.1	pantothenate kinase 2	3.35E-04	-0.0365048
XP_010938431.1	glutathione S-transferase F4	0.00243606	-0.0364449
XP_010908925.1	Zinc-binding ribosomal protein family protein	0.00151498	-0.0364231
XP_010918136.1	aconitase 1	0.00251653	-0.0363643
XP_010937888.1	Pleckstrin homology (PH) domain superfamily protein	0.00387469	-0.0362564
XP_010918518.1	membrane-associated progesterone binding protein 3	0.00195104	-0.0362271
XP_010929516.1	calreticulin 1a	0.00305602	-0.0361908

XP_010913597.1	enolase 1	0.00375813	-0.0360876
XP_010916712.1	GroES-like zinc-binding dehydrogenase family protein	0.00255846	-0.0360858
XP_010932591.1	ketose-bisphosphate aldolase class-II family protein	0.00562797	-0.0360785
XP_010910942.1	chlorophyll a-b binding protein 6	0.0022919	-0.0360007
XP_019710331.1	proteasome inhibitor-like protein	5.69E-04	-0.0358564
XP_010942223.1	Tryptophan synthase beta type 2	9.76E-04	-0.0355244
XP_019706271.1	Heat shock protein 70 (Hsp 70) family protein	0.00356143	-0.03543
XP_019711064.1	homoserine kinase	0.00151427	-0.0354059
XP_010939848.1	Tyrosine transaminase family protein	0.00316108	-0.0352882
XP_010928158.1	Chaperone protein htpG family protein	0.00397795	-0.0352644
XP_010933979.1	NAD(P)-binding Rossmann-fold superfamily protein	7.21E-04	-0.0352379
XP_010929760.1	alpha-soluble NSF attachment protein 2	0.00619188	-0.0352169
XP_010905974.1	Tubulin/FtsZ family protein	0.00112754	-0.035207
XP_010942140.1	WAS/WASL-interacting family protein	0.00258545	-0.0352012
XP_010932864.1	monodehydroascorbate reductase 6	0.00729514	-0.0351704
XP_010917066.1	pyrophosphorylase 1	0.00319327	-0.0351695
XP_019709211.1	GroES-like zinc-binding dehydrogenase family protein	2.81E-04	-0.0351618
XP_010941774.2	DEGP protease 2	0.00179712	-0.0351613
XP_010940091.2	NmrA-like negative transcriptional regulator family protein	4.92E-04	-0.0351524
XP_010926766.1	polyphenol oxidase, chloroplastic-like	0.01111564	-0.0350877
XP_010922748.1	elongation factor P (EF-P) family protein	5.55E-04	-0.0349987
NP_001306846.1	stem-specific protein TSJT1-like	0.00280853	-0.0348373
XP_019704345.1	Pentatricopeptide repeat (PPR) superfamily protein	0.00335073	-0.0347143
XP_010932113.1	Phosphoribosyltransferase family protein	8.23E-04	-0.0347093
XP_010935814.1	lactate/malate dehydrogenase family protein	0.00280029	-0.034302
XP_010913595.1	heat shock factor-binding protein 1	0.00481346	-0.0342172
XP_010921290.1	hydroxyproline-rich glycoprotein family protein	0.00188749	-0.0342138
XP_010915964.1	SOUL heme-binding family protein	0.00374411	-0.0341399
XP_010930238.1	Pyridoxal-dependent decarboxylase family protein	0.00413571	-0.0340279
XP_010918036.1	Ribosomal RNA small subunit methyltransferase J	9.00E-04	-0.0339578
XP_010920944.1	Peroxidase superfamily protein	0.00233538	-0.0339555
XP_010932235.1	Serine carboxypeptidase S28 family protein	0.00789915	-0.0337954
XP_010914334.1	Coproporphyrinogen III oxidase	1.72E-04	-0.0337887

XP_010942029.1	coatomer gamma-2 subunit, putative / gamma-2 coat protein, putative / gamma-2 COP	0.00335566	-0.0337652
NP_001306842.1	catalase isozyme 2	0.00631765	-0.0337233
XP_010913416.1	Phosphofructokinase family protein	0.0011371	-0.0336459
XP_010914166.1	aldehyde dehydrogenase 6B2	0.00296481	-0.0336247
XP_010912239.1	Aldolase superfamily protein	0.00111197	-0.0336173
XP_010930358.1	glutathione S-transferase zeta 1	0.00270811	-0.0335406
XP_010914406.1	dehydroquinate dehydratase, putative / shikimate dehydrogenase	0.00689211	-0.0334601
XP_010925305.2	Ribonuclease T2 family protein	0.00103562	-0.0333742
XP_010933259.1	Cyclophilin-like peptidyl-prolyl cis-trans isomerase family protein	0.01070208	-0.0333587
XP_010915540.1	2-oxoglutarate (2OG) and Fe(II)-dependent oxygenase superfamily protein	0.00664324	-0.0333253
XP_010910557.1	GroES-like zinc-binding dehydrogenase family protein	0.00148685	-0.0333038
NP_001306845.1	elongation factor 1-beta-like	0.00428666	-0.0332969
XP_010940278.1	Class I glutamine amidotransferase-like superfamily protein	0.00782458	-0.0332588
XP_010919339.1	reduced lateral root formation	0.01389886	-0.0332369
XP_010922329.1	O-Glycosyl hydrolases family 17 protein	0.01368622	-0.033163
XP_019705026.1	Ribose 5-phosphate isomerase, type A protein	0.00696764	-0.0331577
XP_010910140.1	dicarboxylate diiron protein, putative (Crd1)	0.0070748	-0.0331325
XP_010920378.1	aspartate aminotransferase 5	0.00266654	-0.0331005
XP_010934070.2	Ribosome-binding factor PSRP1, chloroplastic	2.87E-05	-0.0330115
XP_010915560.1	hypothetical protein (Protein of unknown function, DUF538)	0.00336262	-0.0329157
XP_010905531.1	cyclophilin 38	0.00938093	-0.0328072
XP_010927211.1	UDP-sugar pyrophosphorylase	2.49E-04	-0.0327862
XP_010916944.1	allene oxide cyclase 3	0.00368297	-0.0327722
XP_010940621.1	TCP-1/cpn60 chaperonin family protein	0.00500349	-0.032761
XP_010922672.1	LURP-one-like protein (DUF567)	0.009945	-0.0327609
XP_010921891.1	O-Glycosyl hydrolases family 17 protein	0.00638322	-0.0327518
XP_010921619.1	sucrose synthase 1	0.00391477	-0.0327399
XP_010939055.1	WPP domain protein 2	0.00338372	-0.0326261
XP_010907209.1	Translation elongation factor EF1B, gamma chain	0.00993651	-0.0325407

XP_010920478.1	Lactate/malate dehydrogenase family protein	0.00156234	-0.0325047
XP_010940010.1	Acetamidase/Formamidase family protein	0.00308998	-0.0324658
XP_010904686.2	dihydropyrimidinase isoform X1	0.00664961	-0.0322247
XP_010916236.1	translocon at the outer envelope membrane of chloroplasts 34	0.01042534	-0.0321029
XP_010935200.1	glutathione S-transferase F4	0.00569443	-0.0320511
XP_010918637.1	AMP-dependent synthetase and ligase family protein	0.00901872	-0.0319679
XP_010941972.1	nitrogen fixation S (NIFS)-like 1	0.0069965	-0.031905
XP_010932997.1	alpha/beta-Hydrolases superfamily protein	0.00848471	-0.0318393
XP_010932417.1	FMN-linked oxidoreductases superfamily protein	0.00751009	-0.0318304
XP_010920972.1	Nitrilase/cyanide hydratase and apolipoprotein N-acyltransferase family protein	0.00426103	-0.0317208
XP_019709538.1	Rhodanese/Cell cycle control phosphatase superfamily protein	0.00206304	-0.0316727
XP_010918323.1	Galactose mutarotase-like superfamily protein	0.00389517	-0.0313404
XP_010920408.1	Ribosomal protein L11 family protein	0.00961785	-0.0313346
XP_010909223.1	pfkB-like carbohydrate kinase family protein	0.0125866	-0.0313083
XP_010941080.1	Chaperone protein htpG family protein	0.01289279	-0.0310082
XP_010905987.1	Ribosomal protein L1p/L10e family	0.00371645	-0.0310044
XP_010936350.1	P-loop containing nucleoside triphosphate hydrolases superfamily protein	0.00462964	-0.0309119
XP_010939851.1	N-terminal nucleophile aminohydrolases (Ntn hydrolases) superfamily protein	0.00826028	-0.0307884
XP_010933602.1	ATP-dependent caseinolytic (Clp) protease/crotonase family protein	0.00764084	-0.0307188
XP_010930575.1	hydroxyproline-rich glycoprotein family protein	0.01247653	-0.0306989
XP_010933455.1	phosphoenolpyruvate carboxykinase 1	0.00559913	-0.0306175
XP_019703725.1	Zinc-binding dehydrogenase family protein	0.0119684	-0.0303815
XP_010917276.1	Adenine nucleotide alpha hydrolases-like superfamily protein	0.0103643	-0.0302132
XP_010933889.1	peroxin 11D	0.01530118	-0.0302049
XP_010928413.1	Plastid-lipid associated protein PAP / fibrillin family protein	0.00589845	-0.0302036
XP_010941664.1	Probable gamma-aminobutyrate transaminase 3, mitochondrial	0.00157103	-0.0301218
XP_010916257.1	Fructose-bisphosphate aldolase 1, chloroplastic	0.001668	-0.0299434

XP_010910548.1	Ion channel POLLUX-like protein, putative (DUF1012)	0.00748804	-0.0298976
XP_010916331.1	RNA ligase/cyclic nucleotide phosphodiesterase family protein	0.00551804	-0.0295796
XP_010920729.1	Tetratricopeptide repeat (TPR)-like superfamily protein	0.00470377	-0.0295721
XP_010911739.2	glyceraldehyde 3-phosphate dehydrogenase A subunit 2	0.01335156	-0.0295183
XP_010939415.1	Zeaxanthin epoxidase, chloroplastic isoform X1	0.00973679	-0.0294256
XP_010915385.1	2-oxoglutarate (2OG) and Fe(II)-dependent oxygenase superfamily protein	0.0075185	-0.0293236
XP_010940546.1	binding to TOMV RNA 1L (long form)	0.01058834	-0.0292657
XP_010924024.2	Adenine nucleotide alpha hydrolases-like superfamily protein	0.01247748	-0.0289275
XP_010920402.1	thioredoxin family protein	0.00831371	-0.02892
XP_010917003.1	3-dehydroquinate synthase	8.28E-06	-0.0288331
XP_010932264.1	RNA-binding (RRM/RBD/RNP motifs) family protein	0.0150354	-0.0287445
XP_010940311.1	Clathrin adaptor complexes medium subunit family protein	0.00501349	-0.0286972
XP_010907599.1	Tetratricopeptide repeat (TPR)-like superfamily protein	0.00649929	-0.0286903
XP_010941975.1	cytochrome c oxidase-like protein	0.00501897	-0.0286634
XP_010908786.1	acetyl Co-enzyme a carboxylase biotin carboxylase subunit	0.01245098	-0.0286013
XP_010909285.1	Aldolase-type TIM barrel family protein	0.00111503	-0.0285928
XP_010923772.1	Tubulin/FtsZ family protein	0.005571	-0.0284376
XP_010925927.1	plasma-membrane associated cation-binding protein 1	0.00495813	-0.0277807
XP_010943899.1	RNA-binding (RRM/RBD/RNP motifs) family protein	0.01434912	-0.0276454
XP_010919638.1	Lipase/lipooxygenase, PLAT/LH2 family protein	0.00232755	-0.0274199
XP_010920509.1	NAD(P)-binding Rossmann-fold superfamily protein	0.01340238	-0.0271592
XP_010913007.1	Thiamine pyrophosphate dependent pyruvate decarboxylase family protein	0.00328451	-0.0267286
XP_010939688.1	Peroxidase superfamily protein	0.01113146	-0.0263671
XP_010933488.1	Peptidase M20/M25/M40 family protein	0.007757	-0.0262363
XP_010929910.2	NAD(P)-linked oxidoreductase superfamily protein	0.00773226	-0.0262221
XP_010907148.1	Heavy metal transport/detoxification superfamily protein	0.00127055	-0.0252522
XP_010937791.2	beta-hexosaminidase 1	0.00484601	-0.0251027
XP_010910878.1	Sec14p-like phosphatidylinositol transfer family protein	0.01362376	-0.024619
XP_019701579.1	phosphoglucosamine mutase family protein	0.01336797	-0.0243823

XP_010914531.2	phosphoribosylformylglycinamidine cyclo-ligase, chloroplast / phosphoribosyl-aminoimidazole synthetase / AIR synthase (PUR5)	0.0043464	-0.0237487
XP_010930888.1	Thioesterase superfamily protein	0.00362563	-0.023023
XP_010938339.1	PYR1-like 2	0.00958779	-0.0220715
XP_010914719.1	Peroxidase superfamily protein	0.00337475	-0.0211177
XP_010943121.2	Peptidase M20/M25/M40 family protein	0.00610583	-0.0202043
XP_010906118.1	Ribosomal protein S5 family protein	0.00798932	-0.0170813
XP_010929184.1	Membrane steroid binding protein 1	0.01129143	-0.0154964
XP_010912634.1	Disease resistance-responsive (dirigent-like protein) family protein	0.01208718	-0.0151228
XP_010942682.1	kinesin-like protein KIN-14B	0.00147039	0.0174757
XP_010930724.1	Aldehyde dehydrogenase 3H1	0.00114819	0.0217816
XP_010906269.1	Subtilisin-like protease SBT1.7	0.00215073	0.0226329
XP_010930088.1	Rubisco methyltransferase family protein	0.01210563	0.0243784
XP_010942312.2	glyceraldehyde 3-phosphate dehydrogenase A subunit 2	0.00942049	0.0247288
XP_010940822.1	UDP-Glycosyltransferase superfamily protein	0.01514608	0.0252904
XP_010933351.1	D-3-phosphoglycerate dehydrogenase	0.00948645	0.026653
XP_010938608.1	alanine:glyoxylate aminotransferase	0.01000878	0.0266636
XP_010930713.1	isopropylmalate dehydrogenase 1	0.00825864	0.0269565
XP_010934474.1	Signal recognition particle, SRP54 subunit protein	0.00584401	0.0272802
XP_010921184.1	Receptor-like protein kinase FERONIA	5.88E-04	0.0274055
XP_010939896.1	Calcium-dependent phosphotriesterase superfamily protein	0.00102019	0.0277378
XP_010931015.1	carotenoid cleavage dioxygenase 1	0.0048701	0.0277608
XP_010936352.2	Double Clp-N motif-containing P-loop nucleoside triphosphate hydrolases superfamily protein	0.00779394	0.0278164
XP_010918336.1	serine hydroxymethyltransferase 2	0.0076553	0.0278593
XP_010943742.1	Dihydrolipoamide succinyltransferase	0.00594702	0.0280088
XP_010934370.1	Phosphoglycerate mutase family protein	0.00520803	0.0281271
XP_010918525.1	NAD-dependent malic enzyme 2	0.00277722	0.0282049
XP_010906338.1	pyrophosphorylase 1	0.00897271	0.0282794
XP_010935683.1	Thiolase family protein	0.01169618	0.0286865
XP_010907410.1	Clathrin, heavy chain	0.01273721	0.0286967
XP_010913749.1	allene oxide synthase	0.01149393	0.0292523

XP_010926399.1	accelerated cell death 2 (ACD2)	0.01002715	0.0294086
XP_010909743.1	glycyl-tRNA synthetase / glycine-tRNA ligase	0.01370126	0.0294491
XP_010936744.2	D-3-phosphoglycerate dehydrogenase	0.01448563	0.0295724
XP_010914656.1	TCP-1/cpn60 chaperonin family protein	0.01437109	0.0297544
XP_010927383.2	Inositol monophosphatase family protein	0.00653915	0.0299259
XP_010912493.1	Aldolase superfamily protein	0.01076311	0.0300085
XP_010941216.1	glycine cleavage system H protein 3, mitochondrial-like	0.00638863	0.0301098
XP_010921937.1	Ribosomal protein S5/Elongation factor G/III/V family protein	0.00303982	0.0301444
XP_010915763.1	Regulator of chromosome condensation (RCC1) family protein	0.00666066	0.0301547
XP_010913825.2	Cyclophilin-like peptidyl-prolyl cis-trans isomerase family protein	0.01305851	0.0301976
XP_010918353.1	Glyceraldehyde 3-phosphate dehydrogenase A subunit 2	0.00122425	0.0303065
XP_010941107.1	Actin 1	0.00814231	0.0303482
XP_010909191.1	bacterial trigger factor	0.0064808	0.0303579
XP_010915593.1	magnesium chelatase i2	0.0148473	0.03036
XP_010937415.2	Haloacid dehalogenase-like hydrolase (HAD) superfamily protein	0.00495867	0.0304251
XP_010911412.1	Glycosyl hydrolase family 35 protein	0.01008093	0.0304847
XP_010935585.1	Prolyl oligopeptidase family protein	0.00547002	0.030542
XP_010907515.1	Peroxidase superfamily protein	0.0011192	0.030731
XP_010934566.1	alpha-L-fucosidase 1	0.00157793	0.0307317
XP_010936238.1	peroxisomal NAD-malate dehydrogenase 2	0.01288766	0.030732
XP_019709713.1	pfkB-like carbohydrate kinase family protein	6.21E-05	0.0308321
XP_010931607.1	high chlorophyll fluorescent 109	0.00870273	0.0312496
XP_010924166.1	PS II oxygen-evolving complex 1	0.01159932	0.0313965
XP_010922416.1	actin 1	0.00901276	0.031398
XP_010933475.1	RNA-binding (RRM/RBD/RNP motifs) family protein	0.00361578	0.0315929
XP_010934591.1	Pheophorbide a oxygenase family protein with Rieske 2Fe-2S domain-containing protein	0.01386277	0.0316068
XP_010917378.1	Tyrosine transaminase family protein	0.00975277	0.0316152
XP_010940102.1	ornithine carbamoyltransferase	0.01363716	0.0317425
XP_010928044.1	Phosphofructokinase family protein	0.01299092	0.0317547
XP_010934639.1	glycine-tRNA ligase	0.01510548	0.0317926

XP_010919589.1	Plastid-lipid associated protein PAP / fibrillin family protein	0.01075131	0.0318574
XP_010930234.1	plastid transcriptionally active 4	0.01424865	0.0319052
XP_010911974.1	methionine adenosyltransferase 3	0.00681457	0.0319434
XP_010929443.1	pyridoxine biosynthesis 2	0.00778433	0.0319781
XP_010935338.1	quinolinate phoshoribosyltransferase	0.01214481	0.032102
XP_010923108.1	thylakoid soluble phosphoprotein	0.00921363	0.0322134
XP_010909136.1	Homeodomain-like superfamily protein	0.00310179	0.0322245
XP_010907914.1	cytidine/deoxycytidylate deaminase family protein	1.58E-04	0.0322698
XP_019702460.1	chloroplastidic phosphoglucan, water dikinase (ATGWD3)	0.00464595	0.0323141
XP_010936160.1	alpha/beta-Hydrolases superfamily protein	0.0043354	0.0323708
XP_010920885.1	serine carboxypeptidase-like 34	0.01430616	0.0324311
XP_010942522.1	Glucose-1-phosphate adenylyltransferase family protein	0.00197254	0.0326034
XP_010926375.1	UDP-Glycosyltransferase superfamily protein	0.01366182	0.032611
XP_010936330.1	Insulinase (Peptidase family M16) protein	0.00848218	0.0326625
XP_010942826.1	O-Glycosyl hydrolases family 17 protein	0.00659226	0.0327294
XP_010930946.2	Peroxidase superfamily protein	0.00309837	0.0327716
XP_010940680.1	Glutaredoxin family protein	0.00863823	0.0328145
XP_010909984.1	Serine protease inhibitor (SERPIN) family protein	0.0131769	0.0328378
XP_010920791.1	6-phosphofructo-2-kinase/fructose-2,6-bisphosphatase isoform X	7.70E-07	0.032952
XP_010943402.1	Glyoxalase/Bleomycin resistance protein/Dioxygenase superfamily protein	0.01140676	0.032967
XP_010924997.1	6-phosphogluconate dehydrogenase family protein	0.00298905	0.0329896
XP_010937470.1	Transducin/WD40 repeat-like superfamily protein	0.00148915	0.0330096
XP_010906951.1	GTP binding Elongation factor Tu family protein	9.33E-04	0.0331242
XP_010920032.1	uridine kinase-like 5	0.00538577	0.0331247
XP_010932642.1	pfkB-like carbohydrate kinase family protein	0.00684966	0.0331436
XP_010909530.1	NAD(P)-binding Rossmann-fold superfamily protein	0.01182276	0.0331514
XP_010931083.1	Thioredoxin superfamily protein	0.01169126	0.0332408
XP_010907880.1	NAD(P)H dehydrogenase B1	0.01011423	0.0333152
XP_010920133.1	Glycosyl hydrolase family 38 protein	0.00715919	0.0334374
XP_010907248.1	chloroplast stem-loop binding protein of 41 kDa	0.00178117	0.0334604

XP_010922826.1	Phosphoglycerate mutase, 2,3-bisphosphoglycerate-independent	0.01123119	0.033556
XP_010930044.1	glucose-6-phosphate dehydrogenase 5	0.00501887	0.033691
XP_010917678.1	Glyoxalase/Bleomycin resistance protein/Dioxygenase superfamily protein	0.00456127	0.0336993
XP_010916645.1	alpha/beta-Hydrolases superfamily protein	0.00701972	0.0337029
XP_010922691.1	Peroxidase superfamily protein	2.01E-04	0.0337055
XP_010924134.1	acclimation of photosynthesis to environment	0.00925224	0.0337249
XP_010922882.1	SMAD/FHA domain-containing protein	0.00689533	0.0337593
XP_010927597.1	elongation factor Ts family protein	0.00192947	0.033865
XP_010916694.1	GRAM domain family protein	0.00297007	0.0339338
XP_010942603.1	Thiolase family protein	0.0078023	0.033935
XP_010932308.1	heat shock protein 70 (Hsp 70) family protein	0.01008457	0.0340166
XP_010906913.1	zinc finger BED domain-containing protein RICESLEEPER 2-like	0.00227185	0.0340838
XP_010934999.1	Single hybrid motif superfamily protein	0.00810033	0.0341469
XP_010925514.1	Oxidoreductase, zinc-binding dehydrogenase family protein	0.0116719	0.0341674
XP_010917710.1	NDH-dependent cyclic electron flow 1	0.00539138	0.0342192
XP_010926057.1	aldehyde dehydrogenase 6B2	0.00116886	0.0342316
XP_010915675.1	thylakoid rhodanese-like protein	0.00932764	0.0342421
XP_010929515.1	histone H2A 8	0.00667332	0.0342536
XP_010921394.1	polyribonucleotide nucleotidyltransferase	8.14E-04	0.0342867
XP_010912644.1	hydroxyproline-rich glycoprotein family protein	0.0101175	0.0343143
XP_010934602.1	Dihydrolipoamide acetyltransferase, long form protein	0.00659992	0.0343431
XP_010942763.1	glycine decarboxylase P-protein 1	0.00310076	0.0343482
XP_010916966.1	disproportionating enzyme	0.00414442	0.0344383
XP_010924043.1	light harvesting complex photosystem II	0.0060343	0.0344692
XP_010909941.1	Glycine cleavage T-protein family	3.93E-04	0.0345172
XP_010934029.1	Subtilase family protein	0.00785028	0.0345641
XP_010916299.1	FAD/NAD(P)-binding oxidoreductase	0.00515321	0.0346302
XP_010913019.2	gamma carbonic anhydrase 3	0.00358082	0.0346609
XP_010938375.1	2-oxoacid dehydrogenases acyltransferase family protein	0.00176786	0.0349564
XP_010940058.1	uridine kinase-like 3	0.00213735	0.0350249
XP_010913041.1	non-photochemical quenching 1	0.00698882	0.0350612

XP_010926970.1	glycoside hydrolase family 2 protein	0.00300207	0.0350685
XP_010907549.1	Nucleotide-diphospho-sugar transferases superfamily protein	0.00390403	0.0351636
XP_010940660.1	Glutamine amidotransferase type 1 family protein	0.00515718	0.0352127
XP_010930060.1	heat shock protein 70 (Hsp 70) family protein	0.00545089	0.0352317
XP_010930337.1	6-phosphogluconate dehydrogenase family protein	0.002515	0.0352368
XP_010915890.1	Glyoxalase/Bleomycin resistance protein/Dioxygenase superfamily protein	0.00826622	0.0352534
XP_010910869.1	alpha/beta-Hydrolases superfamily protein	0.0024159	0.0352548
XP_010912957.2	GTP binding Elongation factor Tu family protein	0.00165093	0.0353742
XP_010938866.1	interactor of constitutive active ROPs protein	0.00708807	0.0353857
XP_010915680.1	NAD(P)-binding Rossmann-fold superfamily protein	0.00223178	0.0353858
XP_010941554.1	Transducin family protein / WD-40 repeat family protein	0.0051558	0.0354004
XP_010939741.1	phosphoglucose isomerase 1	7.73E-04	0.0354202
XP_010938515.1	glycoside hydrolase family 2 protein	0.00450479	0.0354631
XP_010938542.1	NADPH-dependent thioredoxin reductase C	9.94E-04	0.0355544
XP_010905922.1	MICOS complex subunit	0.00254116	0.0356691
XP_010927353.1	glucuronidase 3	0.00318779	0.0357165
XP_010934603.1	Pheophorbide a oxygenase family protein with Rieske 2Fe-2S domain-containing protein	0.00426794	0.0357717
XP_010929106.1	Thiamin diphosphate-binding fold (THDP-binding) superfamily protein	0.00323452	0.0357901
XP_010910622.1	nine-cis-epoxycarotenoid dioxygenase 4	0.00159584	0.0358009
YP_006073121.1	photosystem II protein V	0.00461943	0.0358562
XP_010911877.1	Subtilase family protein	0.00374386	0.0360158
XP_019707035.1	carbonic anhydrase 2	0.00187518	0.0361167
XP_010914777.1	Transducin/WD40 repeat-like superfamily protein	8.80E-04	0.0361681
XP_010909019.1	Leucine-rich repeat protein kinase family protein	0.00395873	0.0362556
XP_010906367.1	Transducin family protein / WD-40 repeat family protein	0.00418085	0.0364543
XP_010932120.1	glutamate tRNA synthetase	0.00379981	0.0365549
XP_010909333.1	Eukaryotic aspartyl protease family protein	2.59E-06	0.0365936
XP_010909027.1	cystatin B	0.00157794	0.0366017
XP_010933762.1	Phosphoglycerate mutase-like family protein	4.28E-04	0.0366115
XP_010933631.1	GroES-like zinc-binding alcohol dehydrogenase family protein	0.00467249	0.0366262

XP_010924161.1	Thiamine pyrophosphate dependent pyruvate decarboxylase family protein	0.00183628	0.0366709
XP_010934256.1	cyanase	0.00226384	0.036696
XP_010915605.1	Lactate/malate dehydrogenase family protein	0.00196588	0.0367391
XP_010942794.1	voltage dependent anion channel 2	0.00197174	0.0367446
XP_010932636.1	dehydroascorbate reductase 1	7.58E-04	0.0367507
XP_010914279.1	aldehyde dehydrogenase 6B2	3.60E-04	0.0369489
XP_010911973.1	Inositol monophosphatase family protein	7.13E-04	0.03701
XP_019704975.1	RNA-binding KH domain-containing protein	0.00157965	0.0370408
XP_010921929.1	NAD(P)-binding Rossmann-fold superfamily protein	7.00E-04	0.037053
XP_010905263.1	alpha/beta-Hydrolases superfamily protein	0.00525816	0.0371235
XP_010943716.1	monodehydroascorbate reductase 6	0.00367013	0.0371508
XP_010909644.1	Germin-like protein 5-1	4.20E-04	0.037168
XP_019704170.1	beta-hexosaminidase 3	9.05E-04	0.0371991
XP_010931079.1	Nuclear transport factor 2 (NTF2) family protein	0.00270231	0.0372298
XP_010910872.1	NAD(P)-binding Rossmann-fold superfamily protein	0.00180187	0.0373245
XP_010921195.1	ABC-2 type transporter family protein	0.00204464	0.037331
XP_010929163.1	Cytosol aminopeptidase family protein	0.00225148	0.0373616
XP_010910627.2	Haloacid dehalogenase-like hydrolase (HAD) superfamily protein	0.00227334	0.0374363
XP_010908347.2	NAD(P)-binding Rossmann-fold superfamily protein	8.20E-04	0.0375
XP_010926986.1	glutamate synthase 1	9.36E-06	0.0375905
XP_010927691.1	Sucrose-phosphate synthase family protein	0.00355718	0.0376366
XP_010932478.1	WCRKC thioredoxin 1	2.01E-04	0.0376424
XP_010927829.1	GroES-like zinc-binding alcohol dehydrogenase family protein	6.96E-04	0.0377184
XP_010918317.1	RNA-binding (RRM/RBD/RNP motifs) family protein	0.00112693	0.037755
XP_010905778.1	signal peptide peptidase	0.00128566	0.0378881
XP_010919663.1	Photosynthetic NDH subunit of subcomplex B 3, chloroplastic	1.50E-04	0.0379942
XP_010912914.1	cyclin delta-3	0.001895	0.0379997
XP_010918986.1	Calcium-dependent lipid-binding (CaLB domain) family protein	0.00172133	0.0381436
XP_010927871.1	Peroxidase superfamily protein	0.00124816	0.0381532
XP_010920296.1	Transducin/WD40 repeat-like superfamily protein	9.20E-04	0.038207

XP_010927963.1	Tyrosine transaminase family protein	0.00105466	0.0383503
XP_010928289.1	adenylate cyclase	0.00206868	0.038406
XP_010910204.1	alpha/beta-Hydrolases superfamily protein	0.00119562	0.0384155
XP_010937153.1	P-loop containing nucleoside triphosphate hydrolases superfamily protein	1.49E-04	0.0384571
XP_010927504.1	Cysteine proteinases superfamily protein	0.00114065	0.0385017
XP_010920113.1	Glycerate dehydrogenase-like	1.57E-04	0.0385597
XP_010922391.1	2-oxoglutarate dehydrogenase, E1 component	9.18E-05	0.0386544
XP_010928919.1	Inositol monophosphatase family protein	0.0014634	0.0386989
XP_010930656.1	Thiamin diphosphate-binding fold (THDP-binding) superfamily protein	7.64E-05	0.0387191
XP_010926584.1	Aldolase-type TIM barrel family protein	0.001213	0.0387452
XP_010912227.1	Thioredoxin superfamily protein	7.87E-04	0.0388011
XP_010943220.1	Lactate/malate dehydrogenase family protein	6.78E-04	0.0388169
XP_010931394.1	AAA-type ATPase family protein	0.00139049	0.038871
XP_010919327.1	Guanylate-binding family protein	7.18E-04	0.0389452
XP_010909122.1	UDP-Glycosyltransferase superfamily protein	0.00109998	0.0390272
XP_010942369.1	Glycosyl hydrolase family 38 protein	1.29E-04	0.0391709
XP_010941978.1	Cytidine/deoxycytidylate deaminase family protein	2.86E-04	0.0392599
XP_010941130.1	Lactate/malate dehydrogenase family protein	0.00106205	0.039266
XP_010919889.1	Rubredoxin-like superfamily protein	2.84E-04	0.0392682
XP_010938258.1	methylcrotonyl-CoA carboxylase alpha chain	4.32E-05	0.0393395
XP_010935853.1	plasma membrane intrinsic protein 1B	0.00108733	0.039585
XP_010927091.1	Inositol monophosphatase family protein	6.11E-04	0.0396098
XP_010923240.1	Ribulose bisphosphate carboxylase/oxygenase activase 2, chloroplastic isoform X2	5.98E-04	0.039665
XP_010917217.1	Isoleucine--tRNA ligase, chloroplastic/mitochondrial isoform X1	2.70E-06	0.0396916
XP_010921365.1	glucose-6-phosphate dehydrogenase 5	4.85E-04	0.0396984
XP_010913971.1	fumarylacetoacetase	0.00146619	0.0397545
XP_010928898.1	Glutamate--glyoxylate aminotransferase 2	3.95E-04	0.0399891
XP_010925018.1	glycine decarboxylase P-protein 1	9.45E-05	0.0400587
XP_010937996.1	Melibiase family protein	2.10E-04	0.0400637
XP_010920579.1	triosephosphate isomerase	6.86E-05	0.040117
XP_010913576.1	aldehyde dehydrogenase 6B2	8.31E-04	0.0401489

XP_010909154.1	Inositol monophosphatase family protein	8.10E-04	0.0402641
XP_010925495.1	Phosphoglycerate mutase family protein	2.94E-04	0.0402733
XP_010937316.1	DC1 domain-containing protein	4.14E-04	0.0403047
XP_010933967.1	isoprenoid F	0.00113721	0.0403666
XP_010931571.1	Saccharopine dehydrogenase	5.02E-04	0.0404049
XP_010923900.1	endoribonuclease L-PSP family protein	1.32E-04	0.0404079
XP_010922360.1	ricin-like	6.54E-04	0.0405272
XP_010931621.1	electron transfer flavoprotein alpha	1.82E-04	0.0405895
XP_010922610.1	NAD(P)-binding Rossmann-fold superfamily protein	8.56E-04	0.0406102
XP_010941282.1	triosephosphate isomerase	4.10E-05	0.0406108
XP_010930682.1	Ultraviolet-B receptor UVR8 isoform X4	1.66E-05	0.0409078
XP_010934233.1	aldehyde dehydrogenase 12A1	1.55E-04	0.0409204
XP_010930178.1	2-phosphoglycolate phosphatase 1	1.40E-04	0.041117
XP_010939233.1	HXXXD-type acyl-transferase family protein	1.03E-05	0.0412561
XP_010939064.1	methionyl-tRNA synthetase / methionine-tRNA ligase / MetRS (cpMetRS)	1.14E-04	0.0412779
XP_010910537.1	glycosyl hydrolase family 35 protein	9.99E-05	0.0414478
XP_010939394.1	Tyrosine transaminase family protein	2.05E-04	0.0415335
XP_010941762.1	Sucrose-phosphatase 2	9.65E-06	0.0415375
XP_010922013.1	peptide deformylase 1B	1.15E-04	0.0415625
XP_010943424.1	Serine carboxypeptidase S28 family protein	3.59E-04	0.0415795
XP_010913236.1	ketol-acid reductoisomerase	3.69E-07	0.0416268
XP_010938005.1	Fe superoxide dismutase 1	1.50E-04	0.0417467
XP_010925672.1	SOUL heme-binding family protein	2.44E-04	0.0417752
XP_010943016.1	alpha/beta-Hydrolases superfamily protein	4.01E-04	0.042037
XP_010915045.1	MAR-binding filament-like protein 1	5.24E-06	0.0422084
XP_010941013.1	nucleosome assembly protein 1;2	3.45E-05	0.0423778
XP_010943476.1	chloroplastic drought-induced stress protein of 32 kD	8.65E-06	0.0424919
XP_010941493.1	monodehydroascorbate reductase 6	2.71E-06	0.0426981
XP_010916365.1	Glycosyl hydrolases family 31 protein	1.72E-04	0.0427295
XP_010925689.2	magnesium chelatase i2	3.07E-05	0.0427967
XP_010906903.1	NAD(P)-binding Rossmann-fold superfamily protein	2.01E-04	0.0428069
XP_010923458.1	Phosphoglycerate kinase, chloroplastic-like	6.72E-05	0.0428358
XP_010923134.1	Inositol monophosphatase family protein	7.26E-05	0.0429131
XP_010917225.1	Cysteine proteinases superfamily protein	2.98E-05	0.0430527

XP_010929878.1	Aconitase 1	1.27E-05	0.0431182
XP_010930476.1	Rieske (2Fe-2S) domain-containing protein	1.01E-04	0.0434167
XP_010934663.1	Transketolase, chloroplastic	5.79E-06	0.0434425
XP_010943013.1	alpha/beta-Hydrolases superfamily protein	4.90E-05	0.0435346
XP_010941398.1	FtsH extracellular protease family	1.03E-05	0.0437232
XP_010935634.1	Protein ABCI7, chloroplastic-like	2.17E-07	0.0437994
XP_010931932.1	glutathione synthetase 2	1.23E-05	0.0439226
XP_010930662.1	histone deacetylase 15	1.11E-04	0.0439306
XP_010928647.1	FGGY carbohydrate kinase domain-containing protein isoform X1	6.66E-06	0.0441048
XP_010918997.1	PGR5-LIKE A	4.63E-05	0.0441726
XP_010943941.1	Expansin-like A2	1.29E-05	0.0442574
XP_010918400.1	nitrilase 1	2.21E-06	0.0443239
XP_010912748.1	hypothetical protein AT2G43945	3.02E-05	0.0445063
XP_010942437.1	Thioredoxin superfamily protein	3.33E-05	0.044625
XP_019710370.1	alpha/beta-Hydrolases superfamily protein	4.17E-06	0.04478
XP_010905827.1	Plastid-lipid associated protein PAP / fibrillin family protein	3.96E-06	0.0449124
XP_010926402.1	3-methylcrotonyl-CoA carboxylase	3.01E-06	0.0449283
XP_010909403.1	NAD(P)-binding Rossmann-fold superfamily protein	1.02E-05	0.045035
XP_010907974.2	ERD (early-responsive to dehydration stress) family protein	1.54E-05	0.045143
XP_010928724.1	ATPase, V1 complex, subunit B protein	8.96E-06	0.0451947
XP_010914695.1	Dihydrolipoyl dehydrogenase 1, mitochondrial-like	3.01E-06	0.0455419
XP_010926485.2	VQ motif-containing protein	2.29E-06	0.0455749
XP_010912146.1	Phosphoenolpyruvate carboxylase family protein	1.75E-09	0.0471989
XP_010909363.1	Glutamine synthetase nodule isozyme	3.99E-08	0.0481688
XP_010912571.1	Lactate/malate dehydrogenase, mitochondrial	5.32E-09	0.0484556

Table S2. List of proteins significant for the cross effect in 2017 (Benjamini-Hochberg correction).

Accession number	Description	Pvalue (Cross effect)	Loading (Cross effect)
XP_010906401.1	thylakoid lumenal protein (Mog1/PsbP/DUF1795-like photosystem II reaction center PsbP family protein)	8.72E-09	-0.0589235
XP_010909272.1	Lactoylglutathione lyase / glyoxalase I family protein	1.68E-06	-0.0579621
XP_010907964.1	Immunoglobulin E-set superfamily protein	1.00E-06	-0.0563502
XP_010907549.1	Nucleotide-diphospho-sugar transferases superfamily protein	4.79E-07	-0.0554304
XP_010907928.1	enolase 1	1.49E-05	-0.0543824
XP_010908796.1	photosystem I light harvesting complex protein 5	2.73E-06	-0.0543069
XP_010907781.1	Class II aaRS and biotin synthetases superfamily protein	3.70E-05	-0.054146
XP_010904873.1	Putative NADB_Rossmann_Superfamily domain protein	4.94E-05	-0.0539226
XP_010905030.1	glutathione peroxidase 1	3.59E-05	-0.0536331
XP_010908773.1	NAD(P)-binding Rossmann-fold superfamily protein	2.28E-04	-0.0534296
XP_010907558.1	haloacid dehalogenase-like hydrolase family protein	1.03E-05	-0.0533291
XP_010905724.1	Histone superfamily protein	8.68E-06	-0.0525129
XP_010905109.1	Remorin family protein	2.13E-04	-0.052495
XP_010907071.1	UDP-XYL synthase 6	2.18E-04	-0.0515244
NP_001306846.1	stem-specific protein TSJT1-like	9.45E-05	-0.0512688
XP_010905138.1	Selenium-binding protein 1 isoform X2	3.04E-05	-0.0507925
XP_010907090.1	catalase 3	4.50E-05	-0.0505154
XP_010908968.1	protein containing PDZ domain, a K-box domain, and a TPR region	5.23E-04	-0.0502807
XP_010906166.1	Wiskott-aldrich syndrome family protein, putative (DUF1118)	6.45E-05	-0.0499977
XP_010905780.1	TCP-1/cpn60 chaperonin family protein	3.22E-05	-0.0499304
XP_010906487.1	chlorophyll a-b binding protein 6	1.21E-04	-0.0492949
XP_010906951.1	GTP binding Elongation factor Tu family protein	1.51E-05	-0.0492328
NP_001290534.1	probable aquaporin PIP1-2	7.84E-05	-0.0491115
XP_010906959.1	photosystem II subunit P-1	3.13E-04	-0.0483905

XP_010905907.1	light harvesting complex photosystem II	4.84E-04	-0.0481734
XP_010909019.1	Leucine-rich repeat protein kinase family protein	4.54E-04	-0.0467512
XP_010909145.1	plastid transcriptionally active 4	4.38E-04	-0.0465141
XP_010909956.1	magnesium-protoporphyrin IX methyltransferase	1.54E-03	-0.0459899
XP_010907351.1	RNA-binding (RRM/RBD/RNP motifs) family protein	6.02E-04	-0.0457176
XP_010912612.1	NAD(P)H:plastoquinone dehydrogenase complex subunit O	0.004969898	-0.0455494
XP_010909453.1	Flavin containing amine oxidoreductase family	1.24E-03	-0.0453924
XP_010911412.1	Glycosyl hydrolase family 35 protein	2.95E-03	-0.0452436
XP_010908755.1	CURVATURE THYLAKOID protein	7.02E-04	-0.0452417
XP_010911837.1	prohibitin 2	0.003287759	-0.0449418
XP_010907411.1	Methionine aminopeptidase 2B	4.47E-04	-0.0443611
XP_010905846.1	glutathione-disulfide reductase	2.56E-04	-0.0441229
XP_010912146.1	Phosphoenolpyruvate carboxylase family protein	0.003684021	-0.0440359
XP_010906004.1	Cobalamin biosynthesis CobW-like protein	5.61E-04	-0.0439277
XP_010905778.1	signal peptide peptidase	5.78E-04	-0.0439185
XP_010911317.1	DPP6 N-terminal domain-like protein	2.88E-03	-0.043805
XP_010910613.2	glycosyl hydrolase family 35 protein	2.08E-03	-0.0437326
XP_010907248.1	chloroplast stem-loop binding protein of 41 kDa	6.37E-04	-0.0437248
XP_010909403.1	NAD(P)-binding Rossmann-fold superfamily protein	1.13E-03	-0.0433443
XP_010910722.1	RmlC-like cupins superfamily protein	2.21E-03	-0.0432221
XP_010912173.1	Putative BCR, YbaB family COG0718	0.003831198	-0.0431682
XP_010912493.1	Aldolase superfamily protein	0.004457294	-0.0430701
XP_010913914.2	PLAT/LH2 domain-containing lipoxygenase family protein	0.007694063	-0.0430004
XP_010911890.1	aspartate aminotransferase	0.003408231	-0.042981
XP_010909191.1	bacterial trigger factor	5.45E-04	-0.0429009
XP_010912312.1	Ribosomal protein S11 family protein	0.004240726	-0.0426549
XP_010915413.1	phosphoribosylaminoimidazole carboxylase, putative / AIR carboxylase	0.010769664	-0.0423098
XP_010907343.2	Glucose-1-phosphate adenylyltransferase family protein	2.98E-04	-0.0421896
XP_010915493.1	Peroxidase superfamily protein	0.011404146	-0.0420771
XP_010906118.1	Ribosomal protein S5 family protein	9.53E-04	-0.0418105
XP_010914941.1	histone H2A 8	0.009835185	-0.0417604

XP_010913171.1	Threonyl-tRNA synthetase	0.006401673	-0.0417374
XP_010909644.1	Germin-like protein 5-1	1.42E-03	-0.0417255
XP_010906493.1	4-hydroxy-3-methylbut-2-enyl diphosphate synthase	8.44E-04	-0.0417173
XP_010906270.2	Subtilase family protein	6.41E-04	-0.0415799
XP_010913676.1	ACT domain repeat 3	0.007453569	-0.0415582
XP_010912515.1	Disease resistance-responsive (dirigent-like protein) family protein	0.004709087	-0.0415527
XP_010910303.1	cobalt ion binding protein	1.85E-03	-0.0415459
XP_010910627.2	Haloacid dehalogenase-like hydrolase (HAD) superfamily protein	2.14E-03	-0.0415163
XP_010910668.1	Lactoylglutathione lyase / glyoxalase I family protein	2.17E-03	-0.0412799
XP_010915505.1	Peptide-N4-(N-acetyl-beta-glucosaminyl)asparagine amidase A protein	0.011568852	-0.0412283
XP_010911739.2	glyceraldehyde 3-phosphate dehydrogenase A subunit 2	0.003180108	-0.041214
XP_010910894.1	glutathione S-transferase F4	2.56E-03	-0.0411836
XP_010911346.1	glyoxalase 2-5	2.92E-03	-0.0410857
XP_010911014.1	S-norcoclaurine synthase 2-like	2.63E-03	-0.0408244
XP_010907436.1	NAD(P)-linked oxidoreductase superfamily protein	9.05E-04	-0.0405411
XP_010911246.1	Peptidase C13 family	2.74E-03	-0.0405287
XP_010911653.2	alpha/beta-Hydrolases superfamily protein	3.11E-03	-0.0404751
XP_010913576.1	aldehyde dehydrogenase 6B2	0.007069007	-0.0402966
XP_010909417.1	TCP-1/cpn60 chaperonin family protein	1.17E-03	-0.0402853
XP_010914866.1	Zinc-binding dehydrogenase family protein	0.009406265	-0.0399738
XP_010915212.1	6-phosphogluconate dehydrogenase family protein	0.010417233	-0.0398956
XP_010912468.1	glycine-rich protein 2B	0.004269677	-0.0398489
XP_010913989.1	PSI type III chlorophyll a/b-binding protein, chloroplastic	0.007890799	-0.0398075
XP_010916095.1	methionine sulfoxide reductase B 1	0.013499331	-0.0393536
XP_010910113.1	Heat shock protein 70 (Hsp 70) family protein	1.62E-03	-0.0390945
XP_010916168.1	Rad23 UV excision repair protein family	0.013645367	-0.0387099
XP_010912957.2	GTP binding Elongation factor Tu family protein	0.006036639	-0.0386016
XP_010914695.1	Dihydrolipoyl dehydrogenase 1, mitochondrial-like	0.008974972	-0.0384914
XP_010912997.1	Cyclophilin-like peptidyl-prolyl cis-trans isomerase family protein	0.006073803	-0.0384293

XP_010915385.1	2-oxoglutarate (2OG) and Fe(II)-dependent oxygenase superfamily protein	0.010691487	-0.0382664
XP_010914839.1	Ribosomal L18p/L5e family protein	0.009355428	-0.0380353
XP_010915202.1	Ribosomal protein S5/Elongation factor G/III/V family protein	0.010356701	-0.0379345
XP_010914166.1	aldehyde dehydrogenase 6B2	0.008046404	-0.0377689
XP_010914484.1	Ribosomal protein L18e/L15 superfamily protein	0.008306678	-0.0377536
XP_010915746.1	Ribosomal protein L21	0.012893206	-0.0372971
XP_010914901.1	root FNR 2	0.009774963	-0.0372487
XP_010915045.1	MAR-binding filament-like protein 1	0.009968561	-0.0365644
XP_010915175.1	Aminopeptidase M1 family protein	0.01034836	-0.0356843
XP_010915675.1	thylakoid rhodanese-like protein	0.012491364	-0.0355053
XP_010913220.1	trigger factor type chaperone family protein	0.006583652	-0.0354615
XP_010911871.1	Chlorophyll A-B binding family protein	0.003386984	-0.0352166
XP_010915489.1	Peroxidase superfamily protein	0.010836938	-0.0351975
XP_010913226.1	Eukaryotic aspartyl protease family protein	0.006587366	-0.0351699
XP_010913971.1	fumarylacetoacetase	0.00788001	-0.0350626
XP_010910415.1	ribosomal protein 5B	1.88E-03	-0.0349491
XP_010916236.1	translocon at the outer envelope membrane of chloroplasts 34	0.013869892	-0.0347781
XP_010915593.1	magnesium chelatase i2	0.011878771	-0.0346677
XP_010916299.1	FAD/NAD(P)-binding oxidoreductase	0.014017126	-0.0345926
XP_010915605.1	Lactate/malate dehydrogenase family protein	0.01208163	-0.03449
XP_010916331.1	RNA ligase/cyclic nucleotide phosphodiesterase family protein	0.014086956	-0.0335111
XP_010915680.1	NAD(P)-binding Rossmann-fold superfamily protein	0.01271038	-0.0332659
XP_010916329.1	Transducin/WD40 repeat-like superfamily protein	0.01403606	-0.0323736
XP_010911167.1	Terpenoid cyclases/Protein prenyltransferases superfamily protein	2.66E-03	-0.0322986
XP_010912298.1	Signal recognition particle, SRP54 subunit protein	0.004210718	-0.0280622
XP_010906968.1	Thioredoxin family protein	2.71E-05	-0.0178601
XP_010905021.1	Translation initiation factor 3 protein	3.73E-07	-0.000351955
XP_010912227.1	Thioredoxin superfamily protein	0.003840377	0.0224047

XP_010912634.1	Disease resistance-responsive (dirigent-like protein) family protein	0.005325531	0.0297088
XP_010909643.1	26S proteasome regulatory subunit, putative (RPN5)	1.38E-03	0.0308826
XP_010912237.1	Phosphoglycerate mutase family protein	0.003865619	0.031568
XP_010915890.1	Glyoxalase/Bleomycin resistance protein/Dioxygenase superfamily protein	0.013482545	0.0317318
XP_010915629.1	Class I glutamine amidotransferase-like superfamily protein	0.012150178	0.0322232
XP_010912031.1	Subtilase family protein	0.003500606	0.0323474
XP_010913586.1	calcium sensing receptor	0.007268593	0.0324958
XP_010915873.1	Double Clp-N motif-containing P-loop nucleoside triphosphate hydrolases superfamily protein	0.013310808	0.033465
XP_010913436.1	aldehyde dehydrogenase 6B2	0.006911564	0.0336807
XP_010913416.1	Phosphofructokinase family protein	0.00677798	0.0341284
XP_010913902.1	Zinc finger C-x8-C-x5-C-x3-H type family protein	0.007668242	0.0342806
XP_010916258.1	TCP-1/cpn60 chaperonin family protein	0.013922083	0.0343913
XP_010907133.1	Zn-dependent exopeptidases superfamily protein	7.06E-04	0.0356386
XP_010913749.1	allene oxide synthase	0.007466964	0.0357359
XP_010914811.1	Insulinase (Peptidase family M16) protein	0.00921908	0.0360103
XP_010912571.1	Lactate/malate dehydrogenase, mitochondrial	0.004924675	0.0362538
XP_010914334.1	Coproporphyrinogen III oxidase	0.008110582	0.0363262
XP_010909683.1	Cystathionine beta-synthase (CBS) family protein	1.43E-03	0.0364132
XP_010914719.1	Peroxidase superfamily protein	0.009059376	0.0364985
XP_010915872.1	Phosphorylase superfamily protein	0.013071148	0.0369323
XP_010913256.1	Eukaryotic aspartyl protease family protein	0.006618201	0.0369892
XP_010913164.1	thylakoid lumenal 19 kDa protein, chloroplastic	0.006249173	0.0370016
XP_010914939.2	AAA-type ATPase family protein	0.009783819	0.0371685
XP_010915364.1	NADP-malic enzyme 3	0.010668172	0.0372294
XP_010914656.1	TCP-1/cpn60 chaperonin family protein	0.008821954	0.0373947
XP_010913759.1	ATPase, V1 complex, subunit B protein	0.007566223	0.0374891
XP_010912254.1	Heavy metal transport/detoxification superfamily protein	0.004031849	0.0375691
XP_010911772.1	glutathione S-transferase TAU 18	0.003222083	0.0378045
XP_010915650.1	hypothetical protein AT5G24165	0.012198945	0.0378883
XP_010912748.1	hypothetical protein AT2G43945	0.005394097	0.0379369
XP_010912239.1	Aldolase superfamily protein	0.003871126	0.0379748

XP_010916334.1	ABC-2 type transporter family protein	0.014617661	0.0380473
XP_010914386.1	Peroxidase superfamily protein	0.008270764	0.0381624
XP_010915070.1	ATP synthase D chain	0.010126988	0.038328
XP_010913224.1	Chaperone protein htpG family protein	0.006586067	0.0388654
NP_001290536.1	uncharacterized protein LOC105052388	6.78E-04	0.0388698
XP_010914552.1	glutathione-disulfide reductase	0.008752054	0.0390701
XP_010914880.1	Alba DNA/RNA-binding protein	0.00968104	0.0393041
XP_010910872.1	NAD(P)-binding Rossmann-fold superfamily protein	2.40E-03	0.0393077
XP_010911257.2	alpha/beta-Hydrolases superfamily protein	2.82E-03	0.0393254
XP_010911973.1	Inositol monophosphatase family protein	0.003469437	0.0394042
XP_010915365.1	HAD superfamily, subfamily IIIB acid phosphatase	0.010682224	0.0394952
XP_010910405.1	glyceraldehyde 3-phosphate dehydrogenase A subunit 2	1.87E-03	0.0395151
XP_010913855.1	U5 small nuclear ribonucleoprotein helicase	0.007621686	0.0397625
XP_010915496.1	Mitochondrial dicarboxylate/tricarboxylate transporter DTC	0.011551562	0.0400682
XP_010909911.1	Aldolase-type TIM barrel family protein	1.53E-03	0.0401255
XP_010912545.1	isopropylmalate dehydrogenase 1	0.004718178	0.0401495
XP_010910869.1	alpha/beta-Hydrolases superfamily protein	2.38E-03	0.040268
XP_010915515.1	phosphoenolpyruvate carboxylase 1	0.01172645	0.0403365
XP_010910622.1	nine-cis-epoxycarotenoid dioxygenase 4	2.13E-03	0.0403496
XP_010905855.1	Ribosomal protein PSRP-3/Ycf65	7.86E-04	0.0404085
XP_010911931.1	Ribosomal L28e protein family	0.003416822	0.0404515
XP_010910537.1	glycosyl hydrolase family 35 protein	2.03E-03	0.0405701
XP_010912914.1	cyclin delta-3	0.005885762	0.0407588
XP_010909984.1	Serine protease inhibitor (SERPIN) family protein	1.60E-03	0.0407748
XP_010911525.2	glutathione transferase lambda 1	3.08E-03	0.0412148
XP_010913595.1	heat shock factor-binding protein 1	0.007272386	0.0413425
XP_010911806.1	Thioredoxin superfamily protein	0.003256528	0.041408
XP_010911717.2	AAA-type ATPase family protein	0.003145696	0.0415675
XP_010913236.1	ketol-acid reductoisomerase	0.006597141	0.0417208
XP_010913019.2	gamma carbonic anhydrase 3	0.006118588	0.0418695
XP_010914393.1	phenylalanyl-tRNA synthetase class IIc family protein	0.008281983	0.0419199
XP_010914279.1	aldehyde dehydrogenase 6B2	0.008062834	0.0419225
XP_010909258.1	cobalt ion binding protein	1.02E-03	0.042035

XP_010913457.1	cytosolic NADP+-dependent isocitrate dehydrogenase	0.007030559	0.0420423
XP_010909497.1	Mitochondrial substrate carrier family protein	1.31E-03	0.0422354
XP_010912477.1	AMP-dependent synthetase and ligase family protein	0.004433587	0.042347
XP_010910942.1	chlorophyll a-b binding protein 6	2.59E-03	0.0424586
XP_010912630.1	GroES-like zinc-binding dehydrogenase family protein	0.004986382	0.0427847
XP_010912250.1	60S acidic ribosomal protein family	0.003954751	0.0429152
XP_010914488.1	alpha/beta-Hydrolases superfamily protein	0.008615514	0.0430789
XP_010911620.1	NAD(P)-binding Rossmann-fold superfamily protein	3.10E-03	0.0432663
XP_010913398.1	thioredoxin family protein	0.006637219	0.0433232
XP_010913041.1	non-photochemical quenching 1	0.006150825	0.0433936
XP_010909333.1	Eukaryotic aspartyl protease family protein	1.11E-03	0.0436627
XP_010912087.1	pyruvate orthophosphate dikinase	0.003507814	0.0436634
XP_010908643.1	rhodanese-like domain-containing protein / PPIC-type PPIASE domain-containing protein	1.49E-04	0.0436761
XP_010907974.2	ERD (early-responsive to dehydration stress) family protein	4.08E-04	0.0437464
XP_010910204.1	alpha/beta-Hydrolases superfamily protein	1.82E-03	0.0437733
XP_010910533.1	Cystatin/monellin superfamily protein	1.97E-03	0.043873
XP_010910012.1	Chalcone-flavanone isomerase family protein	1.61E-03	0.0439941
XP_010907494.1	sulfoquinovosyldiacylglycerol 1	3.77E-04	0.0442847
XP_010911159.1	51 kDa subunit of complex I	2.65E-03	0.044428
XP_010909941.1	Glycine cleavage T-protein family	1.53E-03	0.0444605
XP_010907914.1	cytidine/deoxycytidylate deaminase family protein	5.01E-04	0.0447146
XP_010909154.1	Inositol monophosphatase family protein	7.90E-04	0.0447862
XP_010910148.1	polyphenol oxidase, chloroplastic-like	1.79E-03	0.0448195
XP_010909894.1	Ribonucleoprotein 28 kDa, chloroplastic	1.52E-03	0.0451572
XP_010910856.1	alpha/beta-Hydrolases superfamily protein	2.24E-03	0.0451968
XP_010909959.1	thylakoid lumenal 16.5 kDa protein, chloroplastic isoform X1	1.54E-03	0.0453012
XP_010907269.1	phospholipase D delta	1.16E-05	0.045439
XP_010908520.1	Tetratricopeptide repeat (TPR)-like superfamily protein	8.32E-04	0.0454763
XP_010906967.1	Subtilase family protein	3.88E-04	0.0456636

XP_010911012.2	Isocitrate dehydrogenase [NAD] regulatory subunit 1, mitochondrial-like	2.61E-03	0.0456642
XP_010907175.1	aspartate aminotransferase	6.11E-04	0.0457377
XP_010909483.1	P-loop containing nucleoside triphosphate hydrolases superfamily protein	1.27E-03	0.0457465
XP_010907405.1	ATP binding cassette protein 1	6.58E-04	0.0457592
XP_010910878.1	Sec14p-like phosphatidylinositol transfer family protein	2.51E-03	0.0459127
XP_010905827.1	Plastid-lipid associated protein PAP / fibrillin family protein	8.98E-04	0.0459292
XP_010909285.1	Aldolase-type TIM barrel family protein	1.10E-03	0.046165
XP_010906559.1	Cystathionine beta-synthase (CBS) family protein	7.05E-05	0.0462739
XP_010905215.1	PLAT/LH2 domain-containing lipoxygenase family protein	6.33E-04	0.0463137
XP_010910557.1	GroES-like zinc-binding dehydrogenase family protein	2.06E-03	0.0466182
XP_010910143.1	Glycinamide ribonucleotide (GAR) synthetase	1.75E-03	0.0466911
XP_010909122.1	UDP-Glycosyltransferase superfamily protein	1.56E-04	0.0468478
XP_010909722.1	RmlC-like cupins superfamily protein	1.47E-03	0.0469228
XP_010909363.1	Glutamine synthetase nodule isozyme	1.12E-03	0.0470934
XP_010905354.1	anthranilate synthase 2	6.61E-04	0.0471146
XP_010906903.1	NAD(P)-binding Rossmann-fold superfamily protein	5.81E-04	0.0473063
XP_010907117.1	RmlC-like cupins superfamily protein	2.26E-04	0.0475959
XP_010905143.1	Oxidoreductase, zinc-binding dehydrogenase family protein	5.37E-04	0.047844
XP_010910002.1	Melibiase family protein	1.60E-03	0.0480911
XP_010907515.1	Peroxidase superfamily protein	2.50E-04	0.0481228
XP_010906730.1	alpha/beta-Hydrolases superfamily protein	9.26E-04	0.0481672
XP_010908010.1	Leucine--tRNA ligase, cytoplasmic	5.02E-04	0.0481919
XP_010909126.1	Peptidase family M48 family protein	8.03E-04	0.0483424
XP_010909261.1	2Fe-2S ferredoxin-like superfamily protein	1.85E-04	0.0484448
XP_010909277.1	4-hydroxy-3-methylbut-2-enyl diphosphate reductase	1.28E-04	0.0485917
NP_001306842.1	catalase isozyme 2	5.99E-05	0.048809
XP_010908653.2	UDP-Glycosyltransferase superfamily protein	3.64E-04	0.0488148
XP_010905666.1	Ribosomal protein S10p/S20e family protein	4.44E-05	0.0490073
XP_010906509.1	photosystem II subunit R	4.69E-04	0.0493095

XP_010909027.1	cystatin B	3.23E-05	0.0493568
XP_010909223.1	pfkB-like carbohydrate kinase family protein	7.15E-04	0.0493742
XP_010907209.1	Translation elongation factor EF1B, gamma chain	2.37E-04	0.0495681
XP_010905226.1	Rhodanese/Cell cycle control phosphatase superfamily protein	1.55E-04	0.0496264
XP_010909203.1	alanine:glyoxylate aminotransferase	1.08E-04	0.0500448
XP_010907304.1	Aldolase-type TIM barrel family protein	2.86E-05	0.050412
XP_010904844.1	chlorophyll a-b binding protein of LHCII type 1	8.01E-05	0.0506318
XP_010904849.1	protein THYLAKOID FORMATION1, chloroplastic	9.29E-05	0.0511776
XP_010907538.1	2Fe-2S ferredoxin-like superfamily protein	6.63E-05	0.0512464
XP_010907984.1	methyl-CPG-binding domain 11	1.61E-04	0.0512548
XP_010907756.1	Cysteine proteinases superfamily protein	4.26E-05	0.0512862
XP_010906765.1	adenylosuccinate synthase	2.58E-04	0.0512947
XP_010905235.1	dehydrin COR410	1.29E-04	0.0515288
XP_010908644.1	glutamate dehydrogenase 2	1.56E-05	0.0518017
XP_010905956.1	F-type H+-transporting ATPase subunit delta	2.15E-04	0.0521441
XP_010908502.1	nuclear protein	6.59E-05	0.0523937
XP_010906011.1	Transducin family protein / WD-40 repeat family protein	1.98E-05	0.0527821
XP_010907155.1	60S Acidic ribosomal protein P2B	1.33E-04	0.0529558
NP_001306845.1	elongation factor 1-beta-like	1.78E-06	0.0530146
XP_010907148.1	Heavy metal transport/detoxification superfamily protein	4.46E-05	0.0531618
XP_010905974.1	Tubulin/FtsZ family protein	1.27E-06	0.0532402
XP_010908745.1	U2 small nuclear ribonucleoprotein A	3.19E-06	0.0535072
XP_010906831.1	ferritin 2	1.61E-05	0.053553
XP_010905156.1	FKBP-type peptidyl-prolyl cis-trans isomerase family protein	4.32E-06	0.0538414
XP_010908786.1	acetyl Co-enzyme a carboxylase biotin carboxylase subunit	5.64E-06	0.0540439
XP_010905531.1	cyclophilin 38	1.38E-04	0.0540854
XP_010908984.1	Ribosomal protein S5 domain 2-like superfamily protein	1.14E-06	0.0541041
XP_010907961.1	methyl-CPG-binding domain 11	6.60E-05	0.0541938
XP_010908744.1	beta glucosidase 42	4.66E-07	0.0552687
XP_010909270.1	alpha/beta-Hydrolases superfamily protein	2.74E-06	0.0553578

XP_010905734.1	uricase / urate oxidase / nodulin 35	2.30E-06	0.0558255
XP_010904686.2	dihydropyrimidinase isoform X1	7.76E-06	0.0568673
XP_010907839.1	Ribosomal protein L6 family	1.68E-07	0.0568718
XP_010905450.1	RNA-binding KH domain-containing protein	1.27E-06	0.0572973
XP_010905246.1	alpha/beta-Hydrolases superfamily protein	8.91E-07	0.0574677
XP_010906824.1	NAD(P)-linked oxidoreductase superfamily protein	5.48E-09	0.0587378
XP_010905146.1	glycine-rich RNA-binding protein 2	2.11E-07	0.0598532
XP_010906459.1	cysteine synthase D2	1.03E-07	0.0606693

Table S3. List of proteins with best loading values (first decile) in the proteome-metabolome correlation.

Accession number	Description	pq(corr)[1]	pq(corr)[2]
Proteins with lowest loading along axis 1			
XP_010934663.1	Transketolase, chloroplastic	-0.951801	-0.0141784
XP_010915045.1	MAR-binding filament-like protein 1	-0.937503	-0.0095421
XP_010912571.1	Malate dehydrogenase, mitochondrial	-0.92846	0.0772252
XP_010941762.1	Sucrose-phosphatase 2	-0.918305	0.0861009
XP_010917225.1	Cysteine proteinases superfamily protein	-0.909757	-0.195093
XP_010935634.1	Protein ABCI7, chloroplastic-like	-0.903465	0.287625
XP_010923458.1	Phosphoglycerate kinase, chloroplastic-like	-0.890917	0.0279537
XP_010914695.1	Dihydrolipoyl dehydrogenase 1, mitochondrial-like	-0.889713	0.169268
XP_010943941.1	Expansin-like A2	-0.888542	0.0799758
XP_010920113.1	Glycerate dehydrogenase-like	-0.887695	-0.0211217
XP_010926485.2	VQ motif-containing protein	-0.886522	0.187373
XP_010928647.1	FGGY carbohydrate kinase domain-containing protein isoform X1	-0.886152	0.231633
XP_010928898.1	Glutamate--glyoxylate aminotransferase 2	-0.885398	-0.155932
XP_010909363.1	Glutamine synthetase nodule isozyme	-0.884268	0.263607
XP_010923240.1	Ribulose bisphosphate carboxylase/oxygenase activase 2, chloroplastic isoform X2	-0.884128	-0.304332
XP_010917217.1	Isoleucine--tRNA ligase, chloroplastic/mitochondrial isoform X1	-0.88103	0.289096
Proteins with lowest loading along axis 2			
XP_019705414.1	Ankyrin repeat-containing protein 2, chloroplastic	0.0593793	-0.900044
XP_010909894.1	Ribonucleoprotein 28 kDa, chloroplastic	-0.296422	-0.836573
XP_010921860.1	Nascent polypeptide-associated complex (NAC) subunit alpha-like protein 1	0.039127	-0.82732
XP_010921235.1	YCF54	-0.250693	-0.826772
XP_010933893.1	Protein-ribulosamine 3-kinase, chloroplastic	0.0736326	-0.82161
XP_010937293.1	Chaperonin 20, chloroplastic	-0.402053	-0.819297
XP_010907155.1	60S Acidic ribosomal protein P2B	0.0662751	-0.811489
XP_010912576.1	Dihydrolipoyllysine-residue acetyltransferase, chloroplastic-like	-0.0917118	-0.79465
XP_010940406.1	Protein ABCI7, chloroplastic	0.088755	-0.773534

YP_006073160.1	NADH dehydrogenase subunit 7, chloroplast	-0.0922364	-0.758198
XP_019703921.1	Photosystem II reaction center PsbP, chloroplastic	0.316921	-0.731686
XP_010913989.1	PSI type III chlorophyll a/b-binding protein, chloroplastic	-0.0651103	-0.73036
XP_010939148.1	Insulinase (Peptidase family M16) protein, mitochondrial	0.347864	-0.727947
XP_010926757.2	Small ubiquitin-related modifier 1	0.202066	-0.726011
XP_010920706.1	PsbP-like protein 1, chloroplastic isoform X1	0.141323	-0.723846
XP_010941662.1	Histidine triad nucleotide-binding 2 (Adenylylsulfatase)	-0.234885	-0.723773
Proteins with highest loading along axis 2			
XP_010940353.1	Actin-related protein 4	0.359796	0.677923
XP_010931977.1	Mitochondrial Rho GTPase 1-like	-0.214258	0.679648
XP_010935789.1	Puromycin-sensitive aminopeptidase isoform X2	0.115459	0.684327
XP_010919797.1	Nucleolin isoform X1	0.17686	0.70535
XP_010908010.1	Leucine--tRNA ligase, cytoplasmic	0.130357	0.709809
XP_010920077.1	Glycosyl hydrolases family 31 protein	-0.010478	0.726062
XP_010929086.1	Cofactor-independent phosphoglycerate mutase	-0.135916	0.727142
XP_010909136.1	Homeodomain-like superfamily protein	-0.502455	0.742607
XP_010931898.1	Ubiquitin carboxyl-terminal hydrolase 14	0.0643091	0.746018
XP_010940629.1	Cell division cycle protein 48 homolog (Adenosinetriphosphatase)	0.23024	0.749278
XP_010930536.2	Carboxylesterase 18	-0.352161	0.768025
XP_010942549.1	Ribosomal protein S5/Elongation factor G/III/V family protein (CLO)	0.222977	0.773518
XP_010939835.1	Cleavage and polyadenylation specificity factor (CPSF) A subunit protein	0.0899732	0.777042
XP_010906269.1	Subtilisin-like protease SBT1.7	-0.235805	0.781579
XP_010927876.2	Squamous cell carcinoma antigen recognized by T-cells 3	-0.0304645	0.804897
XP_010941046.1	Transketolase, chloroplastic	0.0799808	0.83384
Proteins with highest loading along axis 1			
XP_010905138.1	Selenium-binding protein 1 isoform X2	0.833784	-0.0183339
XP_010924612.2	Phosphoenolpyruvate carboxylase 2	0.834523	0.175416
XP_010907411.1	Methionine aminopeptidase 2B	0.841124	-0.16696
XP_010918502.1	Heat shock protein 70 (Hsp 70) family protein	0.850082	-0.0139643
XP_010941296.1	Chaperone protein htpG family protein	0.851386	-0.0800271

XP_010942223.1	Tryptophan synthase beta type 2	0.855112	0.0817519
XP_010921546.1	Mannosyl-glycoprotein endo-beta-N-acetylglucosaminidase	0.857424	-0.249529
XP_010941303.1	Methenyltetrahydrofolate cyclohydrolase; Methylenetetrahydrofolate dehydrogenase (NADP(+))	0.860154	0.0643084
XP_010914509.1	Pathogenesis-related protein 1-like	0.860626	-0.0458342
XP_010927580.1	Fructose-bisphosphate aldolase 1, cytoplasmic	0.882182	-0.226271
XP_019709780.1	Probable linoleate 9S-lipoxygenase 5	0.885708	-0.0322151
XP_010922792.1	V-type proton ATPase subunit E	0.88802	-0.0268357
XP_010933076.1	Phosphopyruvate hydratase	0.915126	0.0241922
XP_010926052.1	NAD(P)-binding Rossmann-fold superfamily protein (Cinnamoyl-CoA reductase)	0.915256	-0.237854
XP_010941660.1	Phosphoglycerate kinase 3, cytosolic isoform X1	0.931847	-0.0594275
XP_010934326.1	Adenosine kinase 2-like	0.965006	-0.0183237

D. Supplementary pictures

Picture S1. Characterization of oil palm trees in the field at Socfindo in Indonesia (BBCP07). (a) picture of an oil palm tree, (b) counting of leaves and bunches apparent for foliar emission determination, (c) measure of leaf area with the method of Tailliez and Ballo (1992), (d,e) picture of bunches and inflorescence, and (f) sampling of fruits for analysis.

Picture S2. Construction and installation of the labelling assimilation chamber. (a,b) different steps of the construction of the labelling assimilation chamber, (c,d) insertion of the palm inside the chamber, and (e) closing of the chamber.

Picture S3. (a-d) Aerial view of the labelling chamber settlement.

Picture S4. Pictures of the labelling experiment. Pictures of (a,b) the installation and equipment of the labelling experiment, (c) the gas analyzer (WALZ GFS 3000) used for the experiment, and (d) the water condensation on the chamber due to high air temperature and relative humidity inside the chamber.

Picture S5. Field sampling and laboratory analysis after the labelling experiment. Pictures of (a) the opening of the labelling assimilation chamber, (b) the cleaning of sampled leaflet with deionized water, (c) the fixation of the leaflet with liquid nitrogen, and (d) the metabolite extractions for the different analyses.

Picture S6. Dark respiration experiment in the field. Pictures of (a,b) the complete installation in the dark, (c) sampling of CO_2 respired inside the chamber using a syringe, and (d) insertion of the CO_2 sampled inside an air tight tube.

université PARIS-SACLAY | ÉCOLE DOCTORALE Sciences du végétal : du gène à l'écosystème

Titre : Intéractome C/K dans le métabolisme et l'allocation liés à la production chez le palmier à huile.

Mots clés : Palmier à huile, nutrition K, métabolomique, protéomique, marquage au ^{13}C, rendement

Résumé : Le palmier à huile (*Elaeis guineensis* Jacq.) est l'un des oléagineux les plus productifs au monde. Malheureusement, les effets bénéfiques du potassium (K) pour le développement des fruits, en augmentant non seulement le nombre mais aussi le poids des régimes, sont peu prédictibles car on ignore encore les mécanismes métaboliques sous-jacents.
L'objectif de cette thèse était précisément de regarder les effets de la disponibilité en K sur les voies métaboliques et de voir s'il pouvait y avoir une relation entre les modifications métaboliques et la production d'huile.
Outre les effets attendus sur des traits végétatifs ou les régimes, nos résultats montrent que l'apport en K impacte le métabolisme primaire du carbone et de l'azote aussi bien dans les folioles que dans les fruits.
Cette thèse présente ainsi, pour la première fois, une étude détaillée du métabolisme du palmier à huile au champ, et montre que certains traits métaboliques (métabolites ou enzymes) sont liés à la disponibilité en K, mettant en abyme une potentielle utilisation de biomarqueurs foliaires pour piloter la nutrition minérale du palmier.

Title : C/K interactomic in oil palm metabolism and allocation related to yield

Keywords : oil palm, K nutrition, metabolomic, proteomic, ^{13}C labelling, yield

Abstract: Oil palm (*Elaeis guineensis* Jacq.) is one of the most productive oil crop in the world. Unfortunately, positive effect of K fertilization on fruit development with increasing in bunch weight and number, remain rather difficult to predict because of the lack of knowledge of underlying metabolic mechanisms.
The objective of this thesis was precisely to assess the effect of K availability on oil palm metabolic pathways and determine if metabolic changes could be related to oil production.
In addition to expected effects of potassium on vegetative traits and bunches, our results show that K availability affected carbon and nitrogen primary metabolism in both leaflets and developing fruits.
This thesis presents, for the first time, a detailed metabolic exploration of oil palm in the field and shows that some metabolic traits (metabolites or enzymes) are linked to K availability, thereby opening avenues for the use of leaf biochemical markers to monitor oil palm mineral nutrition.

Université Paris-Saclay
Espace Technologique / Immeuble Discovery
Route de l'Orme aux Merisiers RD 128 / 91190 Saint-Aubin, France